International
Progress Report

IPR-99-22

Äspö Hard Rock Laboratory

Äspö Task Force on Modelling of Groundwater Flow and Transport of Solutes

Proceedings from the 12th task force meeting at Gimo, Sweden, April 20-22, 1999

Part 3 of 3: Task 5 contributions

Mansueto Morosini

Svensk Kärnbränslehantering AB

September 1999

Svensk Kärnbränslehantering AB
Swedish Nuclear Fuel
and Waste Management Co
Box 5864
SE-102 40 Stockholm Sweden
Tel 08-459 84 00
+46 8 459 84 00
Fax 08-661 57 19
+46 8 661 57 19

Äspö Hard Rock Laboratory

Äspö Hard Rock Laboratory

Äspö Task Force on Modelling of Groundwater Flow and Transport of Solutes

Proceedings from the 12th task force meeting at Gimo, Sweden, April 20–22, 1999

Part 3 of 3: Task 5 contributions

Mansueto Morosini

Svensk Kärnbränslehantering AB

September 1999

Keywords: Groundwater flow, solute transport, tracer test, fractured rock, underground laboratory, stochastic modelling, deterministic modelling.

Appendix C – Task 5 Data and Predictive modelling

Contents:

Presentation of chemistry data.

M. Laaksoharju (SKB/Intera)

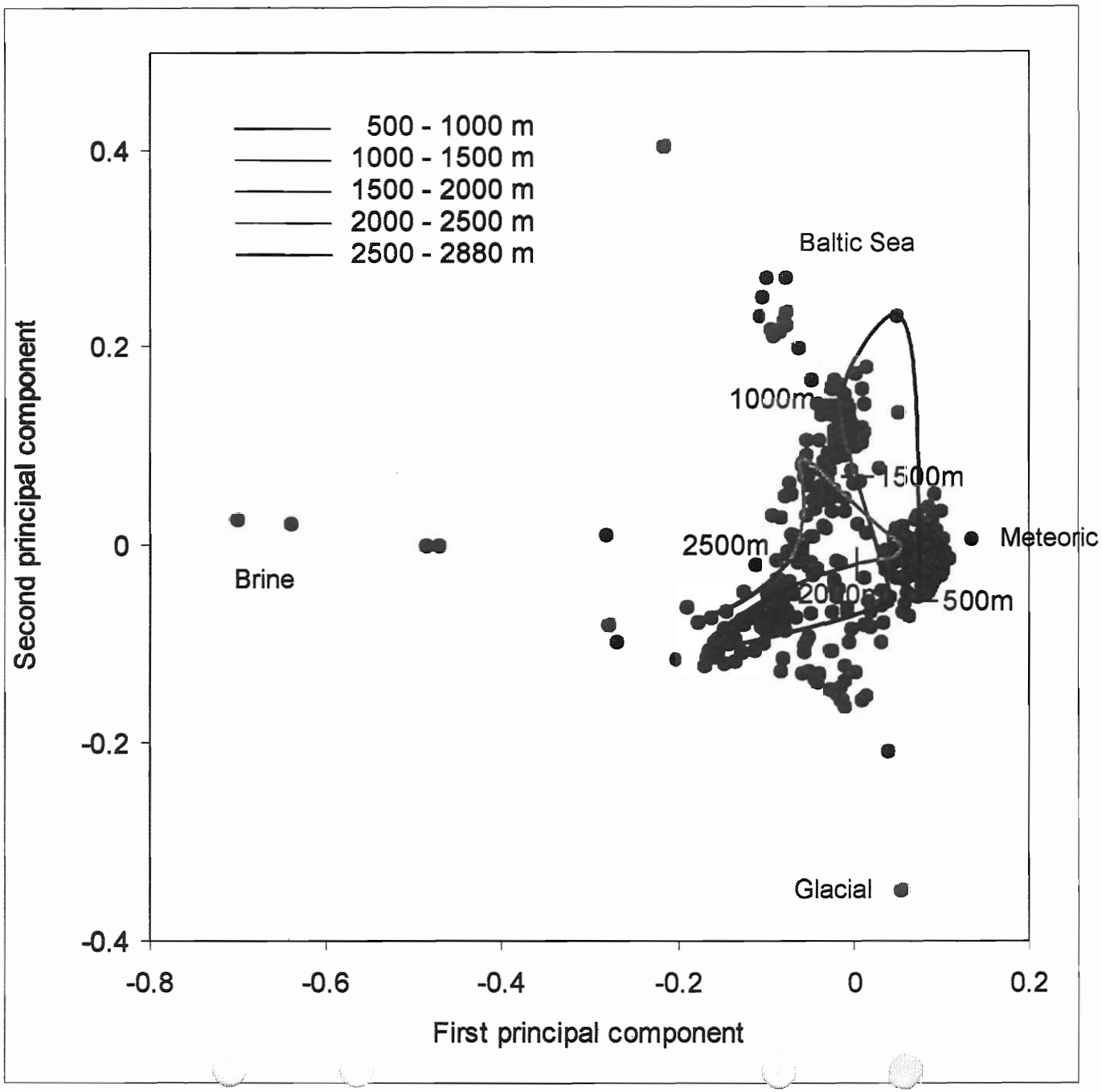
Tunnel position in the PCA, first observation
500 - 1000 m
1000 - 1500 m
1500 - 2000 m
2000 - 2500 m
2500 - 2880 m
Baltic Sea
1000m
1500m
2500m
500m
Meteoric
Brine
Glacial
0.4
0.2
0
-0.2
-0.4
-0.8
-0.6
-0.4
-0.2
0
0.2
Second principal component
First principal component

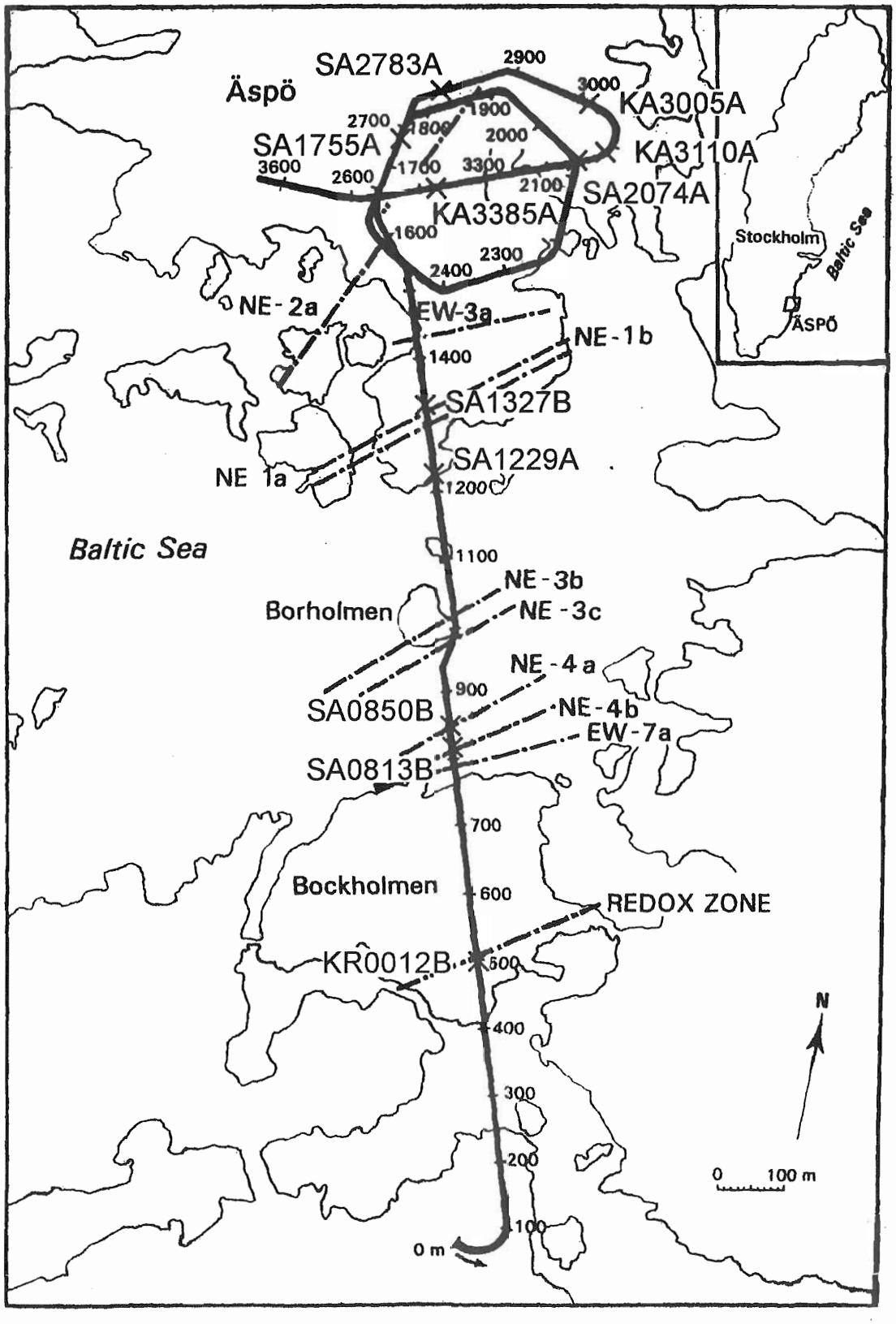
SA2783A
Äspö
2900
3000
KA3005A
2700
1800
1900
2000
SA1755A
KA3110A
3600
2600
1700
3300
2100
SA2074A
KA3385A
1600
2300
2400
Stockholm
Baltic Sea
ÄSPÖ
NE-2a
EW-3a
NE-1b
1400
SA1327B
SA1229A
NE 1a
1200
Baltic Sea
1100
NE-3b
Borholmen
NE-3c
NE-4a
900
SA0850B
NE-4b
EW-7a
SA0813B
700
Bockholmen
600
REDOX ZONE
KR0012B
500
400
300
200
100
0 m
N
0
100 m

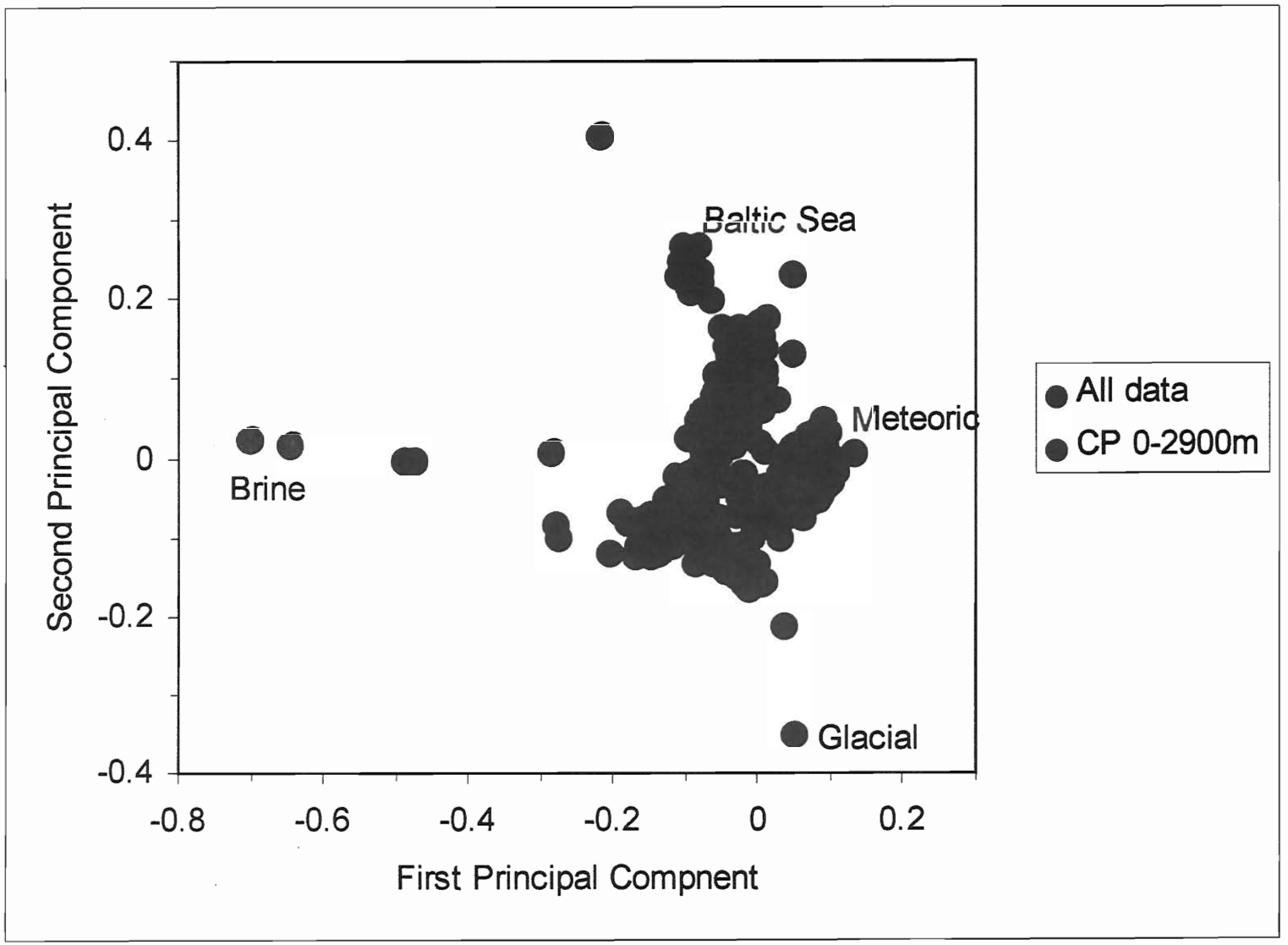
0.4
0.2
0
-0.2
-0.4
-0.8
-0.6
-0.4
-0.2
0
0.2
Second Principal Component
First Principal Compnent
Baltic Sea
Meteoric
Brine
Glacial
All data
CP 0-2900m

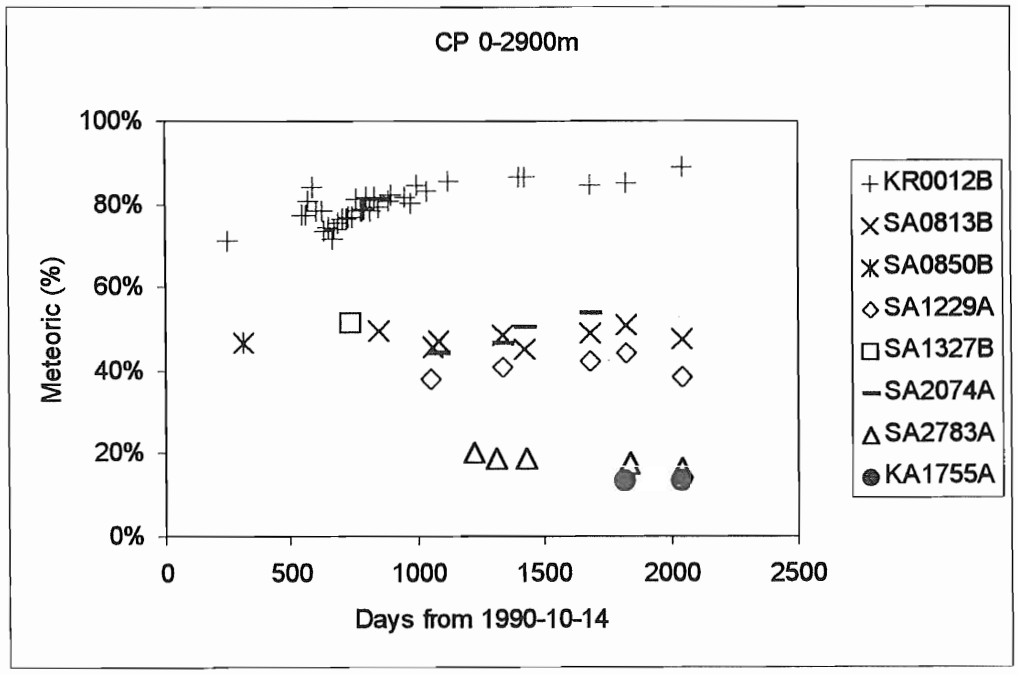
CP 0-2900m
Meteoric (%)
100%
80%
60%
40%
20%
0%
0
500
1000
1500
2000
2500
Days from 1990-10-14
KR0012B
SA0813B
SA0850B
SA1229A
SA1327B
SA2074A
SA2783A
KA1755A

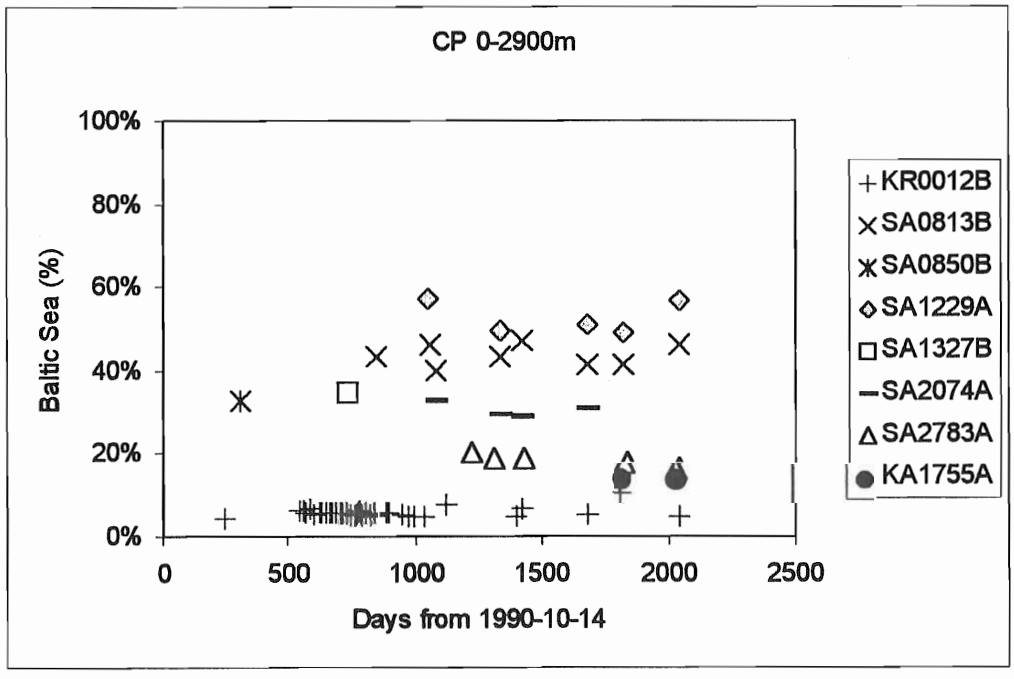
CP 0-2900m
Baltic Sea (%)
100%
80%
60%
40%
20%
0%
0
500
1000
1500
2000
2500
Days from 1990-10-14
KR0012B
SA0813B
SA0850B
SA1229A
SA1327B
SA2074A
SA2783A
KA1755A

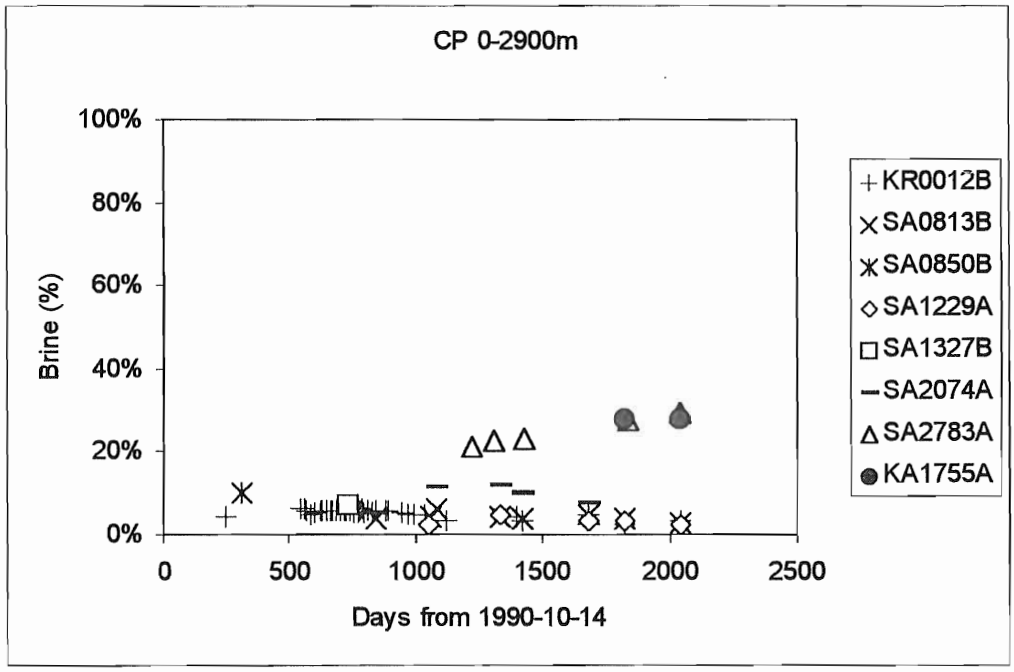
CP 0-2900m
100%
80%
60%
40%
20%
0%
Brine (%)
0
500
1000
1500
2000
2500
Days from 1990-10-14
KR0012B
SA0813B
SA0850B
SA1229A
SA1327B
SA2074A
SA2783A
KA1755A

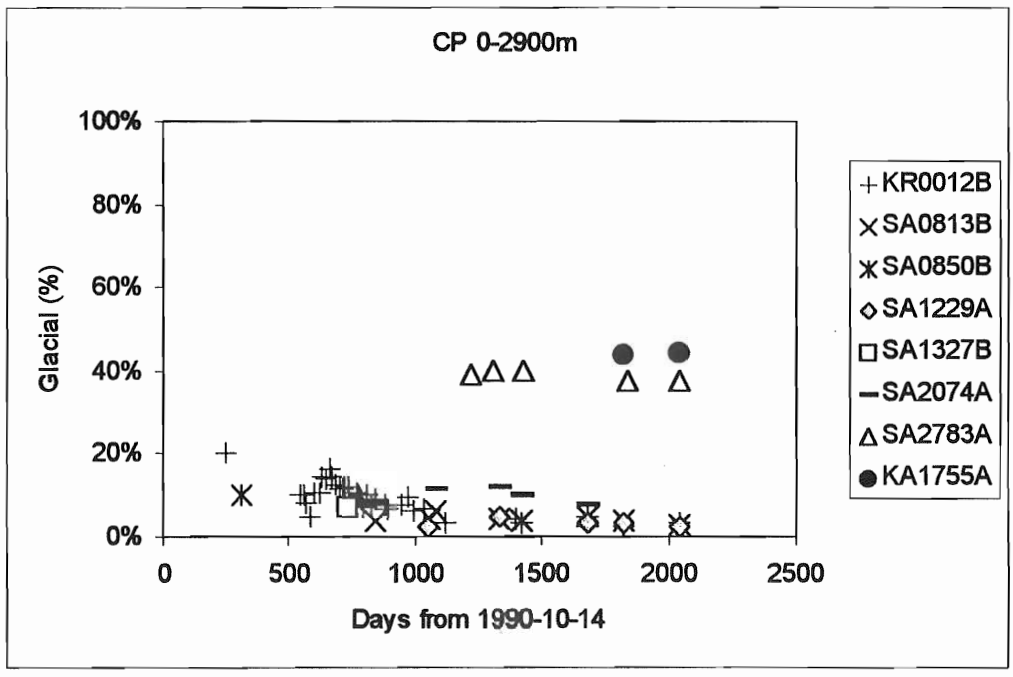
CP 0-2900m
100%
80%
60%
40%
20%
0%
Glacial (%)
0
500
1000
1500
2000
2500
Days from 1990-10-14
KR0012B
SA0813B
SA0850B
SA1229A
SA1327B
SA2074A
SA2783A
KA1755A

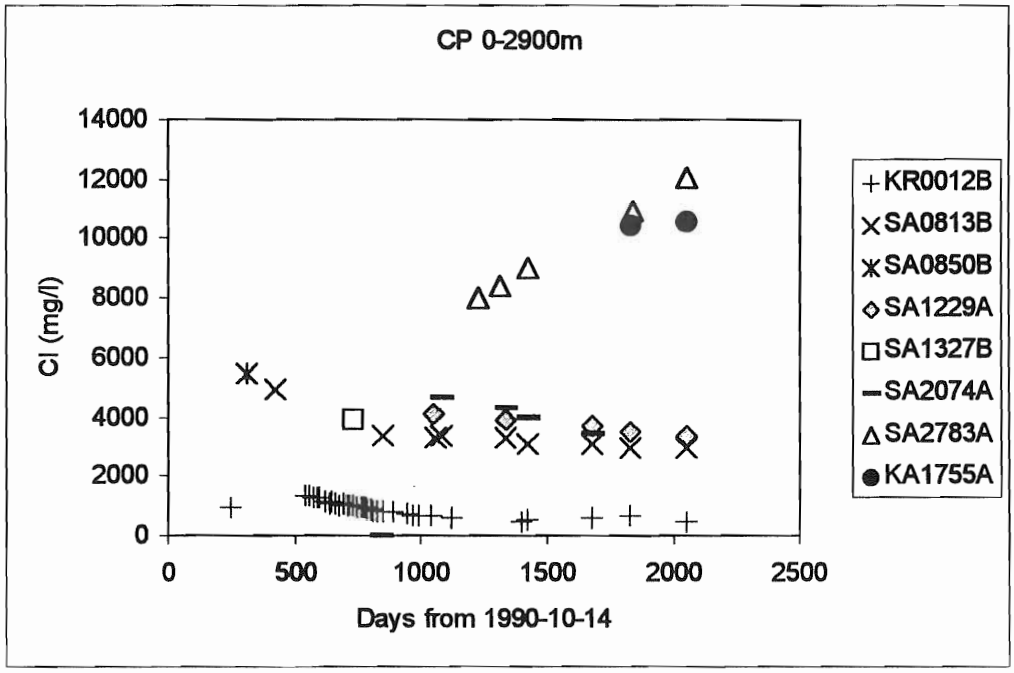
CP 0-2900m
Cl (mg/l)
14000
12000
10000
8000
6000
4000
2000
0
0
500
1000
1500
2000
2500
Days from 1990-10-14
KR0012B
SA0813B
SA0850B
SA1229A
SA1327B
SA2074A
SA2783A
KA1755A

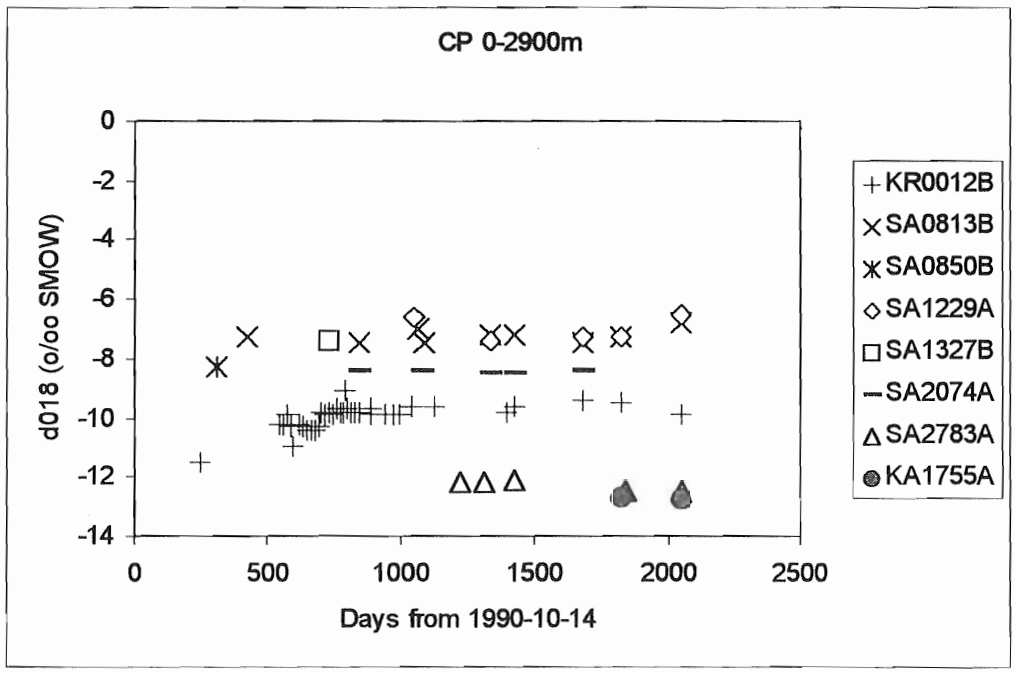
CP 0-2900m
d018 (o/oo SMOW)
0
-2
-4
-6
-8
-10
-12
-14
0
500
1000
1500
2000
2500
Days from 1990-10-14
KR0012B
SA0813B
SA0850B
SA1229A
SA1327B
SA2074A
SA2783A
KA1755A

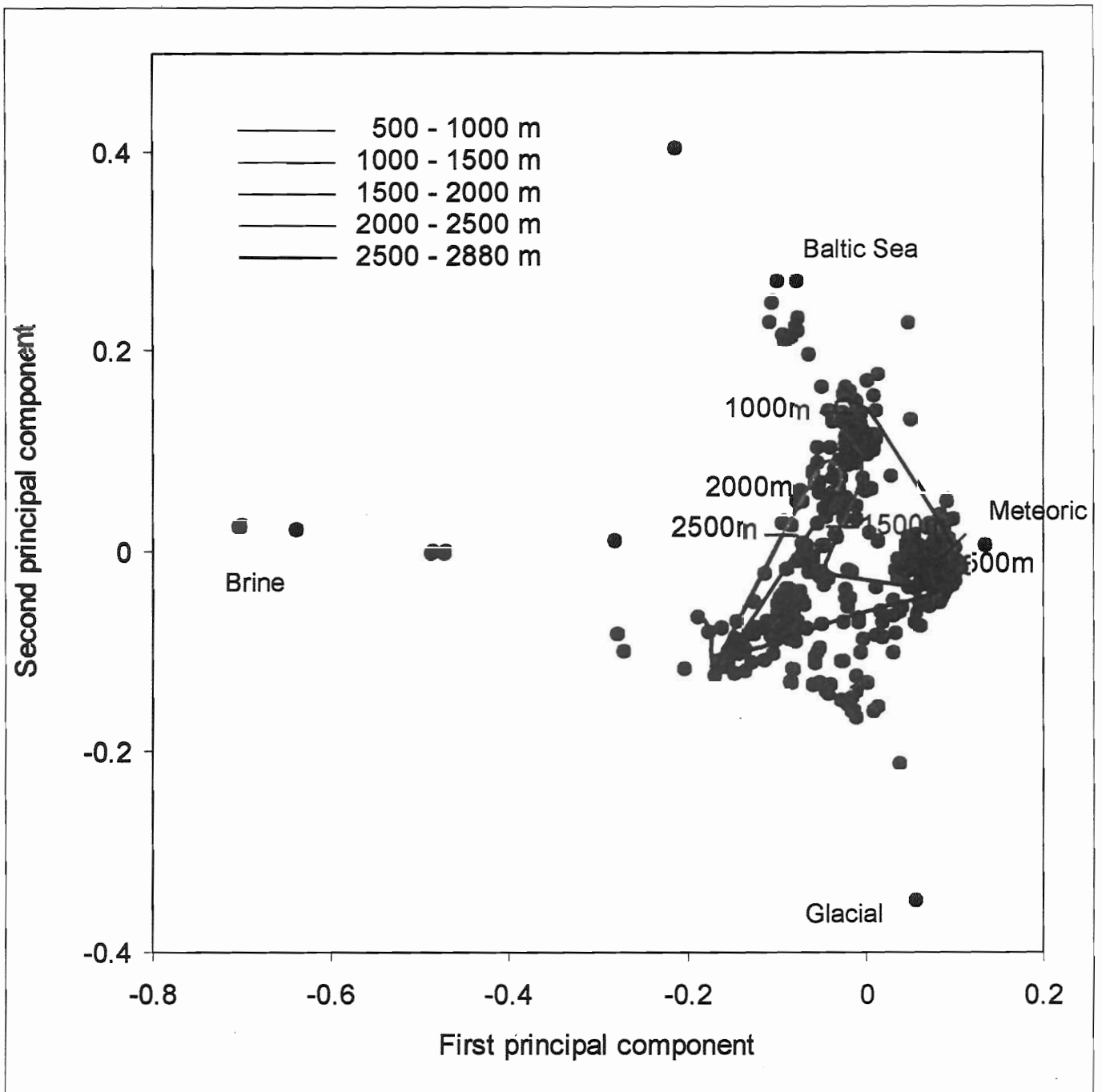
Tunnel position in the PCA, last observation
500 - 1000 m
1000 - 1500 m
1500 - 2000 m
2000 - 2500 m
2500 - 2880 m
Baltic Sea
1000m
2000m
2500m
1500
Meteoric
500m
Brine
Glacial
Second principal component
First principal component
0.4
0.2
0
-0.2
-0.4
-0.8
-0.6
-0.4
-0.2
0
0.2

Modelling the composition of the groundwater leaking into the Äspö HRL.

U. Svensson (SKB/CFE)

Modelling the Composition of the Groundwater Leaking into the Äspö HRL

- An attempt to identify some facts and uncertainties

Urban Svensson
Computer-aided Fluid Engineering AB
April 1999

1 BACKGROUND

The focus of the modelling in Task #5 is given already in the title of the task; "Impact of the tunnel construction on the groundwater system at Äspö, a hydrological-hydrochemical model assessment exercise", Wikberg (1998). From the same reference we may quote another sentence; "The key to a successful integration of the hydrochemical and hydrological models must be to understand the mechanisms behind the processes controlling the evolution and the dynamics of the groundwater system". The present paper will discuss these controlling processes in a mostly qualitative way.

An important step in the Task #5 workplan is "Evaluation, comparison and check of consistency". We are now at this point in the workplan and it seems timely to discuss the basic physical processes that govern the water composition.

The qualitative picture of the situation we are aiming at will be based on all kinds of relevant information, i.e. field data, models, order of magnitude estimates, reasoning, etc. Extensive reference will be made to three reports dealing with numerical models, a regional model study, Svensson (1997a), a site-scale model, Svensson (1997b) and a Task #5 draft report, Svensson (1999). These will in the following be referenced to as the "regional model", the "site-model" and the "Task #5 model".

2 OBJECTIVES

The main objective of the paper is to discuss the physical processes that govern the composition of the groundwater leaking into the spiral part of the Äspö tunnel. In doing so, we will try to identify facts and uncertainties about the processes. Hopefully this can stimulate a discussion and also be of assistance when formulating "basic conceptual assumptions" of a model.

3 METHOD

The approach is straight forward: we will state that the water leaking into the tunnel may origin from surface water (Meteoric or Baltic) or Brine from below 800 metres depth or from a horizontal flow. The different sources are discussed one by one and possible facts and uncertainties are noted.

4 LIMITATIONS

From the hydrochemical point of view, four water types (Meteoric, Baltic, Glacial and Brine) have been found to characterise the water leaking into the tunnel. In this paper we will accept this characterisation and only discuss the hydrogeological aspect of the problem. In line with the objectives of Task #5, only conditions before (as initial conditions), during and after tunnel construction are dealt with. It is however realised that processes during the last 12 000 years, since the last glaciation, are essential for a full understanding of the present situation.

5 ANALYSIS

All processes will be discussed with reference to Figure 1. The spiral part of the tunnel is enclosed in a control volume and we will discuss the composition of water entering through the top, bottom and sides of this box.

5.1 Precipitation on Äspö

Precipitation minus evapotranspiration, P-E, has been estimated to be about 200 mm/year, Rhén et al (1997). Under natural conditions most of this will take a rather direct route to the sea and only a small fraction will contribute to deep infiltration. With Äspö HRL present the groundwater table will be below mean sea level and a much larger fraction of P-E will infiltrate. In the site model report it was estimated that about 100 mm/year will infiltrate. The area above the depressed ground water table is about 5×10^5 m^2 which gives a net flow of 1.5 l/s. The inflow to the spiral part of the tunnel (1 400 → 3 600 metres) is about 14 l/s. From this we can conclude:

Precipitation on Äspö can not alone provide the inflow to the spiral part of the tunnel. If the Meteoric water from Äspö is the only source of Meteoric water, the average fraction of Meteoric water in the tunnel is about 10 %. The uncertainty concerning the magnitude of the deep infiltration will directly influence the estimated proportion of Meteoric water in the tunnel.

5.2 The Baltic water surrounding Äspö

When the groundwater table on Äspö is lowered to around -80 masl, one can expect that the Baltic water surrounding Äspö flows towards the lowest point of the groundwater table, see Figure 1 (see also site model report, Figure 4-13 and Table 6-1). It is likely that a significant amount of Baltic surface water ends up in the tunnel but it is not possible to estimate how much. The salinity of the Baltic surface water is 0.6 %, while the average salinity of the inflow to the spiral part of the tunnel is 0.9 %. This leads to the following conclusion.

Due to the salinity balance, Meteoric water and surface Baltic water can not alone provide the inflow to the tunnel.

Below the Baltic a clay layer of a few meters thickness is normally found. This was considered in the site model, and in the Task #5 model, by prescribing a conductivity of 10^{-9} m/s to a 3 metres thick layer, centred 5 metres below the sea bed.

It is uncertain how this clay layer affects the rate of Baltic surface water found in the tunnel.

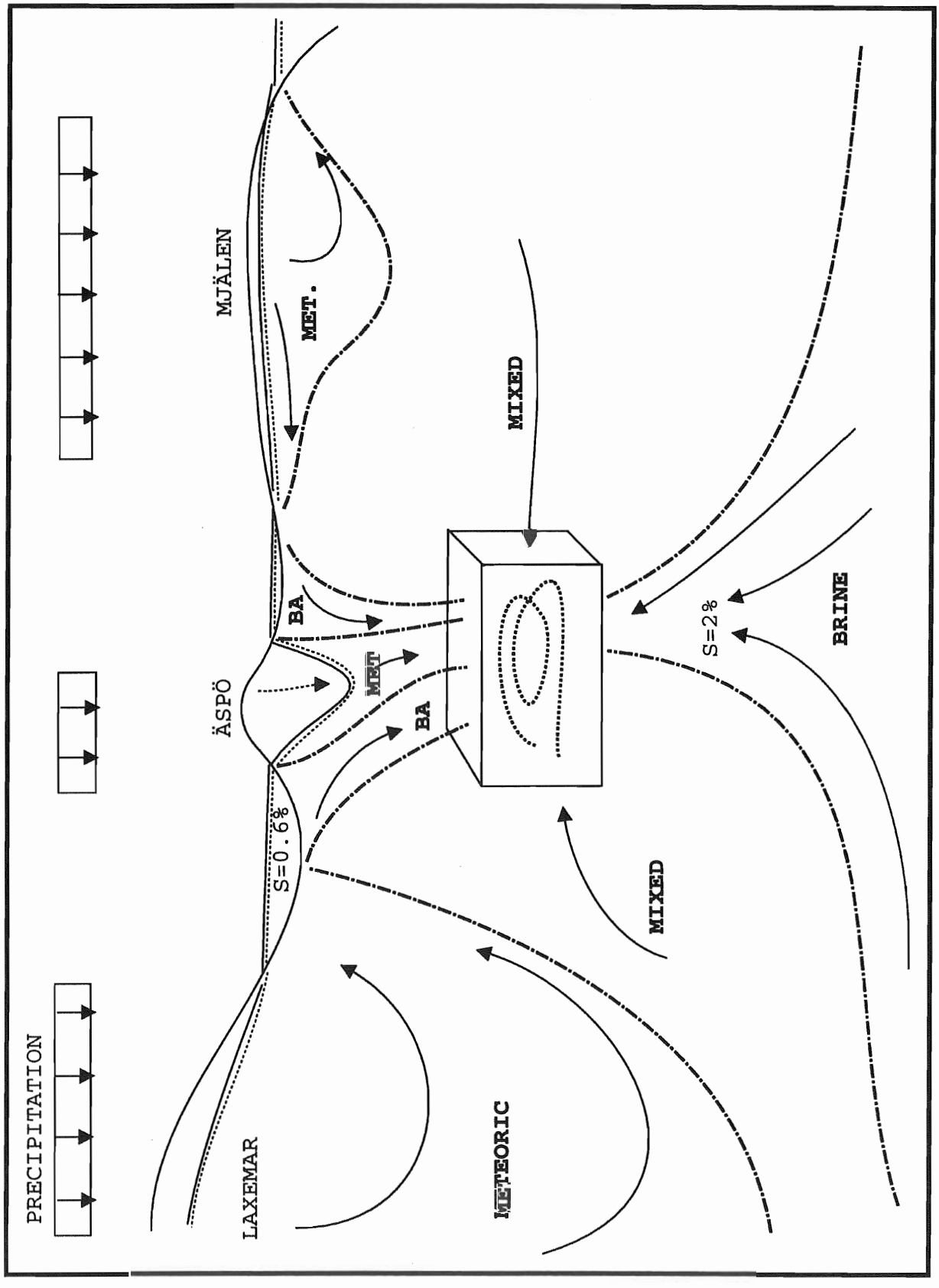

Figure 1. *Illustration of physical processes affecting the composition of groundwater leaking into the spiral part of the tunnel.*

5.3 The Brine

Measurements prior to the tunnel construction show that below a depth of about 800 metres a very old water is found. It has a salinity of about 2 % and we shall call this water type Brine. The Brine is now, from field measurements, found to be one of the water types that make up the tunnel inflow.

About upconing

In order to understand why the Brine is found at laboratory level we look at an idealised situation, see Figure 2. If we have a two-layer situation and the groundwater table is lowered, the saltwater will rise to counter-balance the pressure gradient from the groundwater table. If we estimate the height of the upconing from the Ghyben-Herzberg relation we find that the upconing is about 4 000 metres for a $\Delta\rho$ of 15 kg/m^3 and a groundwater table that is -60 masl. This is of course totally unrealistic but shows anyway that the Brine is exposed to a force that will lift it to laboratory level and higher if it was not "extracted" by the tunnel.

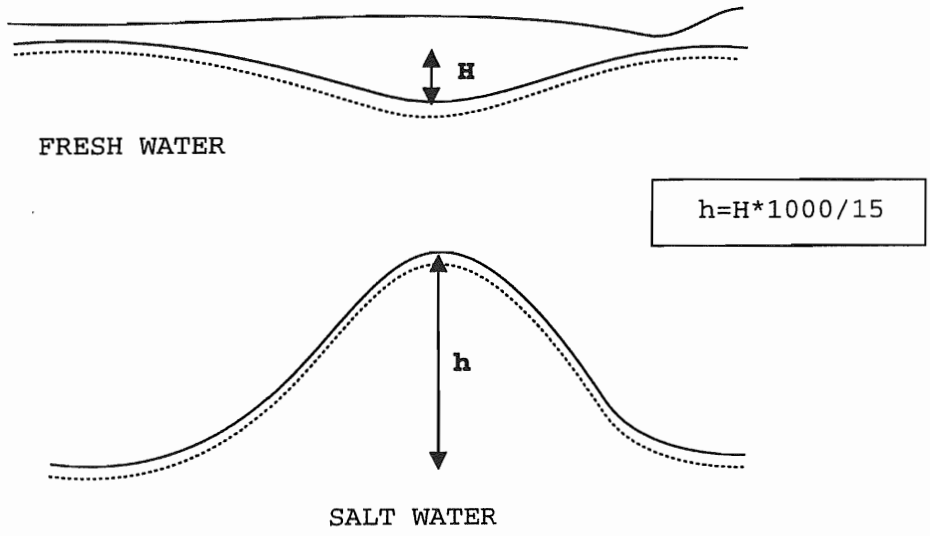

Figure 2. *Upconing in a two-layer system.*

The conclusion is:

The upconing effect is a direct consequence of the lowering of the groundwater table and is thus a persistent and stable effect. The upconing is "cut off" by the inflow to the tunnel.

Water composition

If we assume that the inflow to the tunnel is composed of Meteoric, Baltic and Brine water types we can write:

Flow rates: $Q_M + Q_{Ba} + Q_{Br} = 14 \times 10^{-3}$

Salinity balance: $Q_M \times 0 + Q_{Ba} \times 0.6 + Q_{Br} \times 2.0 = 14 \times 10^{-3} \times 0.9$

If $Q_M = 1.5$ l/s we have two equations and two unknowns. The resulting water composition is 11% Meteoric, 63% Baltic and 26% Brine. This is however not a realistic solution as we have to consider the horizontal flux component at laboratory level; there is a head gradient towards the laboratory and hence there is a flux.

5.4 The horizontal flux at laboratory level

The composition of the horizontal flux component is harder to estimate for several reasons:

- There is no obvious "infinite source" from which all horizontal flux originates.
- The horizontal flux is established in an environment with a density stratification. Presumably the selective withdrawal principle will apply.
- Timedependence. It can be expected that the water composition will change with time as the origin of the water will vary in time.

These aspects of the horizontal flux will now be discussed.

The selective withdrawal principle

Withdrawal of fluid in a continuously stratified (with respect to density) fluid is known as the selective withdrawal problem. The main result, see Figure 3, is that fluid is withdrawn from a certain density, in our case salinity, interval. Close to the spiral the head gradient is so large that it completely dominates the gravitational effect. Further away (300 to 400 metres according to Figure 4-21 in the site model report) the density stratification will govern the flow pattern and flow in a certain salinity interval will result. The flow will of course be weaker far away from the laboratory and the gradient in the horizontal flux is compensated by a vertical flux component, see Figure 3. As a result one can expect that Meteoric or Baltic surface water will increase at laboratory level. This tendency is supported by numerical simulations (regional model report Figure 4-16, Task #5 report Figure 6-18) and the deepening of Meteoric water in KLX02. This was also the result of the analysis by Gurban et al (1998). We can thus conclude:

If the selective withdrawal principle applies one can expect that the horizontal flux is withdrawn from a certain salinity interval. It is also likely that Meteoric or Baltic surface water will increase with time, at laboratory level. The origin of the horizontal flux component is however timedependent and hence uncertain.

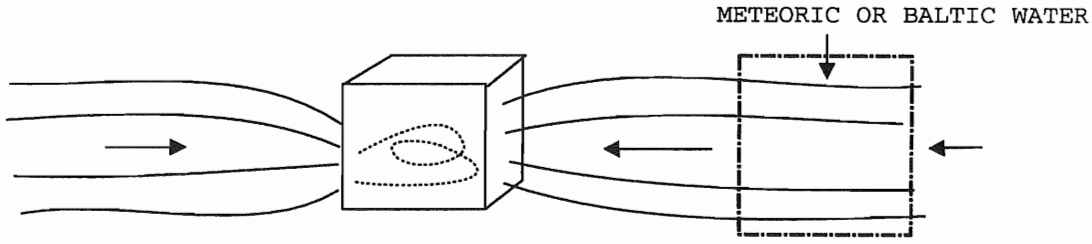

Figure 3. *The selective withdrawal principle.*

Timedependence

As mentioned, the composition of the horizontal flux can be expected to change with time. It is of interest to estimate the timescale for these changes. This can be done by estimating the pore-velocity in the fracture zones and the typical exchange time for a volume enclosing the laboratory.

Pore-velocity: A typical head-gradient at a distance of a few hundred metres from the laboratory is 0.1. Typical data for fracture zones, see Rhén et al (1997) are: $T = 2\times10^{-5}$ m^2/s, width = 10 m and kinematic porosity = 0.005. This gives a pore-velocity of 4×10^{-5} m/s or 1 260 m/year.

Exchange time: Another estimate can be made by enclosing the laboratory in a certain volume and estimate the typical exchange time due to the inflow to the tunnel. If we choose a volume of 1 x 1 x 1 km^3 with a kinematic porosity of 10^{-3} we find that the exchange time is one year (using 30 l/s as the total inflow to the tunnel).

From these estimates we conclude:

The horizontal flux component has a advective velocity of the order 1 km/year. Large volumes may thus be affected by the tunnel inflow.

5.5 Estimate of water composition

It is now time to compile the different estimates made and make an attempt to calculate the water composition of the water leaking into the spiral part of the tunnel.

It was earlier noted that gravitational forces are of little importance close to the tunnel. In the box in Figure 1, we can therefore assume that the flux is equal across all six faces (a similar analysis is made in the site model report, see Table 6-2). The flux over one face is then 2.3 l/s. As we have estimated the volume flux from Meteoric water on Äspö to 1.5 l/s we find that Baltic water through the top of the box is 0.8 l/s. We can now estimate the salinity of the horizontal flux from:

$$Q_{Ba}\times 0.6 + Q_{Br}\times 2.0 + Q_H \times S_H = 14\times10^{-3}\times 0.9$$

which gives $S_H = 0.8$ %. The composition of the horizontal flux is best determined from field data. From Gurban et al (1998) the compositions in KLX01, KLX02 and KAV01 can be

found together with salinity profiles. At the depth where the salinity is 0.8 % one can estimate the following composition: Baltic 10 %, Meteoric 40 %, Glacial 40 % and Brine 10 %. With this composition of the horizontal flux, we can calculate the average composition of the inflow to the spiral part of the tunnel. The result is: Meteoric 38 %, Baltic 12 %, Glacial 27 % and Brine 23%.

Needless to say, this composition is based on a number of rough calculations, estimates, interpretations of field data, etc. The main significance is probably that it is at all possible to arrive at a composition which is based on considerations of all physical processes believed to be important.

5.6 Future evolution

It has already been mentioned that changes with time can be expected. If a timespan from the completed tunnel (1995) to a few years ahead is considered, the following suggestions may be relevant.

- The contributions from the Baltic surface water and the Meteoric water from Äspö can be expected to be in a steady state as both the sources and the driving force are persistent.

- Also the upconing and the associated Brine flux can be expected to be constant in time. The upconing does not however counterbalance the tilt of the groundwater table, as discussed earlier, which means that pressure gradients will be found well below 800 metres (see regional report Figure 4-15). As a result saltwater from deeper levels may be affected which in turn would increase the salinity of the Brine contribution.

- The horizontal flux has a large proportion of Glacial water. As there is no source of this water type it can be expected to decrease with time. Probably the fraction of Meteoric water from the areas surrounding Äspö will increase, according to the water exchange due to the selective withdrawal principle (see also Task #5 report Figure 6-18).

6 CONCLUDING REMARKS

The objective of this paper is to stimulate a discussion about the physical processes believed to be important in the Task #5 modelling exercise. Hopefully such a discussion is of value for the "Evaluation, comparison and check of cosistency" step in the workplan.

In the discussion of various processes "facts" and "uncertainties" have been identified. The most important ones of these can be summarised as:

The sources related to Baltic surface water, Meteoric water from Äspö and the Brine from below 800 metres depth can be expected to be steady and persistent. Sources associated with the horizontal flux can be expected to vary with time as the origin of the sources will vary with time. Presumably, the Glacial component will decrease and the Meteoric component increase.

7 REFERENCES

Gurban I., Laaksoharju M., Andersson C. 1998. Influences of the tunnel construction on the groundwater chemistry at Äspö. SKB Technical Note TN-98-16g.

Rhén I (ed), Gustafson G., Stanfors R., Wikberg p. 1997. Äspö HRL – Geoscientific evaluation 1997/5. Models based on site characterization 1986-1995. SKB Technical Report 97-06.

Svensson U, 1997a. A regional analysis of groundwater flow and salinity distribution in the Äspö area. SKB Technical Report 97-09.

Svensson U, 1997b. A site scale analysis of groundwater flow and salinity distribution in the Äspö area. SKB Technical Report 97-17.

Svensson U, 1999. The origin and composition of groundwater leaking into the Äspö tunnel. Draft Report, SKB Task #5.

Wikberg P. 1998. Äspö task force on modelling of groundwater flow and transport of solutes. Plan for modelling Task #5. SKB progress Report HRL-98-07.

Hydraulic DFN modelling of Task 5

D. Shuttle & W. Dershowitz (Golder), M. Uchida (JNC)

PAWorks Pathways Analysis in Support of Task 5

Stage 1: Hydrogeological Conditioning

Äspö Modeling Task Force Meeting
21 April, 1999

Dawn Shuttle/Golder
Bill Dershowitz/Golder
Masahiro Uchida/JNC

JNC サイクル機構

JNC/Golder Task 5 Goals and Approach

- Demonstrate the Value of Geochemical Data for Construction and Validation of Hydrogeological and Pathway Models
- Stage 1: Calibrate and Predict Based on Hydrological Data Only (4/99)
- Stage 2: Update based on Geochemical Data, Repeat Predictions (8/99)

JNC/Golder Task 5 Approach : Stage 1

- Updated Äspö DFN Hydrogeological Model
  - SKB 1999 Äspö Structural Model
  - Background Fracturing Based on Tunnel Maps
  - Weir Flux Boundary Condition
- Model Calibration Based on Borehole Pressure Response ONLY
  - Same Analysis Approach as "Task 3" (Uchida et al 1997)
  - Demonstration of PAWorks (1-D Elements) comparison to MAFIC (2-D Elements)
- Stage 1 Prediction (from Hydrogeological Data Only)
  - Prediction of Borehole Pressure Response and Geochemical Breakthrough 2900m to 3600 m
  - Pathways Analysis from Initial Geochemical Spatial Pattern to Tunnel Breakthrough
  - Predict End Member Breakthrough at Control Points

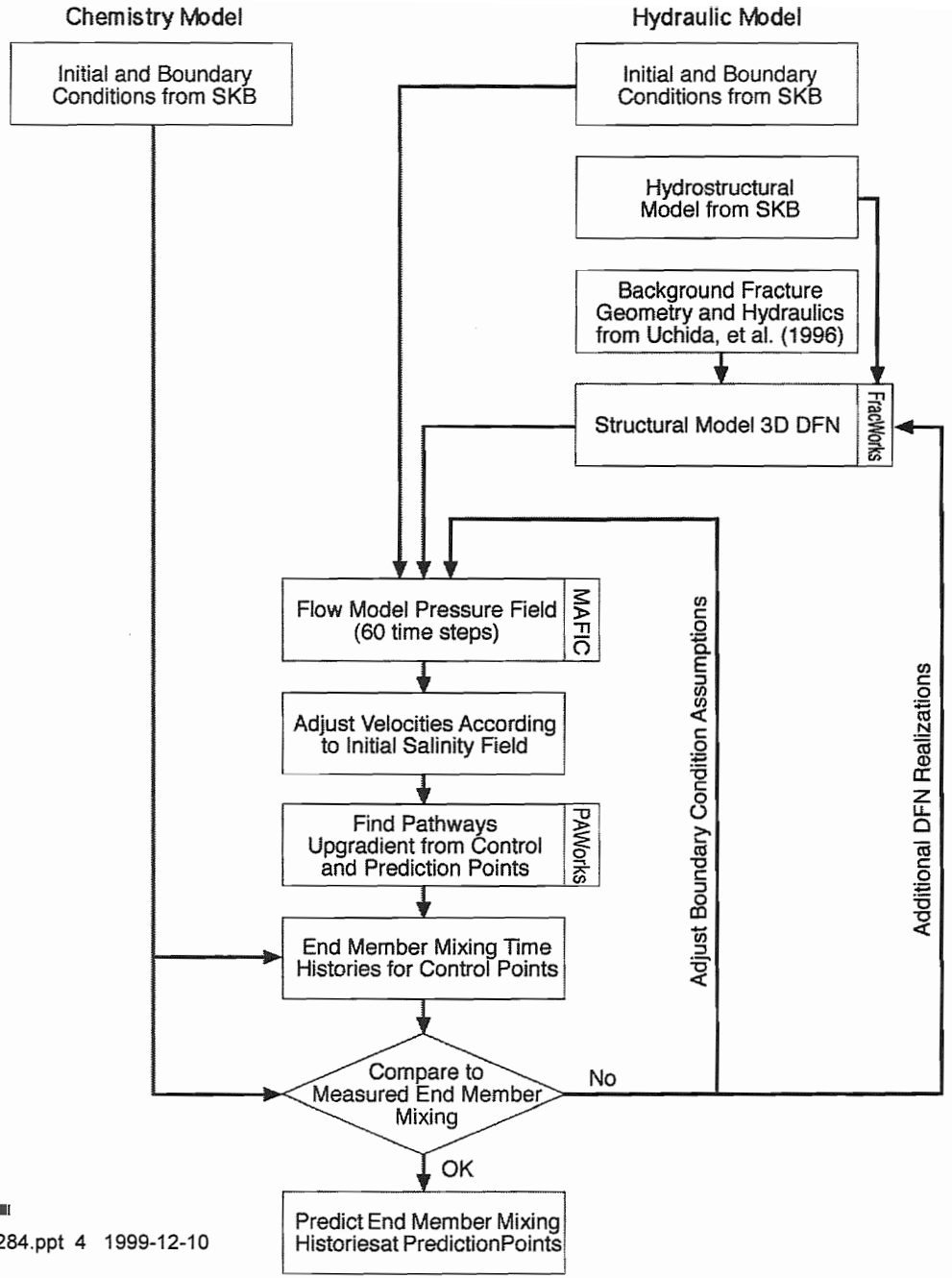
Chemistry Model
Initial and Boundary Conditions from SKB
Hydraulic Model
Initial and Boundary Conditions from SKB
Hydrostructural Model from SKB
Background Fracture Geometry and Hydraulics from Uchida, et al. (1996)
Structural Model 3D DFN
FracWorks
Flow Model Pressure Field (60 time steps)
MAFIC
Adjust Velocities According to Initial Salinity Field
Find Pathways Upgradient from Control and Prediction Points
PAWorks
End Member Mixing Time Histories for Control Points
Compare to Measured End Member Mixing
No
OK
Predict End Member Mixing Historiesat PredictionPoints
Adjust Boundary Condition Assumptions
Additional DFN Realizations

サイクル機構

Task 5 Technical Issues

- **Transient Flow Due to Ongoing Excavation**
  - Time Varying Weir Flux Boundary Condition
  - Limited Conditioning to Hydrologic Measurements ONLY
- **Density Effects on Flow**
  - Environmental Head: Appropriate where Flow is Vertical
  - Freshwater Head: Appropriate where Flow is Horizontal
  - Task 5 Approximation: Assumes pressures from constant density simulation are correct, heads are then corrected based on density and flow direction

Density Effect Approach

Relative Velocity versus Dip of Pipe

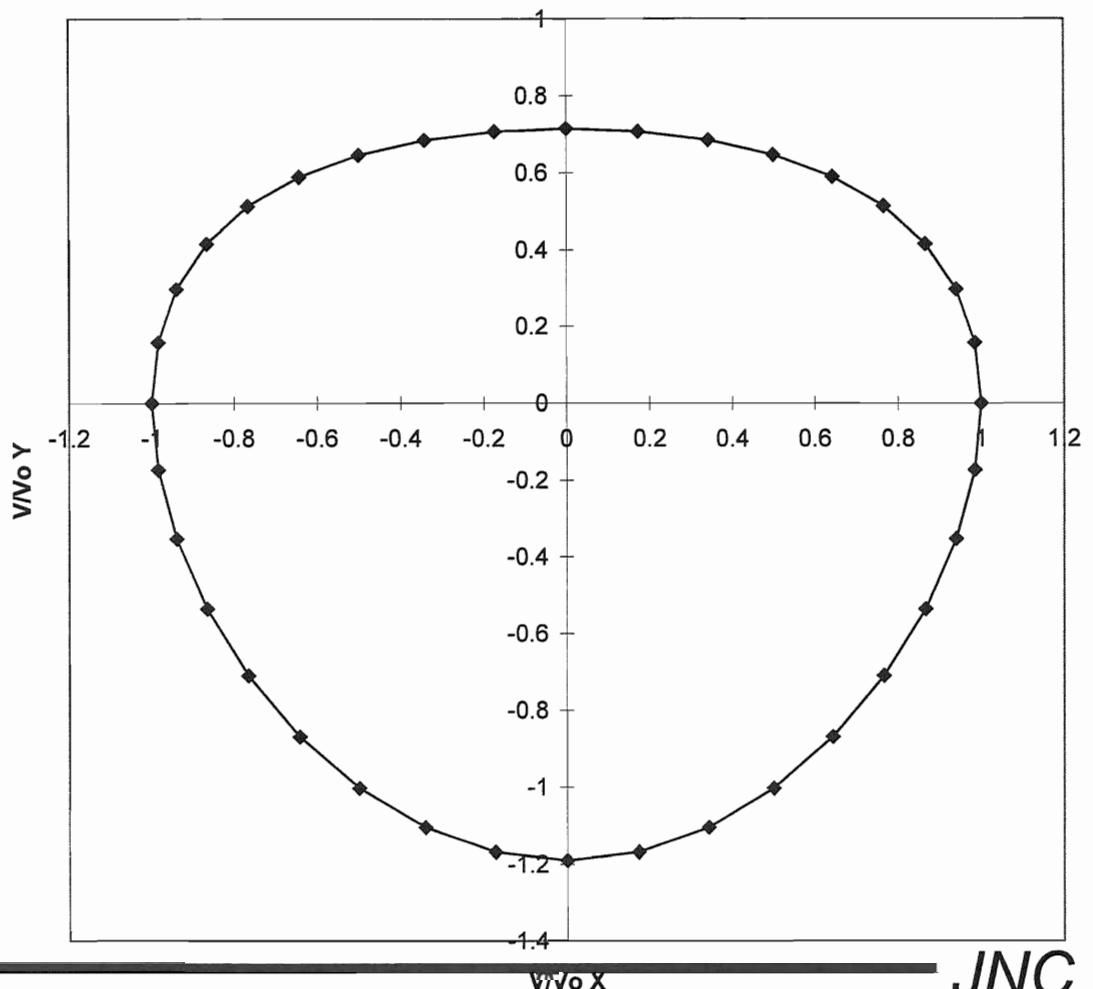

JNC サイクル機構

Density Effect Approach

Relative Velocity V/V0 for Vertically Upward Flow

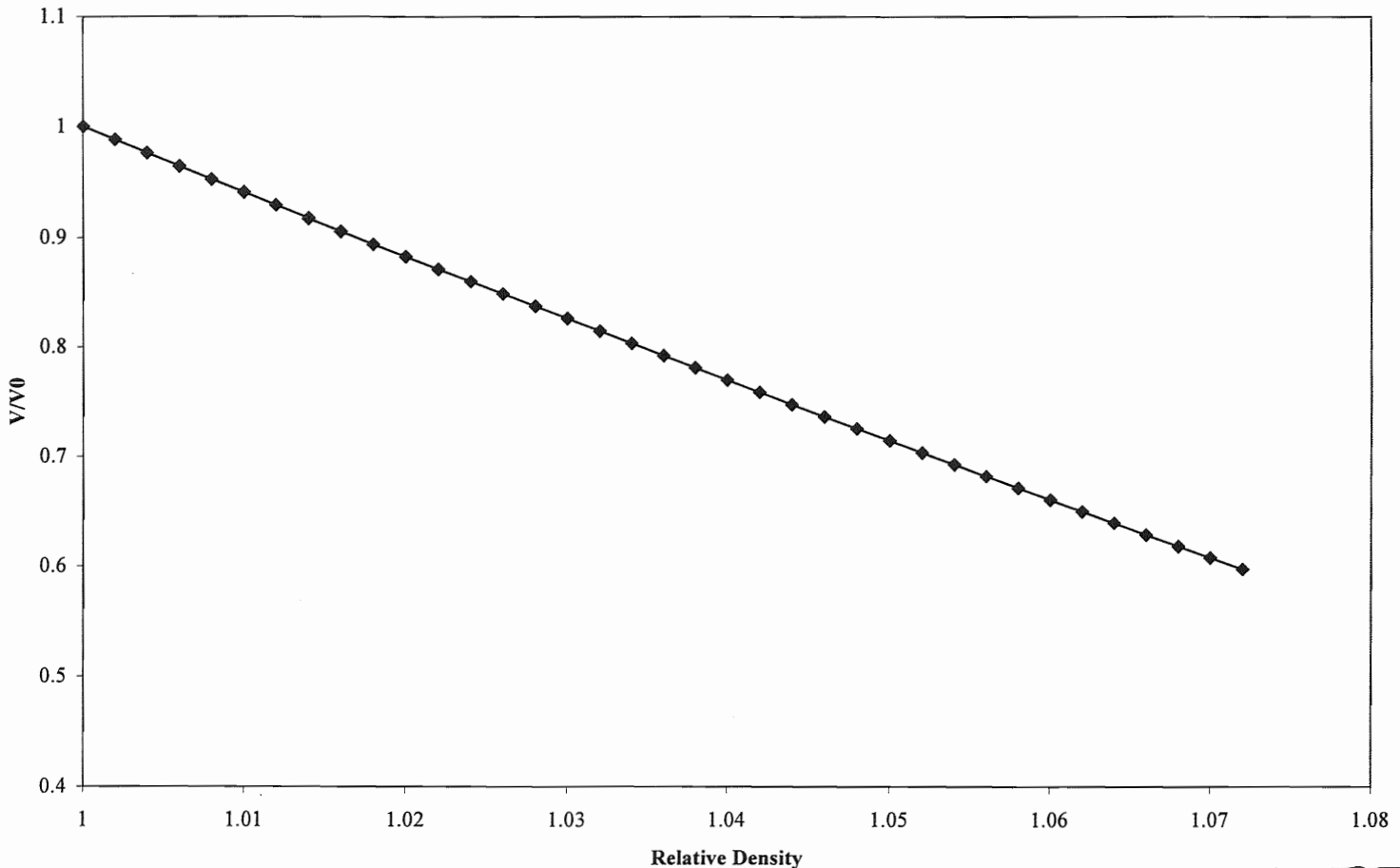

JNC サイクル機構

Task 5 DFN Model

- Latest SKB Structural Model
- Background Fracturing Same as "Task 3"
- Deterministic Fracturing from SR97
- Implement DFN using PAWorks Channel Network Approach

Task 5 DFN Model

■ Fracture Model Parameters (Geometry, Flow)

Fracture Set	Deterministic Fracture Zones	Background Fracture Properties
Name	Fracture Zone Fractures	Background fractures
Location	22 Planar Homogeneous Zones	Baecher/Bart Model
Size	Surface Traces Mean = 1420m	LogNormal (μ = 13.7m, σ = 12.7 m)
Orientation	3 Point Solution	Bootstrap SKB, 1994 Fractures Mapped in Tunnels
Transmissivity (m^2/s)	TR-91-22 & Olsson, 1995a	LogNormal (μ = 9×10^{-7} m^2/s, σ = 5×10^{-6} m^2/s)
Storativity	$0.001\ T^{1/2}$	$0.001\ T^{1/2}$
Intensity (m/m^2)	Surface traces P_{21} = 7.83×10^{-3}	P_{32} = 0.020214

Task 5 DFN Model - Large Scale Features

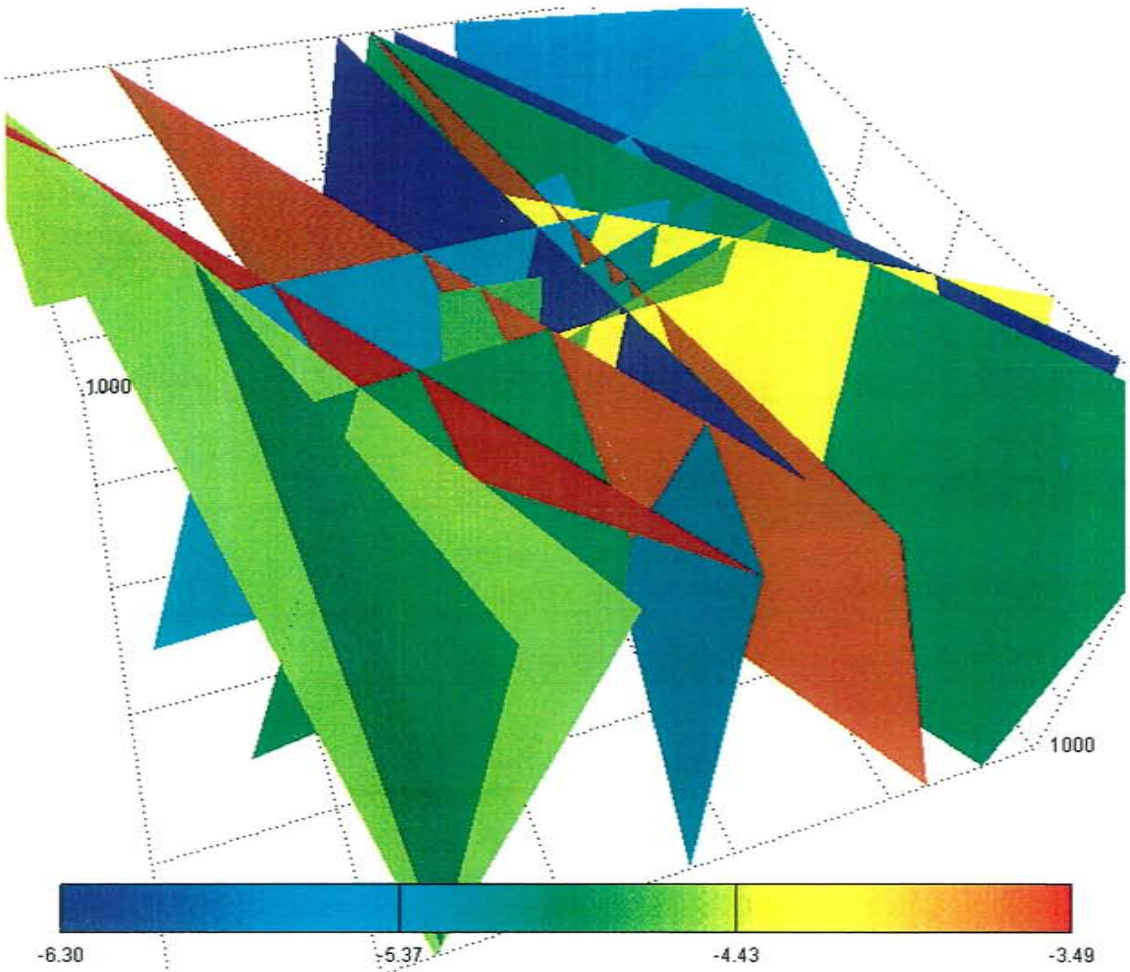

JNC サイクル機構

Task 5 DFN Model - Background Fractures

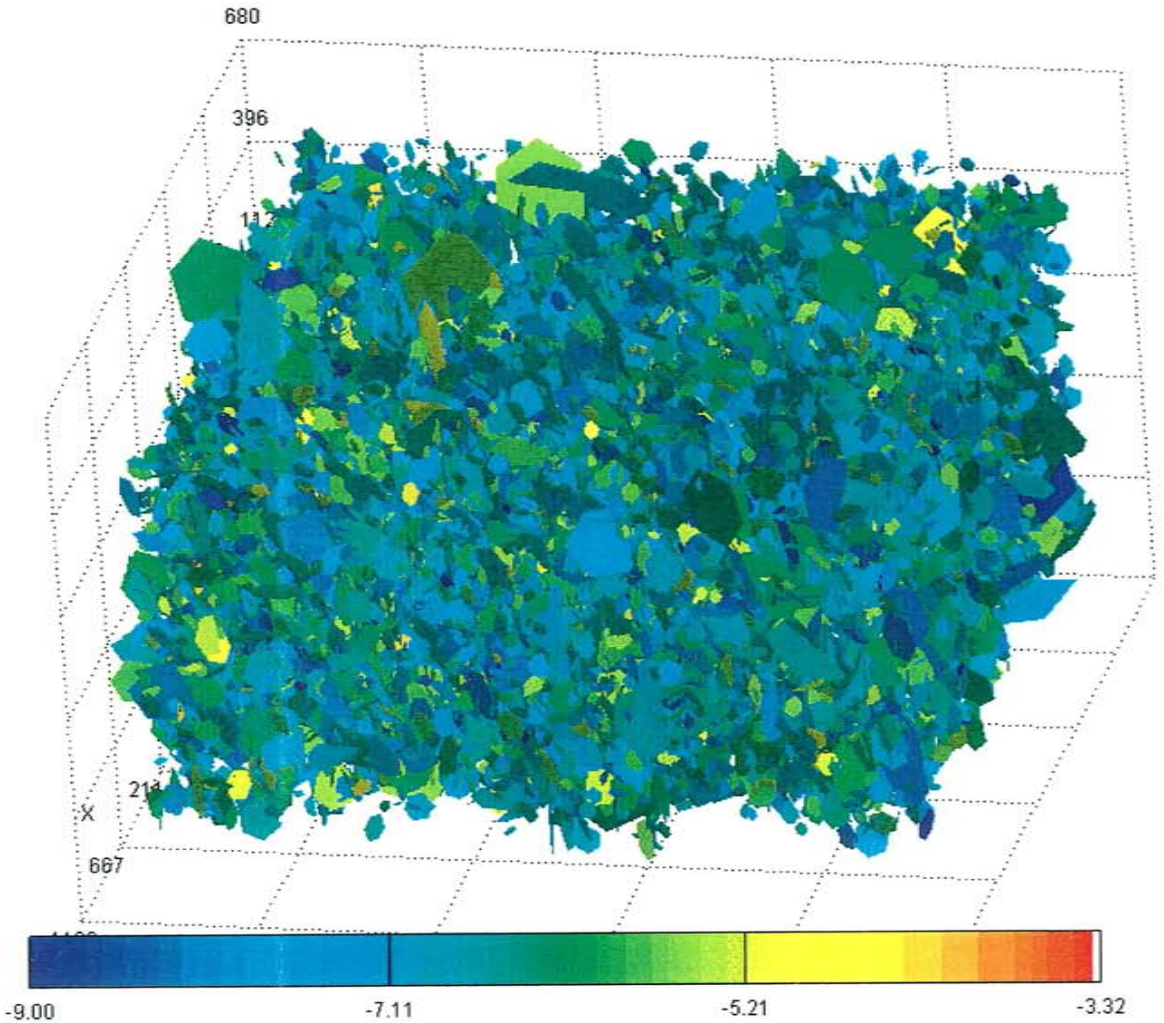

JNC サイクル機構

Task 5 DFN Model - Deterministic Fractures

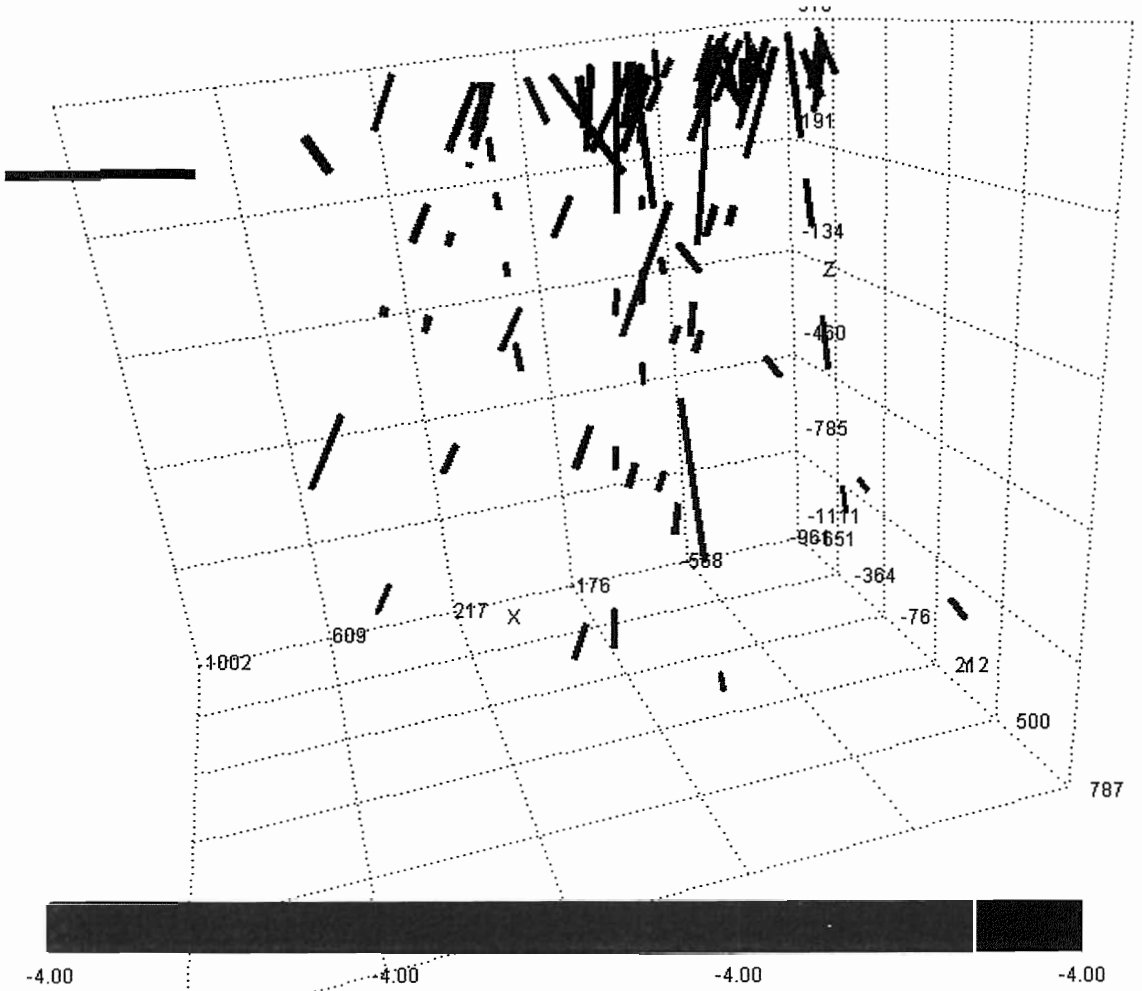

JNC サイクル機構

Task 5 DFN Model Tunnel to MP 3600

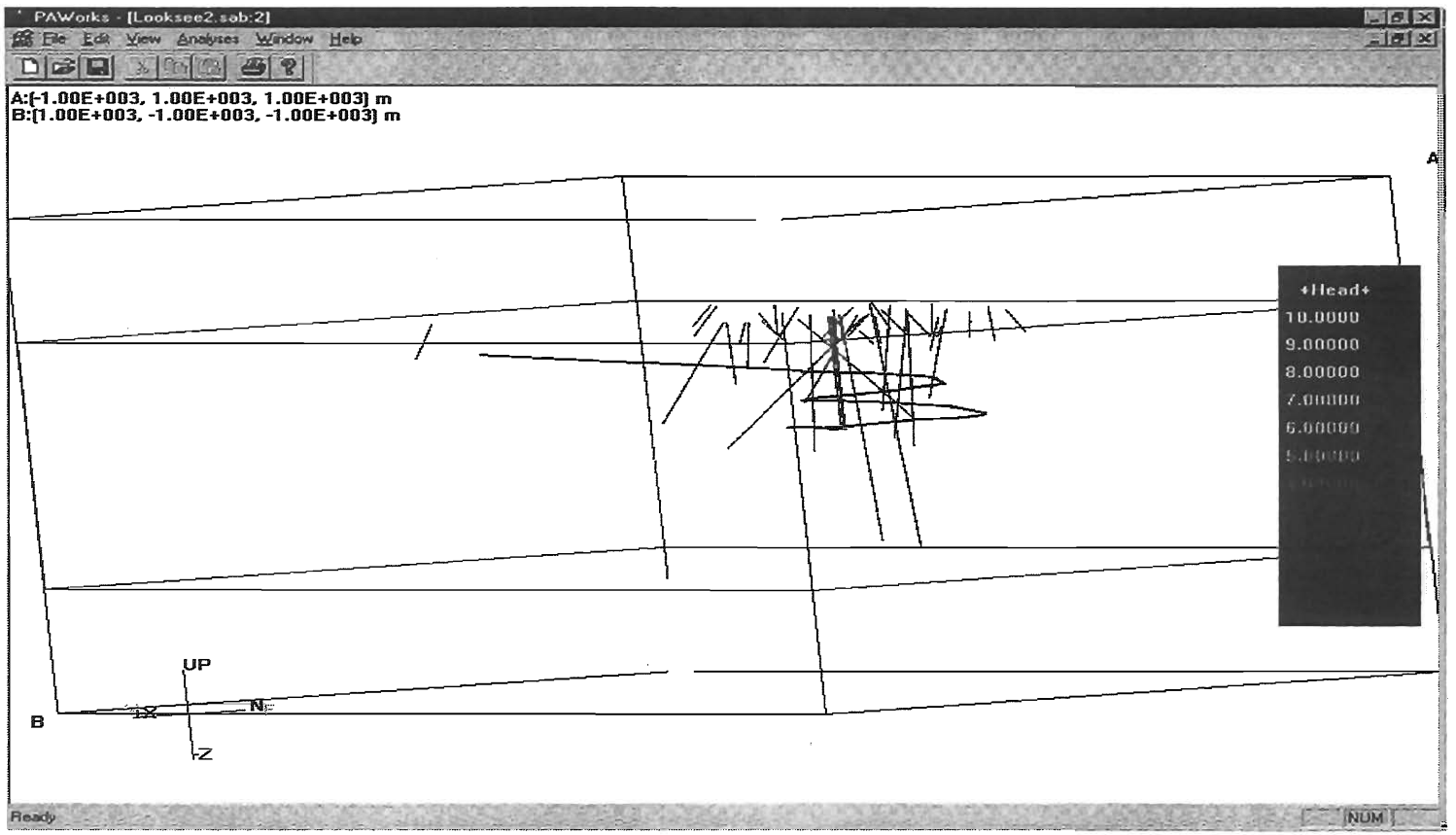

JNC サイクル機構

Stage 1a: Hydrogeological Modeling

- Implement "Task 3" for Calculation of Drawdawn to Specified Control Points
- Adjust Boundary Conditions and Material Properties based on Drawdown Response (not formal calibration/optimization at this point)
- Calculate Head Field for 68 Time Steps to 67 Months (Tunnel Weir Flux Boundary Condition)
- Calculate "Task 3" Drawdown Performance Measurement

Task 5 DFN Model Boundary Conditions

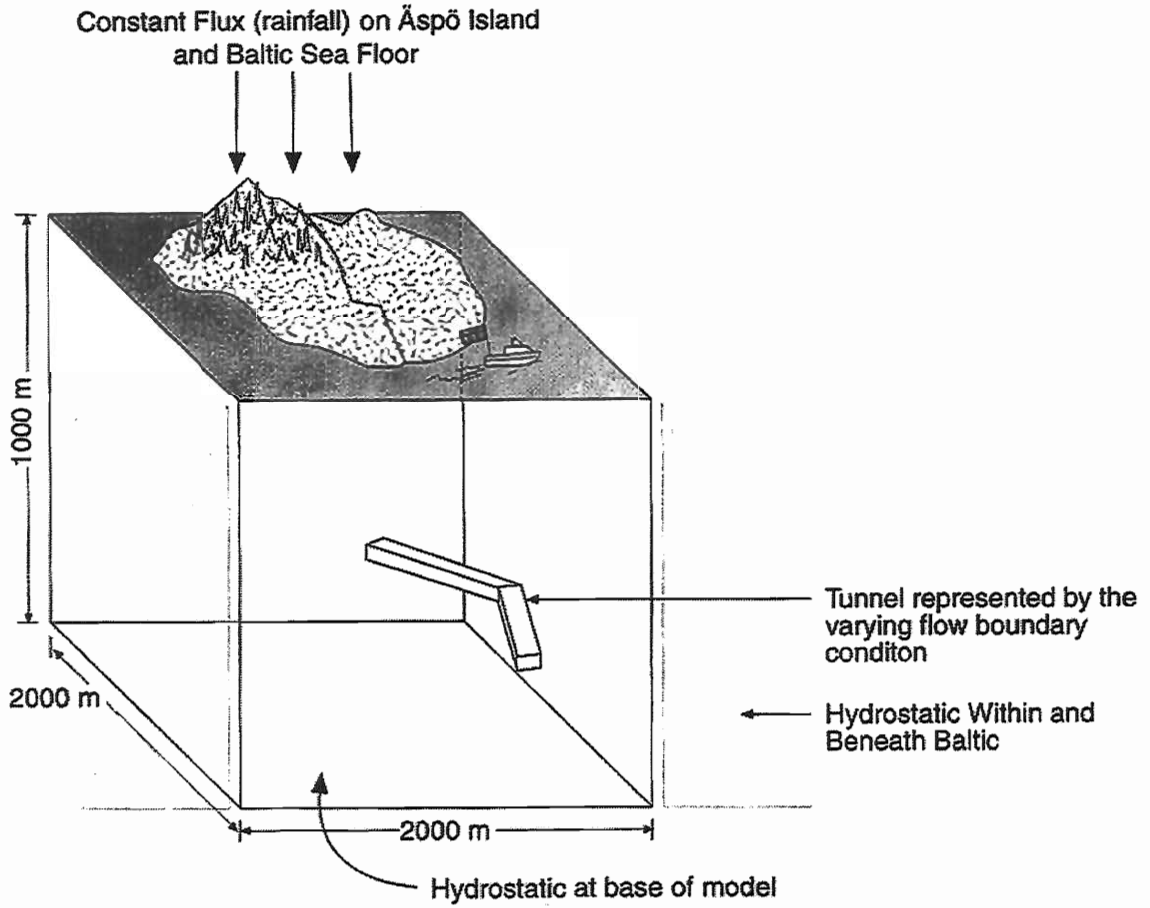

Schematic- Not to scale

JNC サイクル機構

Task 5 DFN Model Boundary Conditions

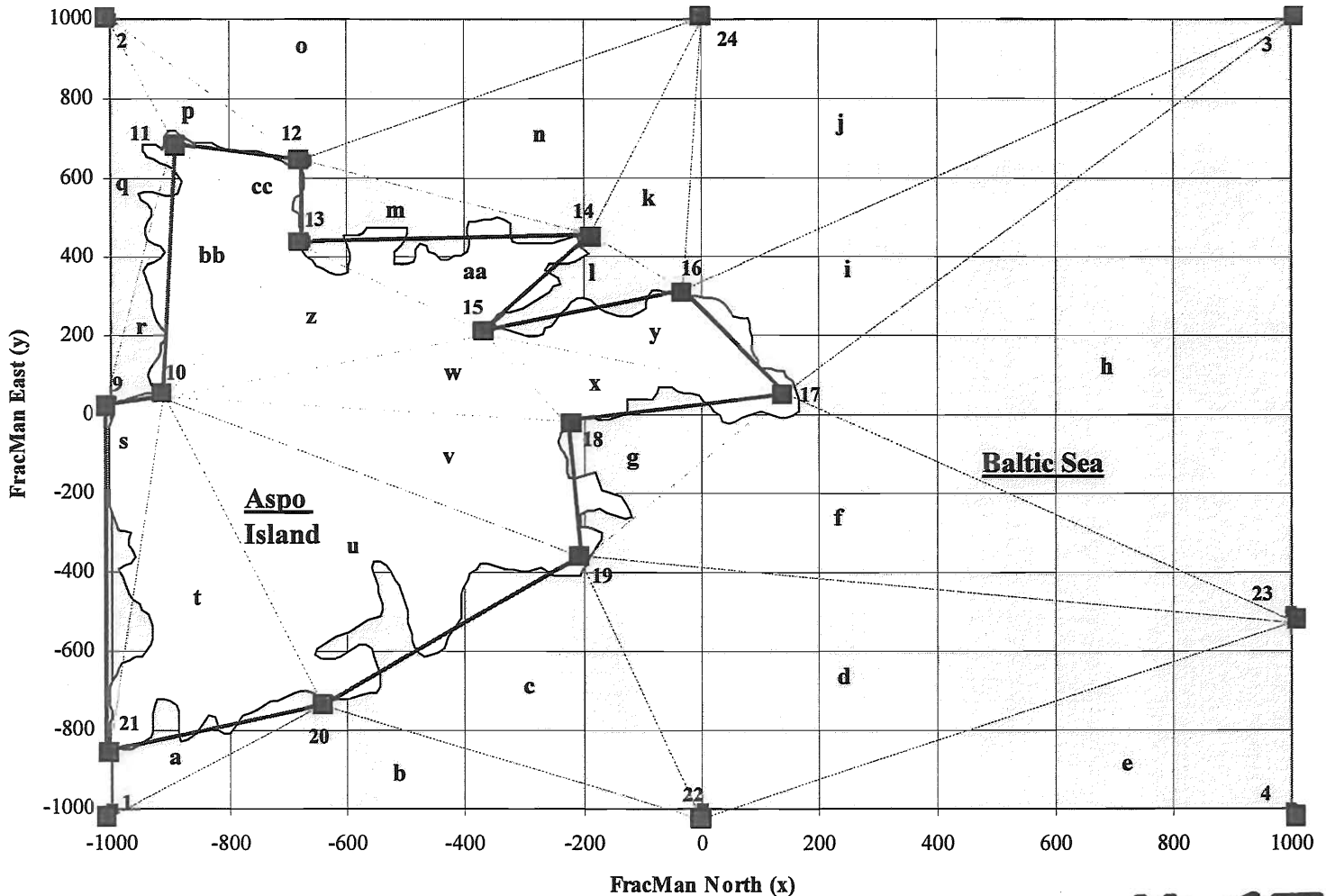

JNC サイクル機構

Weir Flux Time History Boundary Condition

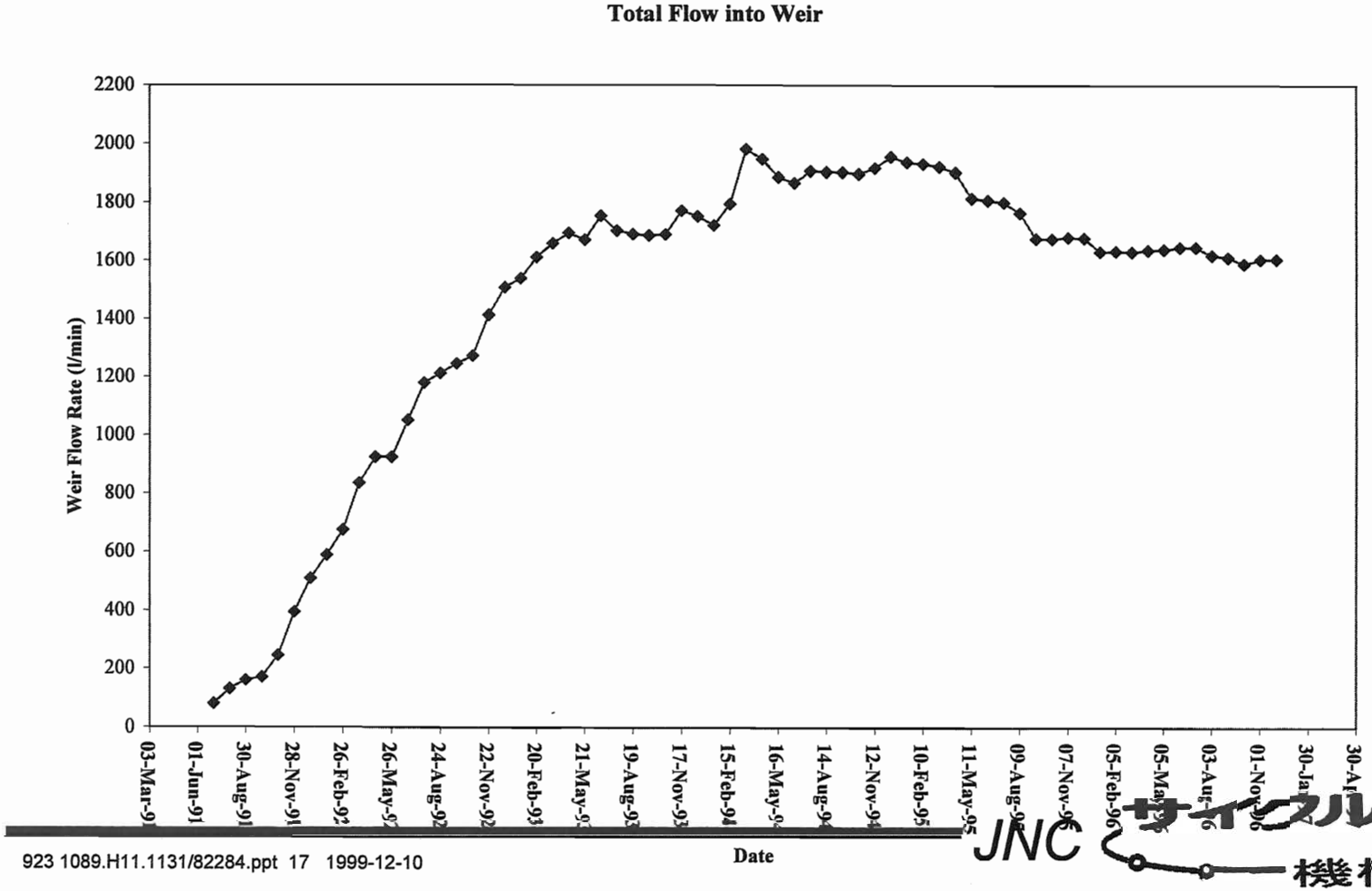

Hydrologic Model Results

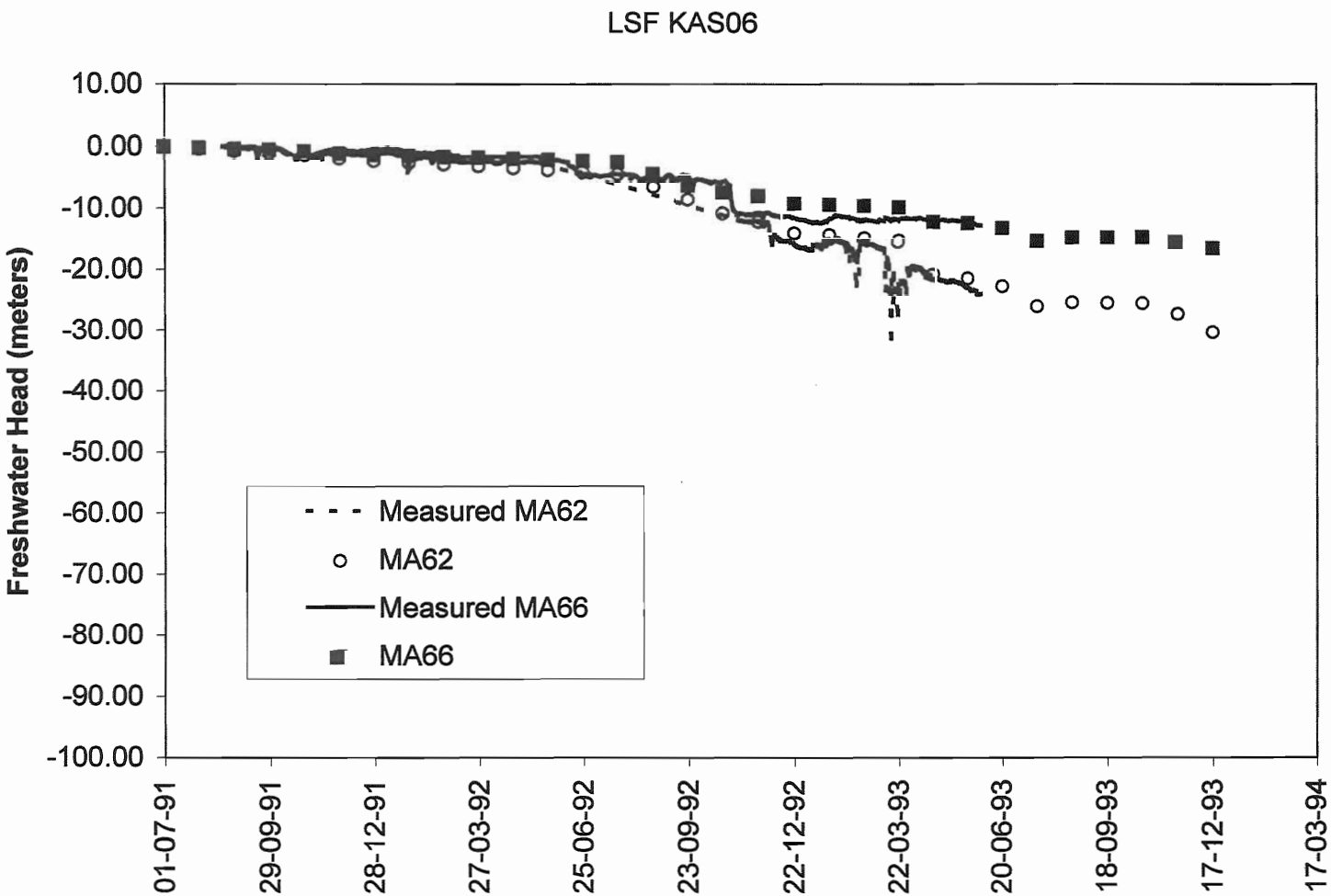

JNC サイクル機構

Hydrologic Model Results

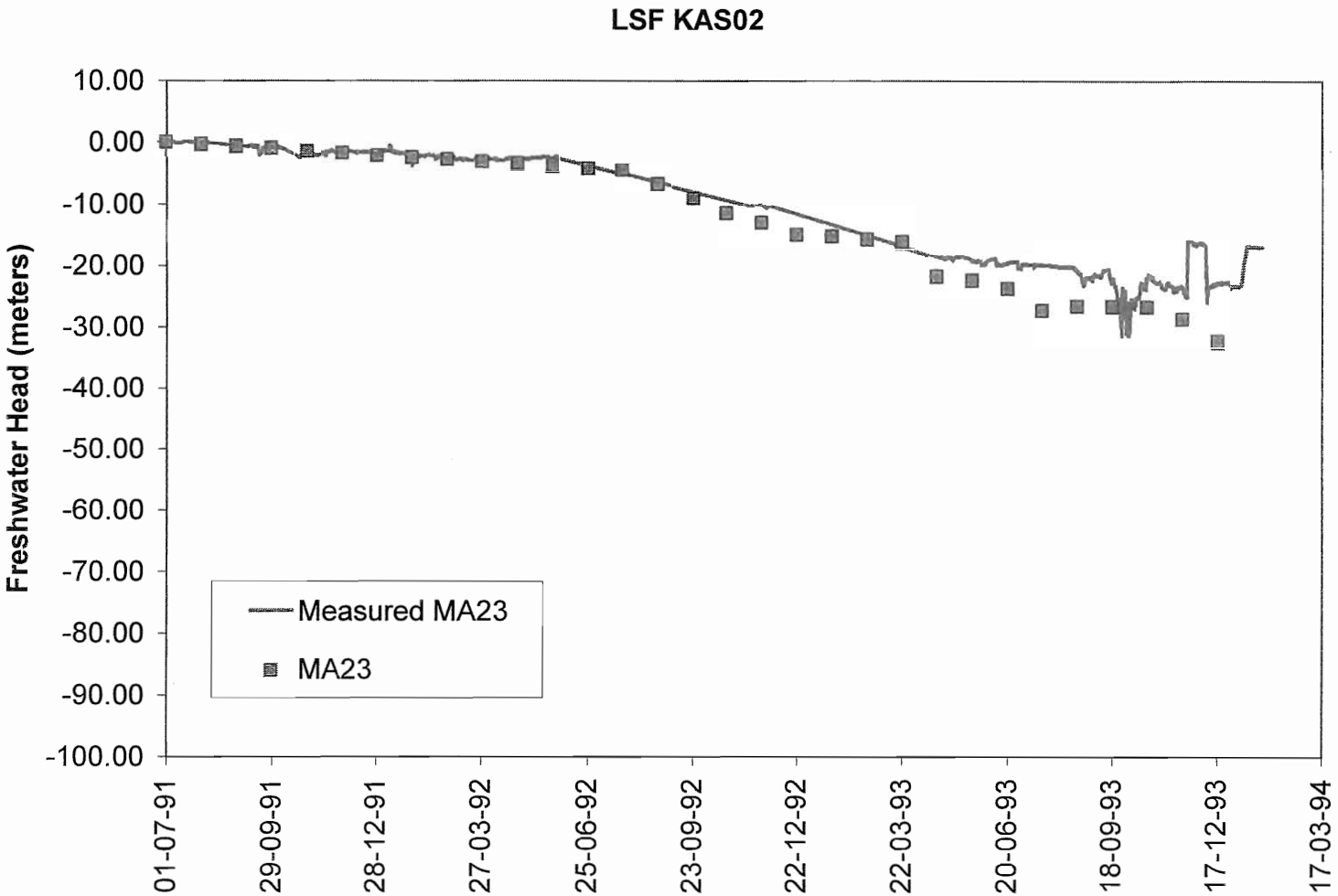

JNC サイクル機構

Hydrologic Model Results

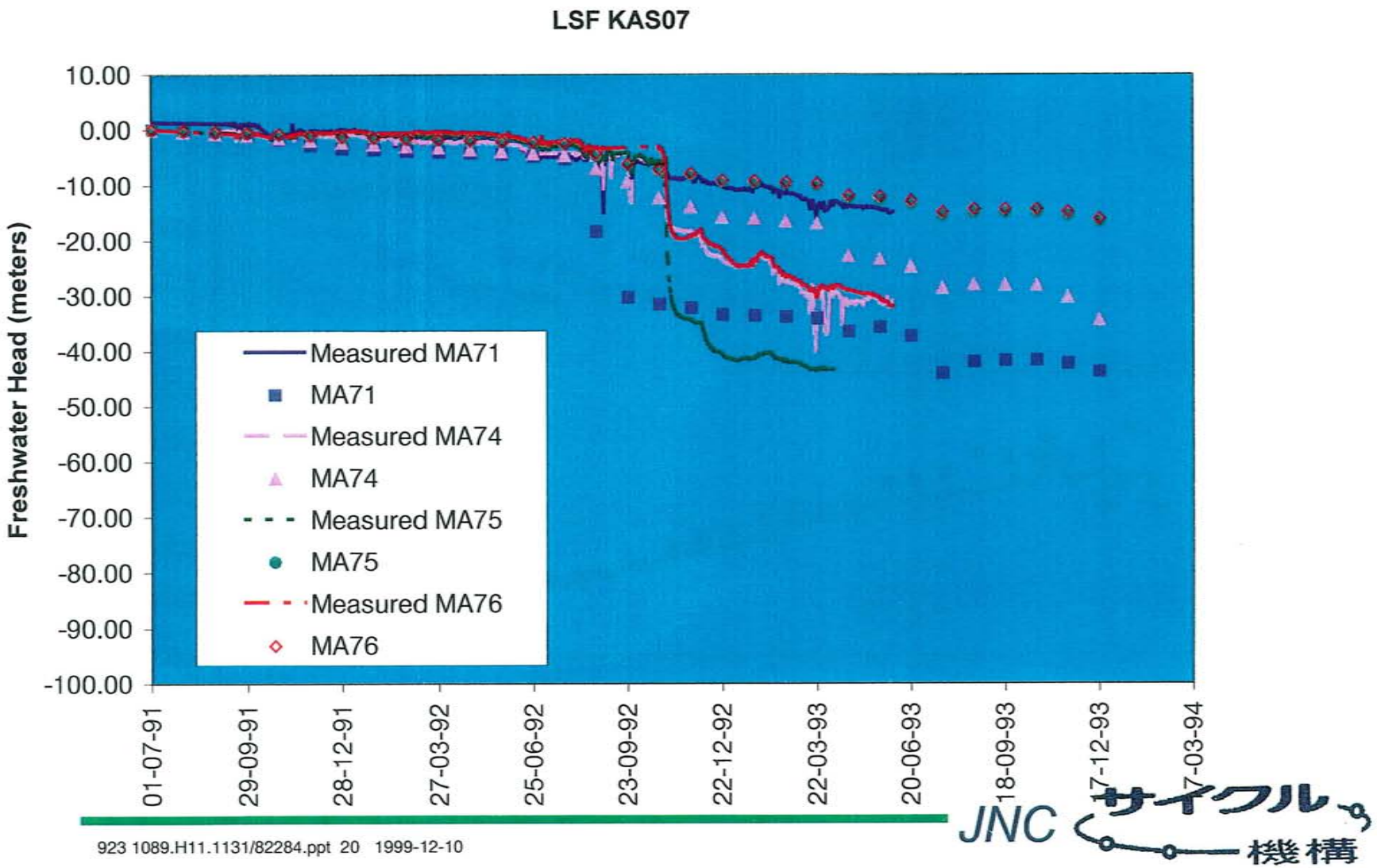

JNC サイクル機構

Stage 1b: Geochemical Modelling
Based on Hydrological Analysis Only

- Identify Transport Pathways to Tunnel Under Changing Head Field (PAWorks Pathways Analysis)
- Calculate Pathway Travel Times Including Rock Mass Storage Effects (500x pathway storage)
- PAWorks Identifies the Original Locations of Waters Arriving to Tunnel by Month
- Calculate End Member Mixing Based on Assumed Initial Conditions

Geochemical Initial Conditions

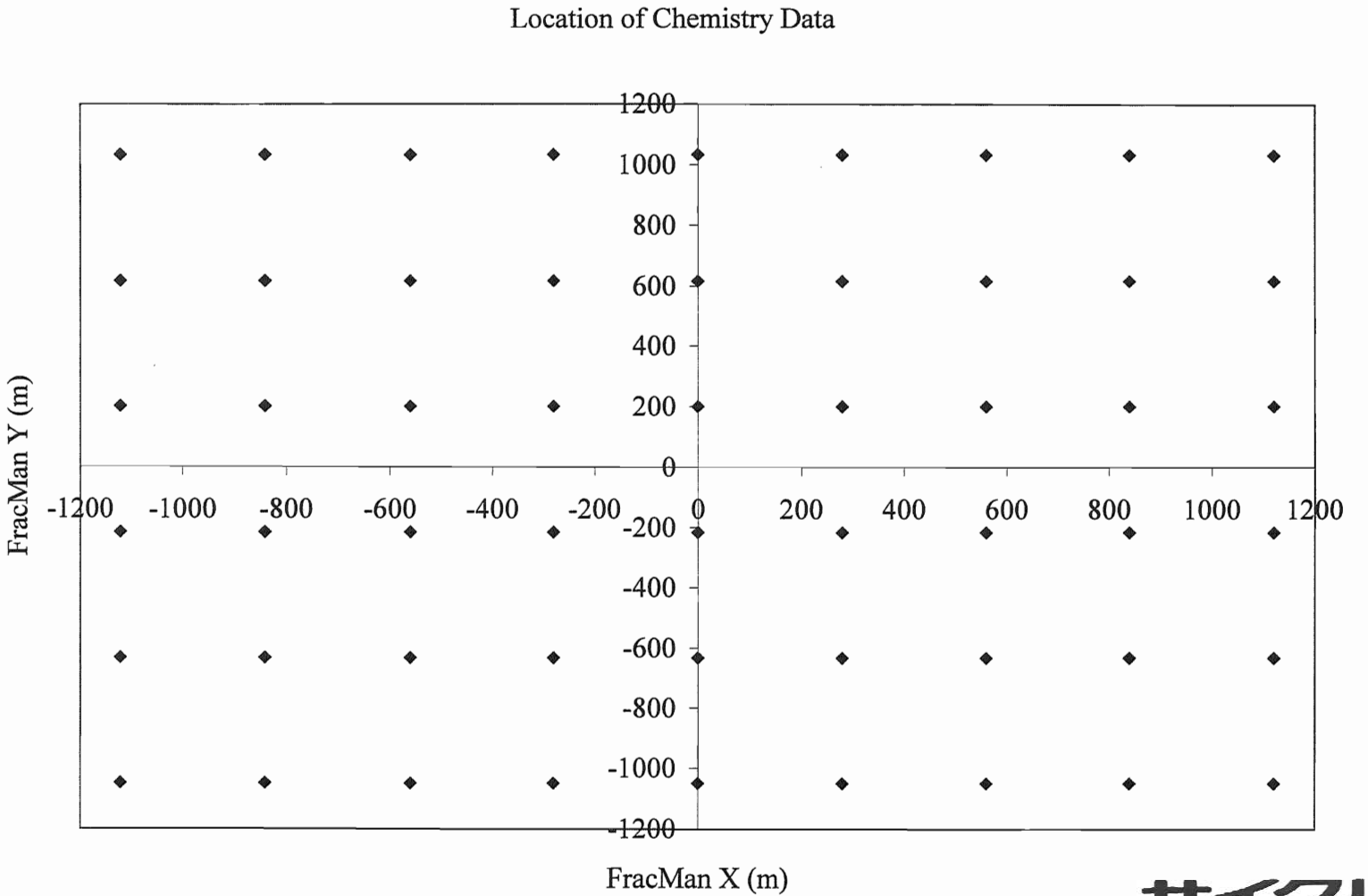

JNC サイクル機構

Pathways Analysis

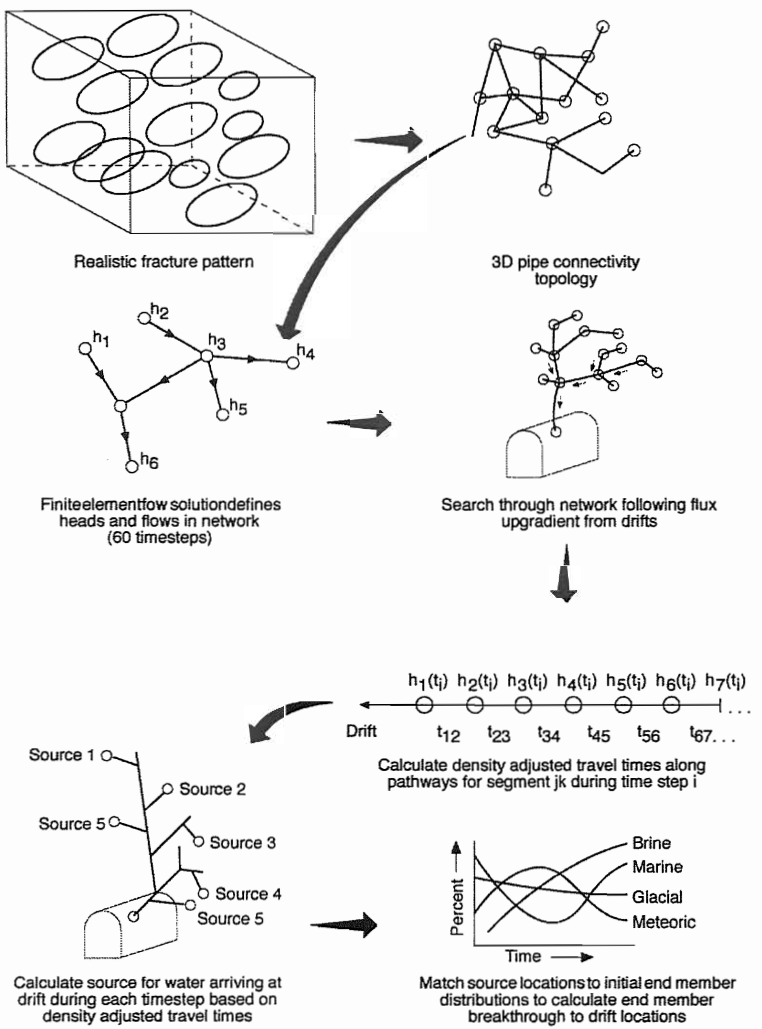

JNC サイクル機構

Stage 1 Geochemical Prediction
Based on Hydrogeology Only

- **Overprediction of Baltic Seawater**
- **Primary Water Supply from Baltic Boundaries**

End Member Geochemistry

Fracture NE2a-1

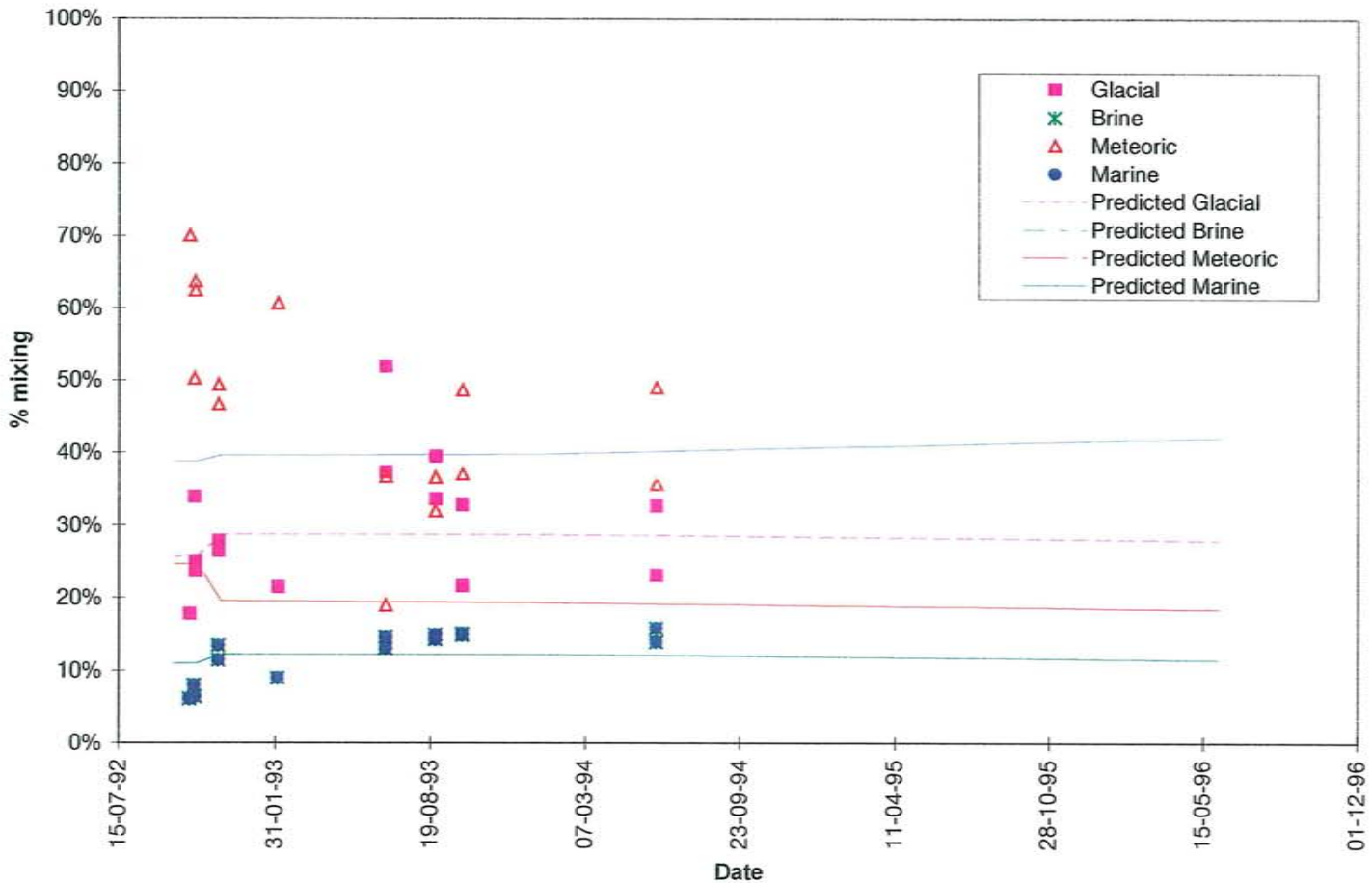

JNC サイクル機構

End Member Geochemistry

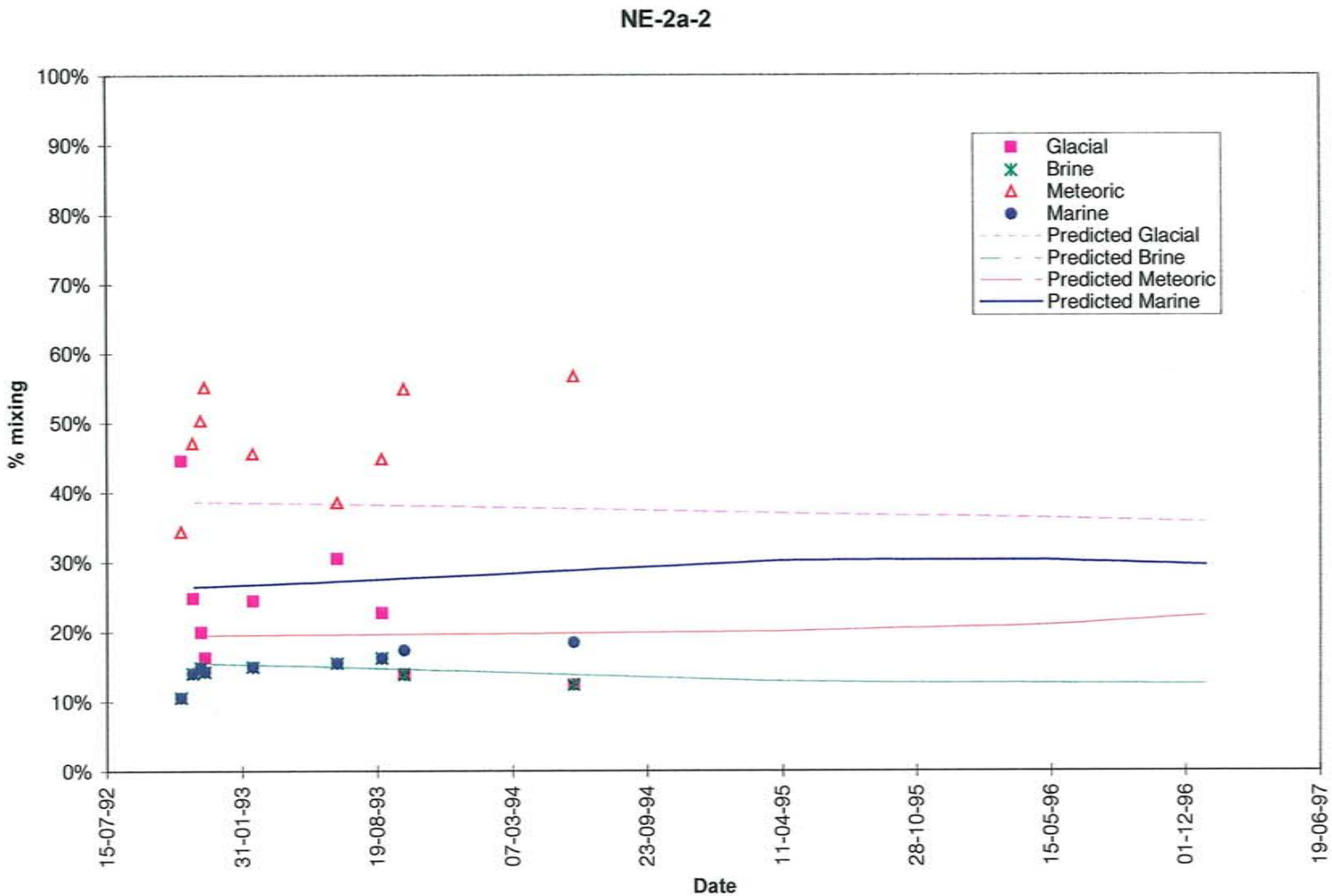

End Member Geochemistry

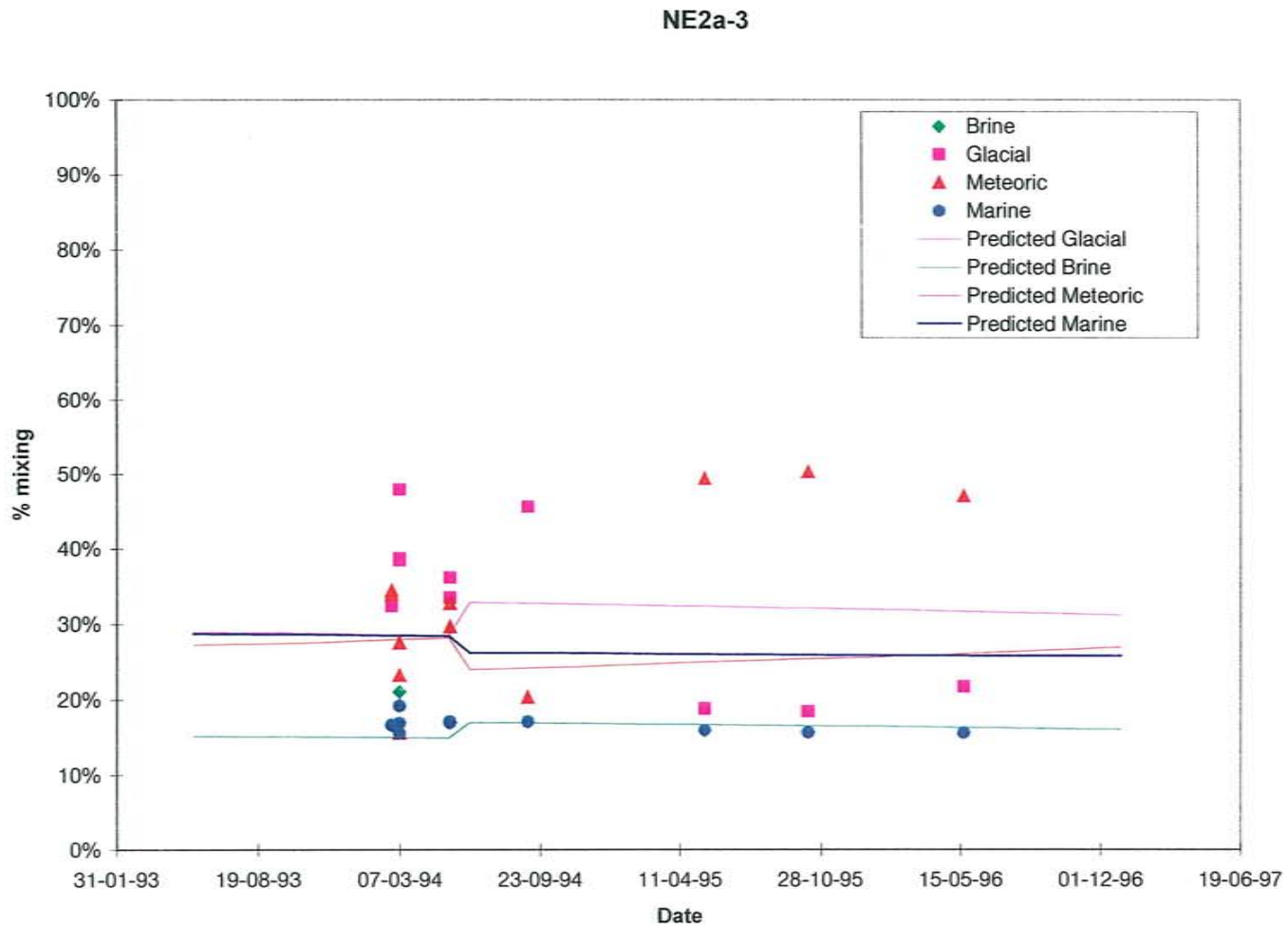

Stage 2: Geochemical Calibration

- **Assess the Value of Geochemical Data**
- **Re-calibrate 3D DFN Model Using Geochemical Data**
- **Predict Hydrological and Geochemical Measures**
- **Schedule: 5/99 - 8/99**

Conclusions

- Demonstrate Model Development based on Hydraulic Data Only
- FracMan/PAWorks Pathway Analysis
- Repeat "Task 3" Using Update SKB Structural Model, Validating PAWorks (pipe) vs MAFIC (plate)
- Large Scale (>1000 m) Transport Pathway Prediction under Transient Pressure Conditions
- Stage 2 Predictions Based on Geochemical Conditioning to Follow Over the Summer

The proportion of water from different sources in the water drained from the Äspö HRL.

L. Liedtke and N. Klennert (BMWi/BGR)

BMWi

SKB

BGR

ÄSPÖ HARD ROCK LABORATORY
The 12th meeting of the Task Force on Modelling of Groundwater Flow and Transport of Solutes

April 20-22, 1999
Gimo Herrgård, Sweden

The proportion of water from different sources in the water drained from the Äspö HRL

Federal Institute for Geosciences and Natural Resources, Hannover

BGR:

Dr. Lutz Liedtke
Dipl.-Geol. Nicole Klennert

DRAFT

ABSTRACT

This study deals with the influence of tunnel construction on the groundwater system at the Äspö site concerning changes in the flow pattern as well as the disturbance of the chemical balance. Hydraulic and transport models were constructed to simulate the processes dominating the hydraulic and chemical systems in the investigated area with and without the spiral tunnel.

Transport calculations were carried out for the NE-2 fracture zone based on a hydraulic model calculated for non-steady-state conditions. The conditions before, during and after tunnel construction were simulated. For a better understanding of the influence of tunnel excavation, a hydraulic model that includes additional fracture zones was developed.

Measured piezometric heads and element concentrations at different control points were compared with simulated values. Corresponding to the deviations, input parameters and boundary conditions were varied to achieve a better response of measured and simulated information.

The modelling confirmed the observed drawdown beneath the island of Äspö and the resulting change in the flow pattern. In contrast to initial conditions, the model indicates downward groundwater flow above the tunnel. This results in dilution of dissolved substance by meteoric water flowing into the aquifer. However, upward groundwater flow is observed in the fractures beneath the tunnel.

APPENDICES

LIST OF TABLES

LIST OF FIGURES

1 INTRODUCTION

1.1 BACKGROUND

The pre-investigations for the Äspö Hard Rock Laboratory (HRL) started in 1986 and a large number of investigation boreholes have been drilled on Äspö and adjacent areas since then. The borehole lengths vary from 22 m to 1700 m and they are usually equipped with borehole packers, which separate the borehole into sections representing different hydraulic units. On Äspö, 13 deep cored boreholes have instrumentation with a total of 70 packed-off sections and 22 of these are equipped for chemical sampling as well as for flow measurements.

The Äspö Hard Rock Laboratory has been under construction for four years, from October 1990 to October 1994. The maximum depth of the laboratory is 450 m and the tunnel has a total length of 3.6 km. The tunnel excavation affected groundwater flow and the chemical composition of the groundwater in the fractures, which is reflected in the borehole sections where the measurements are performed.

At the Äspö Hard Rock Laboratory the groundwater flow and chemical composition, and piezometric levels in borehole sections have been monitored at undisturbed conditions and then at successive intervals as the tunnel approaches the HRL target area deep under Äspö island. The change in the chemical composition indicates groundwater flow and transport of solutes.

Different types of groundwater with different origins were identified on the basis of the consistency and composition of element concentrations. Possible chemical reactions must be taken into consideration to explain the present consistency. An important process is to assess the extent of different reactions taking place as water-rock interactions or between different types of groundwater and whether they actually take place. An important aspect during modelling is the influence of different boundary conditions on the mixing of different types of water during tunnel construction due to changes in the flow pattern. The models are based on hydrological and hydrochemical data obtained before and during the tunnel construction.

In this report, hydraulic processes, as well as transport phenomena in specific conductor domains, were investigated. Borehole sections associated with specific major fracture zones have been studied and the change in the chemical composition has been related to simulations. By this the models have been improved using the information resulting from the response.

1.2 OBJECTIVES

The aim of Task #5 is to compare and ultimately integrate hydrochemistry and hydrogeology. The general method is to compare the outcome of the

hydrochemical models with the groundwater flow models. The Task #5 modelling will also be useful for a future assessment of the stability of the hydrodynamic and hydrochemical conditions at ÄSPÖ. This modelling approach could, if successful, then be used for any future repository site investigation and evaluation, especially in a crystalline bedrock environment. The objectives of this study arise from the general objectives stated for Task # 5.

The specific objectives are:

To assess the consistency of groundwater flow models and hydrochemical mixing-reaction models by integration and comparison of the hydraulic and chemical data obtained before, during and after tunnel construction.

To develop a procedure for integration of hydrological and hydrochemical information which could be used for an assessment of potential disposal sites.

1.3 PERFORMANCE

The following procedure has been used during the performance of this working draft:

1. evaluating groundwater flow and chemical composition in fracture zones in the Äspö HRL target area;
   - during undisturbed (natural) conditions before October 1990;
   - during the construction of the tunnel;

2. compare and interpret the undisturbed and influenced conditions with the prediction.

2 SITE DESCRIPTION

The Äspö Hard Rock Laboratory is located about 2 km north of the Oskarshamn Nuclear Power Station on the island of Äspö. The access tunnel extends from Simpevarp island, runs under the sea floor and reaches the spiral part of the HRL beneath the island. The total length of the tunnel is 3600 m and reaches a maximum depth of 450 m.

Extensive field investigations were carried out before and during the construction phase resulting in a detailed data set of geological, hydrogeological and hydrochemical measurements. Figure 2-1 shows the major fracture zones in the investigated area in relation to the HRL tunnel. The structures modelled in this study using a part of the collected data set are pointed out.

The geology of the Äspö site is characterised by two dominating rock types, the "Småland granite" and the "Äspö diorite". The Småland (Ävrö) granite can be described as a medium-grained porphyritic granite to quartz monzonite, whereas the Äspö diorite is a more basic and heavier variety. Furthermore, some intersections with fine-grained alkali granite, altered greenstone and dacitic metavolcanics occur as lenses and dikes. The fine-grained granite is a highly fractured, water-bearing rock.

The mean annual precipitation in the investigated area is about 675 mm. The groundwater recharge (precipitation minus evaporation) is assumed to be 150 – 200 mm/a. Groundwater flow mainly takes place in major tectonic fractures and discontinuities. Due to the excavation of the tunnel the initial natural groundwater system is disturbed and the hydraulic gradients increased as a consequence of the drawdown.

Furthermore, the distribution of the four types of groundwater at the Äspö site, which differ in chemical composition is influenced by the increased gradients. This leads to a mixing of water types depending on the excavation progress and the present groundwater level.

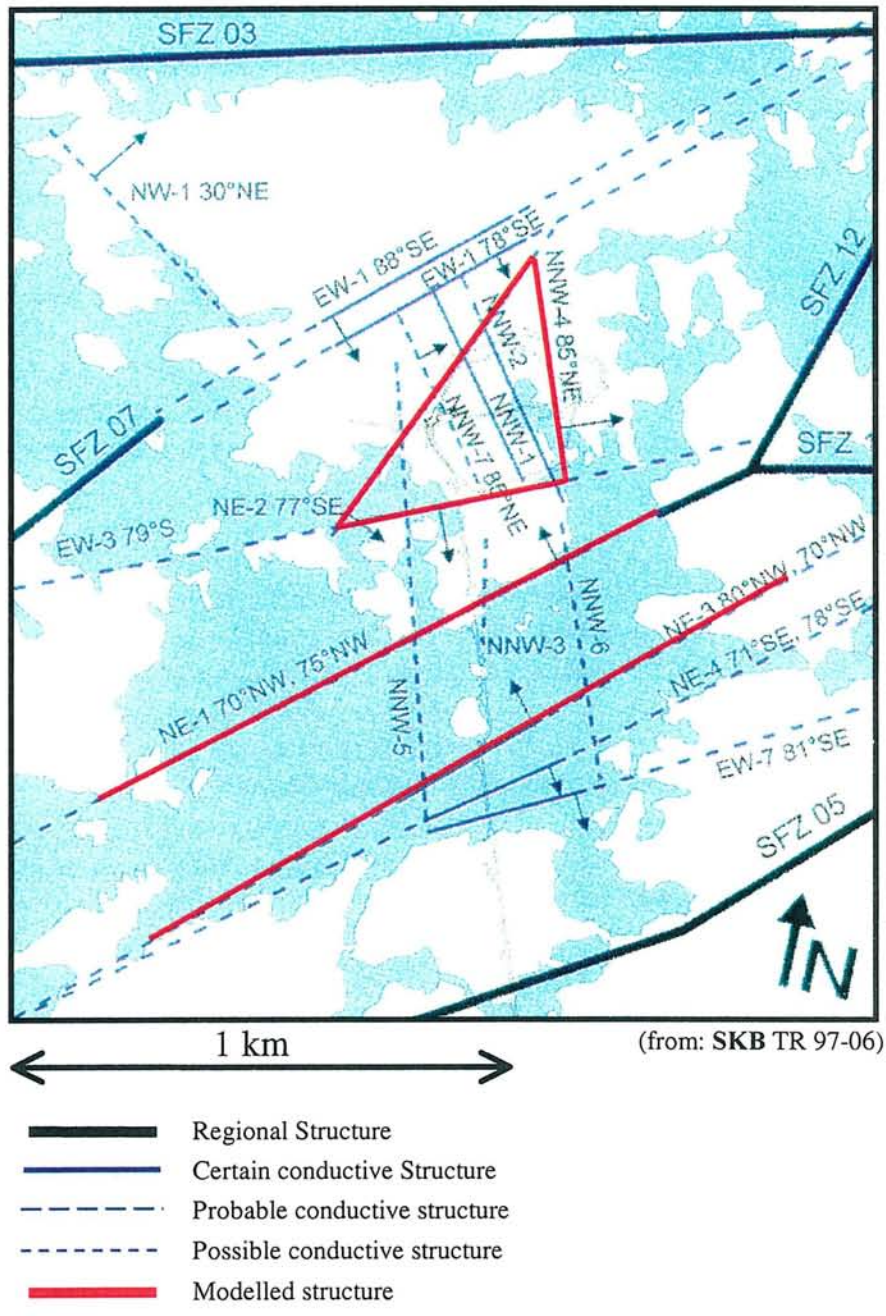

(from: **SKB** TR 97-06)

Fig. 2-1. *Hydraulic conductors at the Äspö site*

3 BASIC CONCEPTUAL ASSUMPTIONS

3.1 PURPOSE OF THE MODELLING

The aim of the modelling is to present the hydraulic conditions in the Äspö area at different stages during the excavation of the HRL and the change of the groundwater dynamics. The corresponding change in chemical composition of the groundwater, as well as the distribution of different water types, has to be analysed. Ultimately, the modelled distribution of the main water types has to be related to measurements. The scope of the groundwater model comprises natural flow and flow to the HRL tunnel. It comprises a time period for the calculation of about 1600 days (1990-10-01 to 1995-02-16) including the prediction of conditions during the excavation of the tunnel section from 2900 m to 3600 m.

The modelling helps understand the interrelationships between the hydrological and hydrochemical processes and to assess possible chemical reactions to explain the existing groundwater composition. Therefore, the information on different water compositions at the selected control points are to be used for the modelling with the chemical data applied as tracer information. The results for different stages have to be compared to assess the influence of the Äspö HRL on the groundwater system.

The hydrological and hydrochemical measurements should be duplicated in order to make predictions of future chemical compositions.

3.2 PROCESSES

The construction of the tunnel has influenced the groundwater flow and the distribution of the main groundwater types: meteoric, marine, glacial and brine. This mainly happens on the way through major fracture zones. Hence, a disturbance of the flow pattern can be observed continuously. The lowering of the water table beneath the island of Äspö is a distinct sign for the influence caused by leakage into the tunnel.

The change in the salinity caused by mixing of different water types causes a change in the distribution of element concentrations and also in the density balance. Chemical reactions may occur which didn't take place under the initial, undisturbed conditions.

3.3 BASIC CONCEPTUAL MODEL

The calculated flow and transport in the selected fracture zones demonstrate the change of the flow pattern during the tunnel construction and the mixing of different types of groundwater. Information about groundwater head and

chemical composition are available from several boreholes from the pre-construction phase (1986 – 1990) and the construction phase (1990 – 1995). As recharge and discharge at the Äspö site is controlled mainly by the major discontinuities it is assumed that groundwater flow can be simulated by considering the processes taking place in the fractures. Possible processes influencing the flux that depend on the rock matrix are neglected in this study.

The fracture zones are considered to be initially completely filled with groundwater. Furthermore, an exponential increase in salinity with depth is assumed, see Figure 5-2. This distribution has been influenced since the beginning of the tunnel excavation and has lead to a dilution of dissolved substances or increase in concentrations.

If the assumption of groundwater mixing leading to the present groundwater consistency is confirmed, chemical reactions can be disregarded. Whereas a combined model for transport and chemical reactions is necessary if chemical processes dominate the groundwater consistency.

4 MODEL CONCEPTS AND FORMULATION

4.1 INTRODUCTION

The DURST/Rockflow software used to simulate flow (SM2 flow model) and solute transport (TM2 transport model) in the modelling of Task #5 is based on the assumption of a double porosity continuum for the fractured rock. This software was developed jointly by BGR and the University of Hannover.

4.2 BASIC ASSUMPTIONS

In particular, the finite element method is used for the numerical simulation of flow and transport in subsurface system. Time derivatives were evaluated by using different schemes of various order of accuracy. The stability of numerical solutions depend on the reference point in time of difference formula. In general, it is distinguished between explicit and implicit schemes. A number of approximate schemes with respect to stability and consistency are examined. The stability criterion by von Neumann states that the eigenvalues of the amplification matrix of the discretized equation must be lower or equal to unity. Important stability criteria are stated in terms of the Courant number Cr, the grid Peclet number Pg, and the Neumann number Fo. For non-linear problems for which no exact discretization criterion exists, the consideration of physical conservativity and the grid convergence test may be appropriate proof of solution stability. Spatial and temporal discretization can introduce spurious dispersion effects where the amount of the (physical) hydrodynamic dispersion is enlarged by a numerical one. To estimate the dispersion actually effective in the numerical approach, truncation errors must be determined.

4.3 EQUATIONS FOR THE GOVERNING PROCESSES

The transient, saturated groundwater flow is described by

$$S_0 \frac{\partial h}{\partial t} + \nabla v = q\,, \qquad (4\text{-}1)$$

where	h	is	the piezometric head,
	t		the time,
	S_0		the specific storativity,
	v		the average fluid velocity vector, and
	q		the fluid sink/source.

The velocity is given by the three-dimensional, linear Darcy law:

$$v = -K \cdot \nabla h\,, \qquad (4\text{-}2.a)$$

where K is the hydraulic conductivity tensor, or by the general form of various non-linear laws for fracture or tube flow:

$$v = -K^* \cdot (\nabla h)^{\alpha}, \qquad (4\text{-}2.b)$$

where K^* is the hydraulic conductivity as a function of the piezometric head or its gradient and
α a coefficient for different non-linear flow laws.

If v is substituted into the mass balance equation (3-1), the equation may be rewritten as follows:

$$S_0 \frac{\partial h}{\partial t} + \nabla(K \cdot \nabla h) = q, \qquad (4\text{-}3)$$

which is the governing equation of the flow model.

The differential equation for solute transport is

$$\frac{\partial}{\partial t}(nc) + v \cdot \nabla c - \nabla(nD \cdot \nabla c) + n\lambda c + q(c - c^*) = 0, \qquad (4\text{-}4)$$

where c is the mass fraction of solute per fluid mass,
n the volumetric porosity,
D the diffusion/dispersion tensor,
λ the radioactive decay constant of the injected radioelement, and
c* the concentration of solute in the source fluid.

This formulation includes dispersion effects described by Fick's first law. The three-dimensional diffusion/dispersion tensor in a ξ,η,ζ-coordinate system oriented according to the flow path is written as

$$Ds = \begin{bmatrix} \alpha_L|v| + d_0 & 0 & 0 \\ 0 & \alpha_T|v| + d_0 & 0 \\ 0 & 0 & \alpha_T|v| + d_0 \end{bmatrix}, \qquad (4\text{-}5)$$

where α_L, α_T are the longitudinal and transverse coefficients of mechanical dispersion and
d_0 is the diffusion coefficient.

This is identical to the Scheidegger approach after transformation of D_s into a global x,y,z-coordinate system.

The term $n\lambda c$ describes the non-conservative behavior of the solute and can be interpreted as a decay term for radioactive solutes, with λ for the decay constant in the decay law.

The last term of equation (4-4) is the source term for fluid sources within the modelled domain.

4.4 NUMERICAL REALIZATION

Equations (4-3) and (4-4) are both solved numerically using a finite-element method. An implicit Crank-Nicolson finite-difference scheme is employed to approximate the time-dependent terms, while in space a Bubnow-Gelerkin technique is used. In this case, the test and shape functions are the same.

The modelling system consists of one-, two- and three-dimensional isoparametric elements with linear shape functions. The positions of nodes and elements in the domain to be modelled can be arbitrary, with the restriction that each quadrangular element must be in a plane; see Figure 4-1.

Time-dependent piezometric heads at the boundaries and time-dependent fluxes at the arbitrary nodes act as the boundary conditions of the flow model. The velocities are used as input data for the transport model. Time-dependent concentrations at the inflow boundary are to be given, as well as the initial concentration distribution.

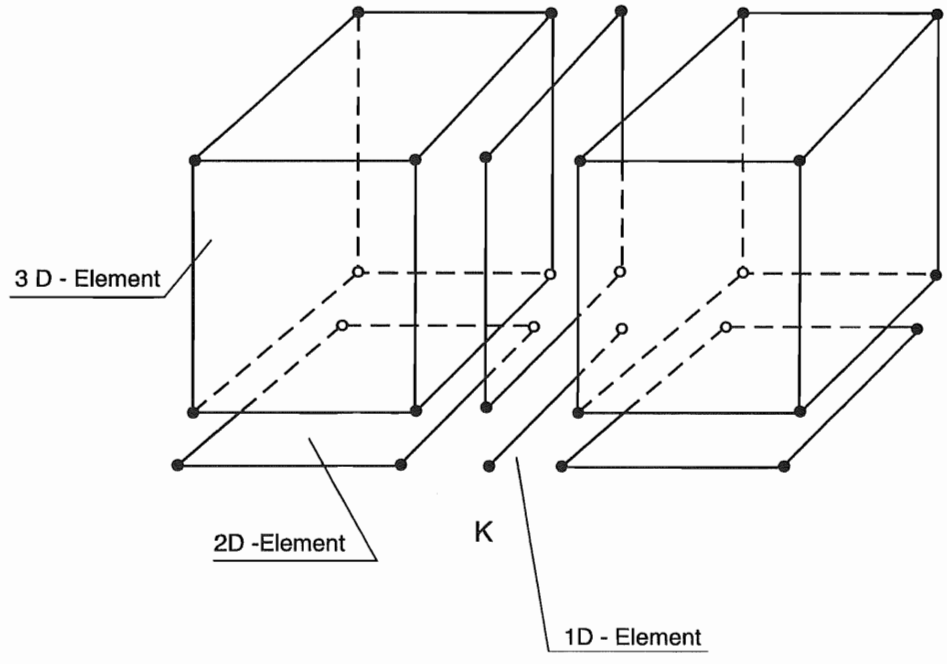

Figure 4-1. *Arbitrary combination of elements of different dimensions*

The time step increments for transport simulations can be controlled in different ways. They can be taken directly from the flow model or described independently. In the latter case, the velocities are linearly interpolated if the

time steps for the transport model are different from the flow field calculation.

Solute transport in the fracture is dominated by advection. A Taylor series expansion describing artificial diffusion was used to modify the numerical formulation in order to reduce the instability of the modelling.

5 SIMULATION MODEL

5.1 INTRODUCTION

The multi-fracture model used for simulating flow includes the aquifers NE-1, NE-2, NE-3, NNW-4 and EW-3. It comprises a time period for the calculation of about 1600 days (1990-10-01 to 1995-02-16). The positions of the working face of the tunnel at different times were included in the model in order to simulate the development of the groundwater system during excavation. They are shown in Appendix x. The model was tested using different specific storage coefficients. The numerical model is based on the linear Darcy law with time-dependent boundary conditions.

Transport calculations were carried out on the single-fracture model including fracture zone NE-2. They are based on a special hydraulic model with a refined FE mesh for NE-2. In addition, the lower boundary of the conductive structure was extended to a depth of 1300 m.

5.2 BASIC APPROACH AND DATA

The first modelling calculations started with two intersecting fracture zones, NE-1 and NNW-4. For a better demonstration of the influence of the tunnel excavation on the groundwater system in the investigated area, three additional fracture zones were added to the model: NE-2, NE-3, and EW-3; see Figure 5-1. The hydraulic contacts and complex connections between the major hydraulic fracture zones are included.

Hydraulic heads were calculated using the multi-fracture model. The extension of the modelled fractures includes the island of Äspö and the Baltic Sea, therefore, different boundary conditions influencing the dynamic system must be considered. In contrast to the previous modelling approaches, recharge on Äspö island is considered. The modelled fractures are intersected by a number of boreholes in which pressure and chemical content are measured for comparison with the calculated data.

Transport calculations were carried out for fracture zone NE-2. In contrast to the first transport calculations for NE-1 and NNW-4, instead of element concentrations, the distribution of the different types of water (brine, glacial, meteoric and Baltic Sea) were simulated.

5.3 GEOMETRIC FRAMEWORK

The model includes the location and orientation of the hydraulic fracture zones EW-3, NE-1, NE-2, NE-3 and NNW-4. They are assumed to be two-dimensional fracture zones, see Figure 5-1.

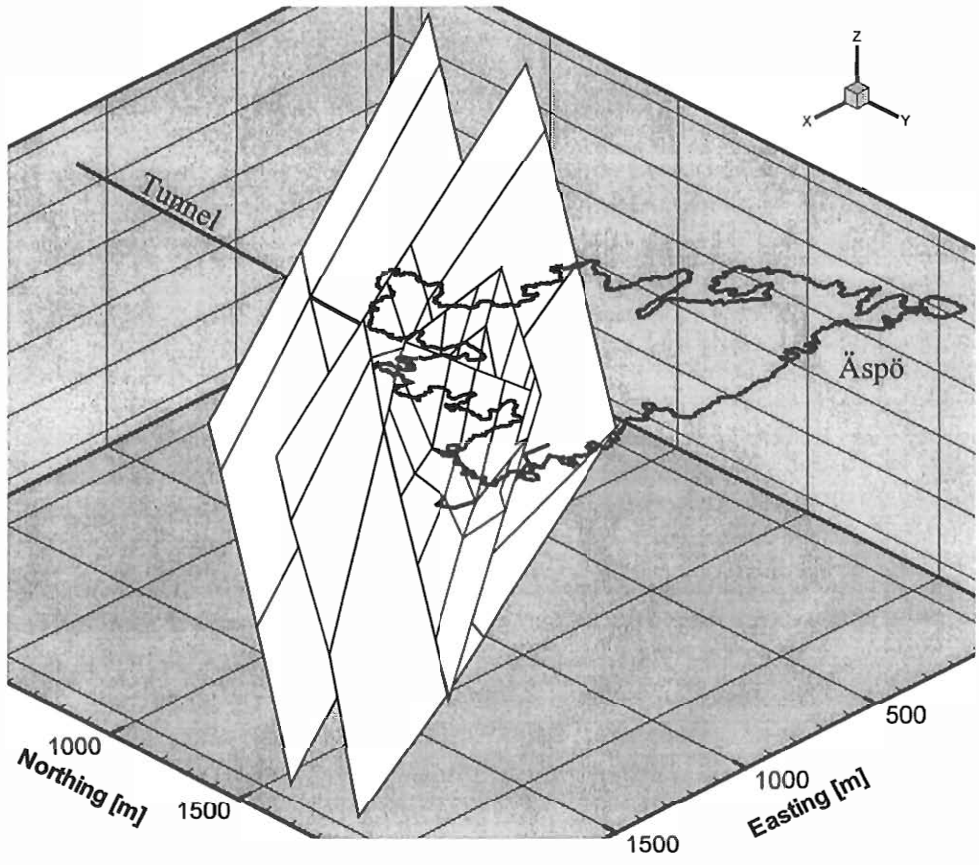

Figure 5-1. *Survey of the modelled structures*

Coordinates or dip and azimuth were included in the model for all modelled fractures, as proposed by Rhén et al. 1997. The planar quadrangular areas of the fracture zones were extended downwards from the surface with respect to assumed hydraulic connections. All fracture coordinates were recalculated.

The coordinates of the corner points and orientations of the fractures are given in Tables 5-1 and 5-2.

The geometry of zone NE-1 was approximated using the average values of x, y, and z for NE-1 with a dip of 70°NW and with a dip of 75°NW, as proposed by Rhén et al. 1997. NE-1 is presented with extensions down to a depth of 1000 m below m.s.l. and a length of 2000 m. NE-1 is assumed to be approximately 60 m wide and to consist of three branches.

Fracture NE-3 is assumed to have a dip between 70°NW and 80°NW. Fracture NE-3 is presented with extensions down to a depth of –1000 m below m.s.l. and a length of 2000 m (Rhén et al. 1998). It is assumed to be about 50 m wide and to dip steeply to the NNW.

Fracture zone EW-3 is found in the tunnel with a width of about 13 m. It consists of a 2–3 m wide crushed section in the centre resulting from a contact of fine-grained granite and Äspö diorite. The intersections of EW-3 with NE-2 and NNW-4 form the boundaries of the planes, see Figure 5-1. To the south, EW-3 stops at fracture NE-1.

Although fracture NNW-4 belongs to a swarm of minor fractures forming a NNW system (Figure 2-1) it is characterised by a clear indication in the tunnel and a significant water inflow that justifies closer consideration. Fracture zone NNW-4 ends to the sides at EW-3 and NE-2 and downwards at NE-1.

Fracture zone NE-2 has been investigated in this study more intense than the other ones. In the multi-fracture model NE-2 meets with EW-3 and NNW-4 and stops at NE-1 at a maximum depth of 1000 m. For transport calculations using the single-fracture model the lower boundary extends to -1300 m. In this way possible influences coming from deeper parts of the site can be taken into consideration.

When constructing the FE-mesh the calculated corner points, points of intersection with the tunnel and intersections with each other were considered. Table 5-3 shows the coordinates where the tunnel penetrates the fractures. All penetration points depending on the geometry of the tunnel and the fracture are considered even if they were not found explicitly in the tunnel.

Quadrilateral, two-dimensional finite elements are used for constructing the mesh of the fracture zones.

After a refining process the modelled domain of the multi-fracture model consists of 2124 two-dimensional elements. The edge lengths of the cells are between 30 and 120 metres. Refinement was carried out in areas of interest e.g. where the tunnel penetrates the fracture zones. Considering the corner points of the computational domain the modelled fractures (NE-1, NE-2, NE-3, NNW-4, EW-3) can be placed in a cube of 1000 x 2000 x 2250 metres.

The FE mesh of fracture zone NE-2 in the single-fracture model consists of 4225 nodes and 4096 elements. The edge lengths of the cells are between 5 and 35 metres.

The tunnel as well as the coast of Äspö are represented by one-dimensional elements.

Table 5-1. Orientation of the fracture planes

	EW-3	NE-1	NE-2	NE-3	NNW-4
Dip [°]	79	72.5	77	74.3	85
Azimuth [°]	282	117.3	324	120	7

Table 5-2. Fracture coordinates used in the multi-fracture modelling study (in Äspö coordinate system)

	Northings	Eastings	Z
EW-3	7048.6	1836.7	0
	7146	2307.2	0
	7097.4	2337.8	-276.6
	6964.9	1921.4	-509.8
NE-1	6306.83	1000	0
	7340.35	3000	0
	6661.8	1000	-1000
	7695.3	3000	-1000
NE-2	7048.6	1836.7	0
	7614.3	2247.7	0
	6964.9	1921.4	-509.8
	7383	2368	-1022.9
NE-3	5928	1000	0
	7081.5	3000	0
	6251.7	1000	-1000
	7405.1	3000	-1000
NNW-4	7146	2307.2	0
	7614.4	2247.7	0
	7097.4	2337.8	-276.6
	7378	2368	-1022.9

Table 5-3. Coordinates of the tunnel intersecting fracture zones (in Äspö coordinate system)

	Northing [m]	Easting [m]	Elevation [masl]	Tunnel Face Position [m]
EW-3	7063.51	2093.16	-196.02	1416.8
NE-1	6944.64	2109.17	-179.23	1296.9
NE-2	7233.29	2034.67	-221.57	1599.6
	7413.71	2174.53	-252.28	1860.1
	7204.39	2045.63	-333.54	2491.6
	7452.75	2239.96	-382.12	2875.3
	7284.64	2134.2	-439.56	3329.1
NE-3	6637.48	2149.79	-135.83	986.9
NNW-4	7350.67	2304.62	-273.05	2021.4
	7261.91	2316.98	-285.29	2121.6
	7423.58	2305.87	-392.22	2947.4
	7318.13	2321.52	-417.74	3138.3

5.4 MATERIAL PROPERTIES

The material properties chosen for the fracture zones EW-3, NE-1, NE-2, NE-3 and NNW-4 in the multi-fracture model are shown in Table 5-4.

Table 5-4. Material properties for the hydraulic conductor domains NE-1, NE-2, NE-3, NNW-4 and EW-3

	NE-1	NE-2	NE-3	NNW-4	EW-3
Width [m]	3	0.001 / 1	3	0.001 / 1	1
Permeability [m/s]	9.9 e-06	1.0 e-06	5.0 e-06	7.0 e-06	5.0 e-06

Spec. storage coeff. [1/m]	0.001	0.001	0.001	0.001	0.001

Transport calculations in NE-2 are based on a hydraulic model calculated for non-steady-state conditions with a specific storage coefficient of 0.001 1/m. The fracture width is set as 0.001 to 1 m with a permeability of $7 \cdot 10^{-5}$ m/s. In Table 5-5 the material properties effective porosity, dispersion length, diffusion and tortuosity assumed for the transport calculations are presented.

Table 5-5. Material properties for transport calculations in fracture NE-2

Eff. Porosity [%]	Dispersion longitud. [m]	Dispersion transversal [m]	Diffusion [m^2/s]	Tortuosity [-]
25	25	2.5	1.0e-08	1

5.5 SPATIAL ASSIGNMENT METHOD

The properties of the hydraulic conductors in the multi-fracture model are given as constant values for every fracture as presented in the previous chapter in Table 5-4. Apart from this the fracture width varies within the fractures NE-2 and NNW-4 where the tunnel intersection is located. The elements around this area are defined with a smaller fracture width in order to control the inflow to the tunnel.

The hydraulic conductors NE-1 and NE-3 show a representative behaviour in changing the flow pattern as a result of the tunnel construction. They also have a great influence on the groundwater system at Äspö resulting from an above-average high inflow to the tunnel and a high transmissivity. For this reason the properties for this two domains are similar and given as constant values with NE-1 showing the highest transmissivity.

The fracture zones NNW-4, EW-3, NE-2 are essentially influenced by NE-1. They represent the central zone of the investigated area and are penetrated by the tunnel several times so that the influence on the groundwater system can be observed clearly. Hence several model calculations were carried out with different coefficients of the specific storativity.

The transport calculations are based on the material properties given in Table 5-5 for fracture NE-2. These were assigned to the computational grid as constant values.

5.6 BOUNDARY AND INITIAL CONDITIONS

Flow calculations were carried out on the multi-fracture model. Transport was simulated using a single-fracture model based on a new flow model. The modelling period starts with the beginning of tunnel construction, representing natural initial conditions in October 1990. Time steps of 10 days were chosen.

The upper boundary conditions of the multi-fracture model are constant pressure heads of zero below the Baltic Sea and pressure heads that vary with time conditions below the island of Äspö. Recharge on Äspö island is assumed to be negligible for the periods before tunnel excavation and the beginning of the drawdown because no significant dilution with meteoric water takes place under natural, undisturbed conditions. The initial recharge rate is set to $7 \cdot 10^{-7}$ m^3/s; after the beginning of the drawdown it is set to $7 \cdot 10^{-5}$ m^3/s.

Prescribed heads corresponding to the geodetic height were assigned to the side and lower boundaries, except in fracture zones EW-3, NE-2 and NNW-4. No boundary conditions were assigned at their intersections and bottom boundaries in order to take the hydraulic connections with fracture NE-1 into consideration.

At the internal boundaries where the tunnel intersects the fractures, constant pressures are given as boundary conditions until the tunnel reaches the fracture. After the construction of the tunnel section a value for the inflow to the tunnel is calculated; see Table 7-1.

A flow model with boundary conditions similar to those of the multi-fracture model is used for the calculation of transport in fracture zone NE-2.

Initial conditions for transport calculations in fracture NE-2 were set according to the available chemical information from boreholes that are not necessarily in contact with NE-2. They were generalised before being used for the fracture. This was done in order to use as much information as possible from the measured distribution of the different types of groundwater. Appendix 3 shows the initial distribution of the reference waters with depth assumed for NE-2.

The assumed proportions of the different types of groundwater largely depend on depth or distance from the Äspö coast line, where Baltic Sea water and meteoric water are in direct contact. Apart from this, constant proportions are assumed. The curve fitted to salinity/depth data in fracture NE-2 measured in several borehole sections; see Figure 5-2. The exponential increase with depth is reflected in the initial distribution of the water types in Appendix 3.

Initial conditions for the transport calculations were assigned to each node in the FE mesh.

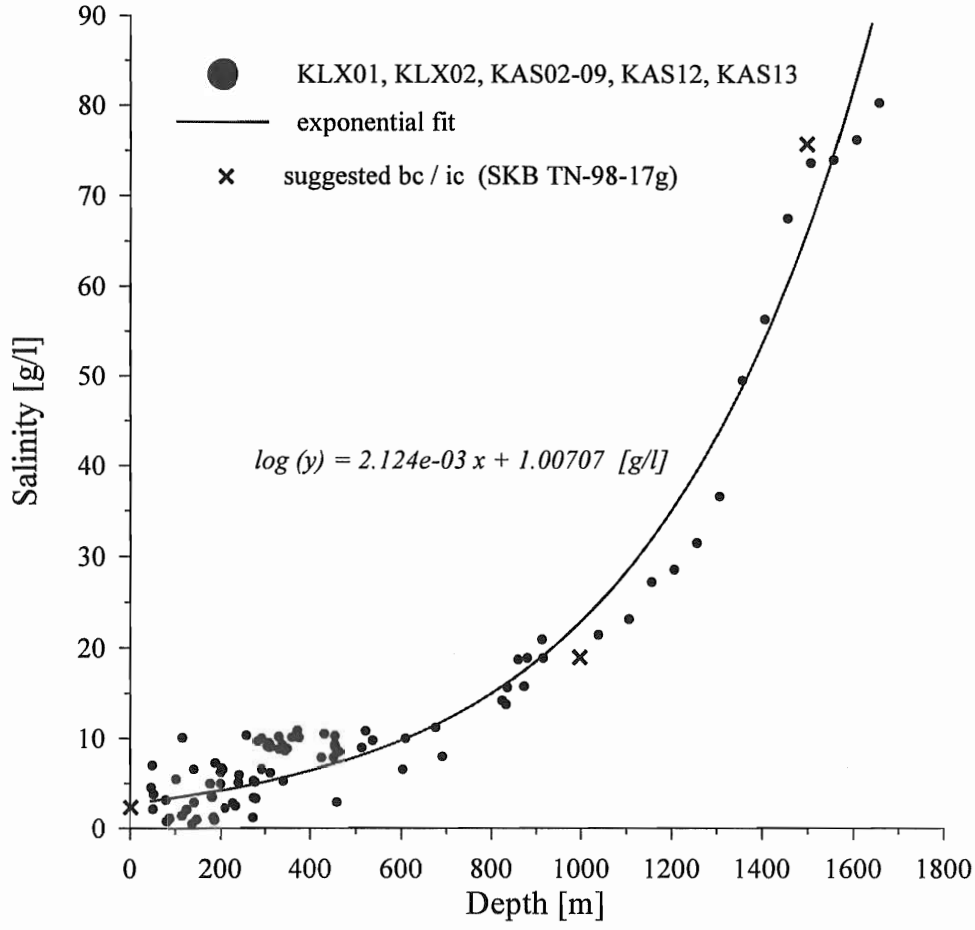

Figure 5-2. *Measured increase of salinity with depth and fitted exponential curve*

The chemical concentrations assigned to the model boundaries depend on the initial proportions of the different types of water. The upper boundary in the area of the Baltic Sea is assigned the concentrations of 100 % of Baltic Sea water, the island of Äspö those of 100 % meteoric water. The lower boundary is assigned constant values representing the initial conditions. Corresponding to the hydraulic model no concentrations were assigned to the vertical boundaries.

6 CALIBRATION

6.1 INTRODUCTION

The modelling work presented in this study is based on two modelling approaches. A multi-fracture model was used for simulation of flow in a larger area than the single-fracture model used for the transport simulations. This was done in order to understand the main processes leading to mixing.

Boundary conditions used in the multi-fracture hydraulic model were used for the single-fracture model to ensure the validity of the results for the transport simulations.

Fracture NE-2 was chosen for transport calculations because several boreholes supplied apparently sufficient chemical data. Some of these boreholes were defined as control points, nevertheless not all measurements are for a long time period.

6.2 CALIBRATION CRITERIA AND PROCESS

Non-steady-state flow and pressure were calculated for the hydraulic conditions – with and without the tunnel – using head measurements to calibrate permeabilities. Furthermore, the permeability of the fractures was chosen on the basis of the calculated inflow to the tunnel at the intersections of the tunnel with the fractures. The permeability values were varied to approximate a flux that corresponds to the measured values in December 1995 at the "weirs" downstream from the intersection; see Figure 6-1.

The storage coefficient was varied to fit the simulated drawdown values to the measured ones at selected control points; see Figure 6-2. The main criterion for calibrating the numerical model is acceptable agreement between measured and simulated heads or distributions.

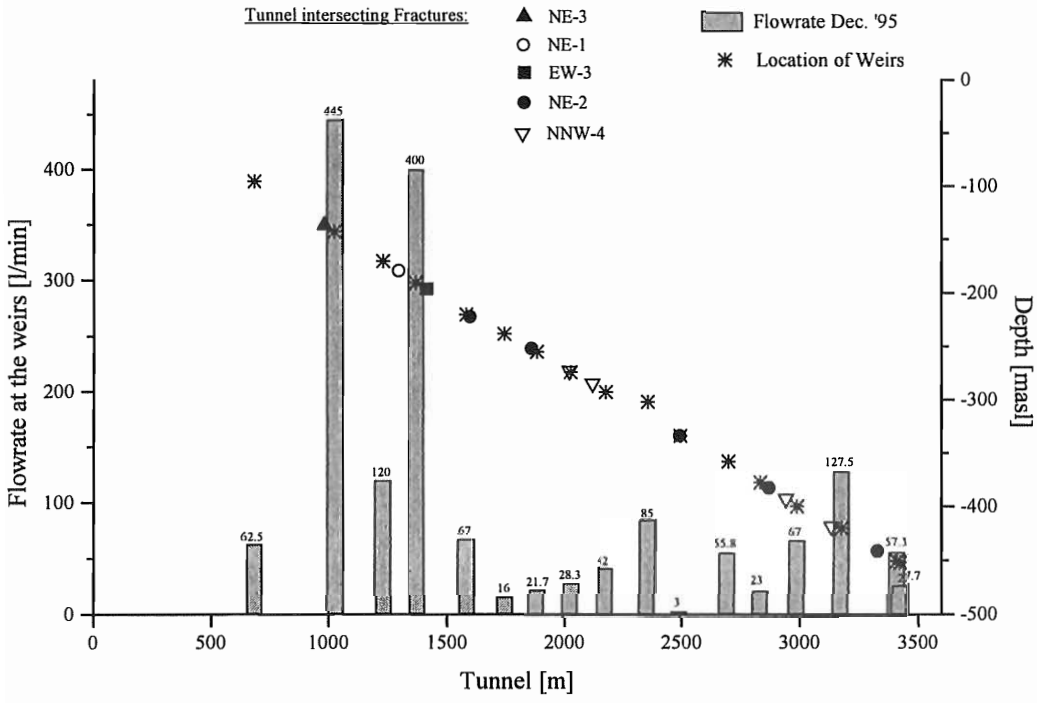

Figure 6-1. *Flow rates at the weirs in December 1995*

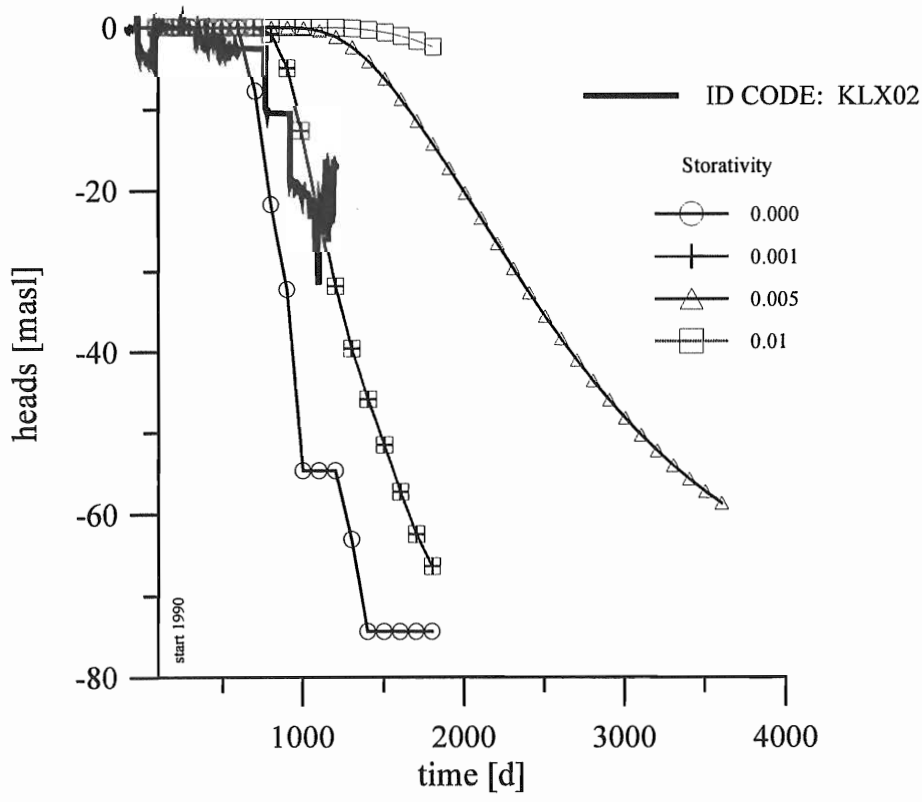

Figure 6-2. *Drawdown versus specific storativity and time in conductive structure NE-2*

For the numerical calculations, no priority was given to any of the required parameters. Parameter values, e.g., transmissivity, geometry of fractures, and storage capacity, were varied iteratively and the calculated drawdown and flow into the tunnel compared with the measured values. The drawdown in borehole KAS11 was compared to modelled results depending on the specific storage coefficient so that the order of magnitude of the storage capacity could be assessed.

The multi-fracture model contains additional fracture zones. They reveal a distinctive groundwater dynamic system that can be explained by the large influence of fracture NE-1. Non-steady-state flow was calculated to demonstrate the main connections and to construct a more detailed pressure model for further transport calculations.

Transport calculations for different types of groundwater in fracture NE-2 were carried out to calibrate transport properties using the measured proportions of water types at the control points. Proportions measured before construction of the tunnel was begun and only a few days after the tunnel crossed the fracture were taken as starting values. The locations of the control points in NE-2 are shown in Figure 6-3.

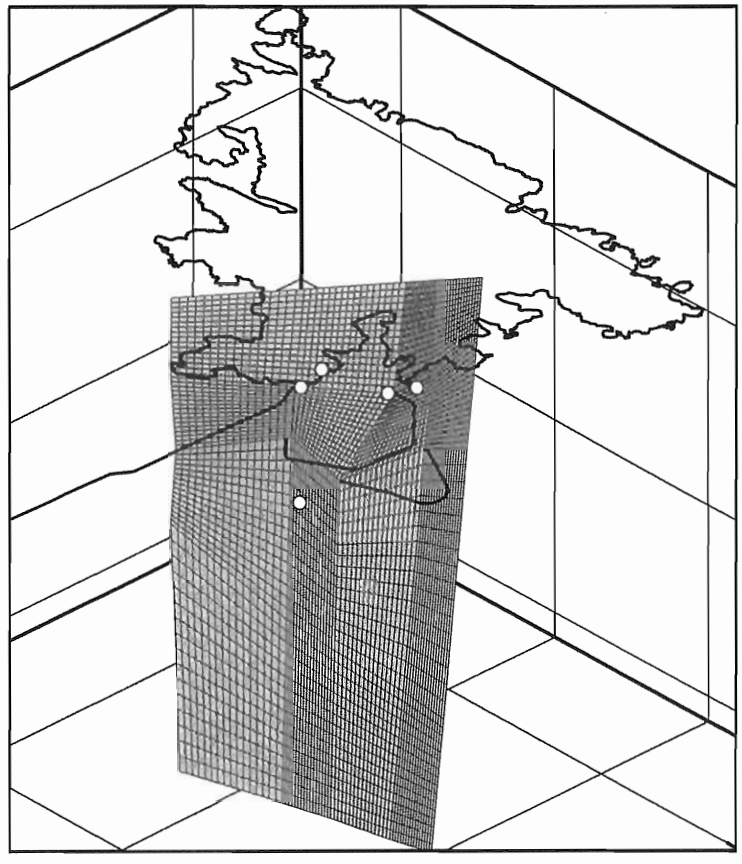

Figure 6-3. *Locations of control points (○) for comparison of the calculated and observed chemical data in fracture NE-2*

7 MAIN RESULTS

7.1 INTRODUCTION

The numerical model leads to results concerning the groundwater pressure at every node and the inflow to the tunnel at the intersection points with the fractures. Different stages during the tunnel construction have been considered so that main flow directions can be derived from the contours or from flow paths, see section 7.3.

The transport calculations give the distribution of the four types of groundwater at different control points supported by borehole data. In this way measured values can be compared with the simulated results for hydraulic heads and the chemical composition of the mixed groundwater. Any reactions between the substances that may occur are not considered. Mass balances were checked for specific stages of the excavation drift.

7.2 NATURAL CONDITIONS

As can be seen in Appendix 1 and 2 the initial conditions before the tunnel excavation are characterised by a constantly distributed dynamic system valid for completely water filled fractures. The piezometric heads amount to zero except the recharge areas of the islands where positive values are present. Due to this the very small hydraulic gradients have a very little influence on the distribution of groundwater.

7.3 COMPLETED TUNNEL

7.3.1 FLOW MODEL

The numerical model shows that since the beginning of the HRL excavation a distinctive change in the groundwater system can be observed. Corresponding to the leakage rate into the tunnel a drawdown in the modelled area extends that has also been measured in several boreholes. The observed drawdown leads to an increased change in flow pattern and mixing of different water types.

The development of the flow field in the multi-fracture model and the piezometric heads in fracture NE-2 present Appendices 1 and 2. In Figure 7-1 the measured and simulated piezometric heads in borehole KAS11 penetrating fracture NE-1 are presented.

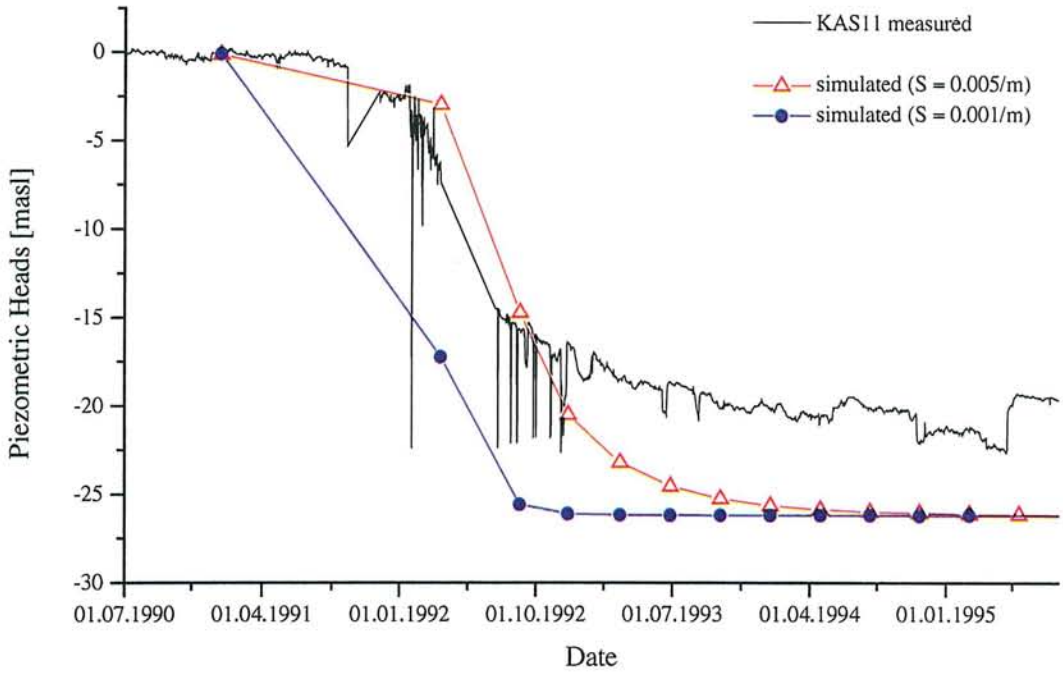

Figure 7-1. *Comparison of simulated and measured heads in the multi-fracture model*

Table 7-1 shows the calculated flow rates using a specific storativiy coefficient of 0.001/m.

Table 7-1. Calculated flow rates at the tunnel intersection points in the multi-fracture model

Q_{out} at the tunnel [l/min]	NE-1	NE-2	NE-3	NNW-4	EW-3
Q_{1st}	46.9	<0.1	27.6	13	10
Q_{2nd}	-	<0.1	-	9	-
Q_{3rd}	-	<0.1	-	20	-
Q_{4th}	-	2	-	20	-
Q_{5th}	-	<0.1	-	-	-

The single-fracture model used for transport calculations is based on it's own flow model which had to be developed corresponding to the assumed conditions in the multi-fracture model. Figure 7-2 shows measured and calculated piezometric heads in boreholes KAS06 and KAS08.

Table 7-2 shows the flow rates for the tunnel locations in fracture NE-2 which have been calculated using a specific storativiy coefficient of 0.001/m.

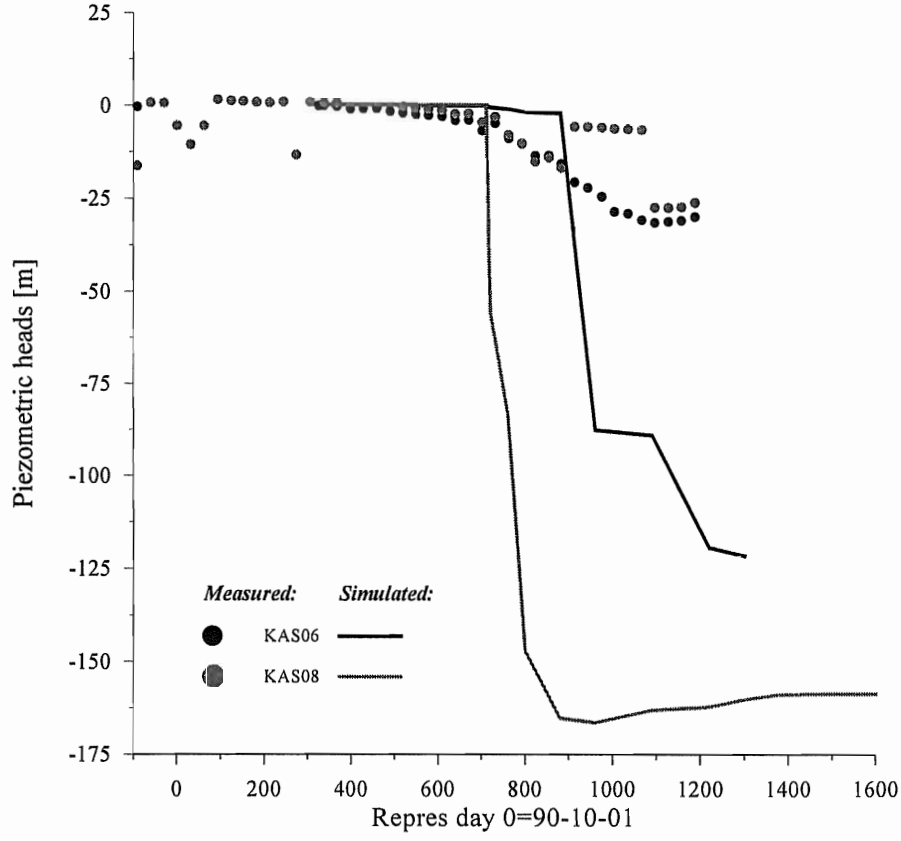

Figure 7-2. *Comparison of simulated and measured heads at control points in the single-fracture model*

Table 7-2. Calculated flow rates at the tunnel intersection points in the single-fracture model after tunnel completion

	Q_1	Q_2	Q_3	Q_4	Q_5
Q_{out} at the tunnel [l/min]	36	46	5	78	84
Tunnel location [m]	1600	1860	2492	2875	3329

The calculated flow rates in the multi-fracture and single-fracture model deviate from the measured inflow at the weirs in the tunnel which shall be used for calibrating the model. The multi-fracture models shows flow rates that are too low, whereas the results of the single-fracture simulation are too high. However, the comparison of the drawdowns in both the multi-fracture and single-fracture model with measured piezometric heads in suitable packed off borehole sections shows a lowering of the water table that is higher than the measured one.

7.3.2 TRANSPORT MODEL

Appendix 4 shows the results of the transport calculations in fracture NE-2 and the comparison of measured and simulated values. The different types of groundwater (brine, glacial, meteoric and Baltic Sea water) were considered separately. The proportions in fracture NE-2 are shown for different stages of tunnel construction, including prediction of conditions during excavation of the tunnel between 2900 m to 3600 m.

The initial distribution of the different types of groundwater is disturbed as a result of the tunnel excavation and the change of the flow pattern. The first crossing of the fracture zone by the spiral tunnel causes a significant change in the initial balance. As a result of the disturbance of the flow field shown in Appendix 1, an increase mainly of meteoric and Baltic Sea water can be observed above the tunnel, which reflects the orientation of the flow lines. They extend downwards to the points in the tunnel where water was extracted. Simultaneously an upconing of the contour lines below the intersections of the tunnel with the fractures is apparent. This leads to a increase in the proportions of glacial and brine water above the tunnel. However, the proportion of glacial water in general decreases with time. It can be concluded that the intersection of the tunnel with the fracture causes an increase in the hydraulic gradients in the vicinity of the tunnel. The disturbed area around the extraction points extends with time, with increased inflow to the tunnel.

In order to check the modelled water distribution in fracture NE-2, the mass balance was checked at different stages. Figure 7-3 shows the mass balance for the position of the working face of the tunnel at 2500 m; at this point the fracture had been crossed for the third time. Apart from an inconsistency in the input data at the top boundary, the deviation generally amounts to ± 5 %.

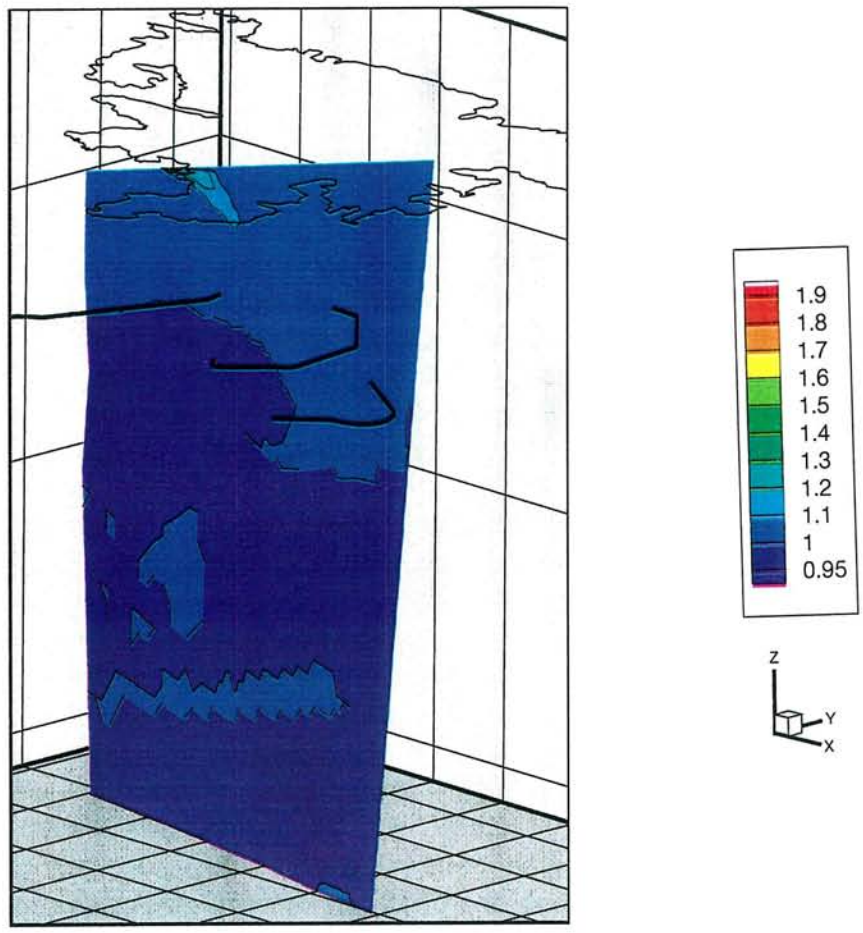

$$\text{best value} = \frac{V_{xyz}\left(c_M + c_S + c_G + c_B\right)_{ii}}{\sum V_{xyz} c_{xyz''}} = 1$$

Figure 7-3. *Mass balance in the single-fracture model (on May 1993 after 960 days)*

7.3.3 BACK TRACKING IN FRACTURE NE-2

In order to estimate the transport velocity of mass less particles in fracture NE-2, the velocity field has to be calculated from the point of time May 31, 1995, taking the construction of the tunnel into consideration. The hydraulic calculations were based on the boundary conditions described in section 5.6. It is the same flow field which has been used at the end of transport calculations for the four different water streams. The heads [m] and velocity vectors are comprised in Figure 7-4 together with the driving points of the spiral tunnels. As the tunnel has been driven from top to bottom, the highest point is also the first point of break through and the lowest point is the last point. The excavation drift influences the heads of pressure and thereby the velocity field as shown in Figure 7-4. The stream lines have been calculated for some areas of the fracture and presented. On the one hand, they are situated from the surface i.e., the island of Äspö or Baltic Sea and on the

other hand from the deep underground to the points of break through of the tunnel. If a particle would move in the fracture water in the direction of the stream lines it would take 1/10 of a year from point to point.

The calculation of this model is showing a residence time of the particle between the ground surface and the tunnel in the area of the NE-2 fracture of less than one year. The duration of the transport of the particles from lower border in 1300 m m.s.l. to the tunnel in -439 m depth takes more than three years.

These calculations are neither taking into account the hydraulic roughness of the fracture, nor the density differences of the fluids, nor the temperature changes in the Earth's mantle. Therefore, a longer travel time of the particles or of the water bearing materials can be foreseen.

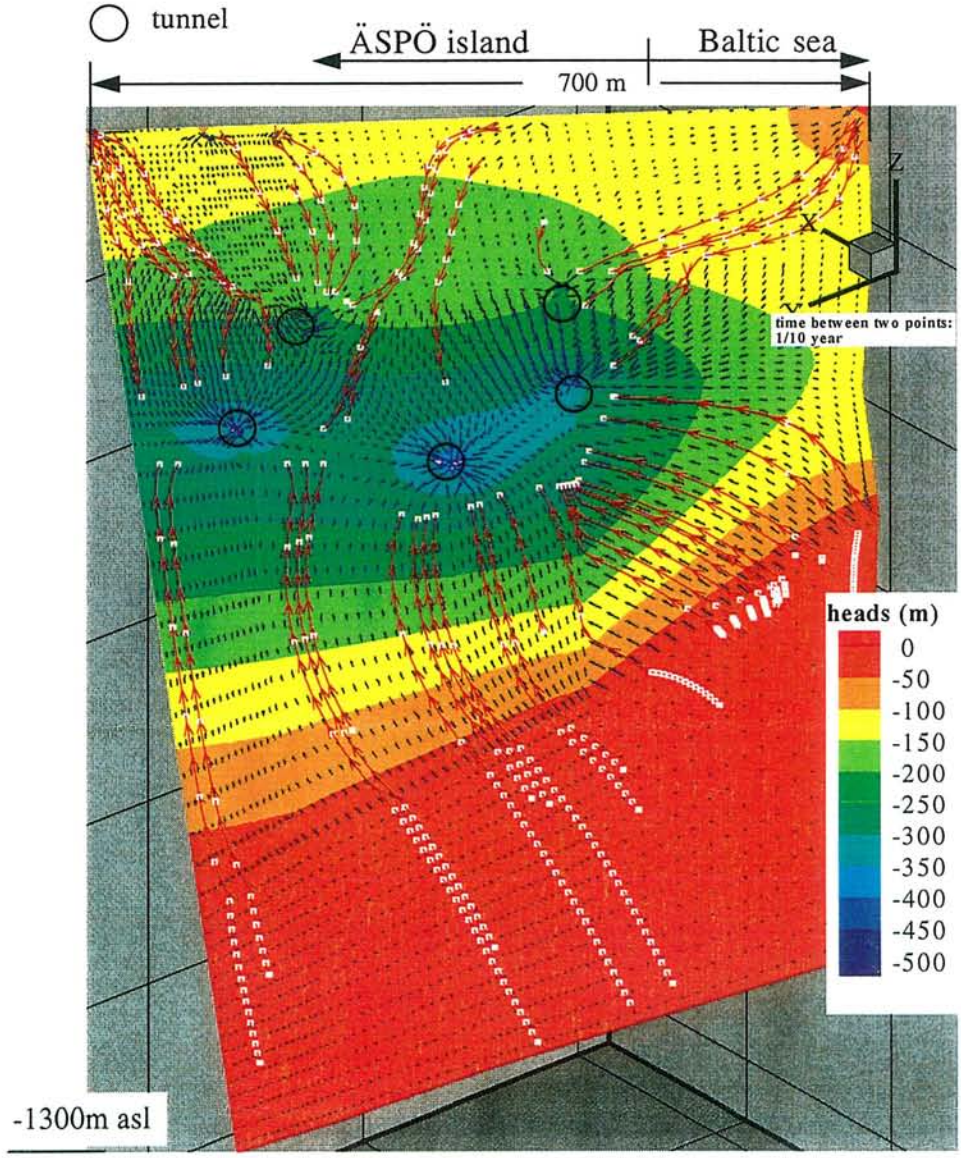

Figure 7-4. *Flow paths, heads [m] and uniform velocity vectors in fracture NE-2*

8 CONCLUDING REMARKS

The numerical results of this study help to understand the processes taking place during groundwater flow. It is intended to improve the model quality by adding chemical information. However, additional calculations are necessary to scrutinize and confirm the obtained information because the modelling results mainly depend on the material properties and boundary conditions.

First of all the pressure response of both the multi-fracture and single-fracture models has to be revised. Corresponding to the calculated flow to the tunnel, the flow rate has consequences on the simulated drawdown which exceeds the measured piezometric heads. This causes discrepancies in the response of chemical simulations shown in Appendix 4 which need to be improved.

It is intended to make additional transport calculations for additional fracture zones in the multi-fracture model. The aim is to construct a transport model that includes as many fracture zones as possible. Additional control points also have to be considered. For further calculations a sensitivity analysis has to be made.

REFERENCES

Ittner T, Gustafsson E, 1995. Groundwater Chemical Composition and Transport of Solutes. Evaluation of the Fracture Zones NE-1, NE-2 and NNW-4 during Preinvestigation and Tunnel Construction. SKB PR HRL-96-03.

Laaksoharju M, Wallin B, 1997. Evolution of the Groundwater Chemistry at the Äspö Hard Rock Laboratory. Proceedings of the Second Äspö International Geochemistry Workshop, June 6-7, 1995. SKB ICR 97-04.

Markström I, Erlström M, 1996. Äspö Hard Rock Laboratory. Overview of Documentation of Tunnel, Niches and Core Boreholes. SKB PR HRL-96-19.

Meszaros F, 1996. Simulation of the Transient Hydraulic Effect of the Access Tunnel at Äspö. SKB ICR 96-06.

Rhén I, Stanfors R, 1993. Passage through Water-Bearing Fracture Zones. Evaluation of Investigations in Fracture Zones NE-1, EW-7 and NE-3. SKB PR 25-92-18.

Rhén I, Stanfors R, 1995. Supplementary Investigations of Fracture Zones in Äspö Tunnel. SKB PR 25-95-20.

Rhén I, Gustafson G, R Stanfors, P Wikberg, 1997. ÄSPÖ HRL - Geoscientific Evaluation 1997/5. Models Based on Site Characterisation 1986 - 1995. SKB TR 97-06.

Rhén I, Magnusson J, Forsmark T, 1998. Äspö Task Force on Modelling of Groundwater Flow and Transport of Solutes - Task #5. Data Compilation: WP A3, WP A 4. SKB TN-98-06g

Wikberg P, 1998. Äspö Task Force on Modelling of Groundwater Flow and Transport of Solutes. Plan for Modelling Task # 5: Impact of the Tunnel Construction on the Groundwater System at Äspö, a Hydrological-Hydrochemical Model Assessment Exercise. SKB PR HRL-97-07.

Appendix 1

Flow field in the multi-fracture model during tunnel construction 2900 m - 3600 m and after completion

TFP at 2900 m
February 1994 / 1220 days

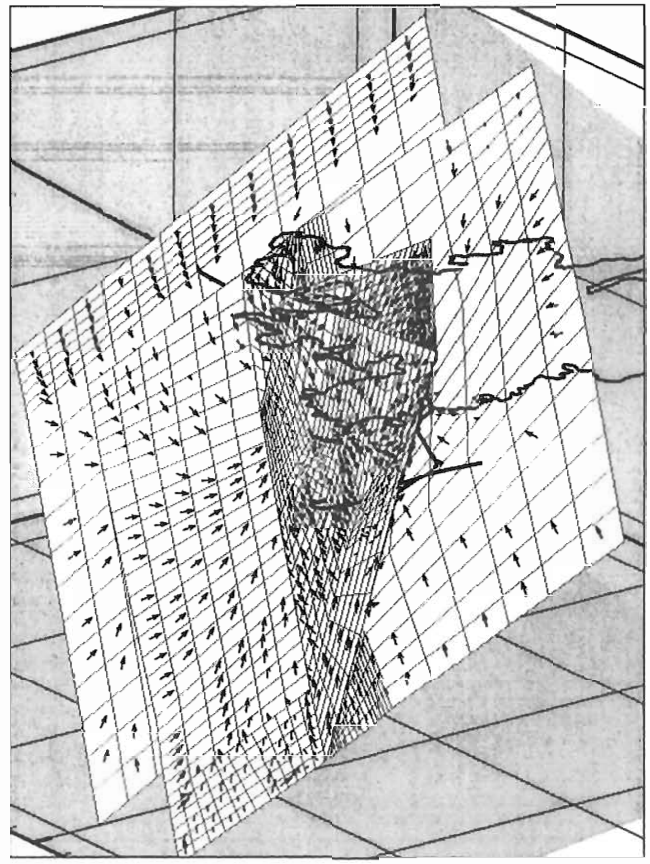

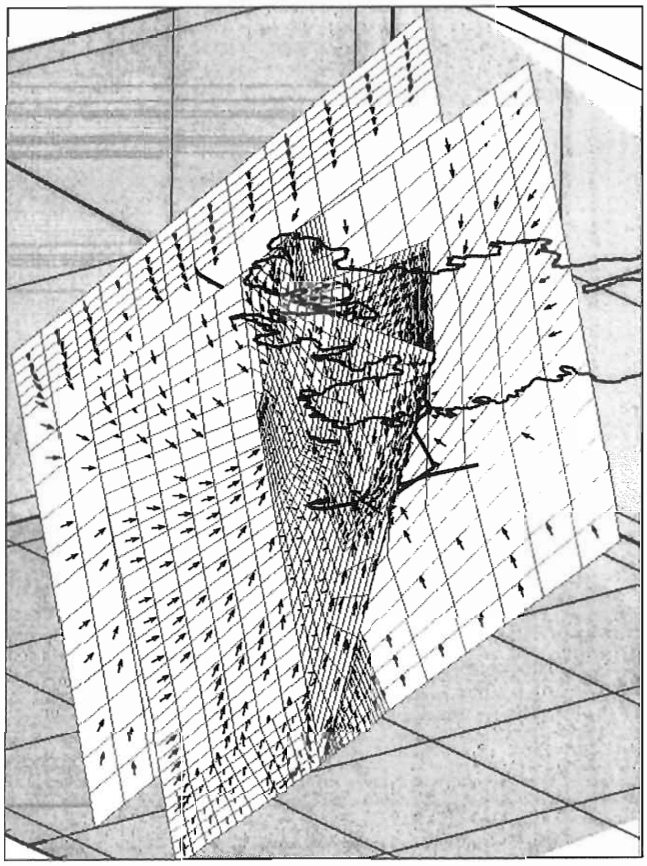

TFP at 3300 m
July 1994 / 1380 days

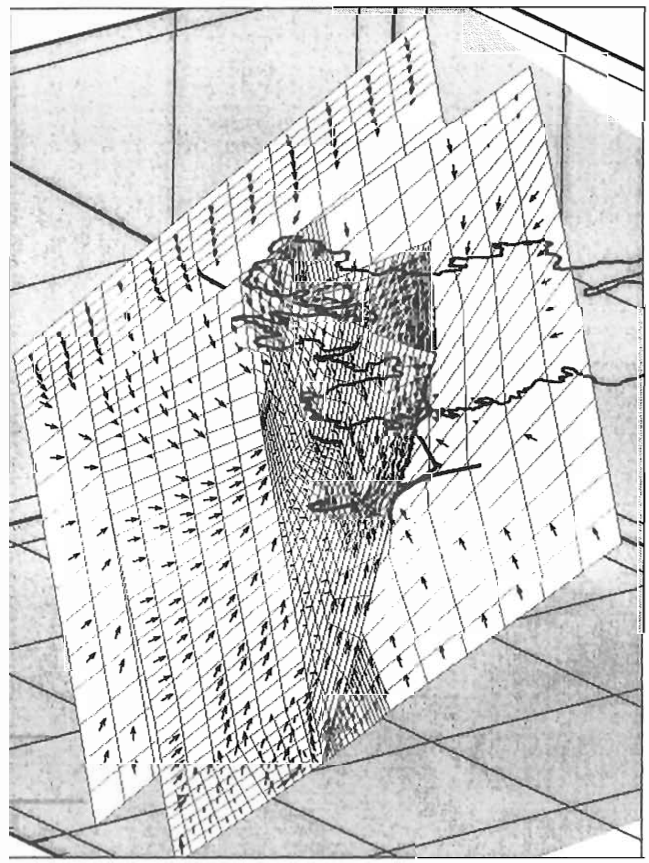

5 months after tunnel construction
February 1995 / 1600 days

Liedtke / Klennert

hydmod4.ppt
04/99

Flow Field in the multi fracture model

BGR

Appendix 2

Piezometric heads in fracture NE-2 before, during and after the tunnel construction

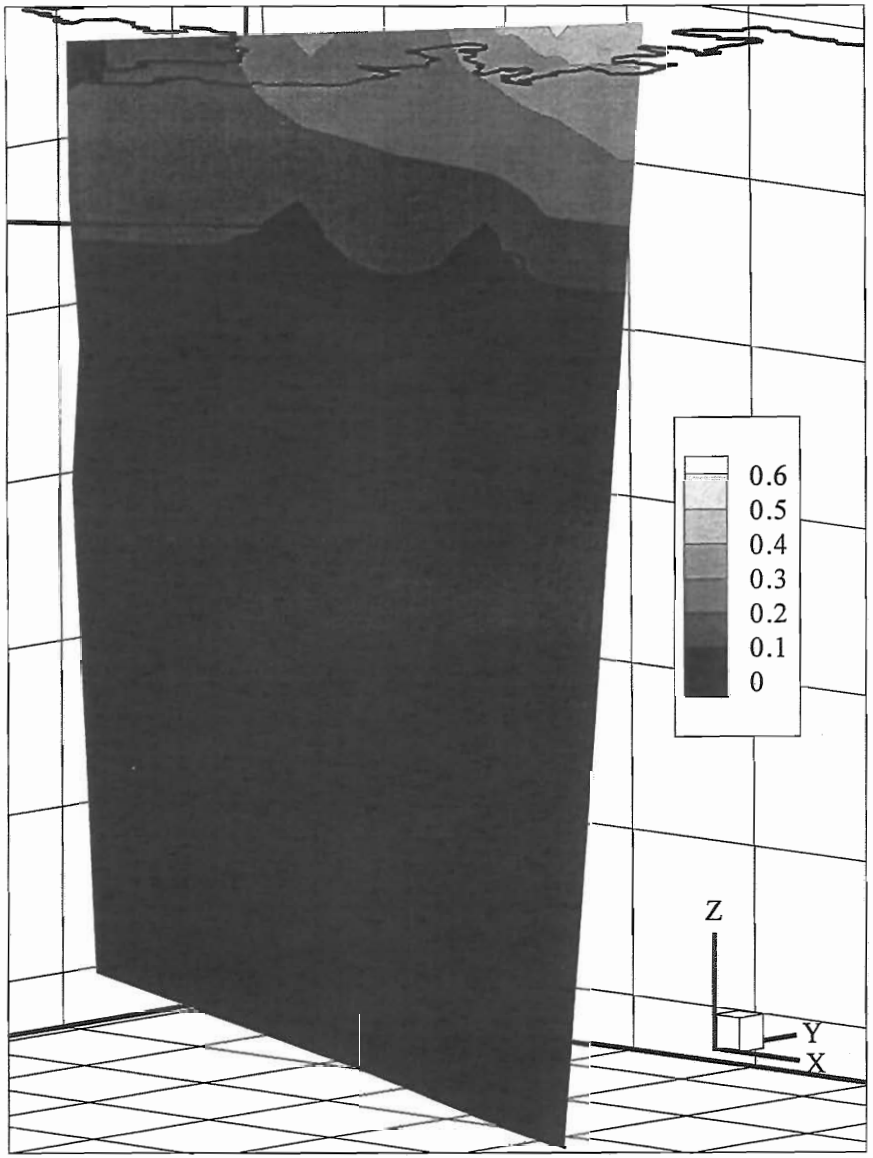

92-08-30 (700 days)

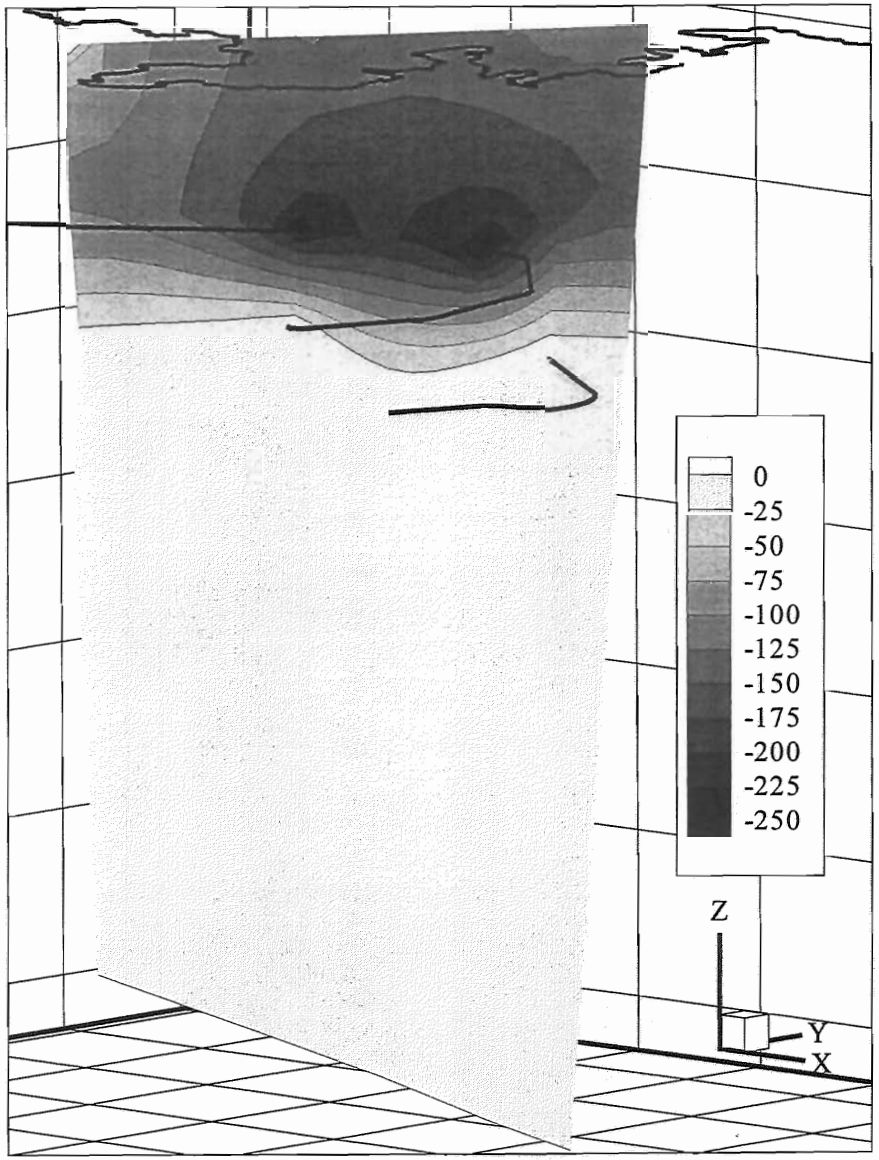

92-12-08 (800 days)

Liedtke/Klennert

headne2b.ppt
03/99

Piezometric Heads [m] in Fracture NE-2 (0 days = 90-10-01)

BGR

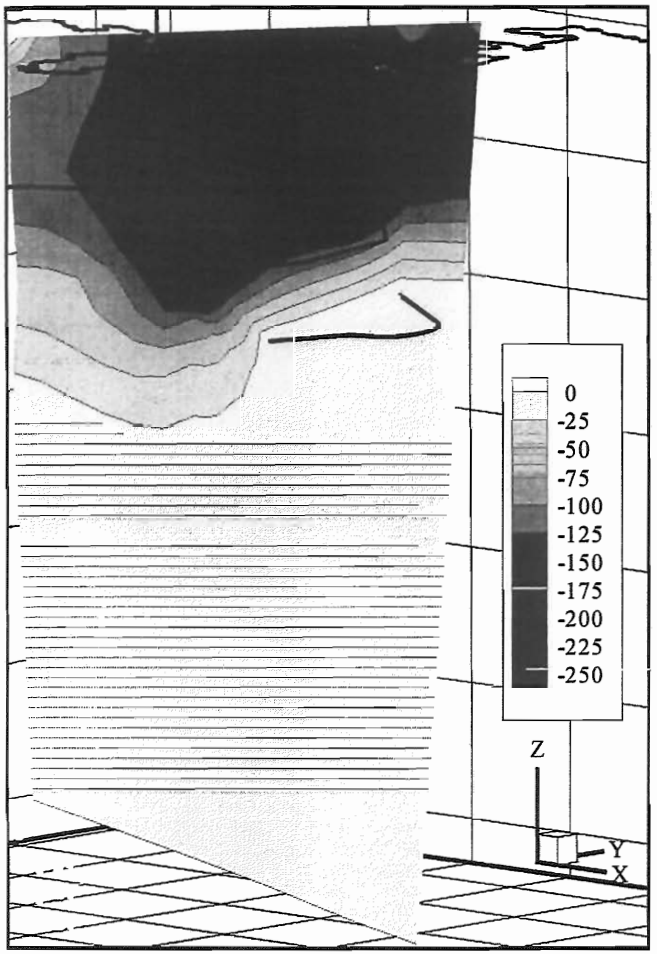

93-05-17 (960 days)

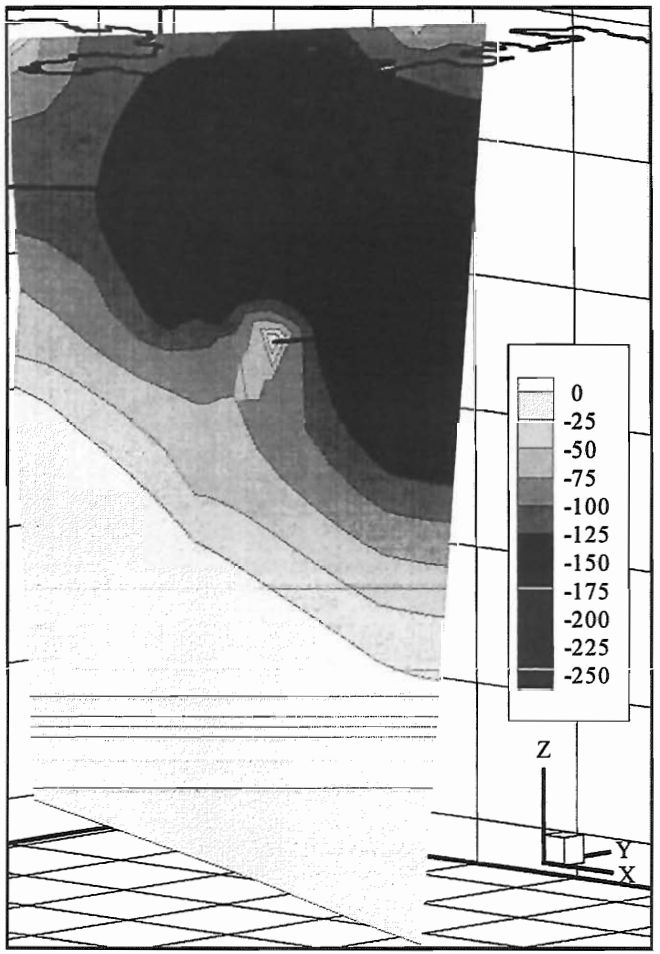

94-02-01 (1220 days)

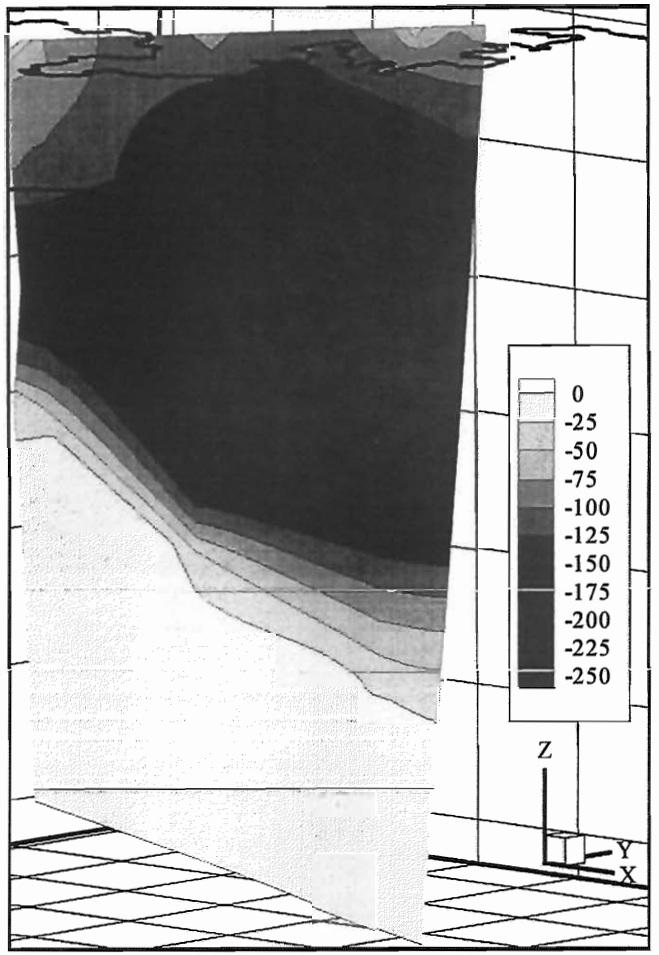

95-02-16 (1600 days)

Liedtke/Klennert

headne2h.ppt
03/99

Piezometric Heads [m] in Fracture NE-2 (0 days = 90-10-01)

BGR

Appendix 3

Fitted initial conditions in Fracture NE-2

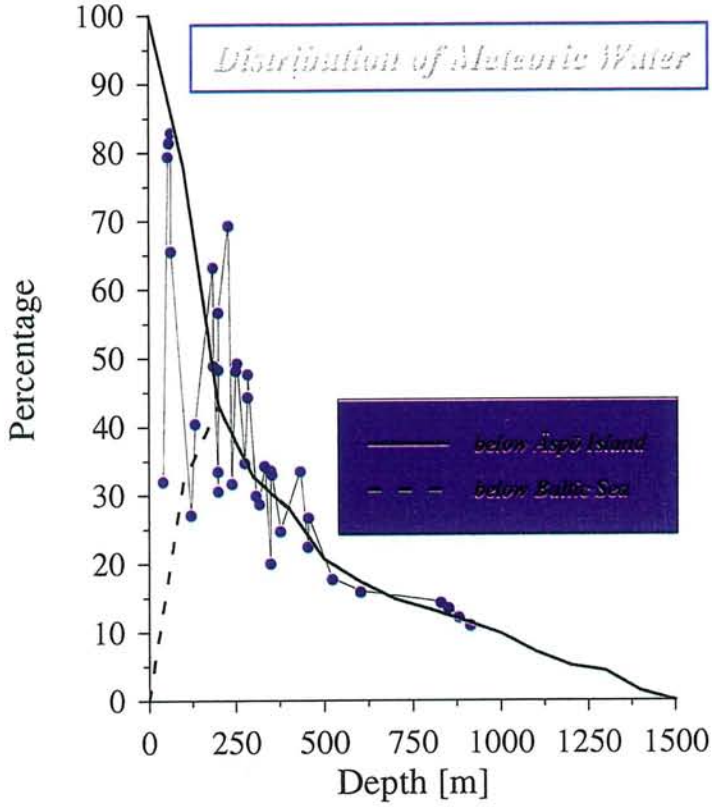

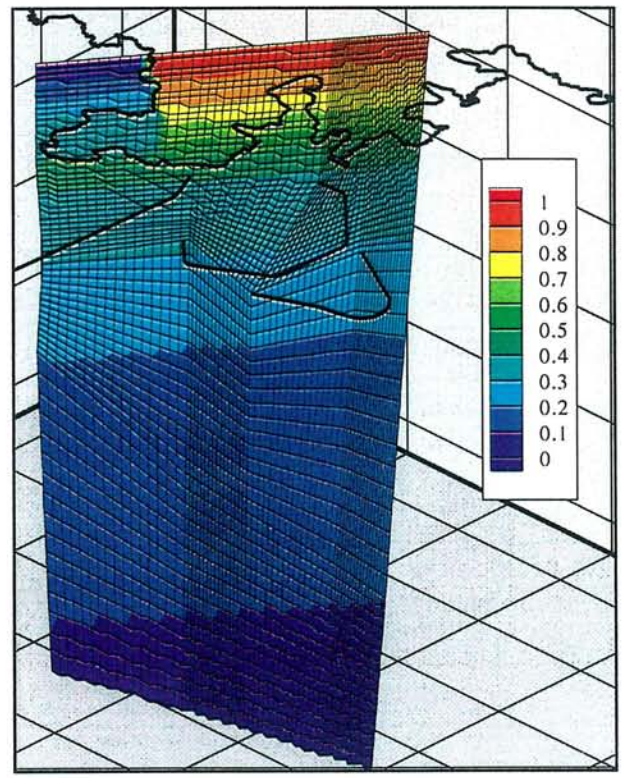

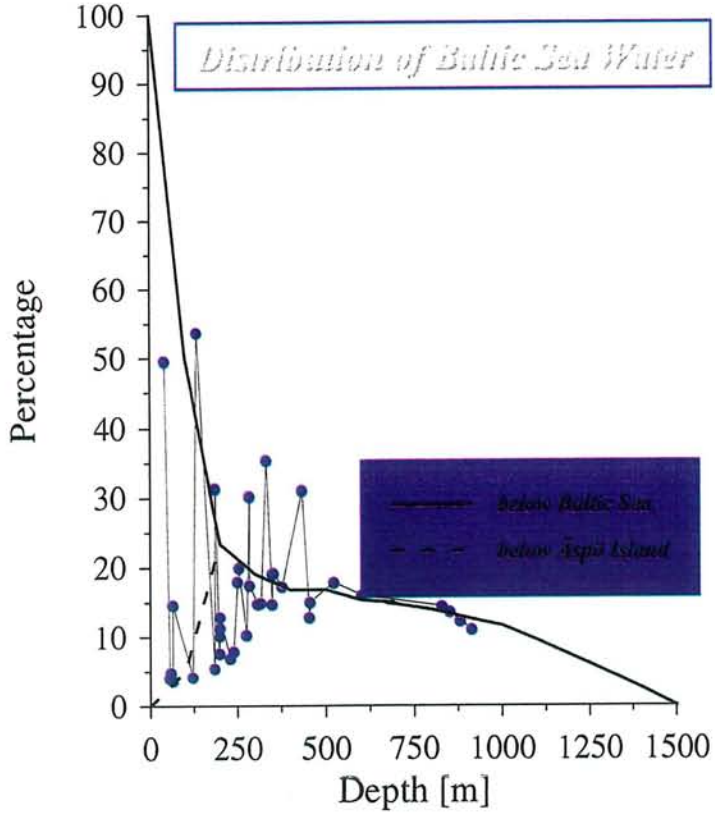

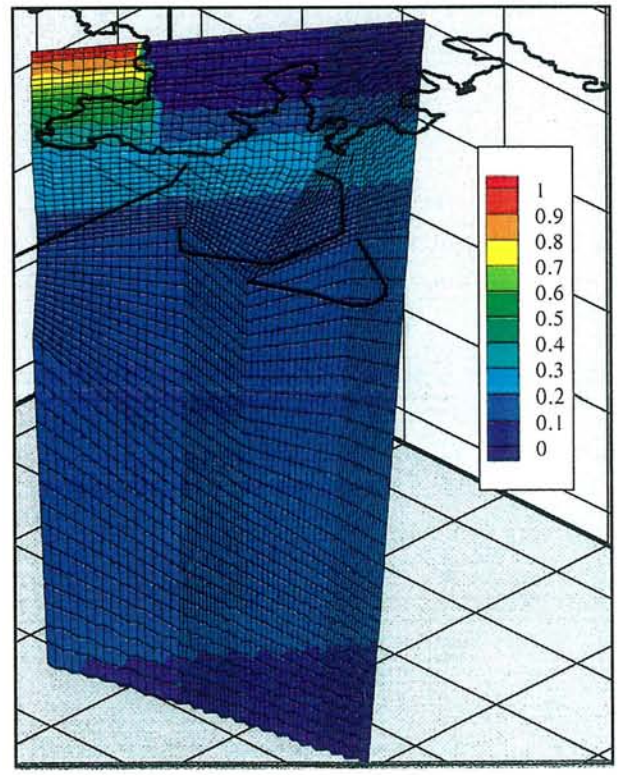

Task 5 - Initial Conditions

BGR

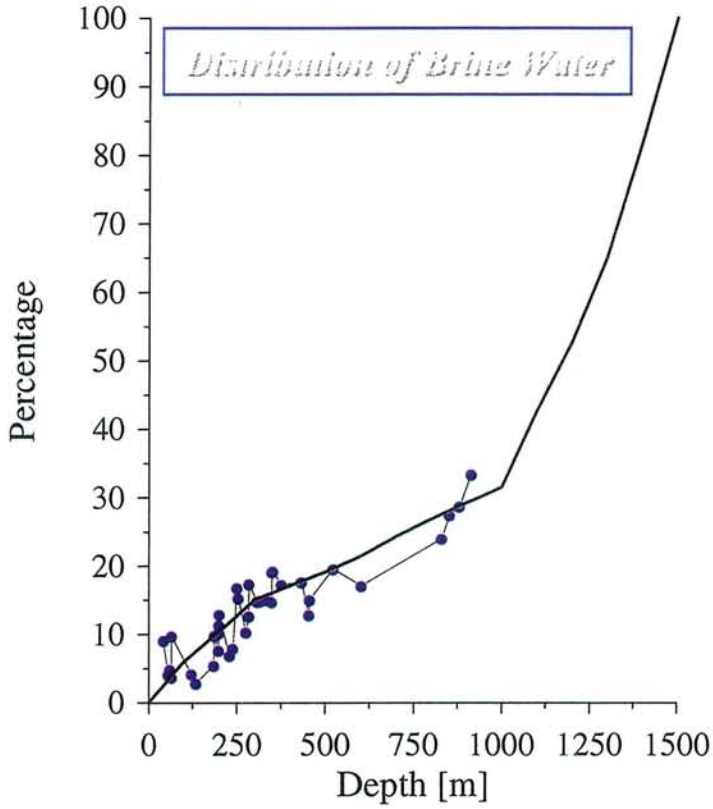

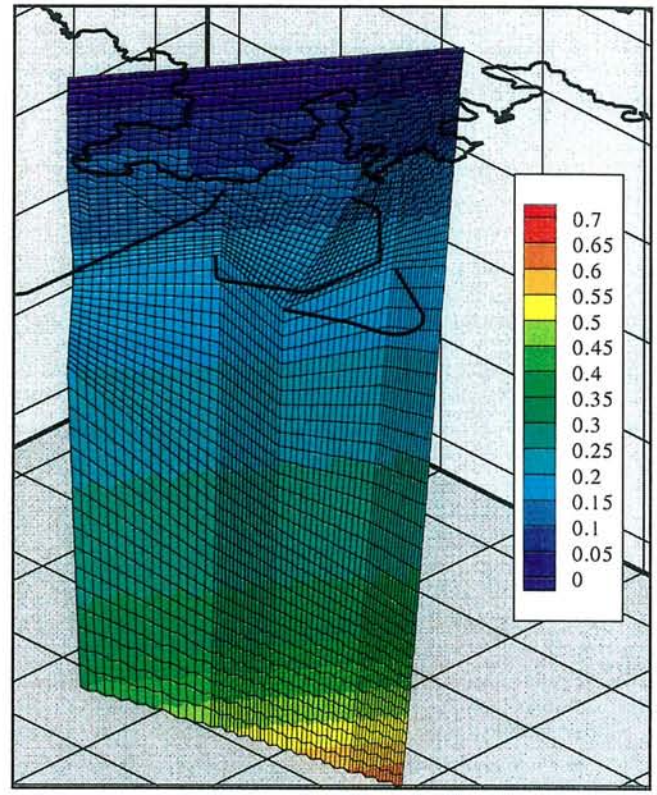

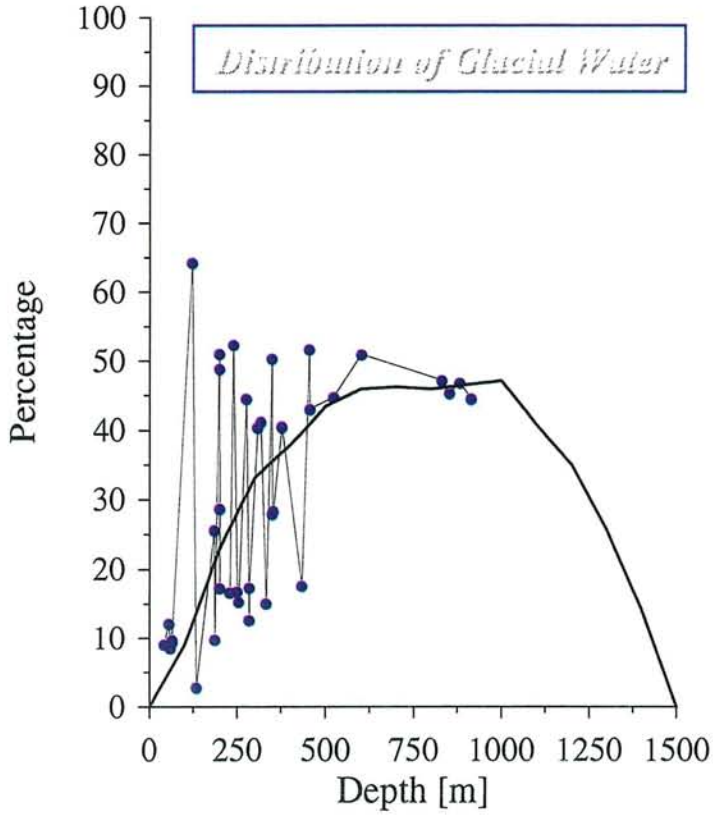

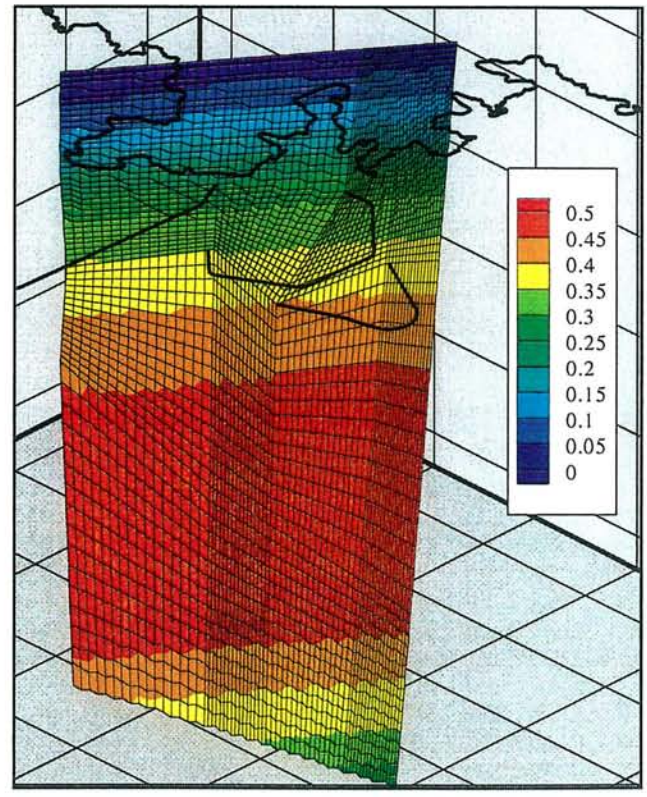

Task 5 - Initial Conditions

BGR

Appendix 4a

Distribution of brine, glacial, meteoric and Baltic Sea water in fracture NE-2 with time

undisturbed initial conditions
October 1990

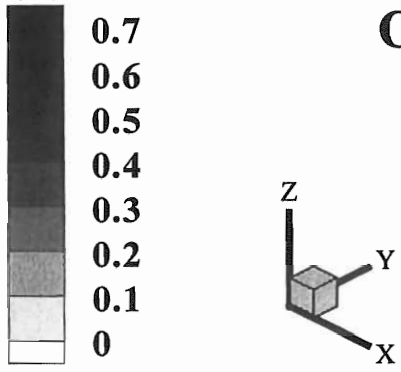

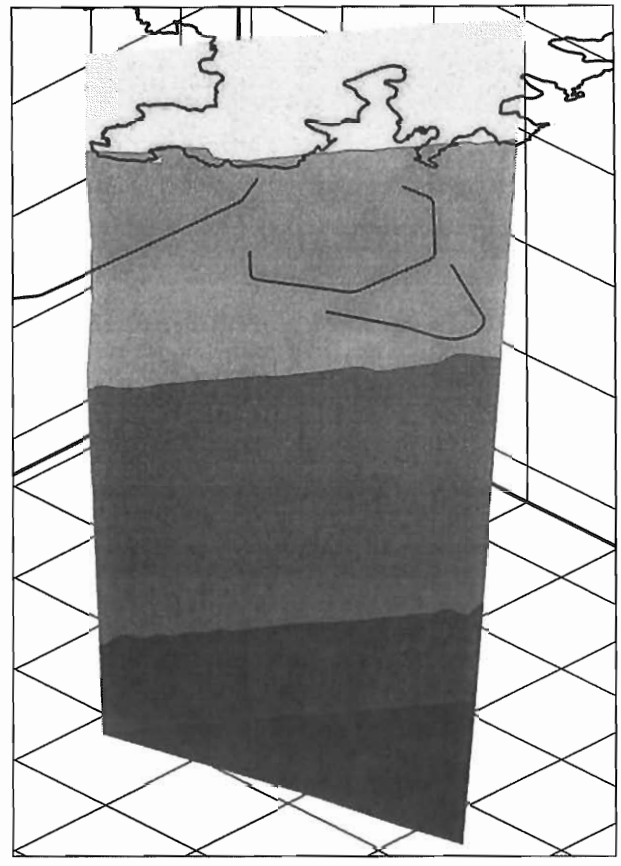

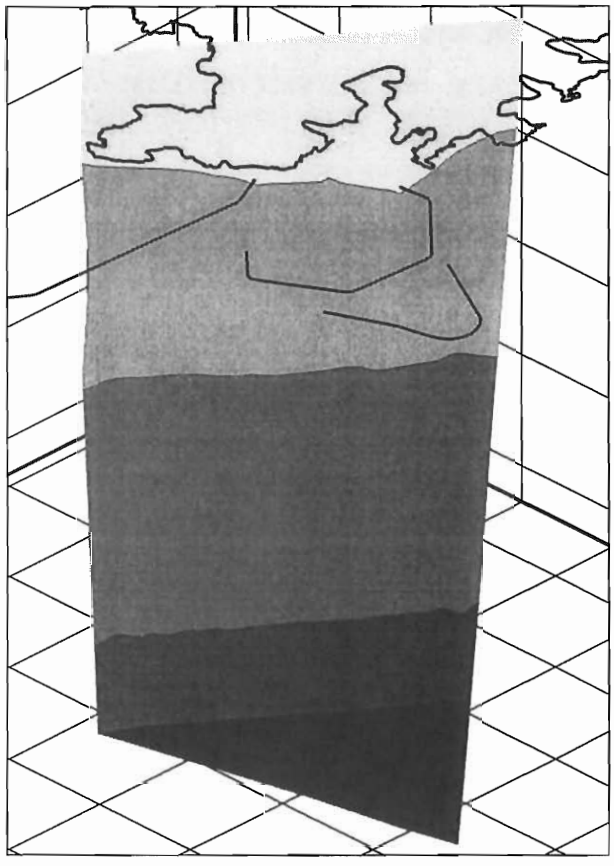

TFP at 1900 m
August 1992

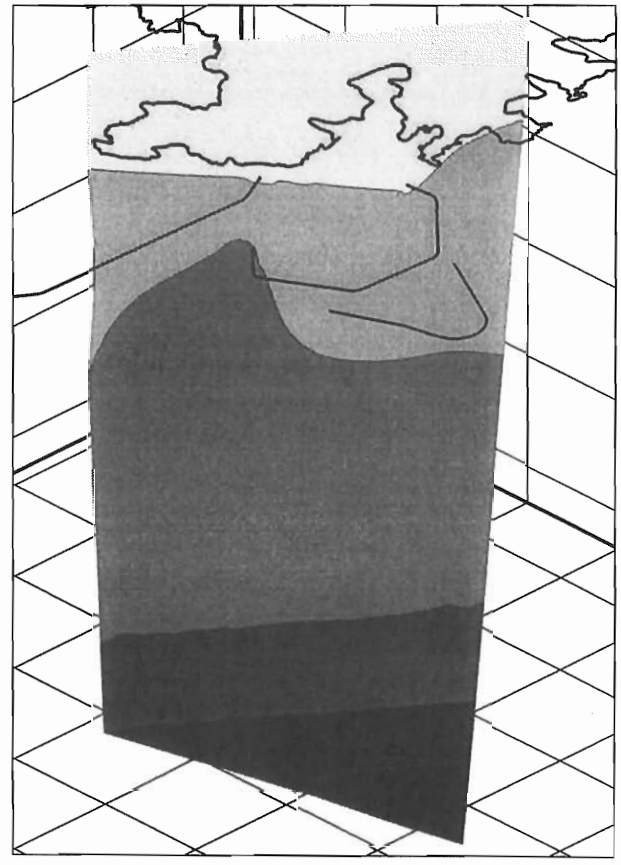

TFP at 2600 m
May 1993

Liedtke/Klennert

brn2ne2.ppt
03/99

Distribution of Brine Water in Fracture NE-2 [100%]

BGR

TFP at 2900 m
February 1994

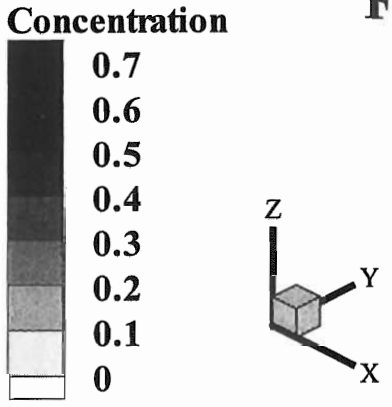

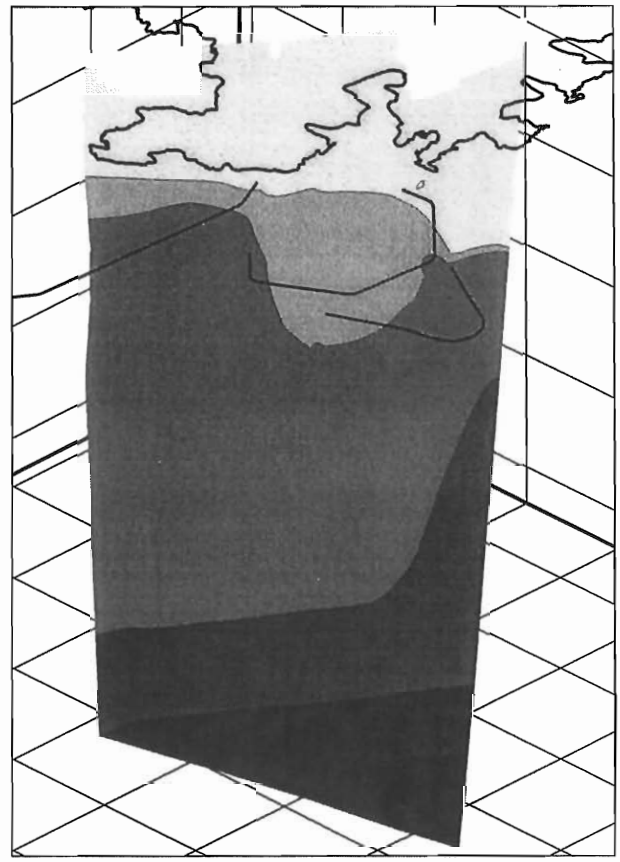

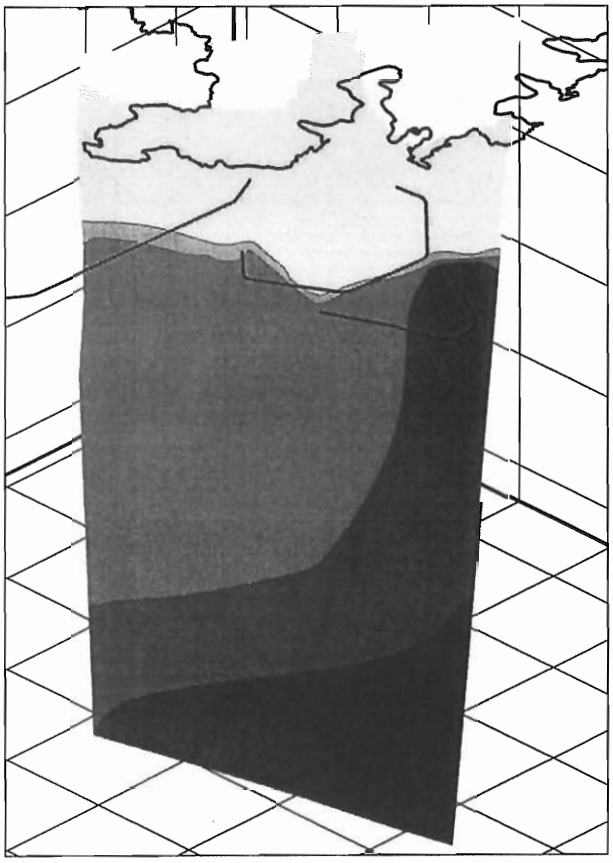

TFP at 3300 m
July 1994

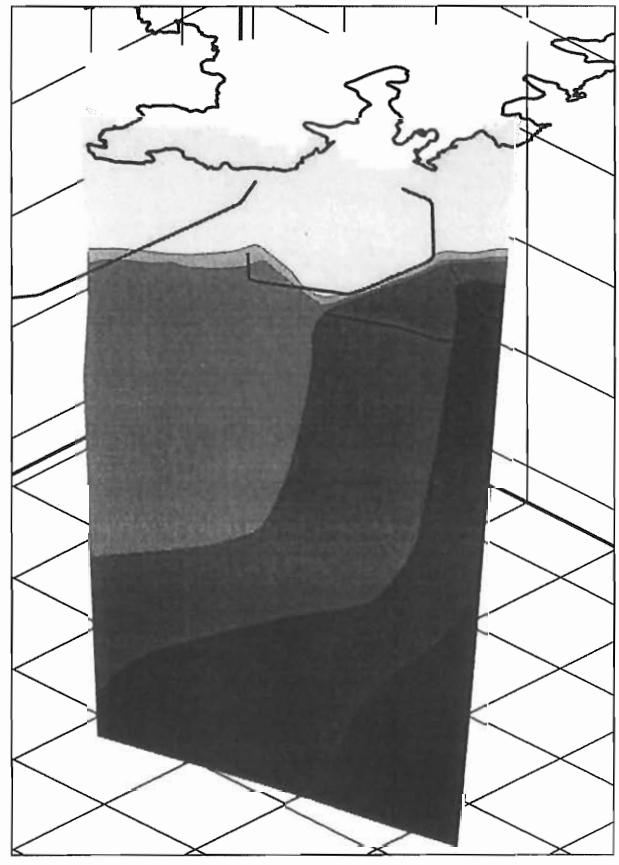

5 months after tunnel construction
February 1995

Liedtke/Klennert

brin2ne2.ppt
03/99

Distribution of Brine Water in Fracture NE-2 [100%]

BGR

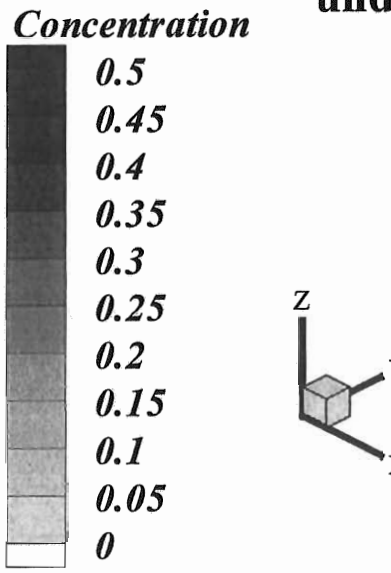

undisturbed initial conditions October 1990

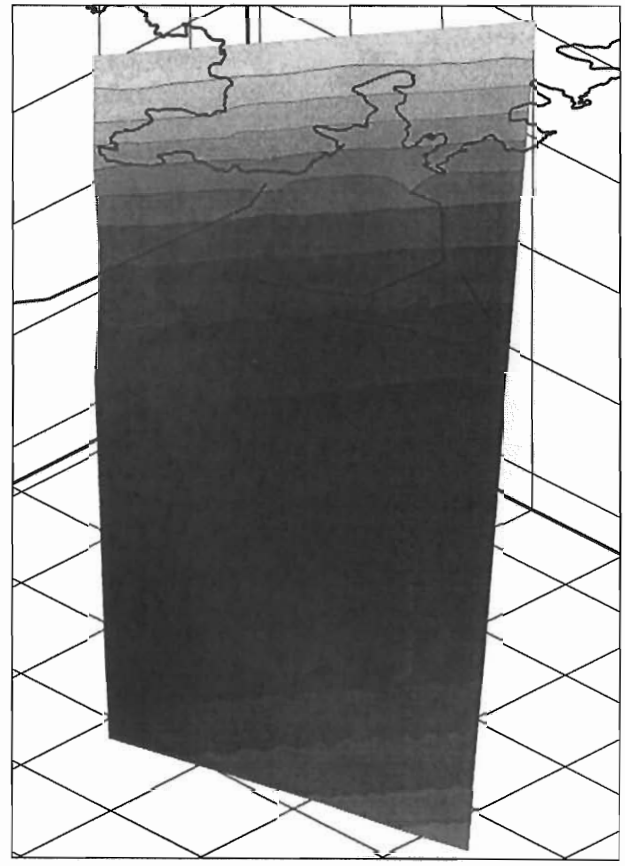

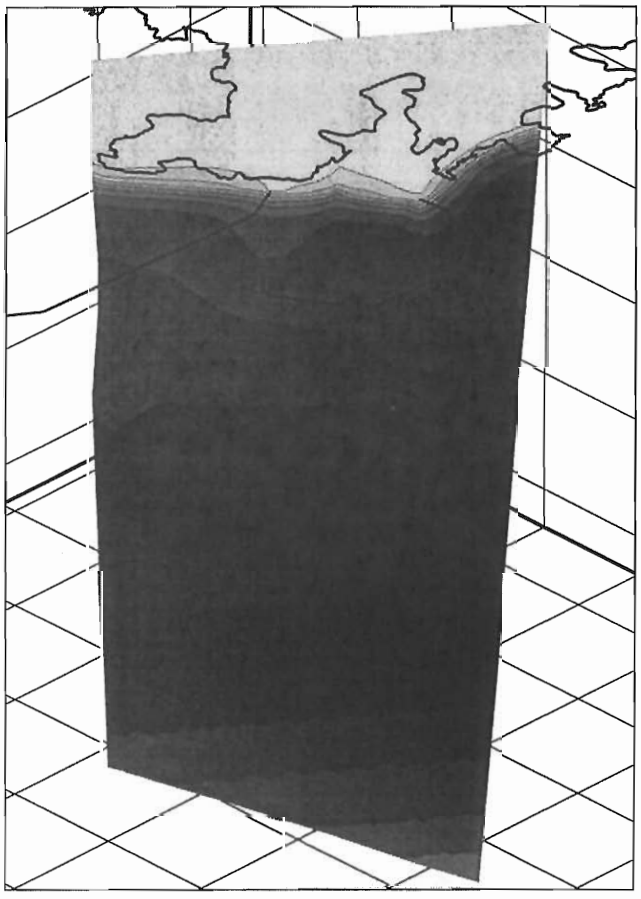

TFP at 1900 m August 1992

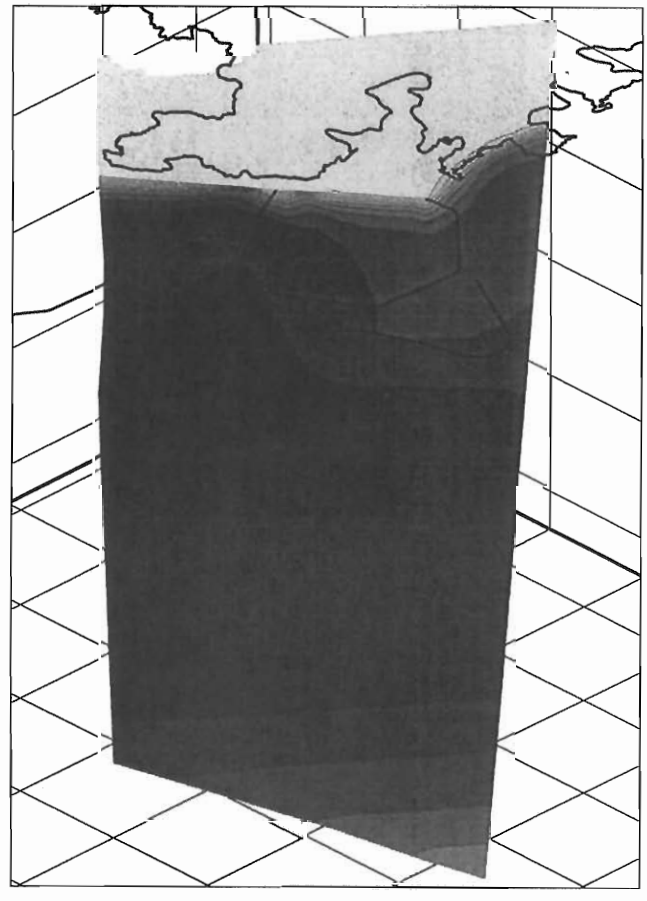

TFP at 2600 m May 1993

Liedtke/Klennert

glac2ne2.ppt 03/99

Distribution of Glacial Water in Fracture NE-2 [100%]

BGR

Concentration

0.5
0.45
0.4
0.35
0.3
0.25
0.2
0.15
0.1
0.05
0

Z
Y
X

TFP at 2900 m
February 1994

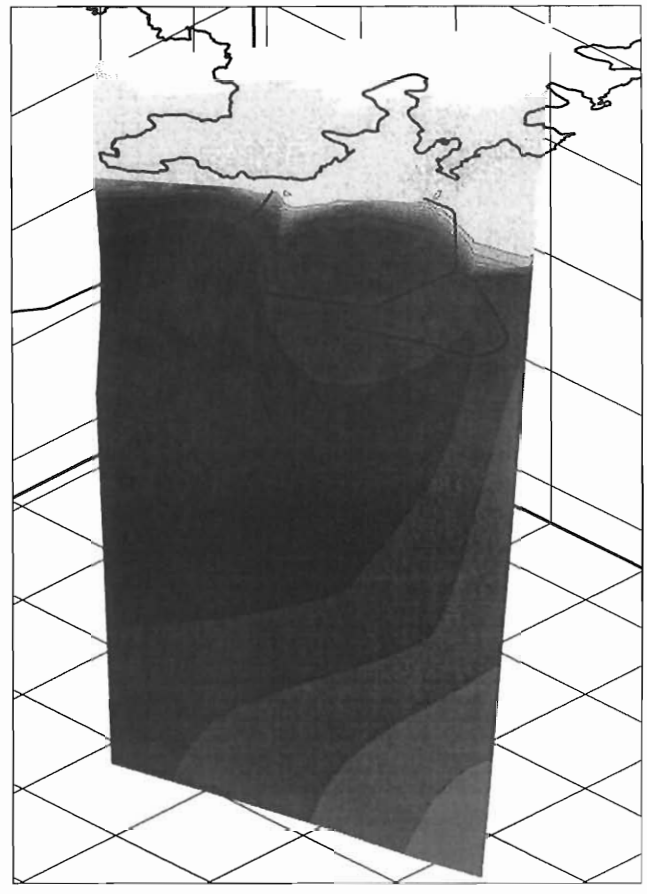

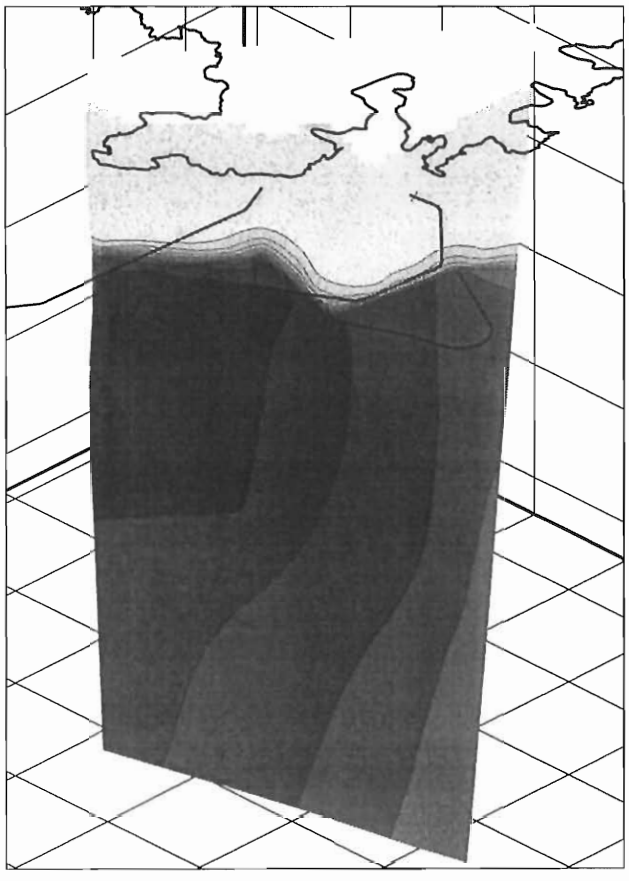

TFP at 3300 m
July 1994

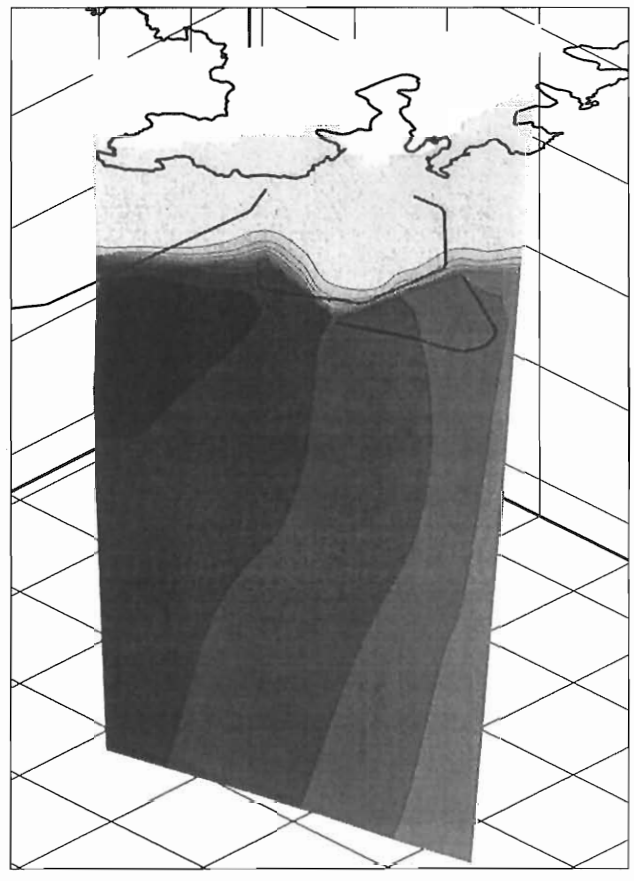

5 months after tunnel construction
February 1995

Liedtke/Klennert

glac2ne2.ppt
03/99

Distribution of Glacial Water in Fracture NE-2 [100%]

BGR

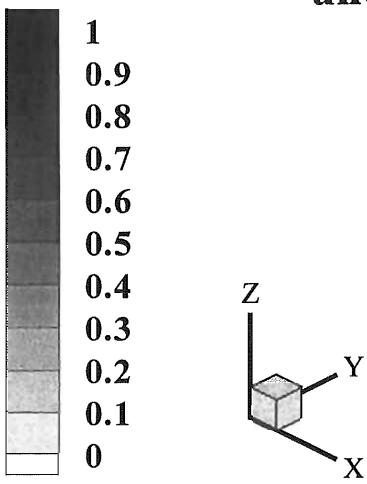

undisturbed initial conditions October 1990

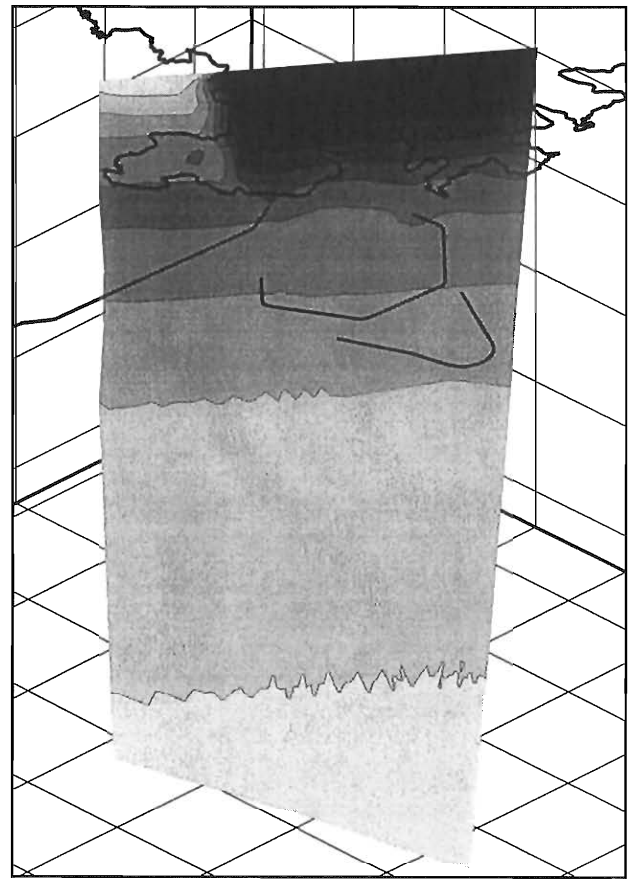

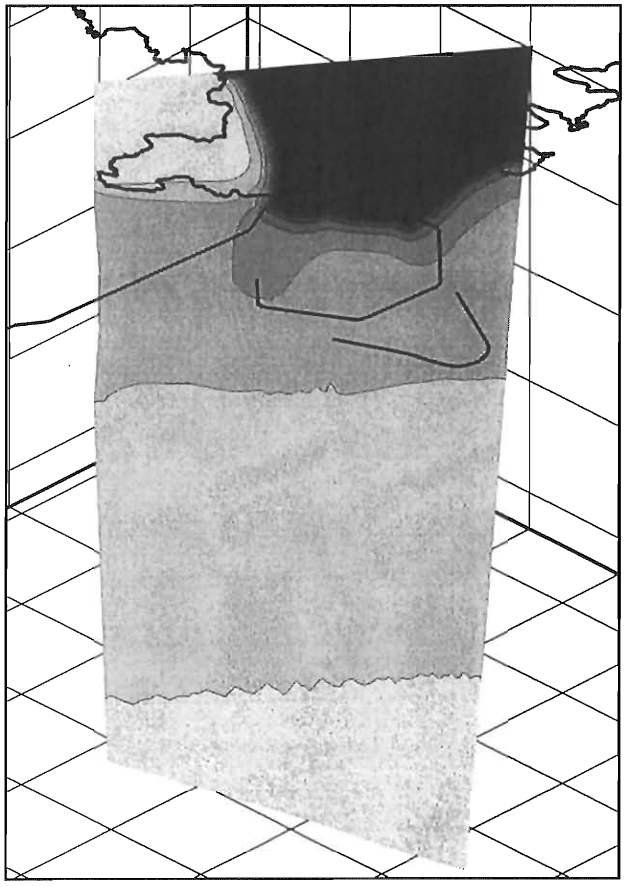

TFP at 1900 m August 1992

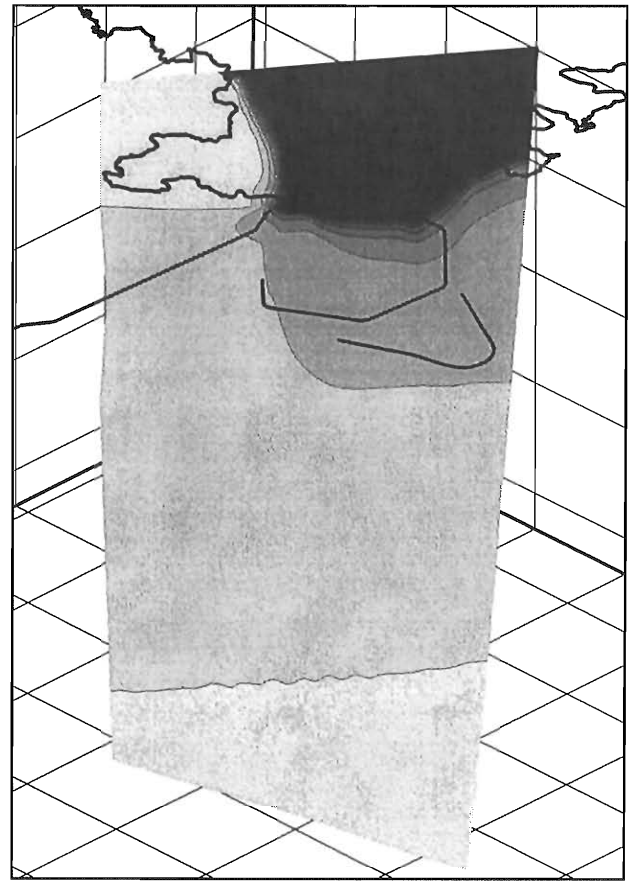

TFP at 2600 m May 1993

Liedtke/Klennert

mete2ne2.ppt
04/99

Distribution of Meteoric Water in Fracture NE-2 [100%]

BGR

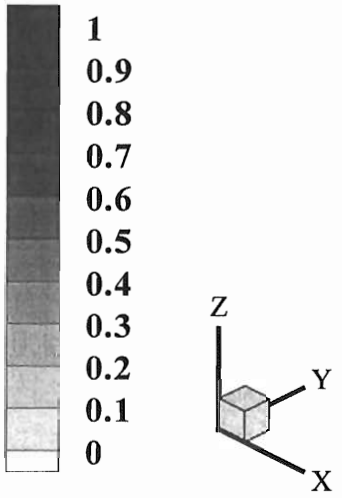

TFP at 2900 m
February 1994

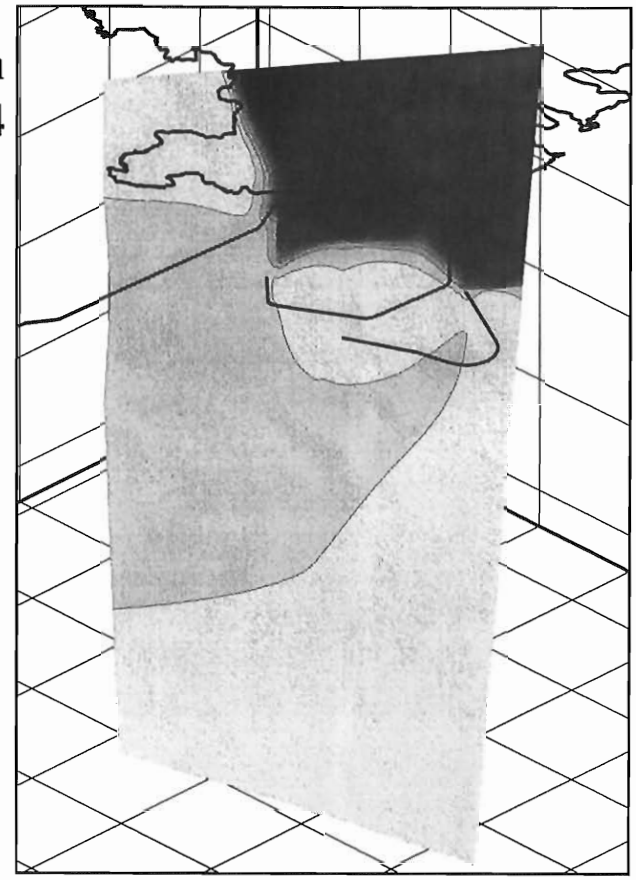

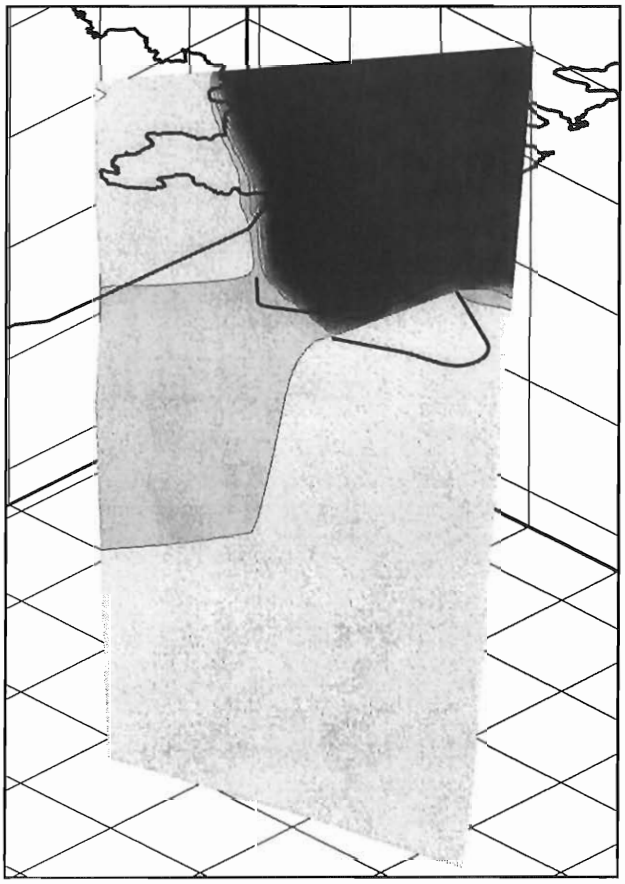

TFP at 3300 m
July 1994

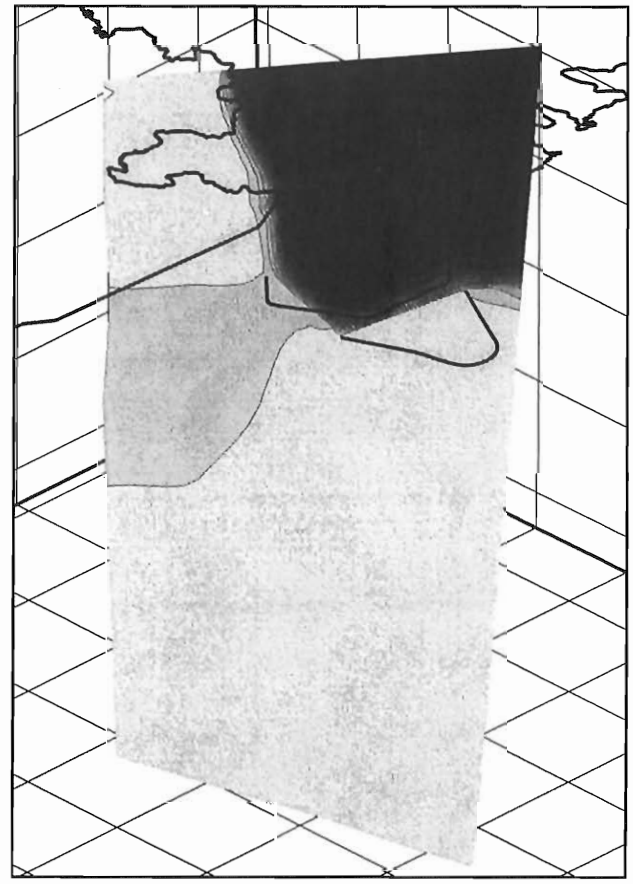

5 months after tunnel construction
February 1995

Liedtke/Klennert

mete2ne2.ppt
04/99

Distribution of Meteoric Water in Fracture NE-2 [100%]

BGR

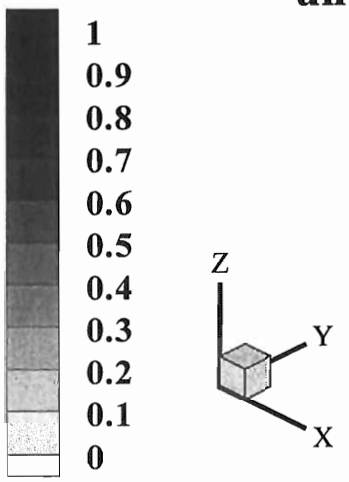

undisturbed initial conditions October 1990

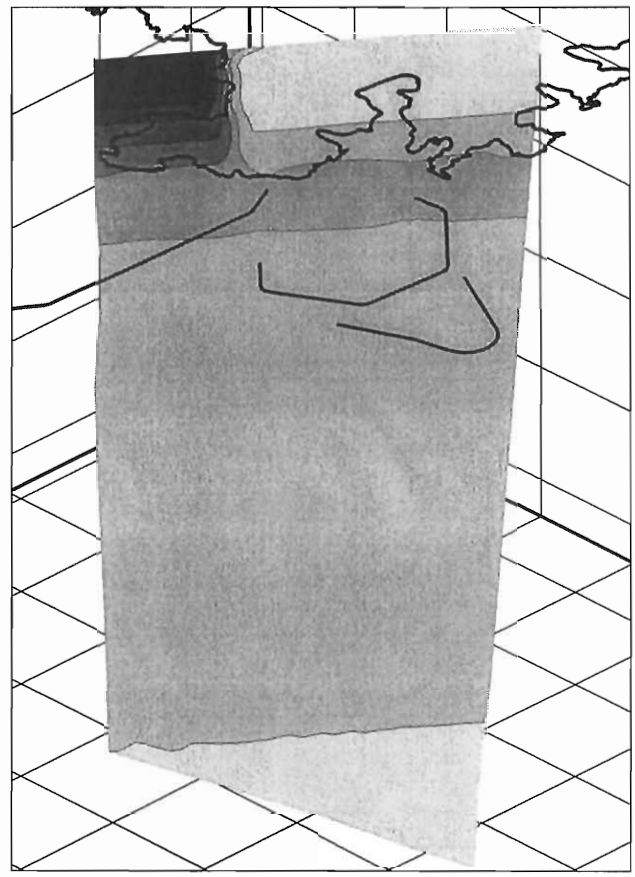

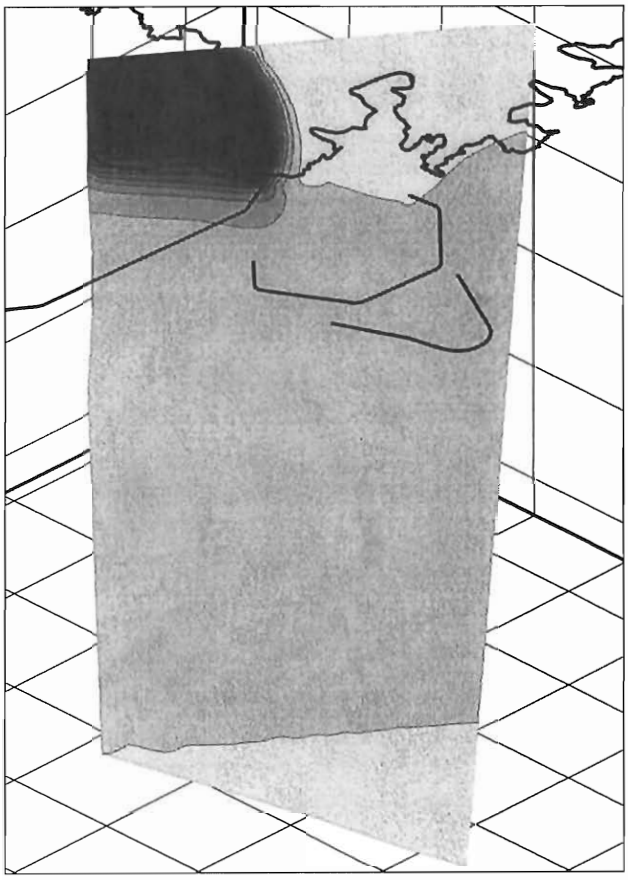

TFP at 1900 m August 1992

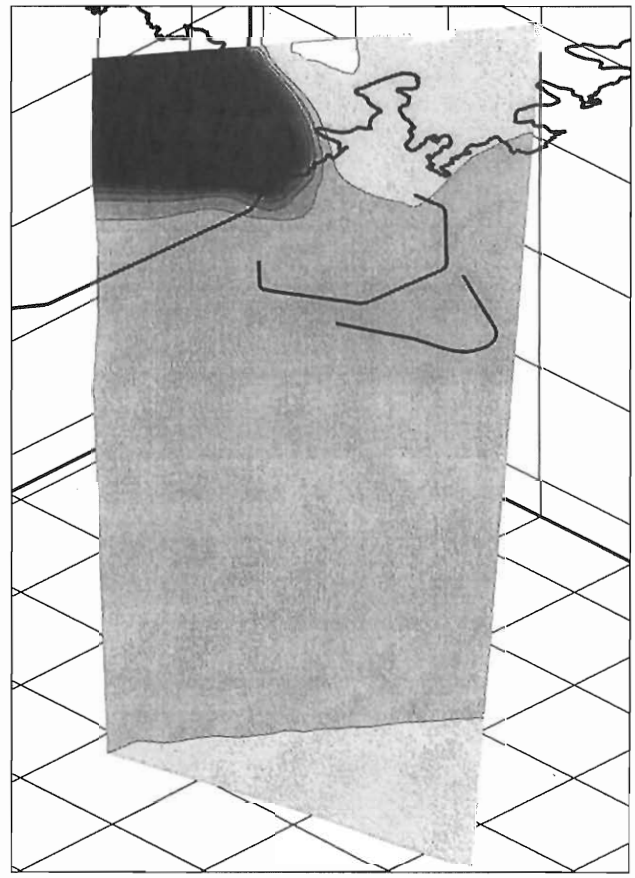

TFP at 2600 m May 1993

Liedtke/Klennert

sea2ne2.ppt 04/99

Distribution of Baltic Sea Water in Fracture NE-2 [100%]

BGR

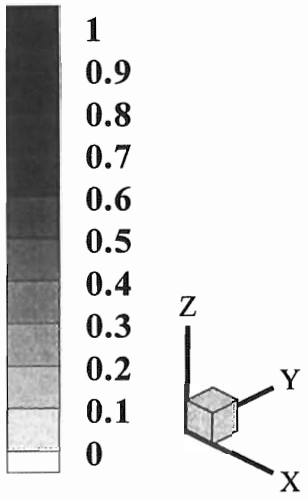

TFP at 2900 m
February 1994

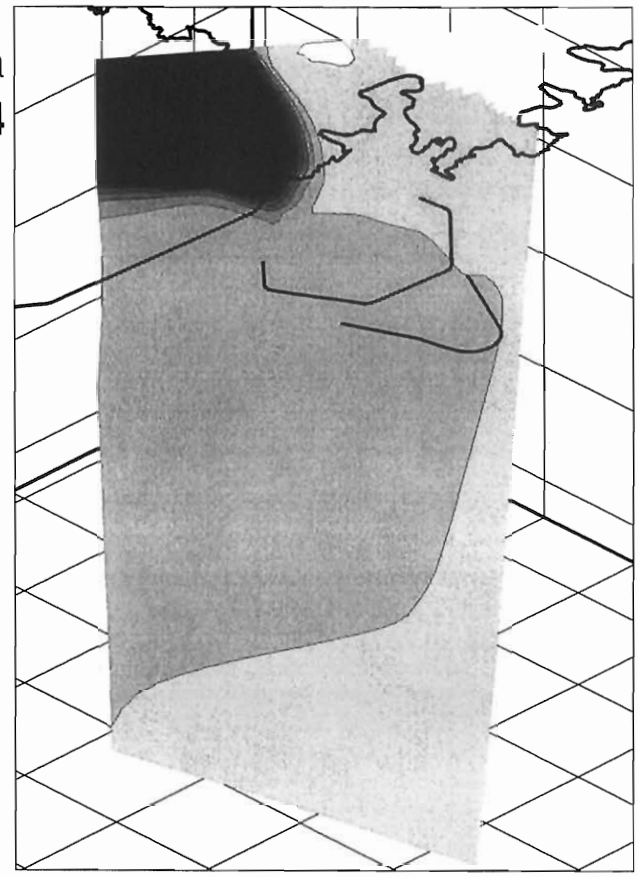

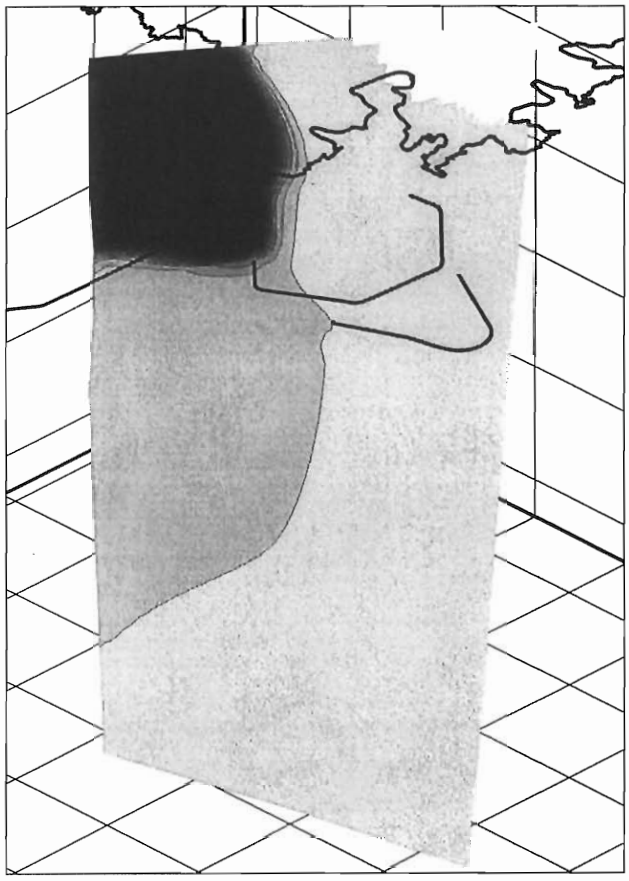

TFP at 3300 m
July 1994

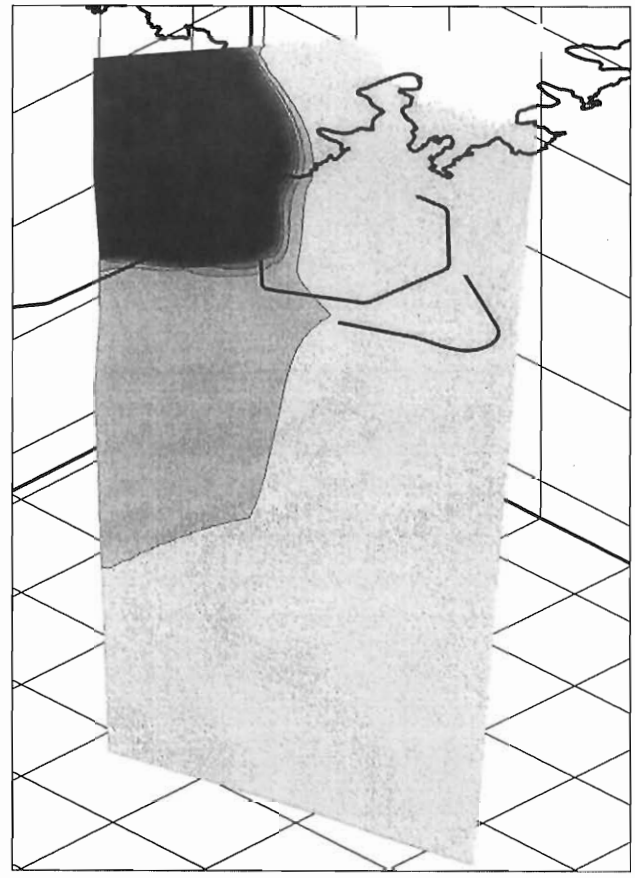

5 months after tunnel construction
February 1995

Liedtke/Klennert

sea2ne2.ppt
04/99

Distribution of Baltic Sea Water in Fracture NE-2 [100%]

BGR

Appendix 4b

Comparison of measured and simulated values

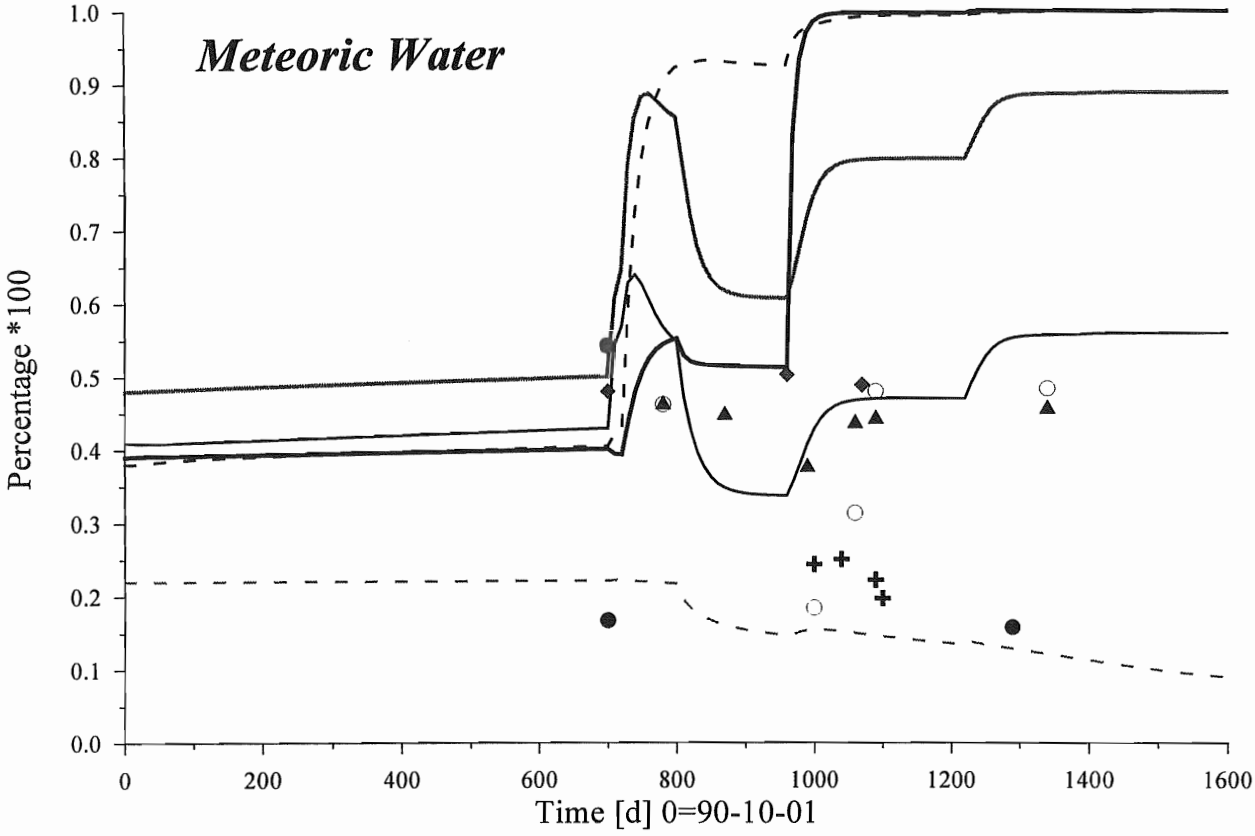

Measured: SA1614B KA1639A SA1828B KAS05 KAS12 KAS13

Calculated:

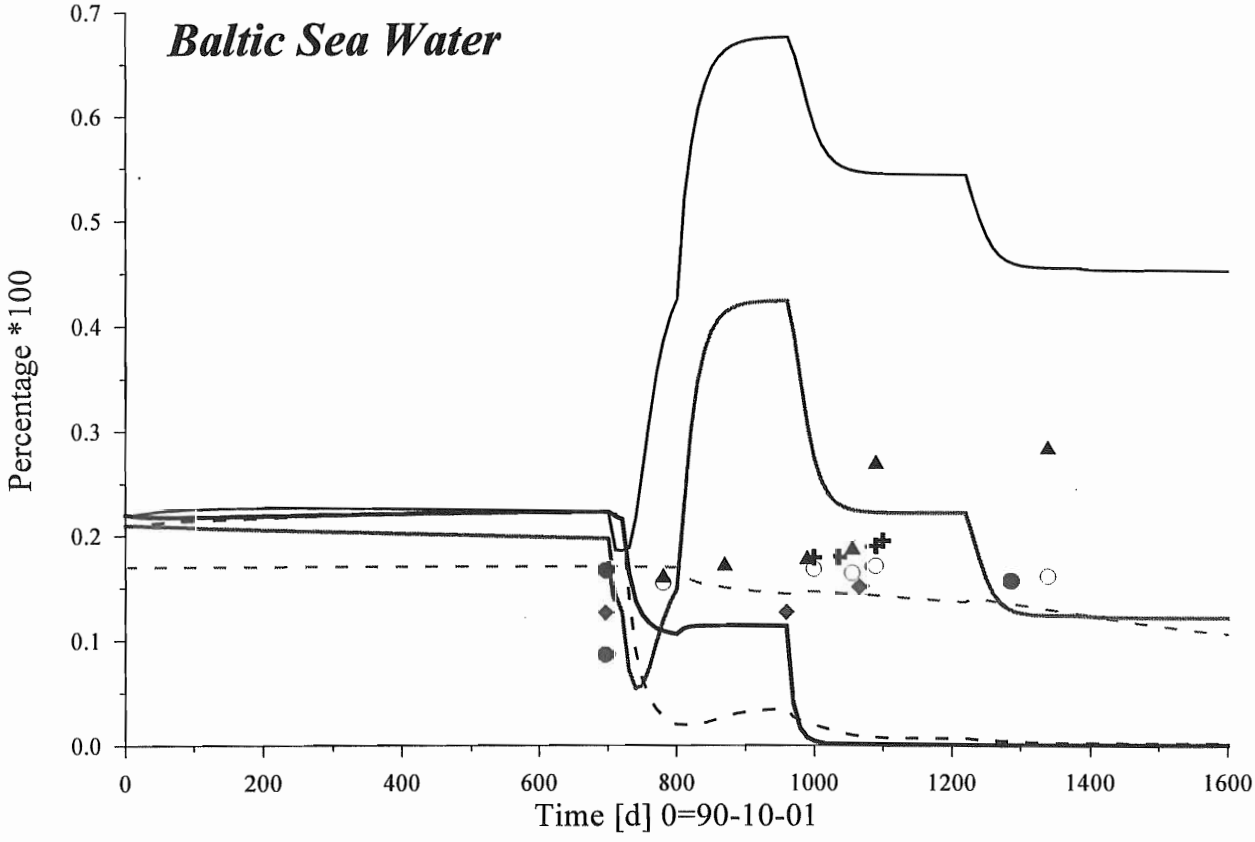

Liedtke/Klennert

appendix.ppt
04/99

Water Composition at Control Points in NE-2

BGR

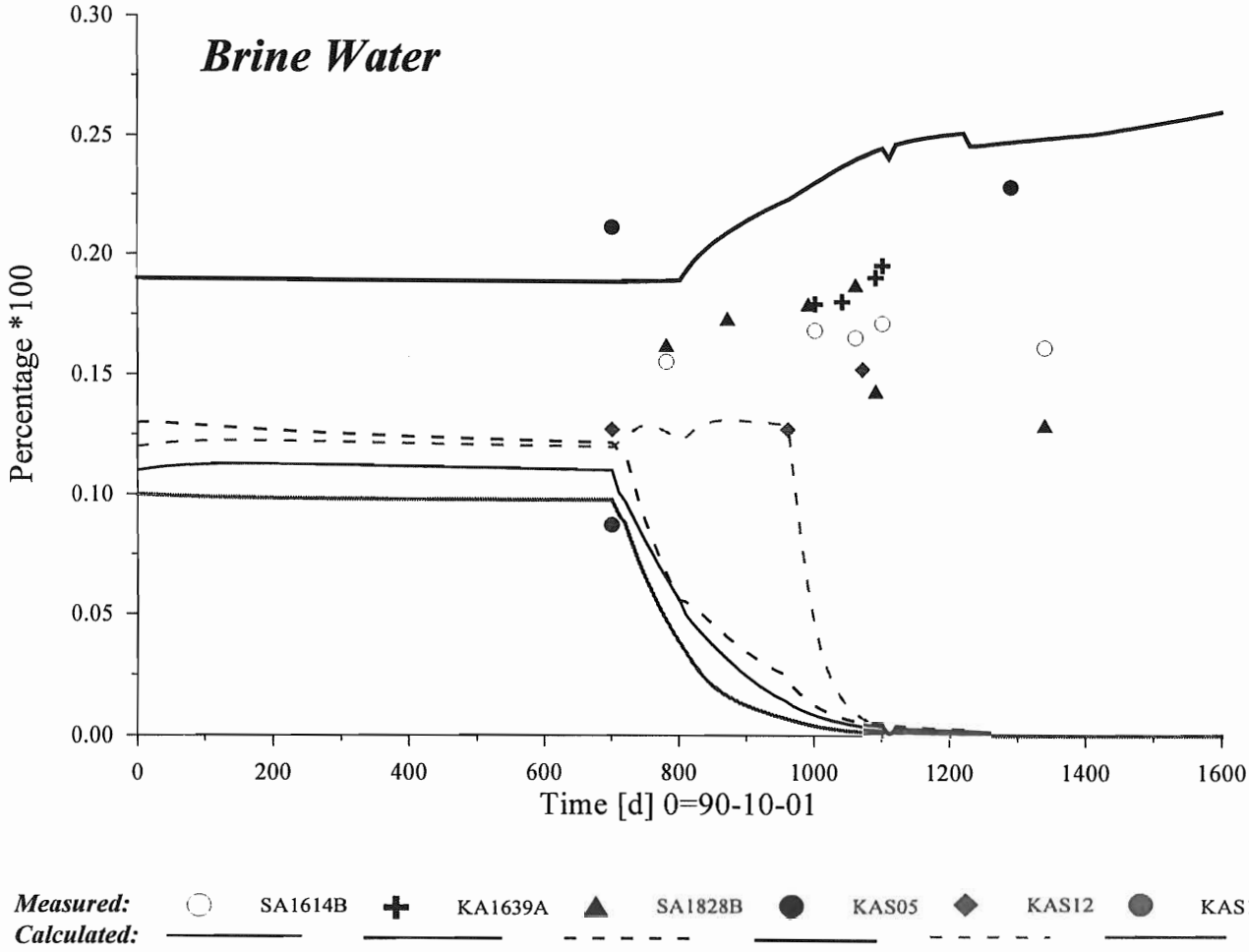

Measured: ○ SA1614B + KA1639A ▲ SA1828B ● KAS05 ◆ KAS12 ● KAS13

Calculated: — — — — — —

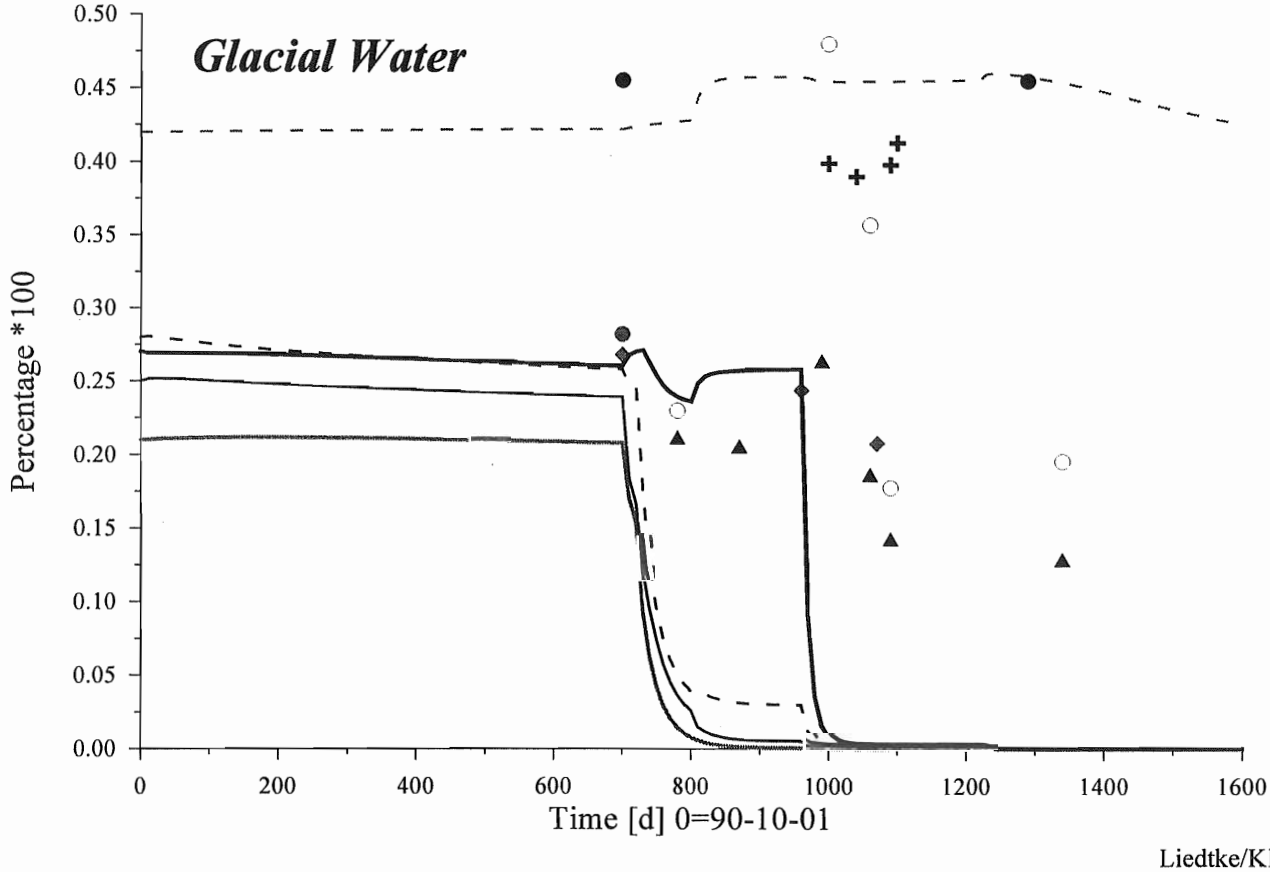

Liedtke/Klennert

appendix.ppt
04/99

Water Composition at Control Points in NE-2

BGR

Executive summary of modelling 2900-3600 m.

E. Kattilakoski (POSIVA/VTT)

Excerpts from a report presented at the meeting.

DRAFT

Task 5: Executive Summary of Modelling 2900—3600 m

Eero Kattilakoski

VTT Energy

April 1999

1 INTRODUCTION

1.1 Background

Task 5 (Impact of the tunnel construction on the groundwater system at Äspö, a hydrological-hydrochemical model assessment exercise) aims for the comparison and ultimate integration of hydrochemistry and hydrogeology. The consistency of groundwater flow models and hydrochemical mixing-reaction models is assessed through the integration and comparison of hydraulic and chemical data obtained before and during the tunnel construction. The modelling task will be useful for a stability assessment of the hydrodynamic and hydrochemical conditions at Äspö. A specific objective is the development of a procedure for the integration of hydrological and hydrochemical information which could be used for disposal site assessments — especially in a crystalline bedrock environment. (Wikberg, 1998)

1.2 Objectives

This work concerns with the groundwater flow modelling part of Task 5. No chemical reactions have been modelled, only mixing. The simulation time steps cover the period from the natural conditions until the completed tunnel and shafts.

The flow model was constructed by including the hydrologic connections recognised during the tunnel construction. The observed properties of water and bedrock were included in the simulation model. The initial salinity boundary condition was fixed in accordance with the observations of the groundwater composition. The hydraulic data gained from boreholes was utilised to confirm the boundary condition in the tunnel.

The FEFTRA code (formerly known as FEFLOW) is used to solve both the coupled equations of pressure and concentration and the transport equations of the different water types. The dual porosity transport model is applied to the equations of the different groundwater types, which are solved using the previously simulated pressure and salinity fields. The calculated mixing ratios are compared with those from a chemistry model. Detailed performance measures (Rhén, Smellie and Wikberg, 1998) will be used for the presentation of the results.

2 MODEL CONCEPTS AND FORMULATION

2.1 Governing equations

The mathematical formulation of the dual porosity approach is explained in detail by Löfman and Taivassalo (1995) and Löfman (1996).

The flow equation is expressed in terms of the residual pressure p — the actual pressure minus the hydrostatic component of freshwater (e.g., Bear, 1979; de Marsily, 1986):

$$\nabla \cdot (\frac{\rho \mathbf{k}}{\mu}(\nabla p - (\rho - \rho_0)g)) = \frac{S_s}{g}\frac{\partial p}{\partial t}, \qquad (2.1)$$

where
- p is the residual pressure (Pa),
- ρ is the density of water (kgm^{-3}),
- ρ_0 is the freshwater density (kgm^{-3}),
- μ is the viscosity of water ($kgm^{-1}s^{-1}$),
- $\boldsymbol{k}$ is the permeability tensor of the medium (m^2),
- g is the gravitational acceleration (ms^{-2}) and
- S_S is the specific storage of the medium (m^{-1}).

The permeability tensor $\boldsymbol{k}$ in Eq. (2.1) can be expressed in terms of the hydraulic conductivity $\boldsymbol{K}$ (m/s):

$$\mathbf{k} = \frac{\mathbf{K}\mu}{\rho g}. \qquad (2.2)$$

In *the dual porosity approach* the equation describing mass transport in the water-bearing fractures is as follows (Huyakorn et al., 1983):

$$\nabla \cdot (\mathbf{D}\nabla c) - \nabla \cdot (\mathbf{q}c) + Q_{in}c_{in} - Q_{out}c + (1-\phi_f)\Gamma = \phi_f \frac{\partial c}{\partial t}, \qquad (2.3)$$

where
- c is the concentration of the solute (g/l),
- $\boldsymbol{D}$ is the hydrodynamic dispersion coefficient, which includes dispersion and diffusion (m^2s^{-1}),
- $\boldsymbol{q}$ is the Darcy velocity (ms^{-1}),
- Q_{in} is the term for sources (s^{-1}),
- c_{in} is the concentration in the inflowing water (kgm^{-3}),
- Q_{out} is the term for sinks (s^{-1}),
- ϕ_f is the flow (fracture) porosity (-) and
- Γ is the rate of solute transfer from the matrix block to the fracture ($kgm^{-3}s^{-1}$).

The components of the hydrodynamic dispersion tensor in Eq. (2.3) are

$$D_{ij} = \varepsilon_T |\mathbf{q}| \delta_{ij} + (\varepsilon_L - \varepsilon_T) \frac{q_i q_j}{|\mathbf{q}|}, \tag{2.4}$$

where ε_L is the longitudinal dispersion length (m),
ε_T is the transversal dispersion length (m) and
δ_{ij} is the Kronecker delta function (-).

The Darcy velocity $\boldsymbol{q}$ in Eq. (2.3) in terms of the residual pressure p is

$$\mathbf{q} = -\frac{\mathbf{k}}{\mu}(\nabla p - (\rho - \rho_0) g). \tag{2.5}$$

The molecular diffusion, which dominates the mass transport in the matrix blocks, can be described with a one-dimensional diffusion equation

$$\frac{\partial}{\partial z'}(D_e' \frac{\partial c'}{\partial z'}) = \phi' \frac{\partial c'}{\partial t}, \tag{2.6}$$

where c' is the concentration of the solute (g/l),
D_e' is the effective diffusion coefficient (m^2s^{-1}) and
ϕ' is the porosity in the matrix blocks (-).

In accordance with Archie's law (Valkiainen, 1992), the connection between the effective diffusion coefficient and the porosity can be stated

$$D_e' = 0{,}71 \cdot D_0 \phi'^{1{,}58}, \tag{2.7}$$

where D_0 (m^2s^{-1}) is the molecular diffusion coefficient in water.

Equations (2.3) and (2.6) are coupled by the continuity of the diffusive mass flux at the interface of the fracture and the matrix block. For a rectangular matrix block unit the rate of solute transfer from the matrix block to the fracture is

$$\Gamma = -\frac{1}{a}(D_e' \frac{\partial c'}{\partial z'}\Big|_{z'=a}), \tag{2.8}$$

where a (m) is half the fracture spacing, i.e., half the matrix block.

2.2 Numerical tool (Löfman, 1996)

The flow equation (2.1) and the transport equation (2.3) are coupled by the density ρ and the Darcy velocity **q** (Eq. (2.5)). This results in a system of two non-linear partial differential equations that can rarely be solved analytically. The finite element code FEFTRA was used in this work for the numerical solution.

Table 3.4. The modelling period with comments on the tunnel and shaft updating.

Time step	Date	Comments on modelling
0	0,5 years before 1.10.1990	Start of modelling period
1	1.10.1990	
2	21.05.1991	First tunnel updating, release of groundwater table over the land
3	10.02.1992	
4	10.08.1992	
5	05.10.1992	
6	10.11.1992	First updating of shafts
7	11.02.1993	
8	03.06.1993	
9	03.11.1993	No updating of tunnel
10	16.02.1994	Second updating of shafts
11	16.06.1994	
12	16.09.1994	
13	24.01.1995	Last updating of shafts
14	25.05.1995	
15	24.10.1995	
16	24.04.1996	
17	23.12.1996	

The tunnel and shaft advance is modelled by giving a residual pressure boundary condition for the flow equation (Eq. (2.1)) and a flow rate boundary condition for the transport equation (Eq. (2.3)) to the nodes describing the tunnel and shafts in each time step (see Section 4).

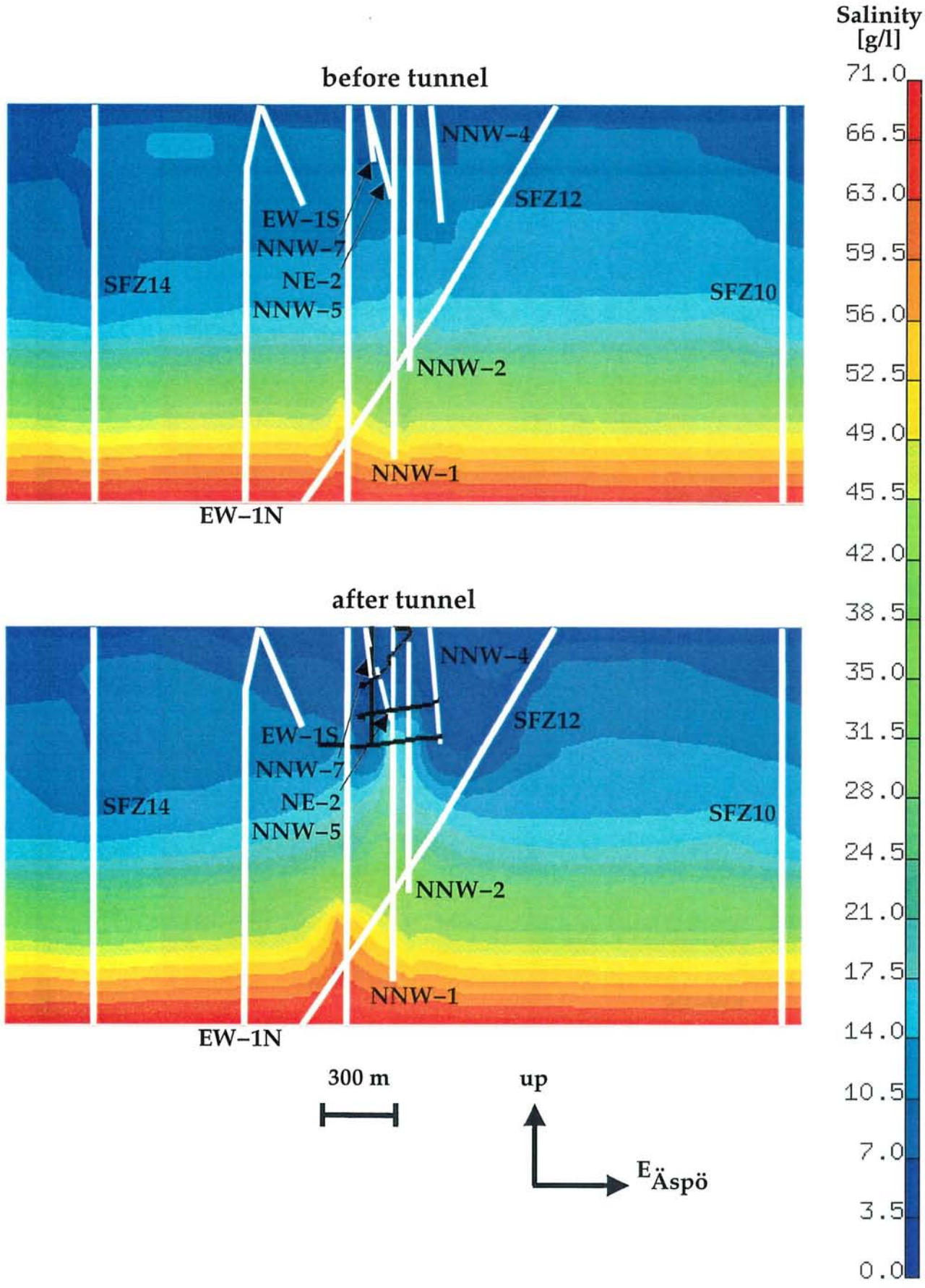
Salinity
[g/l]
71.0
66.5
63.0
59.5
56.0
52.5
49.0
45.5
42.0
38.5
35.0
31.5
28.0
24.5
21.0
17.5
14.0
10.5
7.0
3.5
0.0
before tunnel
NNW-4
SFZ12
EW-1S
NNW-7
NE-2
NNW-5
SFZ14
SFZ10
NNW-2
NNW-1
EW-1N
after tunnel
NNW-4
SFZ12
EW-1S
NNW-7
NE-2
NNW-5
SFZ14
SFZ10
NNW-2
NNW-1
EW-1N
300 m
up
E
Äspö

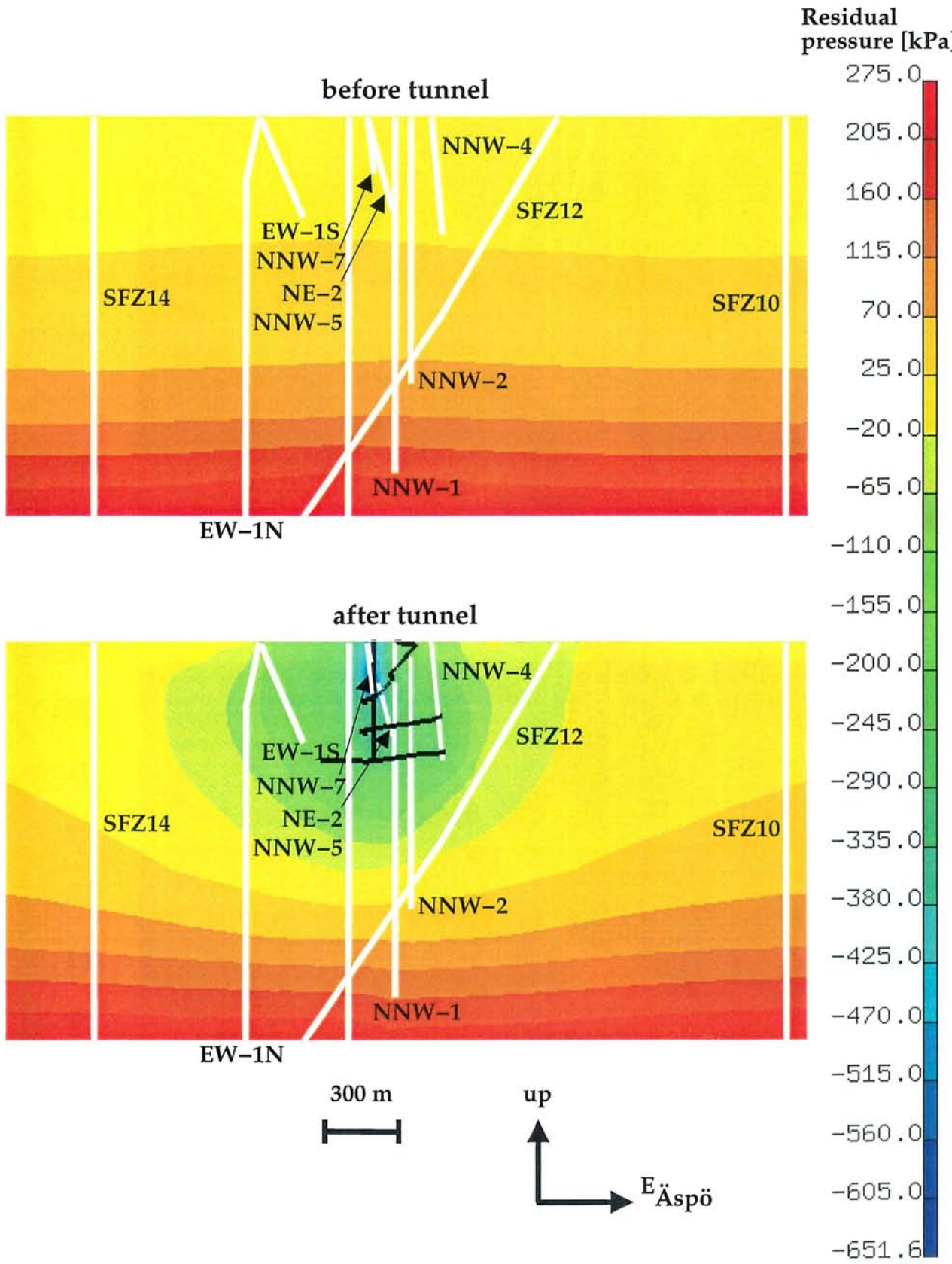
Residual pressure [kPa]
275.0
205.0
160.0
115.0
70.0
25.0
-20.0
-65.0
-110.0
-155.0
-200.0
-245.0
-290.0
-335.0
-380.0
-425.0
-470.0
-515.0
-560.0
-605.0
-651.6
before tunnel
NNW-4
SFZ12
EW-1S
NNW-7
NE-2
NNW-5
SFZ14
SFZ10
NNW-2
NNW-1
EW-1N
after tunnel
NNW-4
SFZ12
EW-1S
NNW-7
NE-2
NNW-5
SFZ14
SFZ10
NNW-2
NNW-1
EW-1N
300 m
up
E Äspö

Table 4.1. Salinity on the vertical boundaries.

Depth (m)	Salinity (g/l)
0	3
200	5
450	10
725	11,6
950	18
1100	40
1500	40

4.3 Residual pressure

The initial residual pressure boundary condition throughout the model was calculated from the salinity given in Table 4.1 using Eq. 3.7. In the first time step the residual pressure in the interior and bottom nodes was released.

The freshwater head assigned with the tunnel nodes is depicted in Figure 4.1. The lowering of the curve in the depth interval 284—348 m is based on a calibration result in the boreholes KAS05—KAS08.

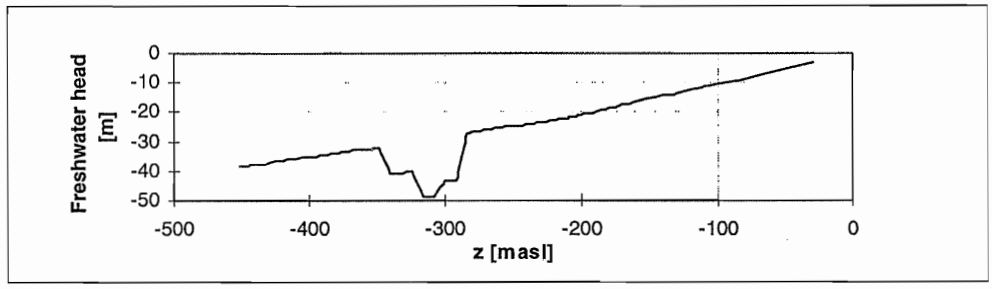

Figure 4.1. The freshwater head (m) used to calculate the residual pressure boundary condition in the tunnel nodes.

The low freshwater head measured in the uppermost packed-off sections of the borehole KAS02 was tried to catch up by assigning the residual pressure corresponding to the freshwater head

$$h_{0,shaft}(z) = -80 \text{ m} \tag{4.1}$$

with the nodes representing the shaft.

The freshwater hydraulic head measured from the boreholes and the calculated residual pressure are related as follows:

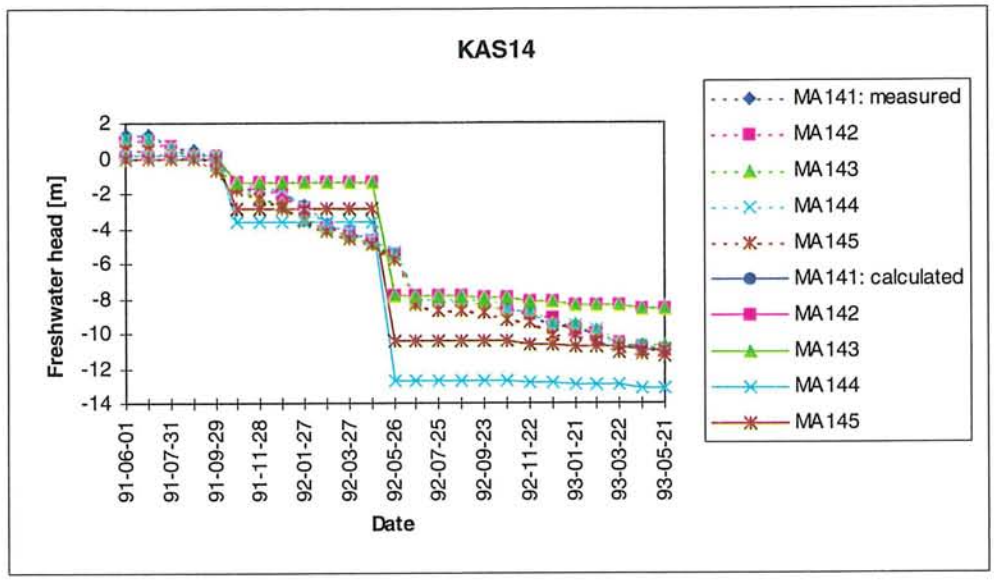

Figure 4.3. (cont.) Calculated and measured freshwater head (m) in the borehole KAS14 as function of time.

4.4 Inflow

Details about the flow measurements can be found in SKB PR 25-95-28, App. 2:4. The flow rates have also been presented by Rhén et al. (1997) (App. 2). However, minor adjustments of the flow rates after August 1995 reported by Rhén et al. (1997) and in SKB PR 25-95-28 have been made in the data delivered.

In each time step the nodes representing the tunnel and the shaft were grouped according to the measurement sections determined by the weirs. The flow rate measured at the weir was then uniformly divided between the nodes.

As suggested, the actual measurements at MA1659G, MA2587G and MA3384G have not been used in the modelling. Tunnel F (parallel and close to tunnel A, approximately section 3400-3510 m) being not modelled, the flow rate in MF0061G was added to MA3411G (50 %) and MA3426G (50 %).

4.5 Mean error and accuracy

The mean error and accuracy are defined as follows (Rhén, Smellie and Wikberg, 1998):

MEAN ERROR

$$dh = \frac{\sum_{i=1}^{n} (h_i^m - h_i^c)}{n}, \tag{4.3}$$

$$dh(abs) = \frac{\sum_{i=1}^{n} \left| h_i^m - h_i^c \right|}{n}, \tag{4.4}$$

ACCURACY

$$Dh = \sqrt{\frac{\sum_{i=1}^{n} (h_i^m - h_i^c - dh)^2}{n-1}}, \tag{4.5}$$

where n is the number of points with measured data used to compare with calculated points, h piezometric level (freshwater head) in metres above sea level (masl). Index m refers to a measured value and c to a calculated one.

These quantities are depicted in the following Figure 4.4 separately in the boreholes KAS02—KAS09, KAS12 and KAS14 and in all the boreholes concurrently.

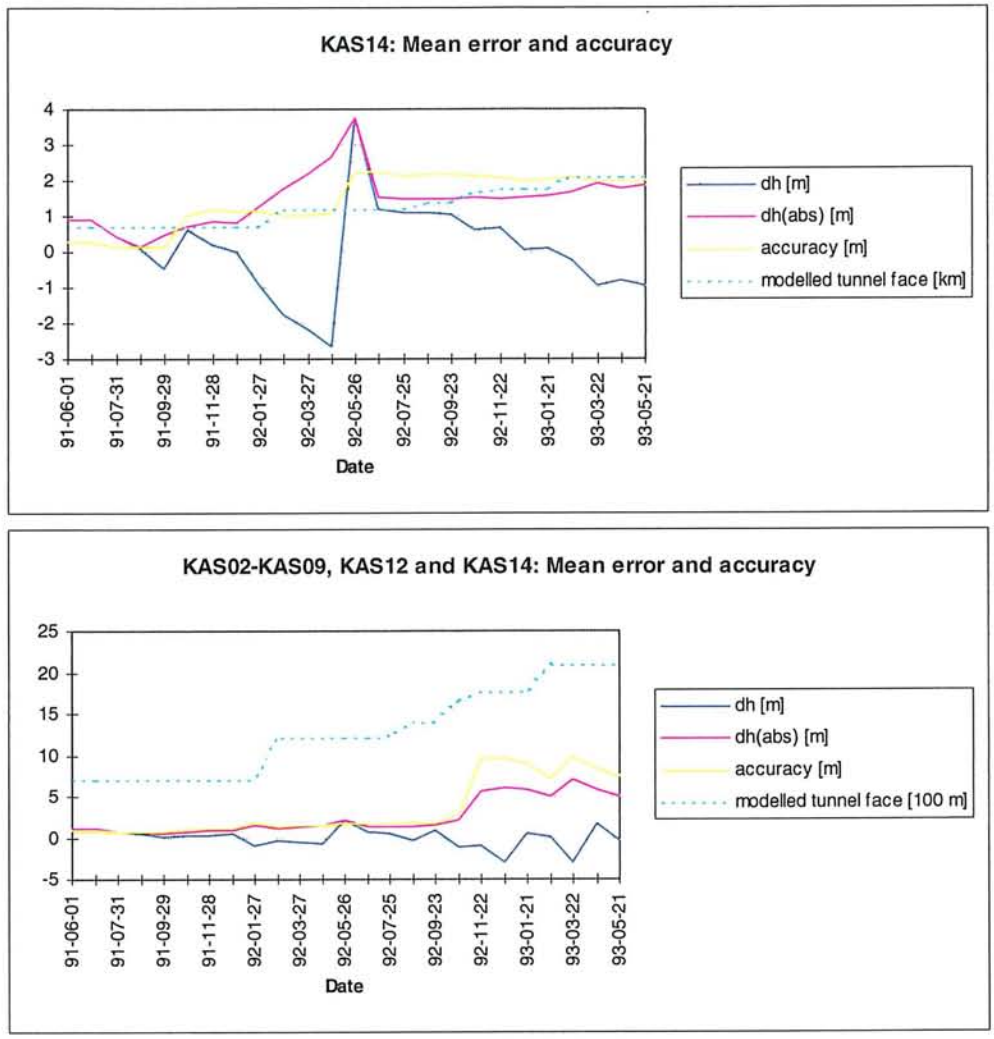

Figure 4.4. (cont.) Mean error and accuracy (m) in the borehole KAS14 and in the whole model as function of time.

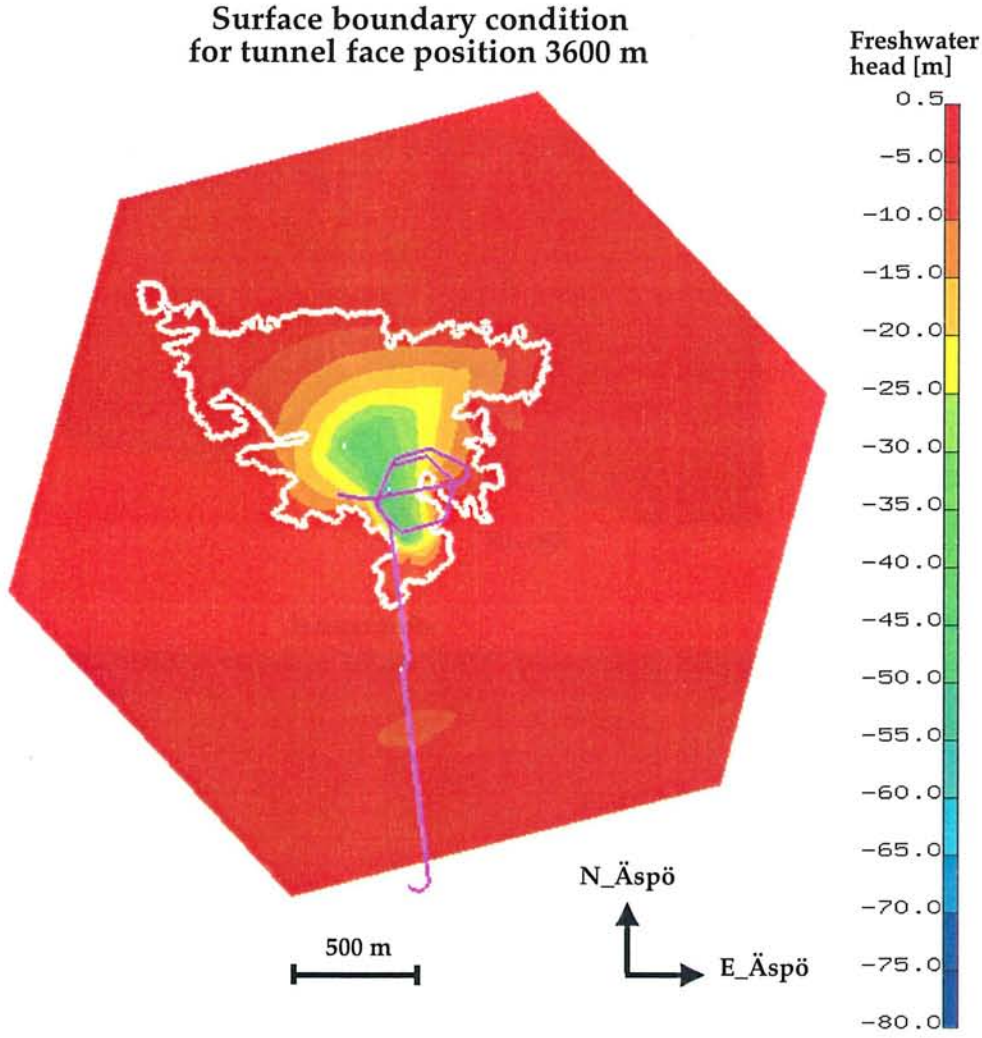

Figure 5.1. (cont.) Surface boundary condition for tunnel face position 3600 m.

5.2 Mixing proportions at control points

The model was firstly solved by using the dispersion lengths 100 m and 10 m for the longitudinal and transversal dispersion lengths, respectively. This usually resulted in an increasing mixing ratio of a water type in a control point. This is illustrated in Appendix B, where the series Cal. 9 depicts this result in the control point SA2783A. This behaviour was tried to change by decreasing the infiltration from the sea by lowering the transmissivity of the uppermost elements of the fracture zones below the sea to the value T=9,3·10^{-9} m^2/s. This did not obviously lead to a better result, however.

After increasing the dispersion lengths tenfold, the behaviour of the mixing ratios as function of time changed considerably (App. B). The mixing ratios could also have been adjusted by lowering the transmissivity of the fracture zones.

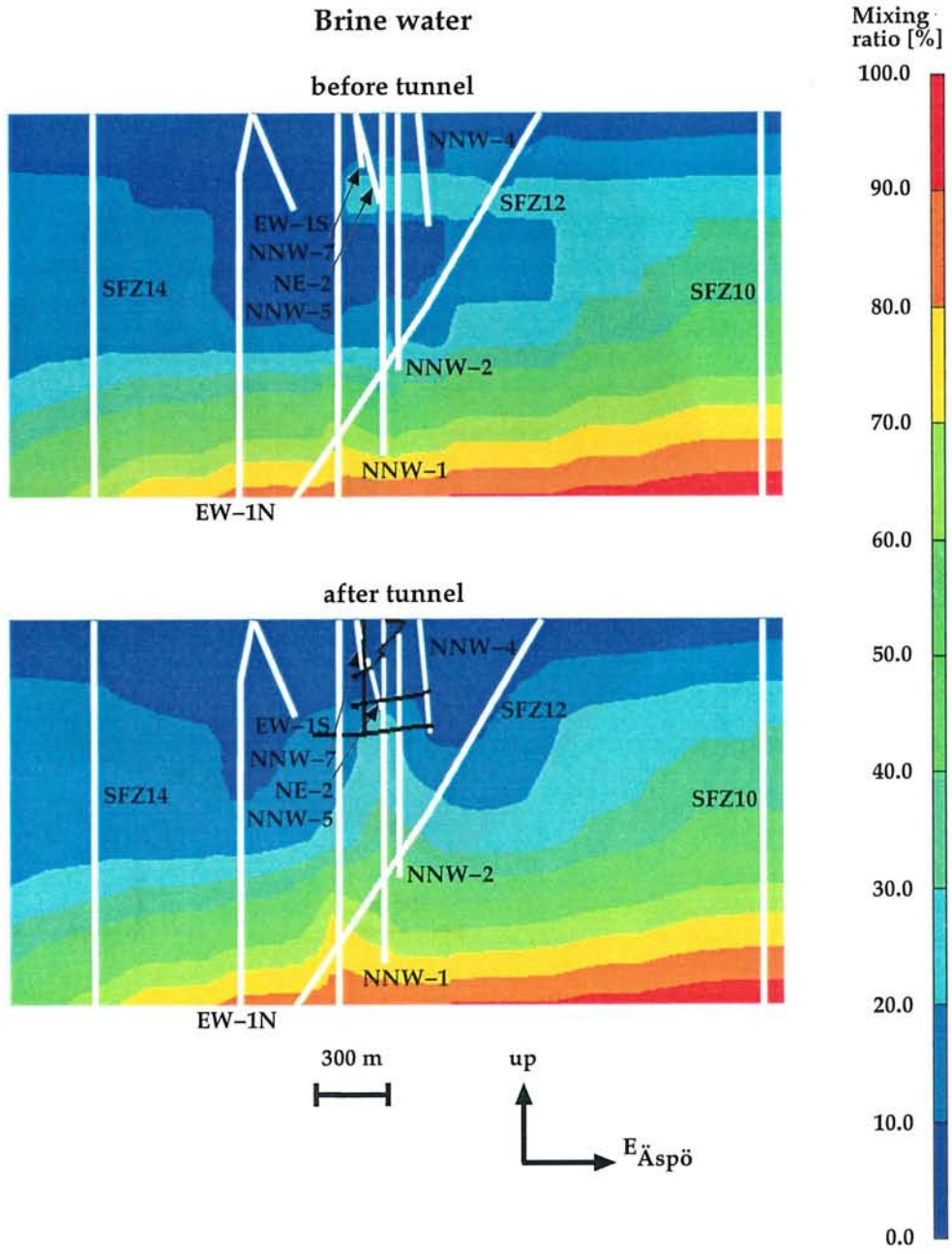

Figure 5.6. The mixing ratio of brine water on an east—west trending cut plane through the control point KA3110A before and after the tunnel construction.

Mixing ratios of brine water in SA2783A; z=-371 m

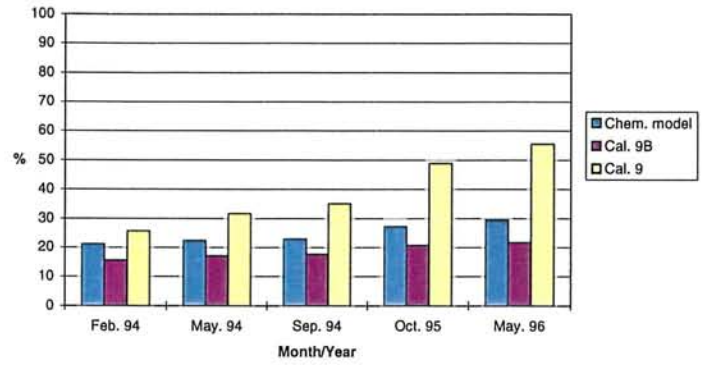

Mixing ratios of glacial water in SA2783A; z=-371 m

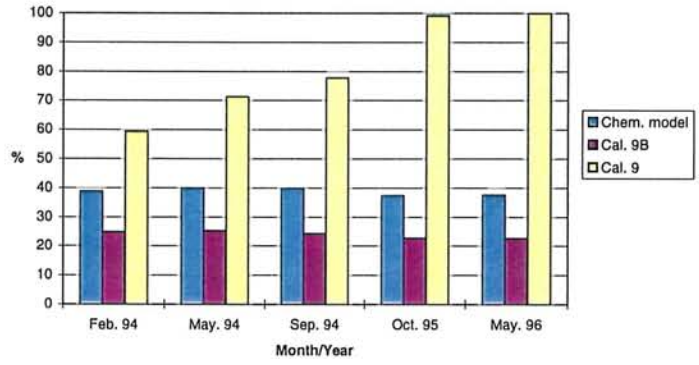

Mixing ratios of meteoric water in SA2783A; z=-371 m

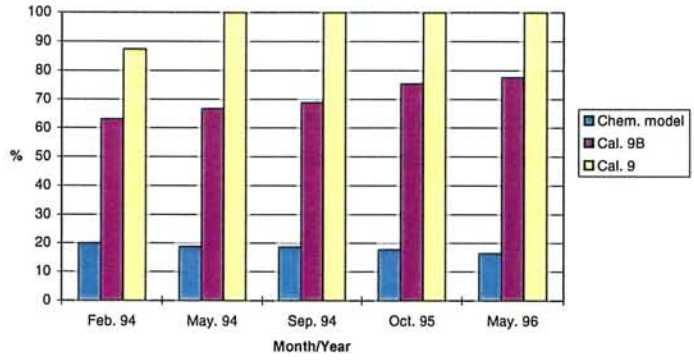

Mixing ratios of baltic water in SA2783A; z=-371 m

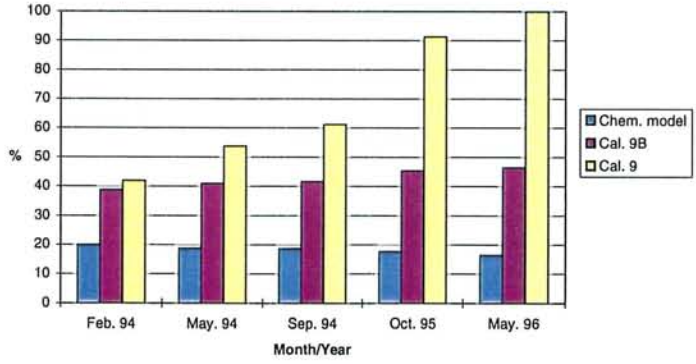

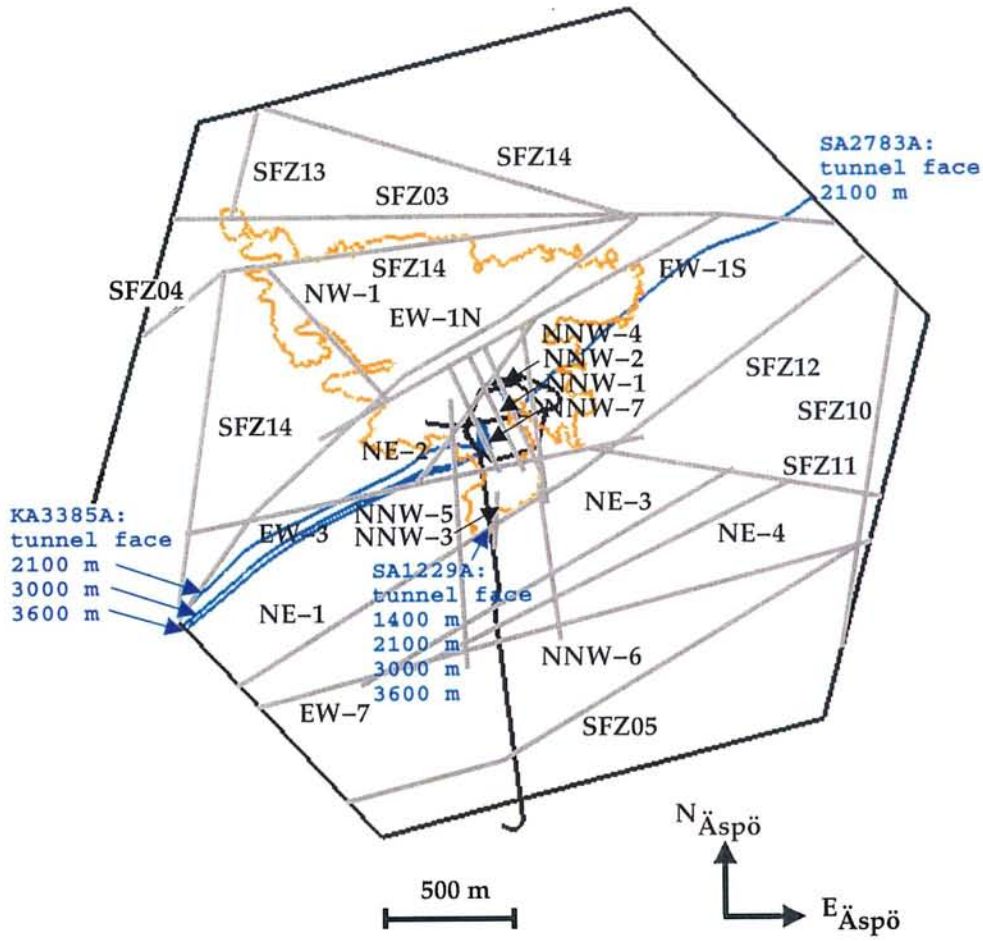

Figure 5.7. Flow paths from SA1229A, SA2783A and KA3385A. The coastline of the Äspö island, the fracture zones at the surface and the model boundaries are also shown.

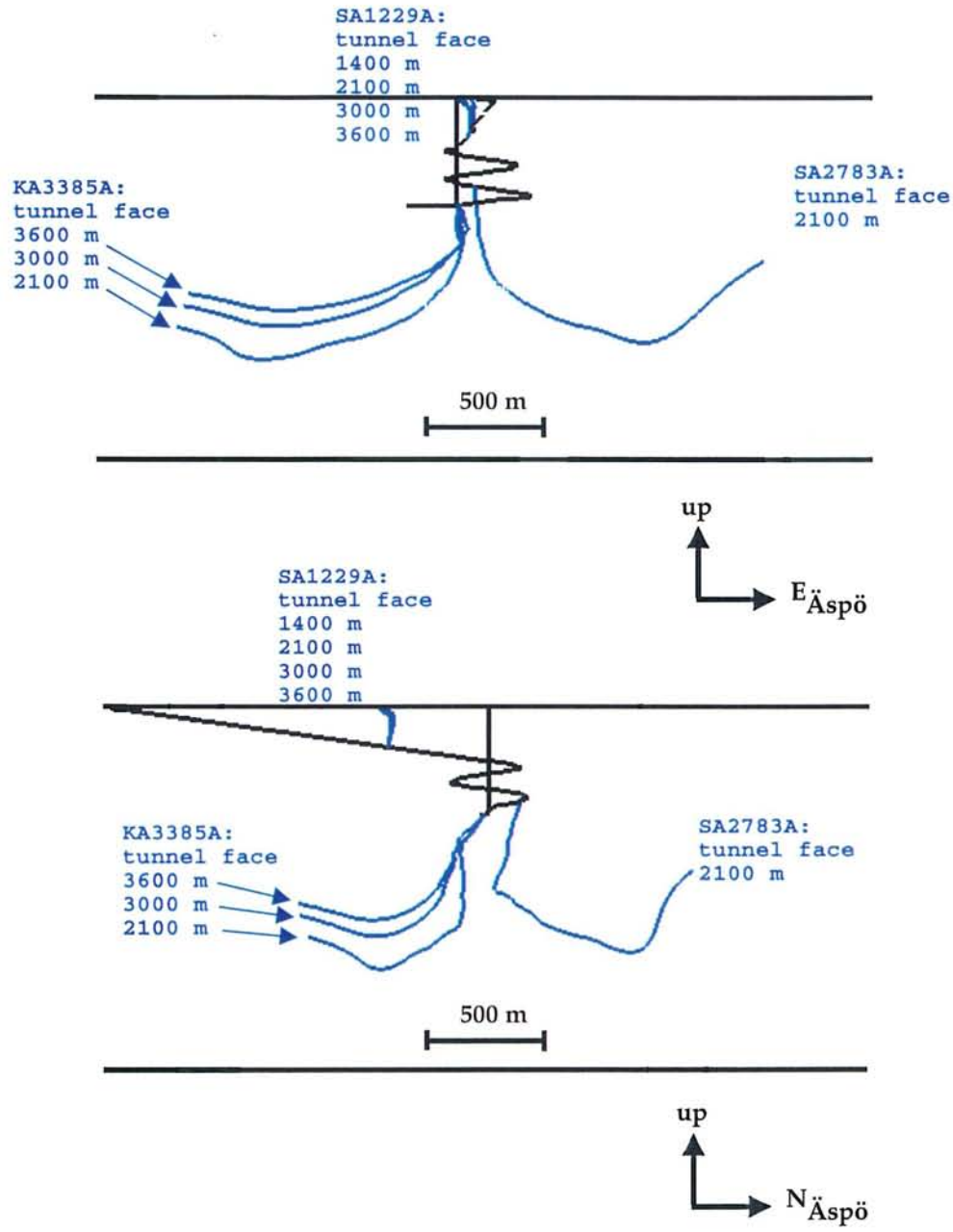

Figure 5.7. (cont.) Flow paths from SA1229A, SA2783A and KA3385A on vertical cross sections.

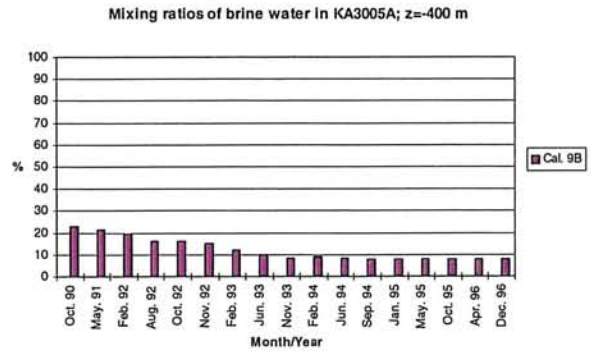

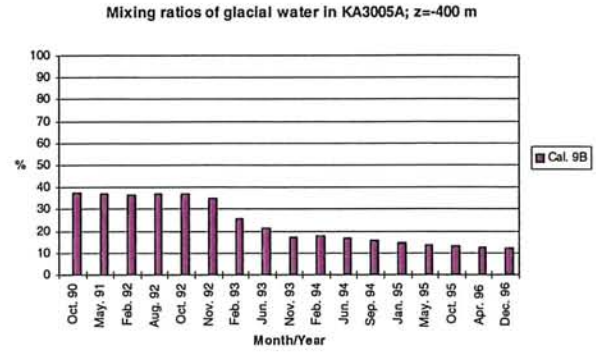

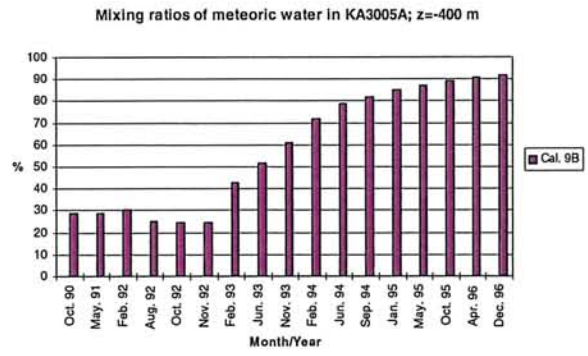

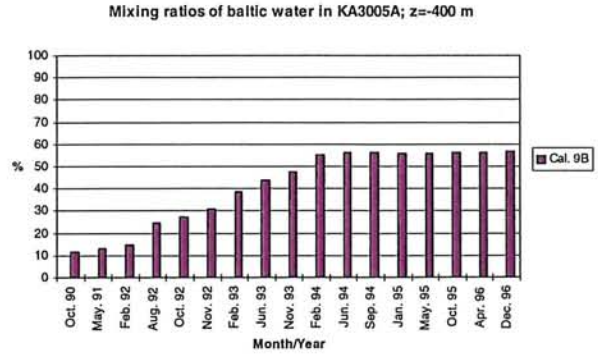

code	date	xmeas	ymeas	zmeas	MEAS: br	gl	me	ba	CALC: br	gl	me	ba
SA0850B	Aug. 91	2146.364	6514.633	-117.736	10.2	10.2	46.7	32.8	7.1	11.5	38.8	48.4

code	date	xmeas	ymeas	zmeas	MEAS: br	gl	me	ba	CALC: br	gl	me	ba
SA1327B	Oct. 92	2111.44	6987.423	-184.085	7	7	51.4	34.7	4.1	7.2	92.4	37.3

Preliminary application of FEGM/FERM to Task 5.

T. Hasegawa, Y. Tanaka, M. Kawanishi and T. Igarashi
(CRIEPI)

Status Report

Preliminary application of FEGM/FERM to Task #5.

Modeling Task #5:

Impact of the tunnel construction on the groundwater system at Äspö,

Hydrological – hydrochemical model assessment exercise

12th Task Force Meeting

20-22, Apr., 1999

By

Takuma HASEGAWA, Yasuharu TANAKA, Motoi KAWANISHI, Toshifumi IGARASHI

CRIEPI

1.Introduction

This document summarizes the modeling approach and results for Task 5 by CRIEPI. Task 5 focus on evaluating the effect of the tunnel construction on groundwater system around Äspö, the changing of the groundwater flow and geochemical distribution. Äspö HRL had been constructed from Oct. 1992 to Sep. 1995. The site scale investigation, ex water head observation and geochemical sampling, has been continued before the tunnel construction. The aim of this study is to check the consistency between groundwater flow and solute transport and to develop the procedure evaluating groundwater system. This kind of work would be useful for disposal assessments.

2.Numerical model description

2.1 Numerical model

The ground water flow and solute transport code called FEGM/FERM have been applied to Task 5. The governing equations are expressed as follows, these codes solve the following continuity equations by using Galerkin method.

Groundwater flow: FEGM

$$F\frac{\partial h}{\partial t} = \nabla \cdot (K\nabla H) + Q \qquad (2.1)$$

$$F = \theta\beta' + \frac{d\theta}{dh} + \frac{\theta}{n}\alpha' \qquad (2.2)$$

Where F is the generalized specific storage coefficient, h is the pressure head, t is the time, K is the hydraulic conductivity tensor, H is the total head, Q is sink/source term, θ is volumetric water content, β' is compressibility of water, n is porosity rate, and α' is compressibility of media.

Solute transport: FERM

$$R\frac{\partial c}{\partial t} = \nabla \cdot (D\nabla c - vc) - \lambda Rc + Q \qquad (2.3)$$

Where R is the retardation factor, c is the concentration, t is the time, D is the dispersion tensor, v is the velocity, λ is the decay constant, and Q is the sink/source term.

2.2 Smeared Fracture model

In order to treat fractures easy, FEGM/FERM have the smeared fracture model which incorporates the property of the fracture into finite element by volume weighted method. When the fracture intersects several finite elements as shown in Fig.2.1, the parameter of shadowed finite element change to volume weighted value.
In this study, this smeared fracture model was used to consider the fracture zone.

3.Modeling description

3.1 Modeling area

In this study, site scale groundwater flow and solute transport was expected, and the important factors of modeling are rainfall on island area, seawater inflow, tunnel and shaft construction. Including aforementioned factor and avoiding interference of boundary condition, modeling area is decided as Fig 3.1. The modeling area was covered with Easting 1000m-3000m, Northing 5500-8000m and depth 0m-1000m on Äspö coordinate.

3.2 Material property

Assuming that the material properties are divided into two categories, rock mass and fracture. Their properties are characterized as follows.

- Rock mass has one property, which does not depend on geometry.
- Fracture zones consist of 17 Fractures, which have the defined orientation and dip.

(1) Hydraulic conductivity

Many hydraulic tests have performed in Äspö HRL. The results of hydraulic test for fracture is summarized in Table 3.1. The values of mean, median, task 3 were used in the modeling work. Otherwise, the conductivity of rock mass tends to depend on test scale. In this study, two isotropic models and one anisotoropic model were used for rock mass; these values correspond to 3m, 15m hydraulic test and 15m hydraulic test in the tunnel. The conductivities of rock mass and fracture were shown in Table 3.2.

(2) Specific storage

The value of specific storage is around $10^{-6}m^{-1}$ by interference test, so $1.0x10^{-6}m^{-1}$ is used as the specific storage.

(3) Dispersion length

Generally, the dispersion length depends on the experiment scale, and the longitudinal dispersion length is 1/10 of the experiment scale, and the transverse dispersion length is 1/10 of longitudinal dispersion length. So 20m and 200m is used as the longitudinal dispersion length.

(4) Effective porosity

On basis of tracer experiment, the linear relationship between conductivity and effective porosity rate are derived as follows,

$$n_e = 34.87K^{0.753} \qquad (3.1)$$

Where n_e is the effective porosity and K is water conductivity (m/sec).

Table 3.2 Input parameters for Fracture zone and Rock Mass zone.

Fracture Zone Model	Rock Mass Zone Model
·Model96(Mean) ·Model96(Median) ·Model94(Task 3 update model) (see TR96-06)	Isotropy model ·1.5 x10^{-9}m/sec ·6.0 x10^{-9}m/sec Anisotropy model ·Kx,Ky,Kz:5.3 x10^{-8},3.0 x10^{-9},3.3 x10^{-9}m/s (Rotating 130 degrees from North to East)

3.3 Boundary conditions

The important factors of Task 5 modeling are rainfall on island area, seawater inflow, tunnel and shaft construction. These factors is modeled as follows,

(1) Groundwater flow

The surface of Äspö Island is modeled as constrained flux boundary to consider the rain infiltration. Baltic Sea surrounds the Äspö Island; the sea area is modeled as constrained head boundary. Tunnel and shaft are modeled as time changing boundary. This time changing rate is decided from progress of these. The progress of tunnel construction is expressed by the transmisivity changing at the line element. In the case of the flux boundary used, tunnel sections are divided by weir section. The bottom of the model is prescribed by no flux boundary, the side boundary of the model is constrained by the hydrostatic head on basis of sea level.

(2) Solute transport

The Äspö Island and Baltic Sea on upper part of model are prescribed as constrained concentration boundary, these salinity are 0% and 0.6%, respectively. Here assuming that salinity of Baltic sea is 6g/liter. The side boundary condition is interpolated from measured initial salinity distribution at Aspo KAS boreholes. The initial salinity distribution tend to depend on depth, so the relationship between salinity and depth is assumed as following equation on the side boundary.

$C_{salinity}=6+0.016Z$ (3.2)

Here $C_{salinity}$ is salinity (g/liter), Z is depth from sea level (m).

Table 3.3 Boundary conditions.

Boundary	Groundwater flow	Salinity concentration
Upper Island area Sea area Lower Side	 Constant flux Constant head: Sea level No flux Constant head: Hydrostatic	 Fresh water:0% Sea water:0.6% No flux Interpolated from sampled data in Äspö boreholes

3.4 Finite element mesh

Figure 3.2 shows the finite element mesh in this study. This finite element mesh consisted of 159,214 hexahedral elements and 349 truss elements. Tunnel and shafts are modeled as line elements.

4. Numerical calculation

4.1 Complementary calculation

To select the material properties in Table 3.2, some numerical calculations were performed to the following matter,

(1) Undisturbed condition (Initial pressure head distribution and Initial salinity distribution)

(2) Long term Ponping Test 2 (it called LPT2.)

(1) Undisturbed condition

Checking the material properties, some calculations were performed to check the consistency of initial pressure head distribution and initial salinity distribution. On basis of meteoric data, about 100mm/year infiltration is expected, but on calculation it makes very high water table. Therefore infiltration rate was estimated by sensitive analyses of material properties. The fracture transmisivities are not so sensitive for water table, so the infiltration rate was estimated for each rock mass model shown in Table 4.1.

Table 4.1 Estimated infiltration rate

Rock Mass Model	Isotropy 1.5×10^{-9}m/s	Isotropy 6.0×10^{-9}m/s	Anisotropy
Precipitation rate (mm/year)	2.6	11.0	25.6

We performed five numerical calculations for initial salinity distribution The measured undisturbed salinity distribution is shown in all figure by asterisk, and the calculated salinity distribution are shown in Fig.4.1 - Fig.4.2. Fig.4.2 shows the sensitivity of the material properties. Fig.4.3 shows the sensitivity of dispersion coefficient. On this calculation10 times dispersion lengths is used. (a_L=10 a_T=200m.)

(2) LPT2 Experiment

We perform the numerical calculation for LPT2 to evaluate the consistency of update Äspö model. The salinity effect is not taken into account these calculations.

We performed five numerical calculations for LPT2 by changing transmisivity of rock mass and fracture in Table 3.2. Fig 4.4 shows the normal probability plot of error that is the difference between measured and calculated. Table 4.2 and 4.3 summarize the results of Fig.4.4. The relationships between drawdown and distance from ponping area are shown in Fig.4.5.

Table 4.2 Sensitive analysis for Rock Mass Model

Fracture Model	Model 96 (Mean)		
Rock Mass Model	Isotropy 1.5×10^{-9}m/s	Isotropy 6.0×10^{-9}m/s	Anisotropy
Average(m)	0.169406	0.369604	0.845347
Standard derivation	2.257223	2.172349	2.26681

Table 4.3 Sensitive analysis for Fracture Zone Model

Fracture Model	Model96 (mean)	Model96 (median)	Task3
Rock Mass Model	Isotropy 1.5e-9m/s		
Average	0.169406	0.872079	1.682574
Standard derivation	2.257223	2.279059	2.358411

Measured salinity distribution (Fig. 4.1) shows the mixing effect of meteoric water could be reached at 200m depth on Kas02 and Kas03. The result that Model96 (mean) and Isotropic (1.5×10^{-9}m/s) used shows the mixing occurred at 200m depth, others shows the mixing occurred at 100m or 300m. On sensitive analysis of dispersion show a_L=200m is better agreement with measured than 20m .So hundred-meter-order dispersion length is expected on the solute transport.

Concerning with LPT2 calculation, The result that Model96 (mean) and Isotropic (1.5×10^{-9}m/s) used is also better than others.

4.2 Groundwater flow and solute transport during tunnel construction

The results of groundwater flow and solute transport during tunnel construction are explained in this section. On this calculation, assuming that 1.5×10^{-9}m/s (isotropic) for the rock mass permeability and mean value in Table 3.2 for fracture permeability were used, since the results of complementary calculation show the result of these values used is better than others.

The progress of tunnel construction is expressed by the transmisivity changing at the line element. The flux boundary is given at weir section on basis of measured flux. The unsteady state calculations were performed by using time depending boundary. On these calculation the salinity effect is not considered.

Initial and boundary condition of solute transport is from the result of VOXEL code developed by SKB and 3D bi-liniear basis function is used to distribute it to nodal point of FEM.

The results of drawdown at KAS02-09, 12, 14 during tunnel construction shows in Fig.4.6. Fig.4.6 shows the result of constrained flux boundary at tunnel weir position. Fig 4.7 shows mean error between measured and calculated head during tunnel construction. Fig.4.8 shows the trajectory used back ward method. It shows the origin point and velocity to control point at certain time. The results of mixing portion at control point are

shown in Fig. 4.8.

5.Main results

1)The model, which Mean value of Model 96 for fracture model and 1.5×10^{-9}m/sec for rock mass model are used, made good agreement with measured. On solute transport hundred-meter-class dispersion length could be expected.

2) The calculated drawdowns at KAS02,04,05 are disagreement with measured. However it will be better by changing the transmisivity of NNW-1, NNW-7.

3) The real velocity in fracture zone is very fast, it is not good condition to calculate solute transport by continuity model. However trajectory shows our calculations are valid on such condition.

Reference

Rhen I. et al, 1997, Aspo HRL- Geoscientific evaluation 1997/5, Models based on site characterization, 1986-1995 TR97-06.

Igarashi T. et al., 1994. Application of three-dimensional smeared fracture model to the groundwater flow and solute migration of LPT2 experiment, ICR94-08.

Tanaka Y. et al., 1996, Application of three-dimensional smeared fracture model to the hydraulic Impact of Aspo tunnel, ICR96-07.

Svensson U., 1997, A site scale analysis of groundwater flow and salinity distribution in the Aspo area, TR97-17.

Table 3.1 Transmisivities of fracture zone.

Task3
data from TR-96-07, Table 3-1

Fracture Zone	Width(m)	T(m^2/sec)	S(-)	Comments
EW-1_{wp}	1	2.00E-05	2.00E-05	
EW-1, N	1	4.00E-07	1.00E-05	
EW-1, S	30	1.40E-04	3.00E-04	
EW-3_r	12.5	2.00E-05	1.25E-04	-200<z<0
lower side		5.00E-07	1.25E-04	z<-200
EW-5_{wp}	100	2.00E-05	1.40E-05	
EW-7_{wp}	1	1.40E-04	1.00E-05	
EW-7_r	15	6.00E-06	1.50E-04	
NE-1_r	30	4.50E-04	2.60E-05	-300<z<0
lower side		2.00E-04	3.00E-04	z<-300
NE-2_r	3.3	5.00E-06	3.30E-05	
NE-3_r	50	4.30E-04	5.00E-04	
NE-4_r	40	3.40E-04	4.00E-04	
NW-1_p	5.5	7.00E-06	5.50E-05	
NNW-1_{wp}	2	2.00E-05	2.00E-05	
NNW-2_{wp}	2	7.00E-05	2.00E-05	
NNW-3_{wp}	2	2.00E-05	2.00E-05	
NNW-4_{wr}	4.3	1.40E-04	4.30E-05	
NNW-5_{wp}	2	5.00E-05	2.00E-05	
NNW-6_{wp}	2	5.00E-05	2.00E-05	
NNW-7_w	2	2.70E-05	2.00E-05	

w:water bearing structure
r:revised sturcture
ppredictive structure
nnew structure

Task5
data from TR-97-06, Table A2-7 and Table A2-8

Fracture Zone	Width	T(mean)	T(median)	S	n_e	Comments
unit	m	m^2/sec	m^2/sec	-	-	
EW-$1N_r$	30	5.20E-07	1.50E-06			
EW-$1S_r$	30	1.20E-05	2.20E-05			
EW-3_r	15	1.70E-05	2.40E-05			-300<z<0 Upperside
lower side	15	5.00E-07				z<-300 Lower side
EW-7_r	10	1.50E-05	6.80E-05			
NE-1_r	30	2.20E-04	3.00E-04	2.60E-05	7.00E-03	S=2.6e-5,ne=7.0e-3
NE-2_r	5	1.20E-07	4.10E-07			
NE-3_r	50	3.20E-04	2.90E-04			
NE-4_r	40	3.10E-05	3.00E-05			NE-4s+Ne-4n
NW-1_{wp}	10	4.10E-07	1.70E-07			
NNW-1_{wp}	10	8.60E-06	1.10E-05	5.00E-06		S=5.0e-6
NNW-2_{wr}	20	2.40E-05	5.60E-05	2.00E-06	0.0034	S=2.0e-6,ne=3.4e-3
NNW-3_{wp}	20	2.00E-05				
NNW-4_{wr}	20	6.50E-05	1.50E-04			
NNW-5_{wp}	10	4.00E-06	2.00E-06			
NNW-6_{wp}	20	1.40E-05				
NNW-7_{wn}	20	7.50E-06	4.80E-06			
NNW-8_{wn}	20	8.40E-06	1.00E-05			

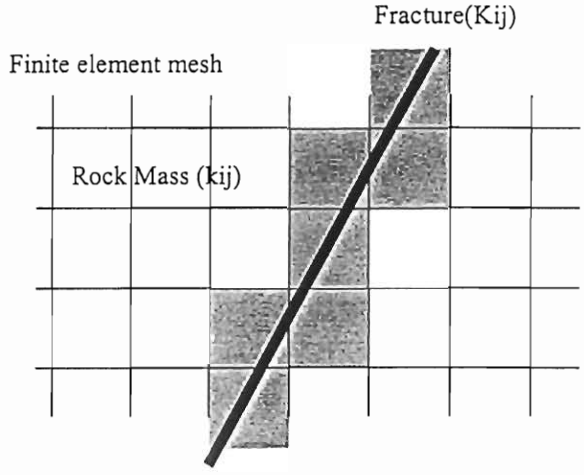

Fig. 2.1 Concept of smeared fracture

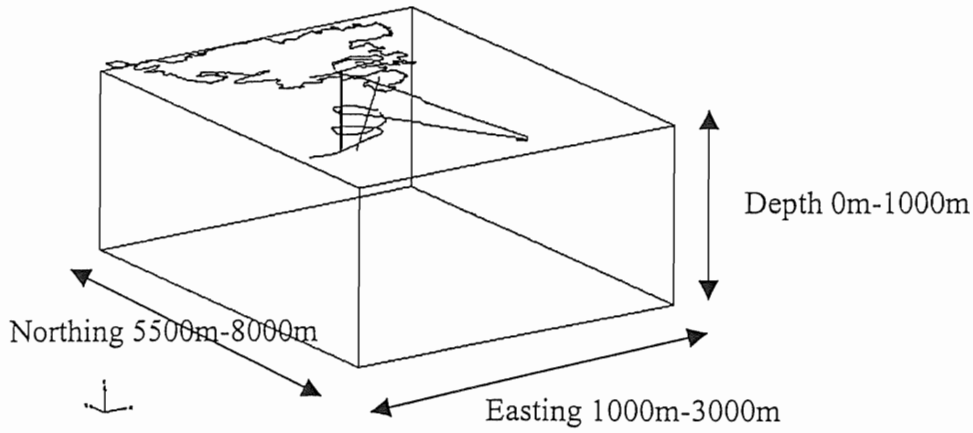

Fig. 3.1 outline of the modeling area.

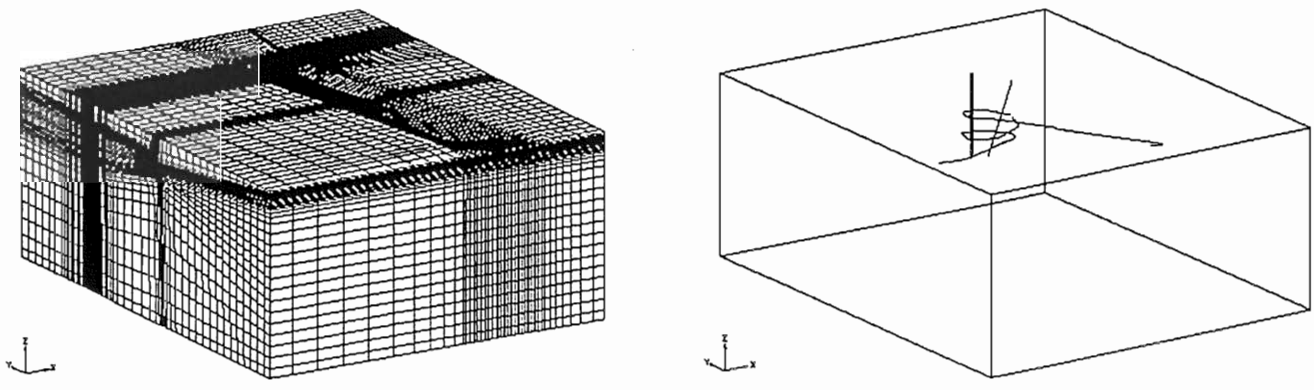

Fig. 3.2 Finite element mesh (159,214 hexahedral element and 349 truss element.)

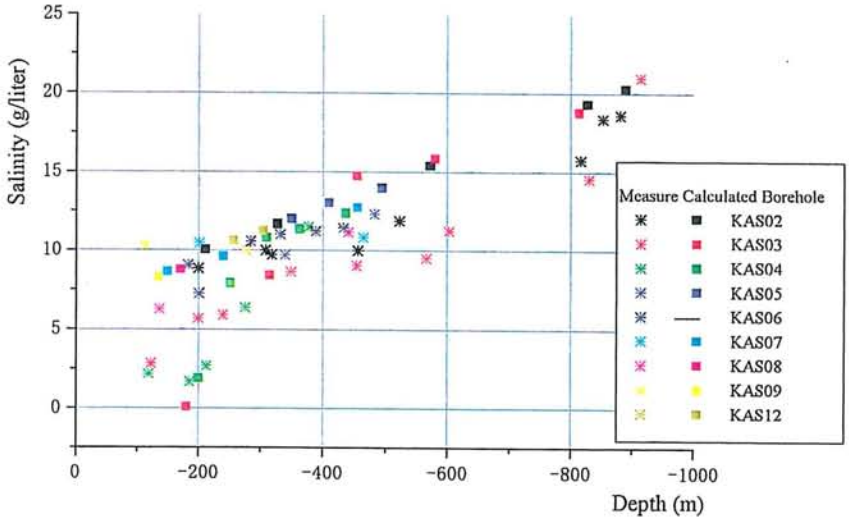

Fig. 4.1 Initial salinity distribution
(Rock mass: $1.5x10^{-9}$m/s, Fracture: Model96 Mean)

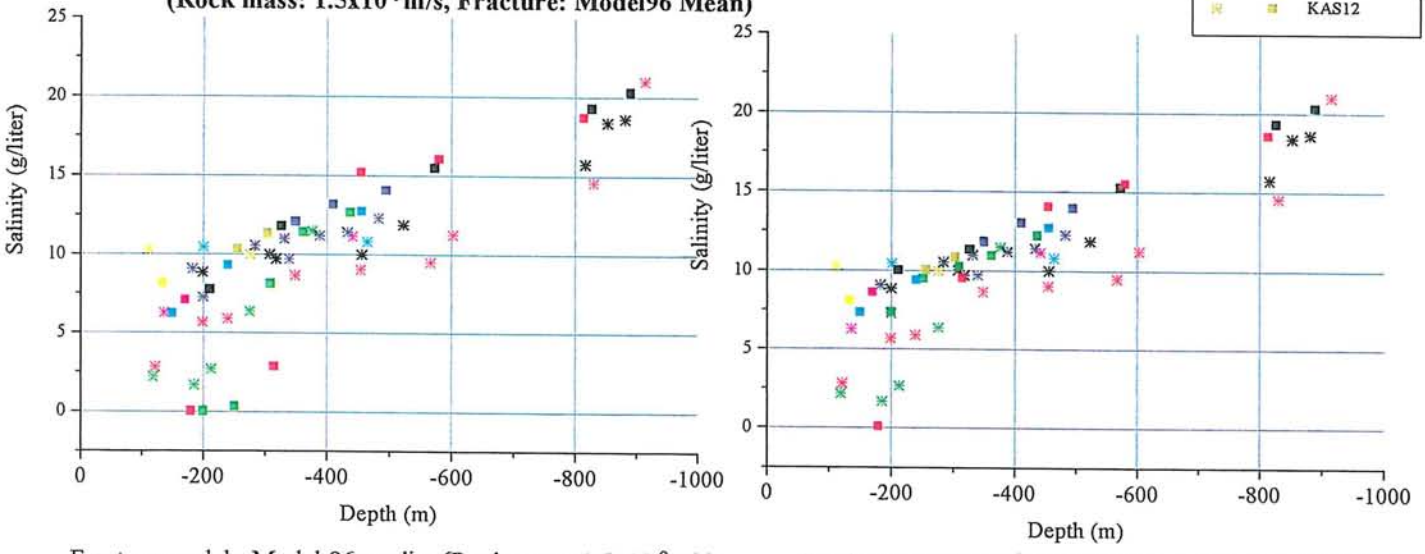

Fracture model : Model 96 median(Rock mass: $1.5x10^{-9}$m/s)

Rock mass: $6.0x10^{-9}$m/s (Fracture model : Model 96 mean)

Fig. 4.2 Sensitive analysis of Intial salinity distribution for Rock mass and fracture model

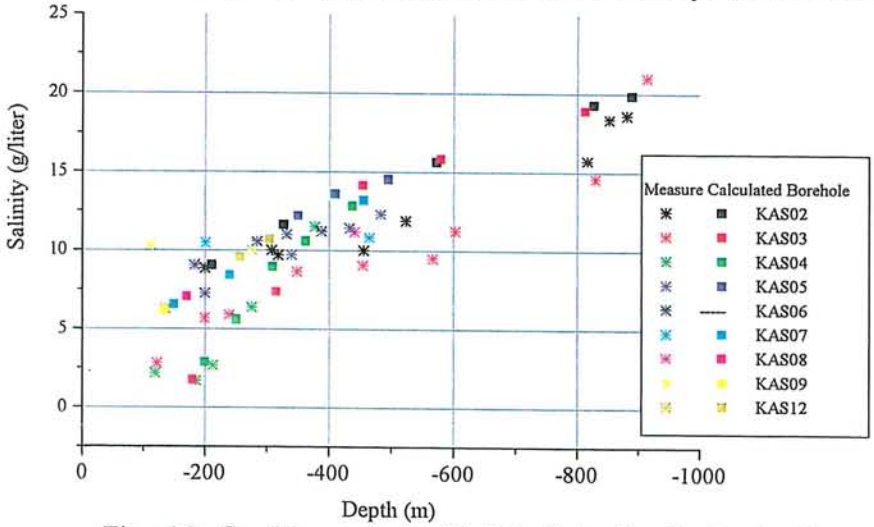

Fig. 4.3 Sensitive analysis of Intial salinity distribution for dispersion parameter
(Rock mass: $1.5x10^{-9}$m/s, Fracture: Model96 Mean
Dispersion Coe. $a_L=10a_T=200$m)

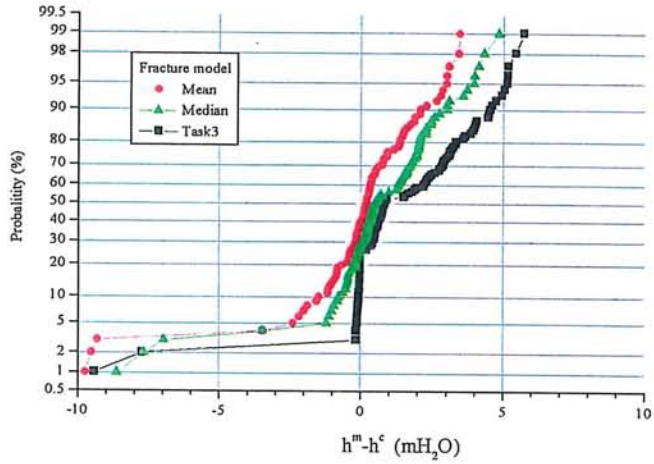

(1) Sensitive analysis of fracture zone model for LPT2
(normal probability plot of errors for LPT2)

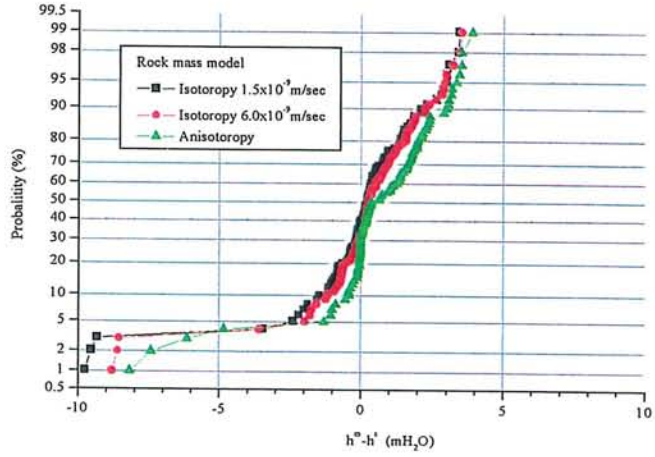

(2) Sensitive analysis of Rock mass model for LPT2
(normal probability plot of errors for LPT2)

Fig.4.4 Sensitivity of Rock mass model and Fracture model for LPT2

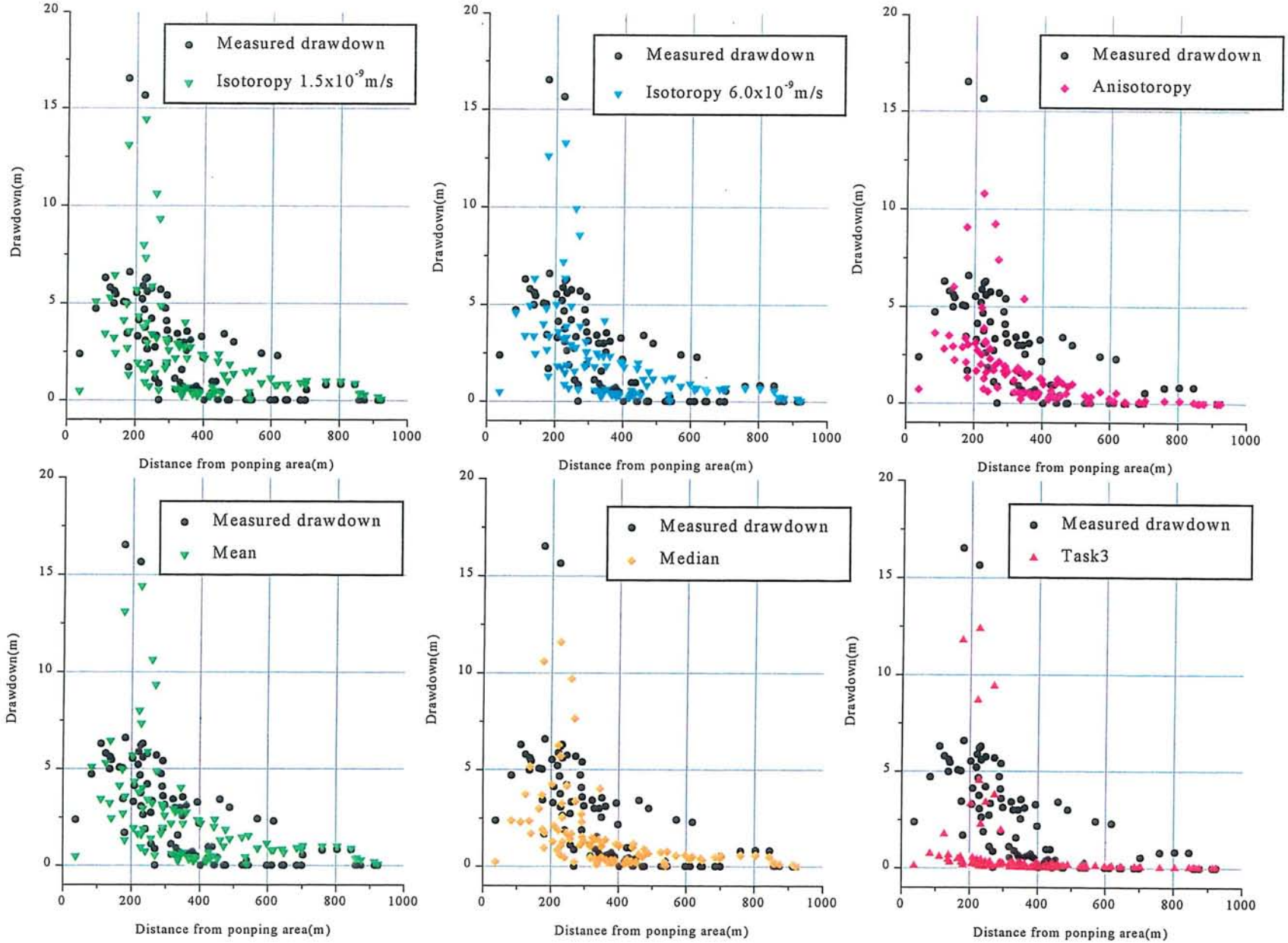

Fig. 4.5 Sensitive analysis of Rock mass model nad Fracture zone model for LPT2

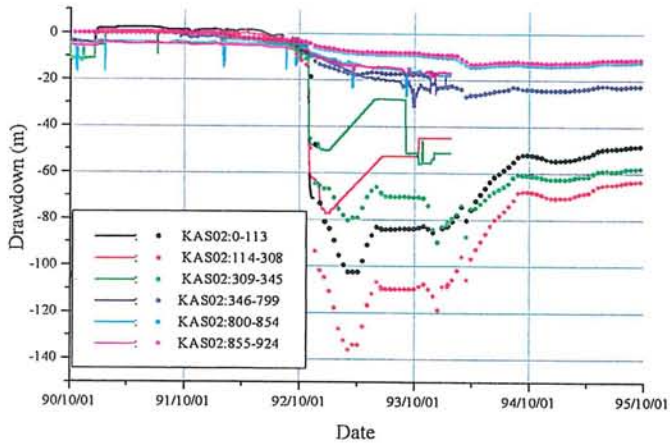

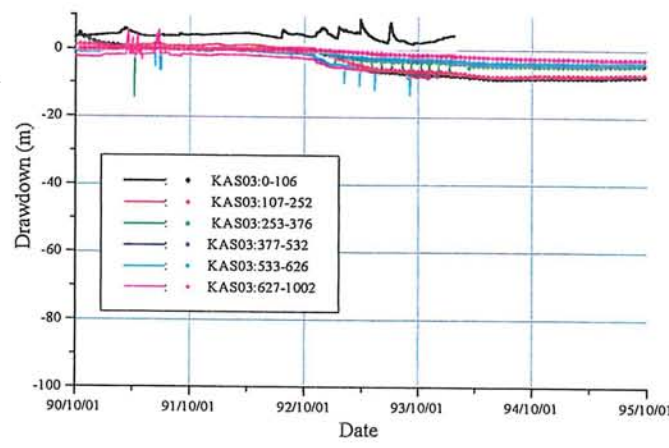

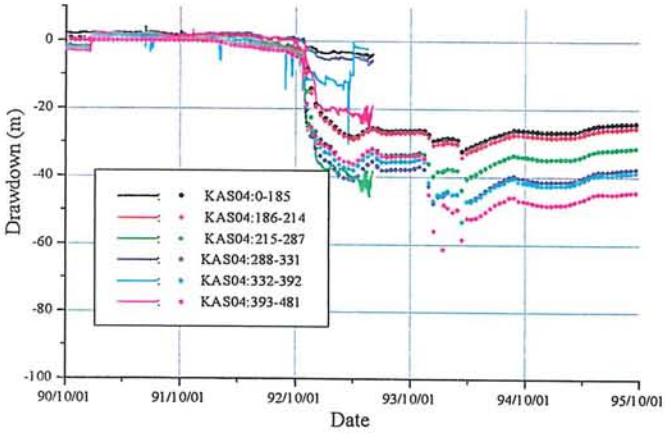

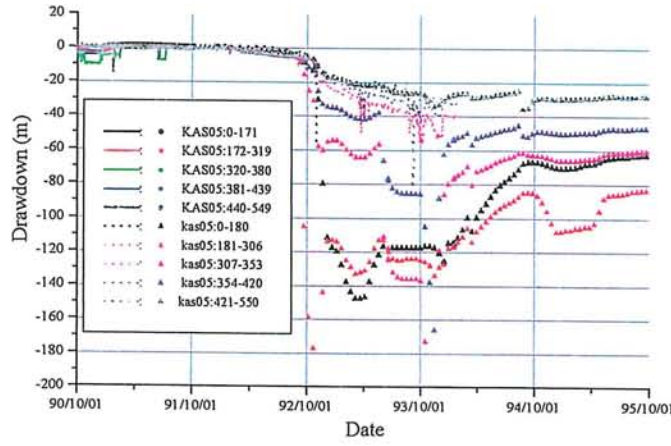

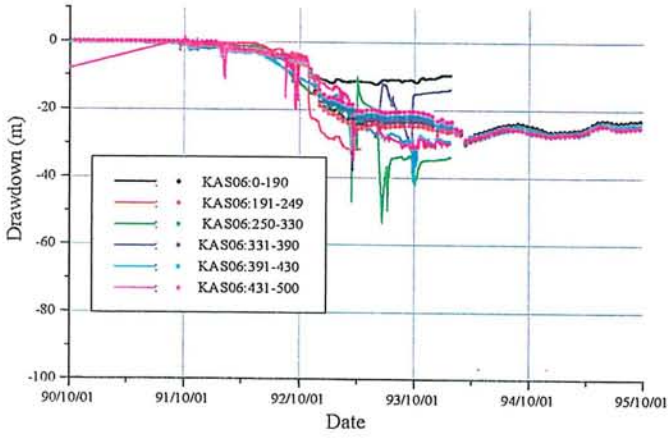

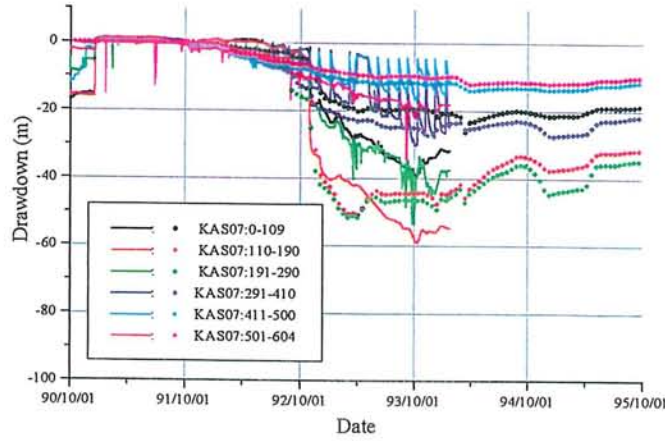

Fig.4.6 Drawdown during tunnel construction(---:measured, ·:calculated)
Constrained flux boundary used (Measured flux at weir)

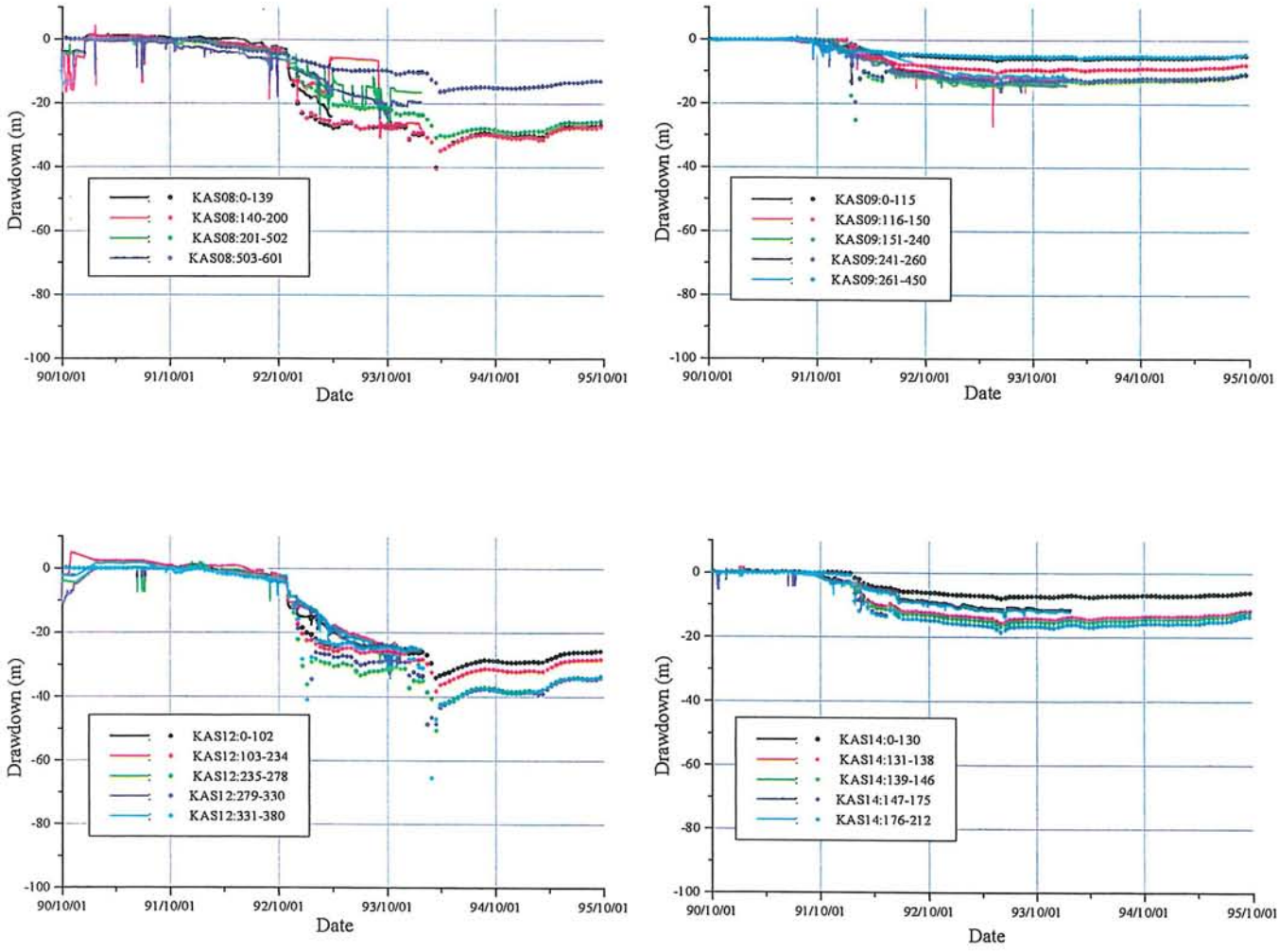

Fig.4.6 Drawdown during tunnel construction(---:measured, ·:calculated)
Constrained flux boundary used (Measured flux at weir)

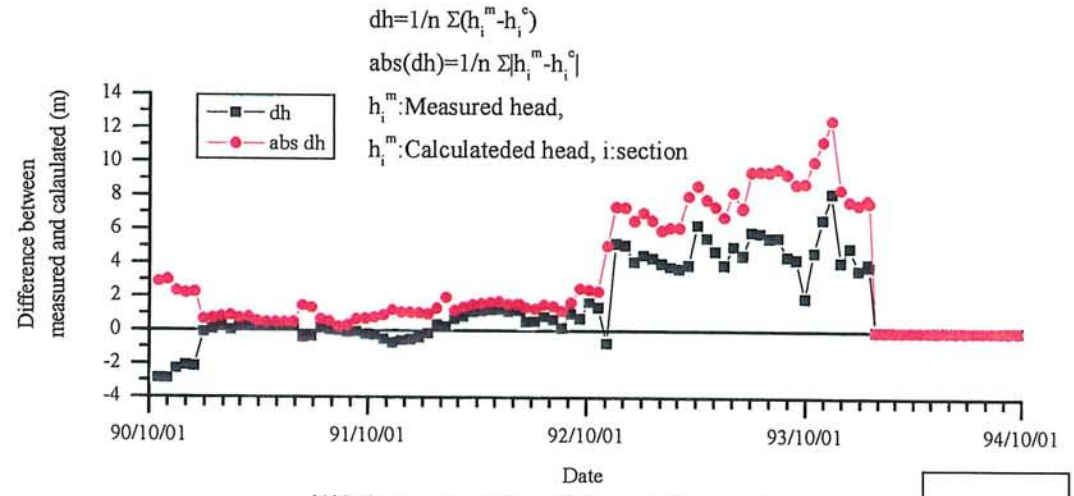

(1)Mean error for all borehole section

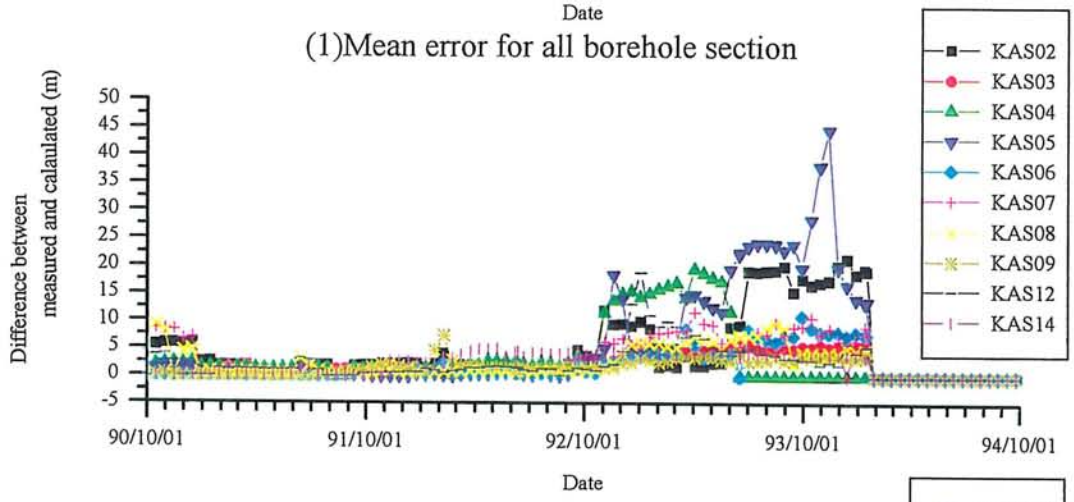

(2)Mean error (abs dh) for each borehole section

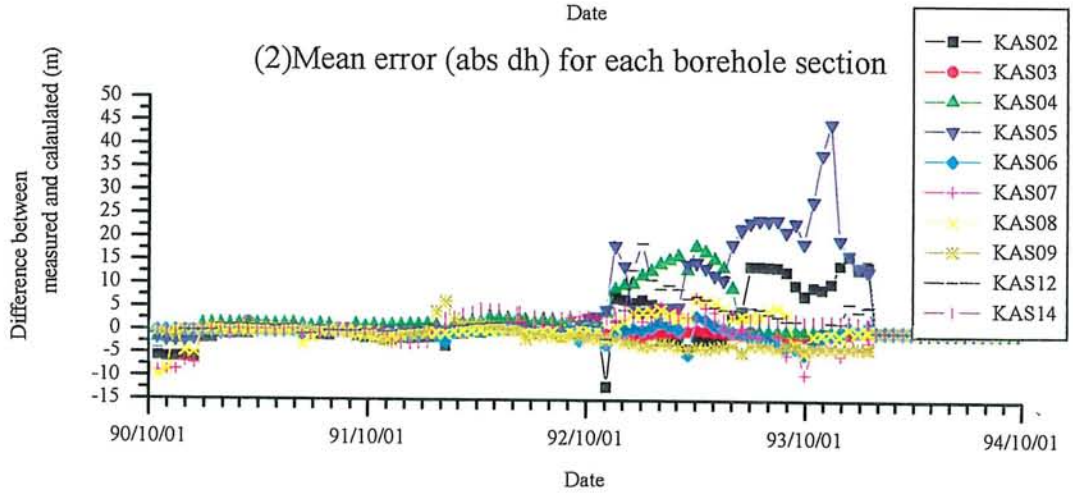

(3)Mean error (dh)for each borehole section

Fig. 4.7 Mean error changing during tunnel construction.

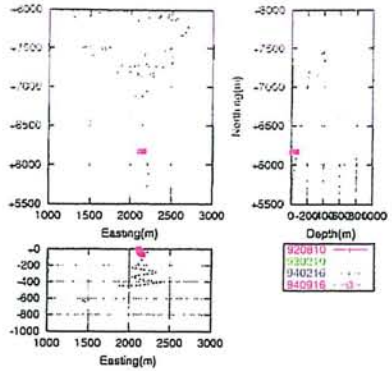

(1)KR0012B

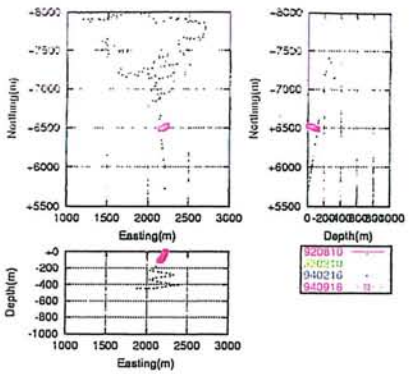

(2)SA0813B

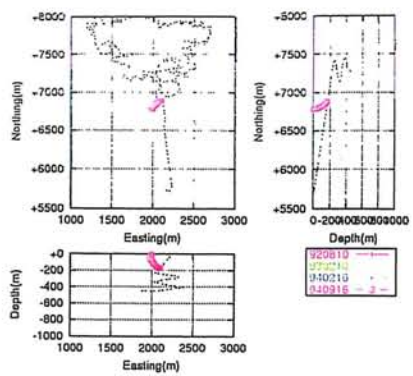

(3)SA1229A

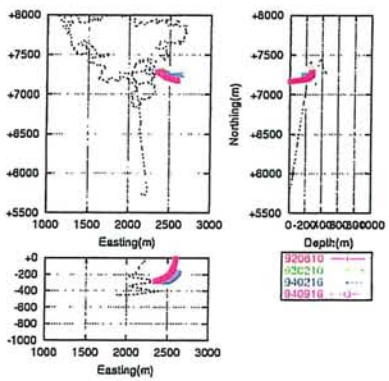

(4)SA2074A

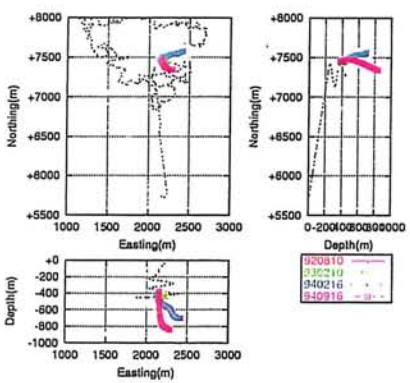

(5)SA2783A

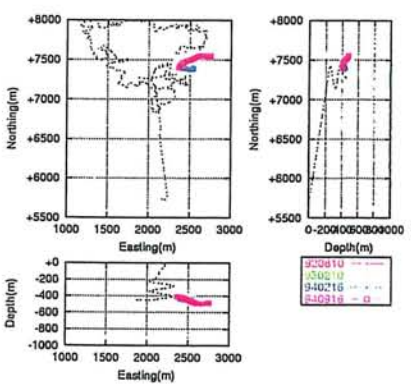

(6)KA3005A

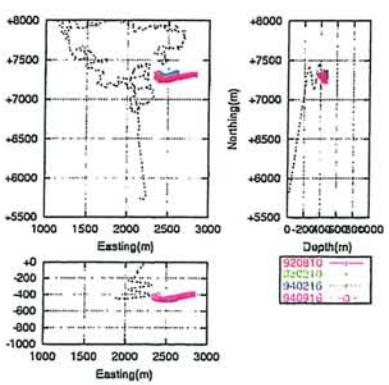

(7)KA3110A

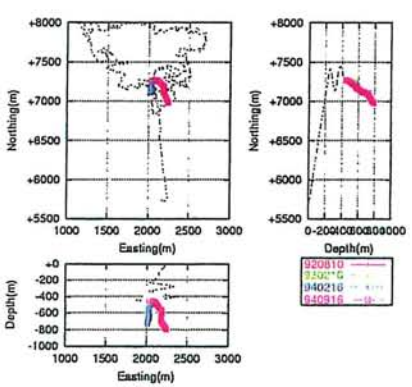

(8)KA3385A

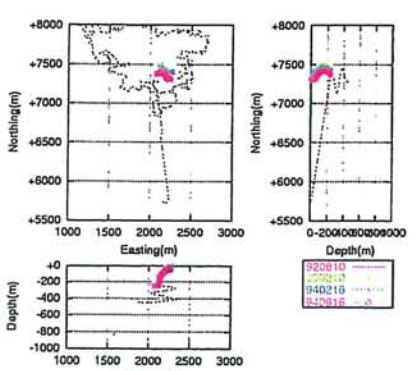

(Option)KA1755A

Fig.4.7 Trajectory to each control point at certain time.

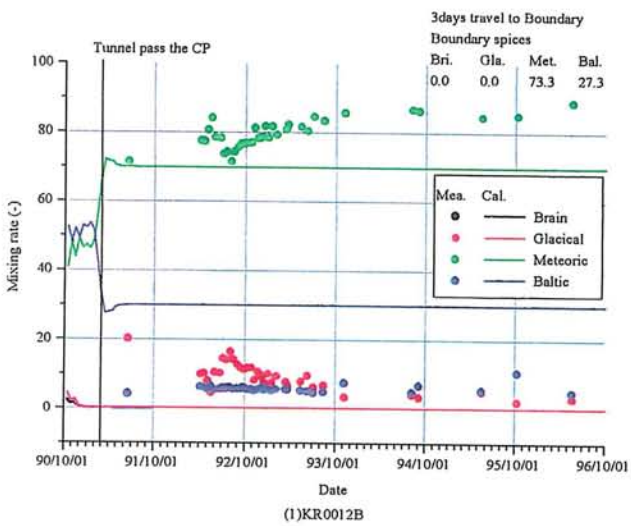

(1)KR0012B

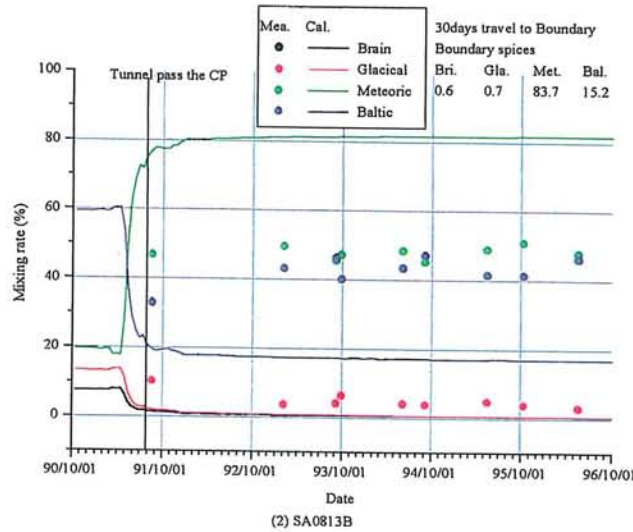

(2) SA0813B

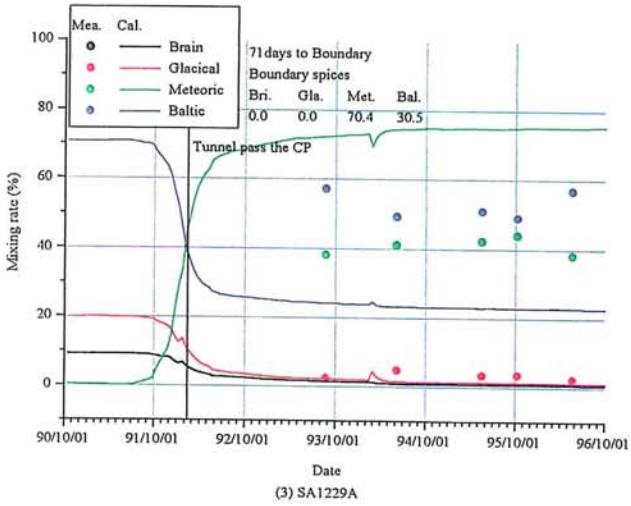

(3) SA1229A

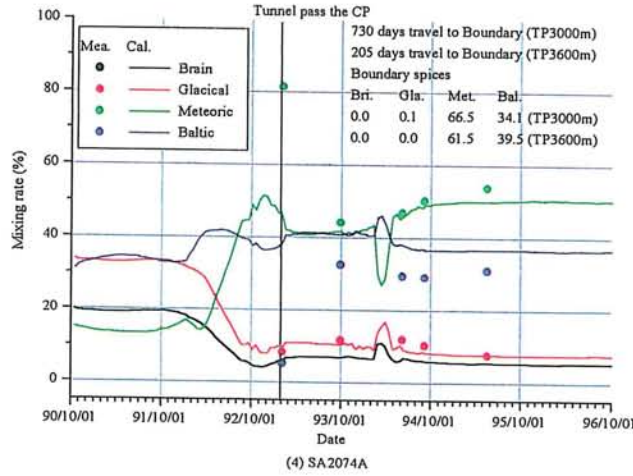

(4) SA2074A

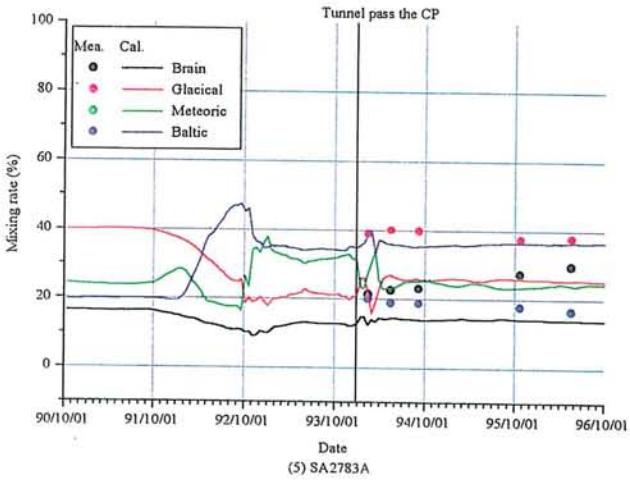

(5) SA2783A

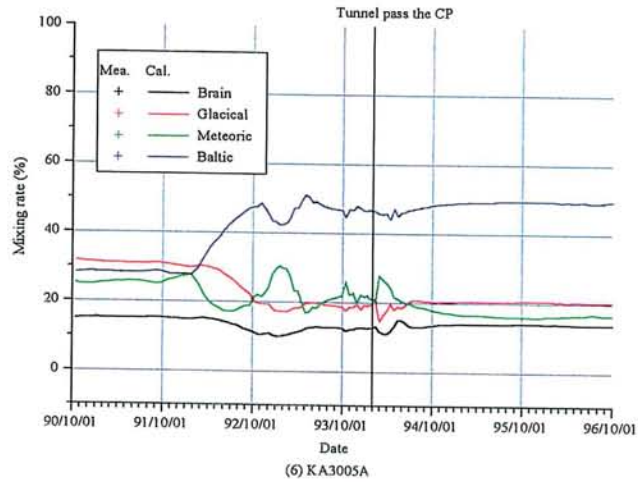

(6) KA3005A

Fig .4.8 Mixing rate changing during tunnel construction

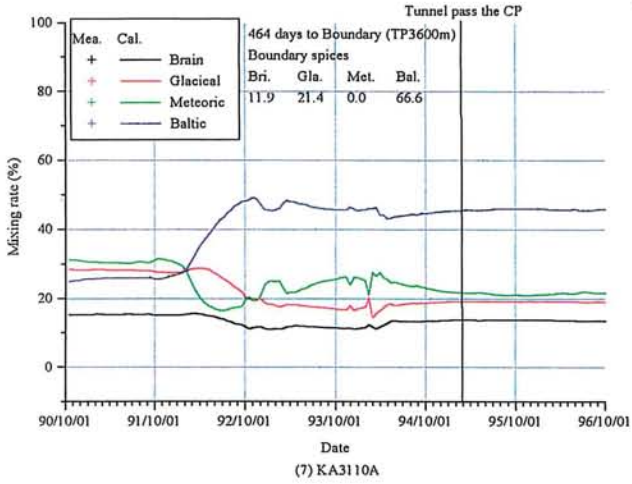

(7) KA3110A

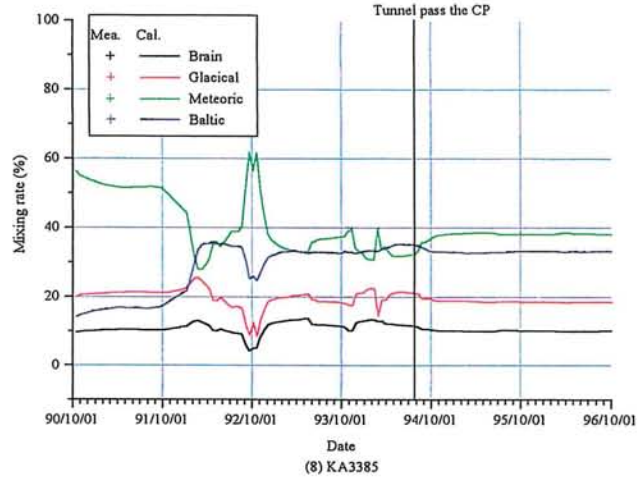

(8) KA3385

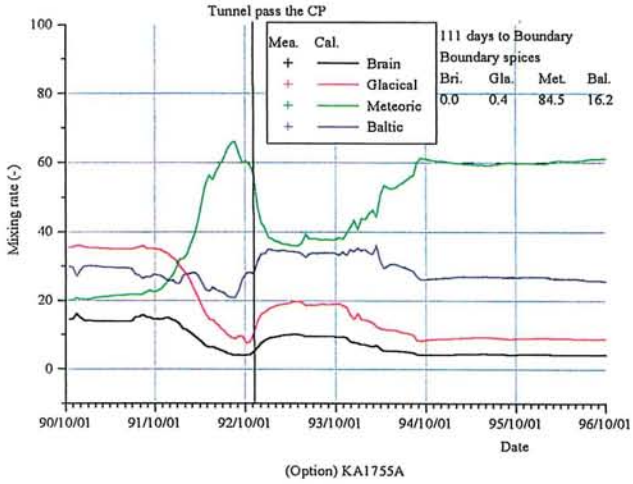

(Option) KA1755A

Fig .4.8 Mixing rate changing during tunnel construction

Appendix I

Table Condensed description of modeling by CRIEPI

CRIEPI's Groundwater flow and solute transport model of the Äspö site Porous media model with smeared fractures			
Process description **Continuity description (Mass rate for groundwater flow and solute transport)** **Equation of motion (Darcy's law with Bousenessq approximation)**			
Concept		**Data**	
Generic frame works and parameters			
Easting 1000-3000m, **Notrhing 55000-8000m** **Depth 0-1000m at Äspö coordinate** **17 fracture zone** **1 rock mass**		**Size2.0 x 2.5 x 1.0km^3** **About 160,00 hex. Element and 300 line Element** **Smeared model**	
Material properties			
Fracture zone **Rock mass** **Storage capacity** **Dispersion length** **Effective porosity**		**Mean value of hydraulic test** **Mean value of 3m-scale hydraulic test** **Assumed ($1.0\times10^{-6}m^{-1}$)** **Assumed ($a_L=10a_T=200m$)** $n_e = 34.87K^{0.753}$: K(m/sec) **Data from Rhen(1997)**	
Spatial assignment method			
Deterministic **Property of Element crossed by fracture calculated as volume-weighted value**			
Boundary conditions			
	Groundwater flow	**Salinity distribution**	**Solute transport**
Upper **Island area** **Sea area** **Lower** **Side**	**Constant flux** **Constant head** **No flux** **Constant head : Hydrostatic**	**Fresh water:0%** **Sea water:0.6%** **No flux** **Interpolated from sampled data**	**Interpolated from the result of VOXEL CODE**
Numerical tool **FEGM/FERM**			
Output parameter **Pressure head, total head, flowrate, salinity**			

Appendix II

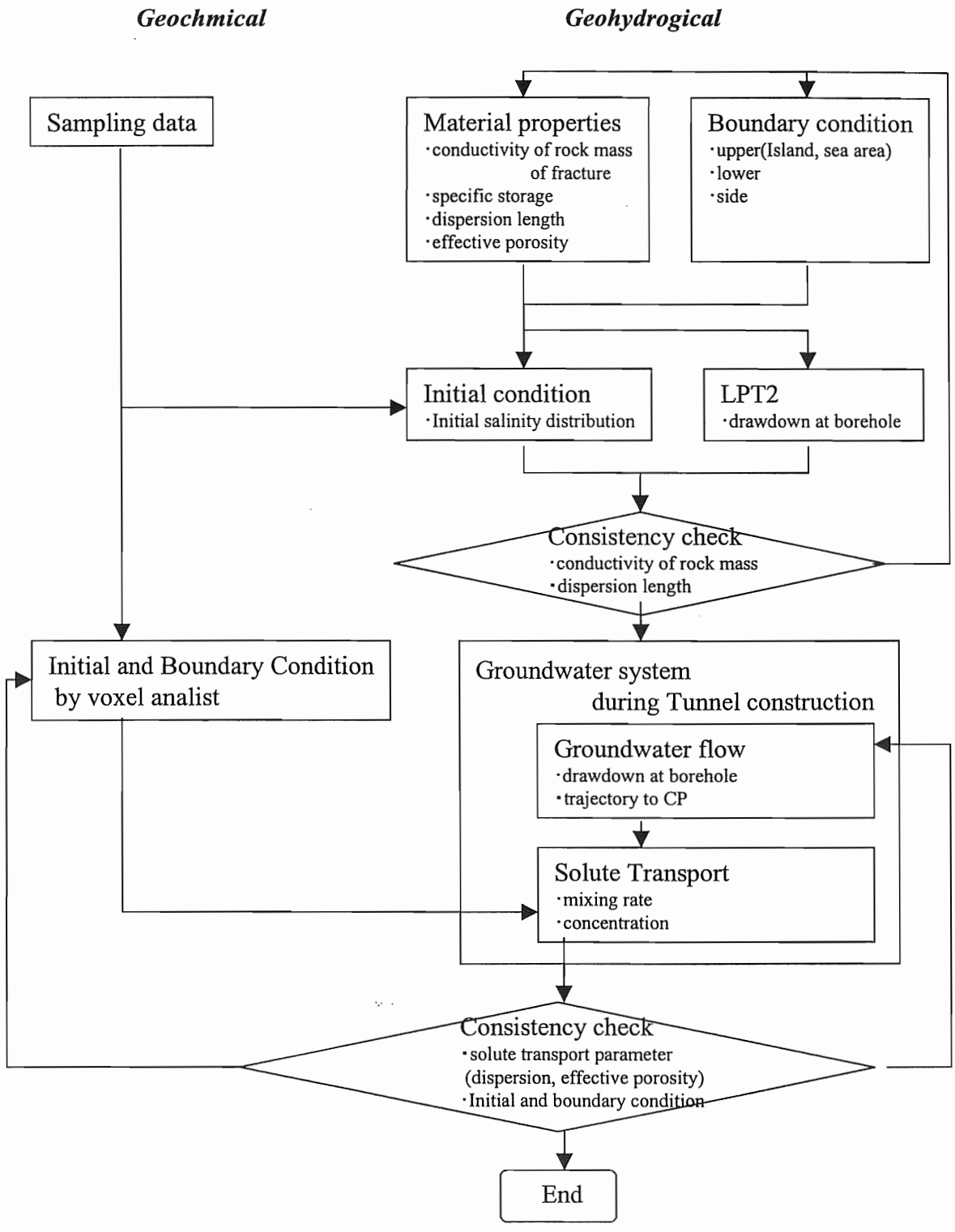

Fig. Flow of modeling work

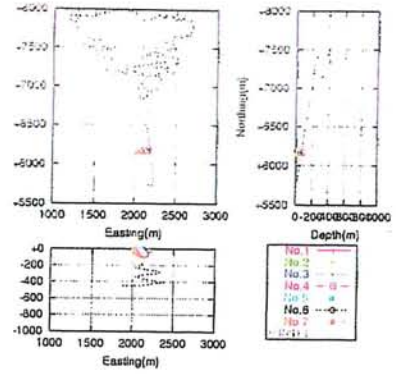

(1)KR0012B

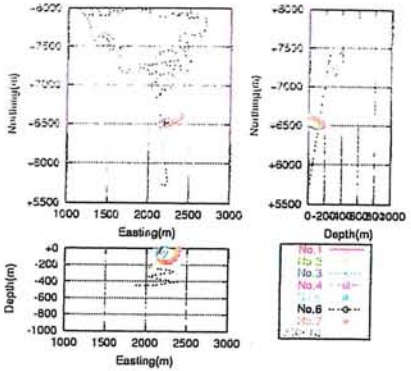

(2)SA0813B

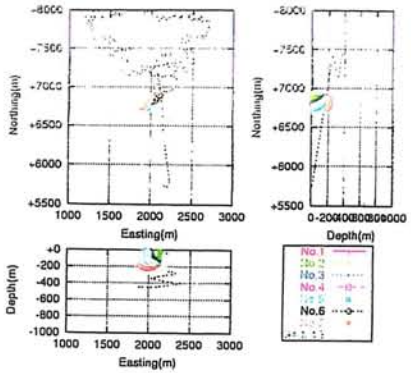

(3)SA1229A

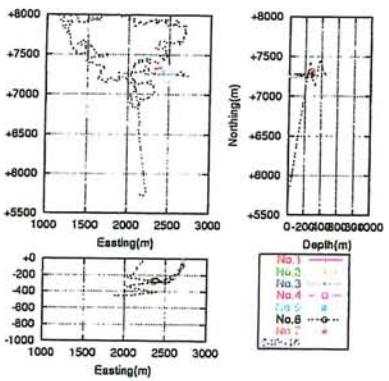

(4)SA2074A

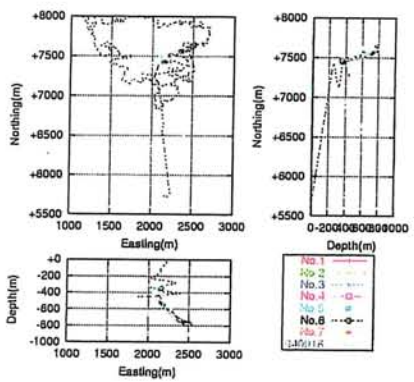

(5)SA2783A

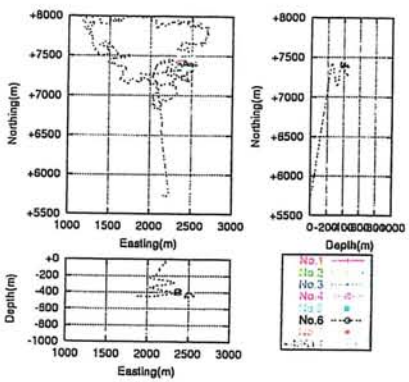

(6)KA3005A

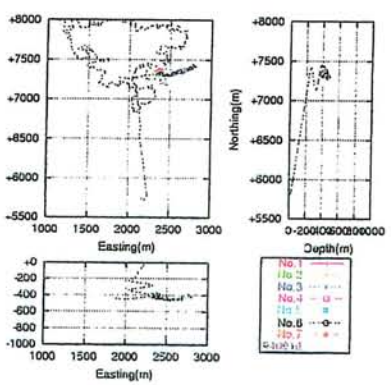

(7)KA3110A

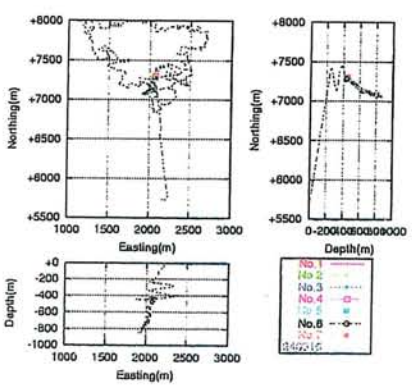

(8)KA3385A

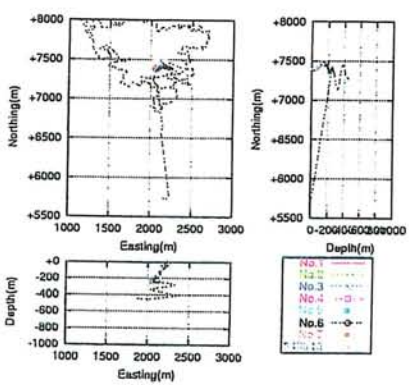

(Option)KA1755A

App. Fig.1 Trajectory to near the control point at 920810.

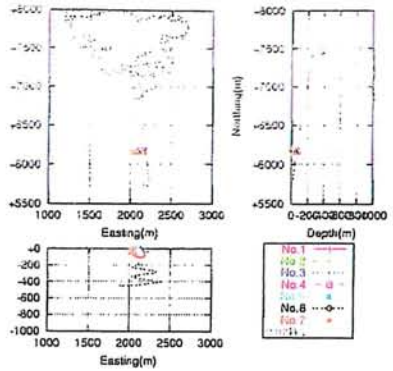

(1)KR0012B

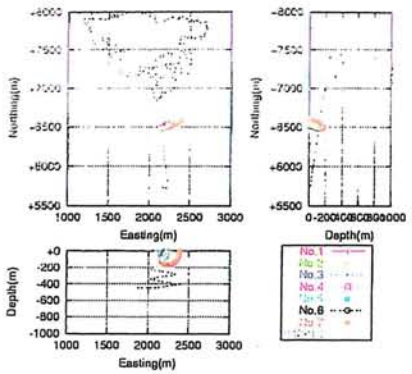

(2)SA0813B

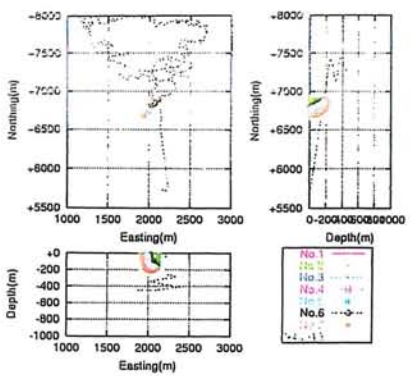

(3)SA1229A

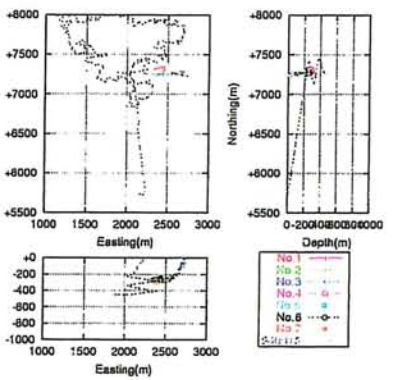

(4)SA2074A

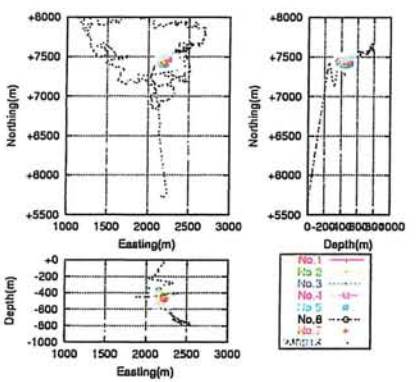

(5)SA2783A

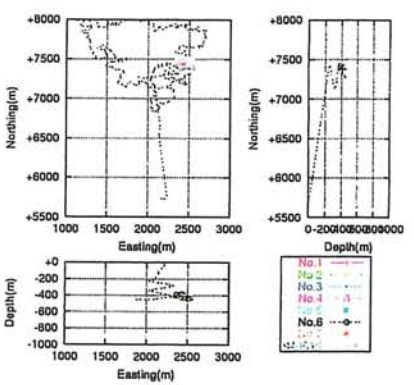

(6)KA3005A

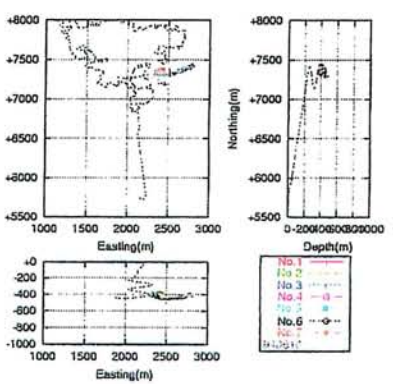

(7)KA3110A

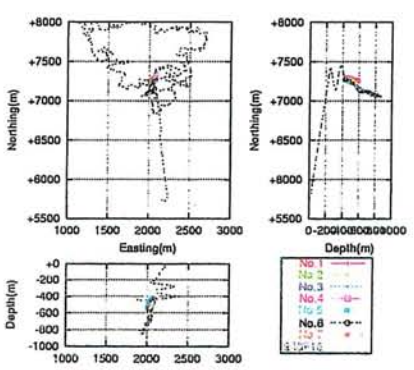

(8)KA3385A

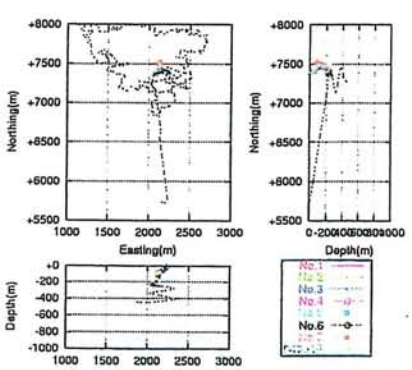

(Option)KA1755A

App. Fig.2 Trajectory to near the control point at 930210.

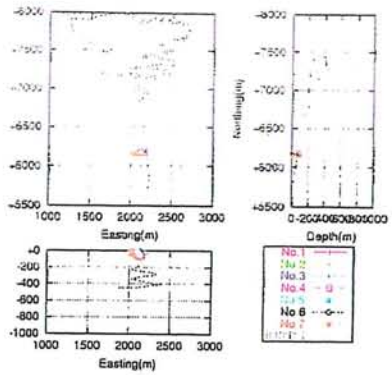

(1)KR0012B

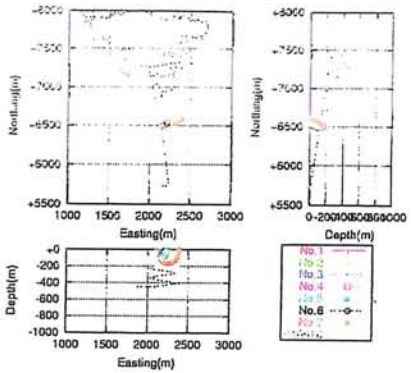

(2)SA0813B

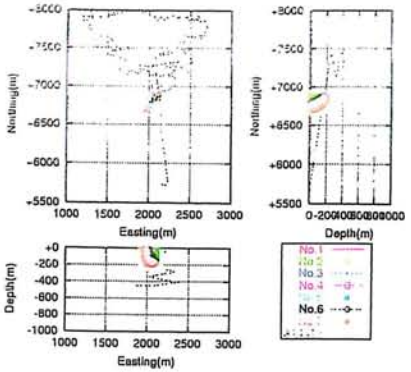

(3)SA1229A

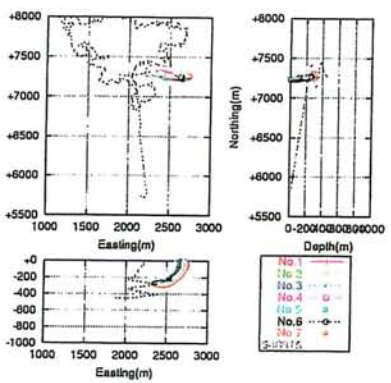

(4)SA2074A

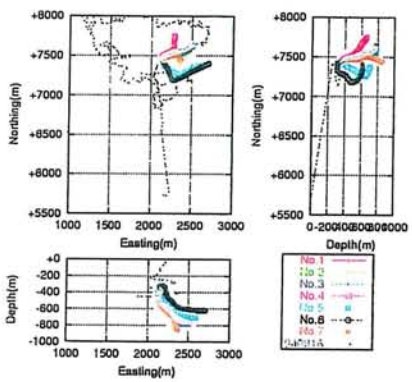

(5)SA2783A

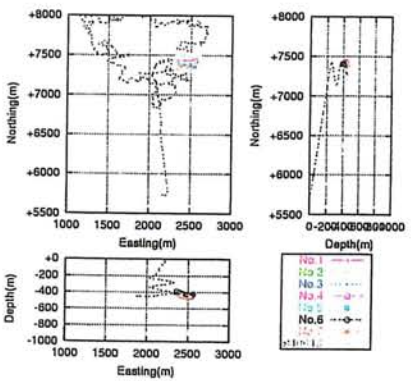

(6)KA3005A

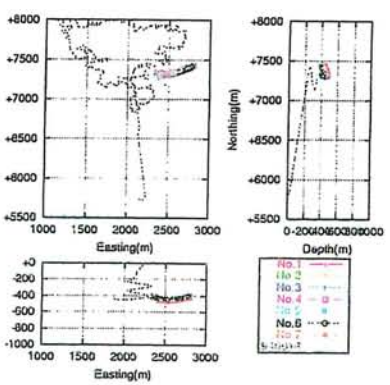

(7)KA3110A

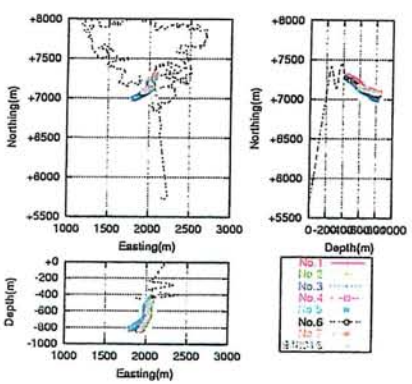

(8)KA3385A

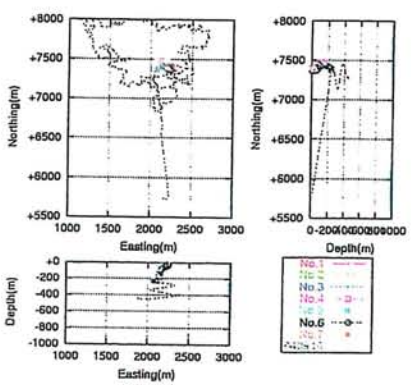

(Option)KA1755A

App. Fig.3 Trajectory to near the control point at 940216.

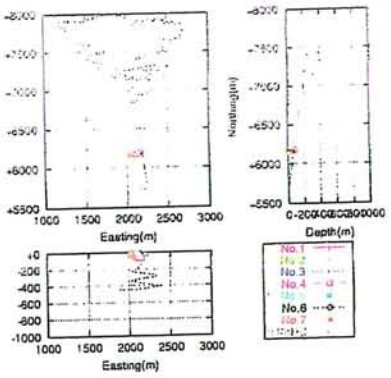

(1)KR0012B

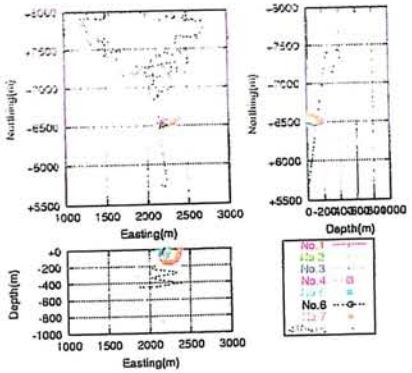

(2)SA0813B

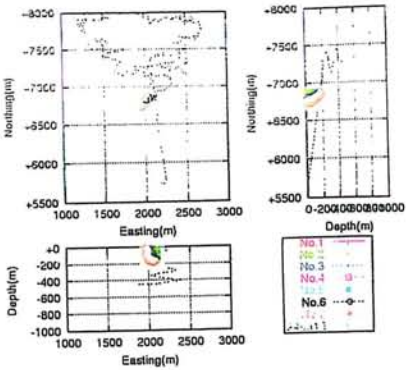

(3)SA1229A

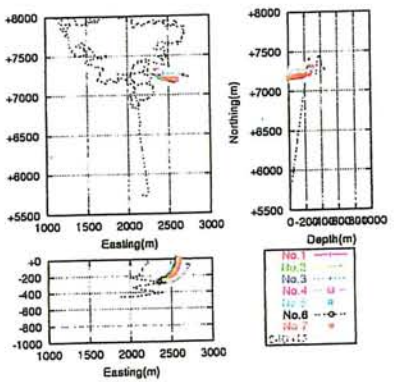

(4)SA2074A

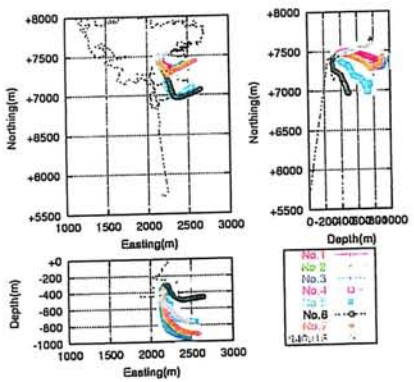

(5)SA2783A

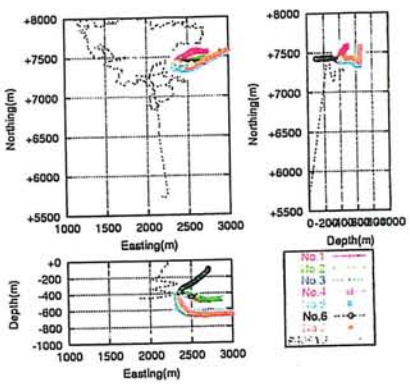

(6)KA3005A

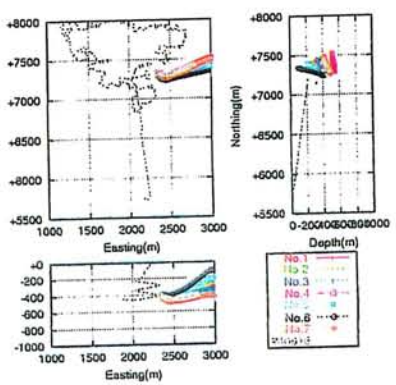

(7)KA3110A

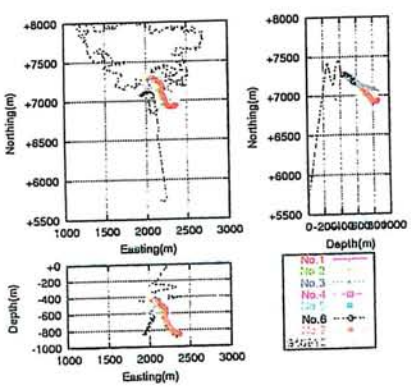

(8)KA3385A

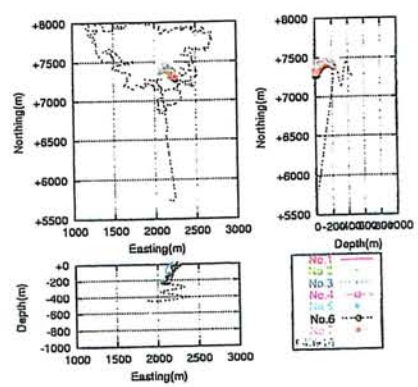

(Option)KA1755A

App. Fig.4 Trajectory to near the control point at 940916.

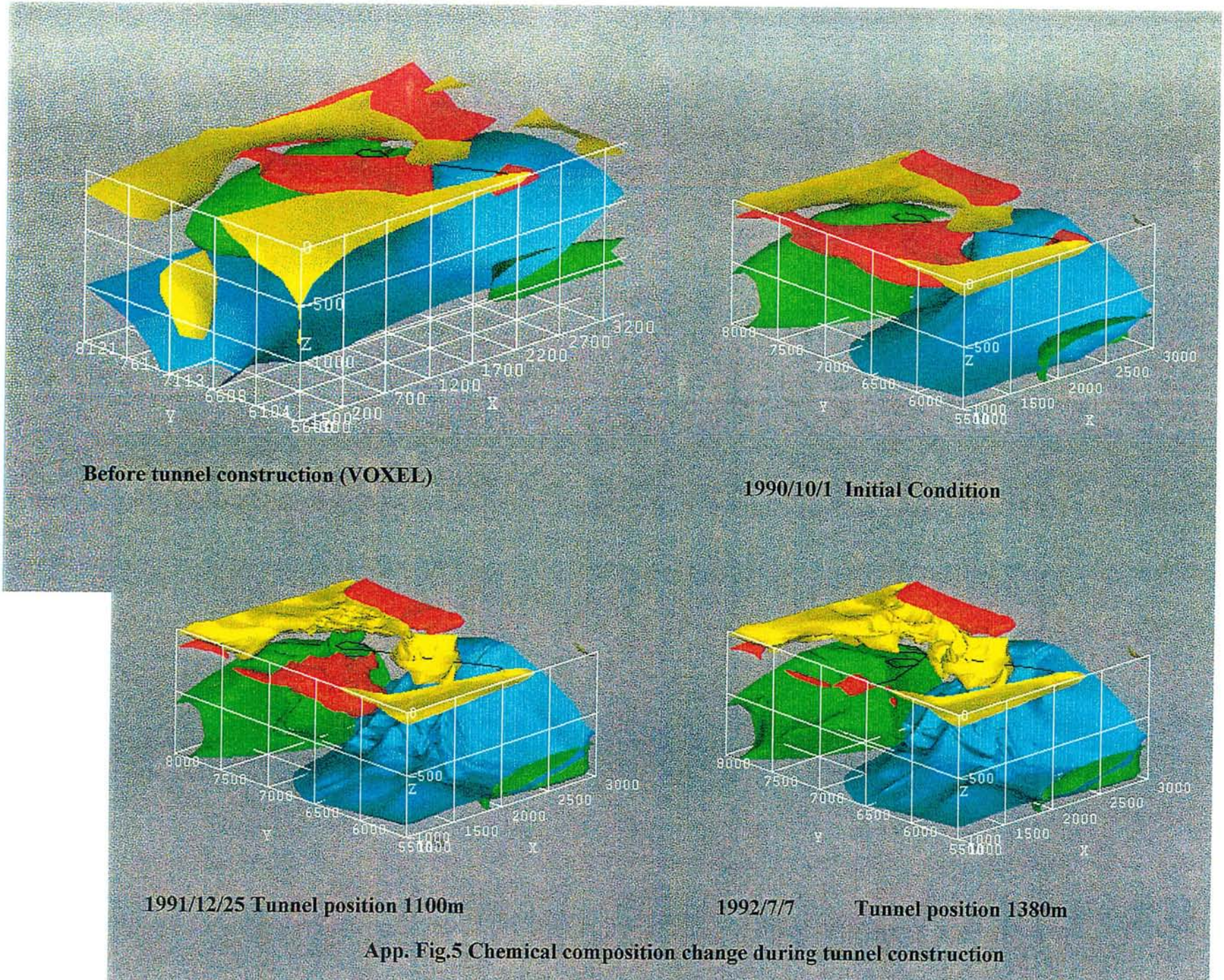

App. Fig.5 Chemical composition change during tunnel construction

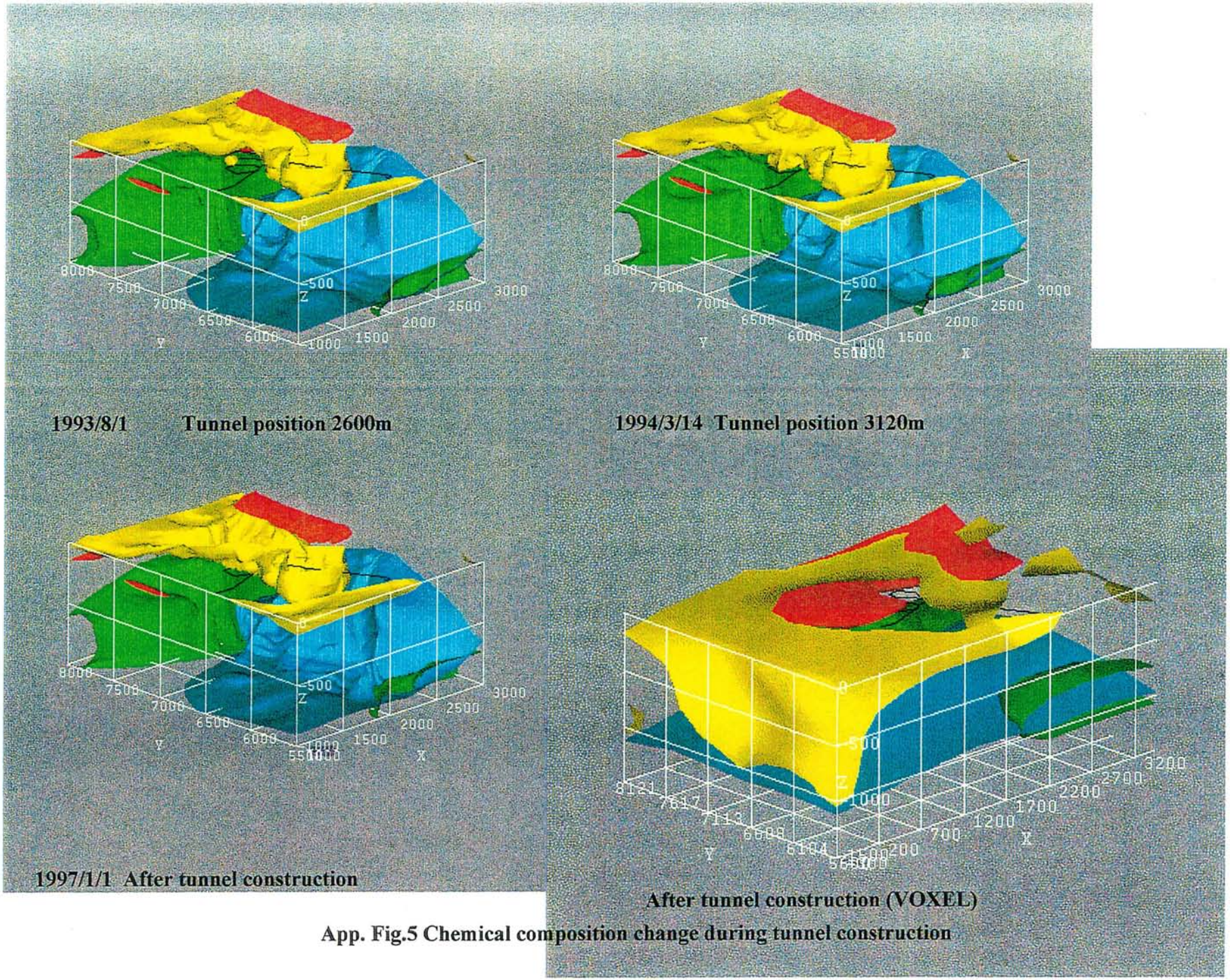

App. Fig.5 Chemical composition change during tunnel construction

Numerical modelling of flow and transport during the tunnel construction of Äspö HRL.

J. Molinero (ENRESA/ULC)

UNIVERSIDADE
DA CORUÑA

E.T.S. INGENIEROS DE
CAMINOS,CANALES Y PUERTOS

EMPRESA NACIONAL
DE RESIDUOS, S.A.

NUMERICAL MODELLING OF THE IMPACT OF THE TUNNEL CONSTRUCTION ON THE GROUNDWATER SYSTEM AT ÄSPÖ

PROGRESS REPORT: *Numerical modelling of the transient groundwater flow and conservative solute transport during the tunnel construction.*
(1990/10/01 – 1997/01/01)

Contribution of ENRESA+University of La Coruña Team
to the Task Force #5.

Jorge Molinero
Javier Samper
Rubén Juanes
Leandro Buján
Gouxiang Zhang

Grupo de Hidrología Subterránea
E.T.S. Ingenieros de Caminos, Canales y Puertos
Universidad de La Coruña
Campus de Elviña s/n
15192 La Coruña
Spain
e-mail: samper@iccp.udc.es
molinero@iccp.udc.es

April, 1999

INDEX

1 INTRODUCTION

1.1 Background

The Äspö HRL is a Laboratory for the development and testing of methods for detailed characterisation of fractured rock volumes. In addition to be a full scale laboratory, the Äspö HRL provides a multitude of data to improve the knowledge of the crystalline bedrock and for testing models of groundwater flow, groundwater composition and solute migration.

After the Regional Geological investigations, the construction of the Äspö HRL underground facilities was started in October 1990 and completed during the summer of 1995.

The Äspö Task Force on Modelling of Groundwater flow and Transport of Solutes was initiated in 1992. The Task Force is a forum for the organizations involved to interact in the area of conceptual, mathematical and numerical modelling of groundwater flow and solute transport in fractured rock. Within these activities, Task Force #5 was initiated in February 1997 with the aim to compare and integrate hydrochemistry and hydrogeology.

The nature of the flow at repository level and the chemical composition of the groundwater are essential for the calculations of nuclide migration. The composition and evolution of the groundwater chemistry depends on: (1) Groundwater flow, (2) Solute transport through fractures and matrix blocks, (3) Heat transport and (4) homogeneous (solute-solute) and heterogeneous (solute-mineral) chemical reactions.

Therefore, it is of interest to combine groundwater flow and chemistry. However, this is difficult for several reasons. First of all, a wide range of physical, chemical, thermal and hydrodynamic processes are involved. A second reason has to do with numerical aspects. The problem involves many partial differential equations together with nonlinear algebraic equations. The simultaneous solution of water flow, reactive solute transport and heat transfer equations requires a numerical effort which is orders of magnitude greater than that required for modelling conservative solute transport or speciation of a static water solution.

In addition of the numerical aspects, carrying out a reactive transport model requires a solid hydrogeological model and a good knowledge of the hydrochemical patterns.

1.2 Objectives

The aim of Task #5 is to compare and ultimately integrate hydrochemistry and hydrogeology. The Task will also be useful for a future assessment of the stability of the hydrodynamic and hydrochemical conditions at Äspö. This modelling approach could then be used for any future repository site investigations and evolution, especially in crystalline bedrock environment.

The specific objectives of the Task #5 are:

- To assess the consistency of groundwater flow models and hydrochemical mixing-reactions models through integration and comparison of hydraulic and chemical data obtained before and during tunnel construction.
- To develop a procedure for integration of hydrological and hydrochemical information which could be used for disposal site assessments.

In the other hand, the main objective of the University of La Coruña (ULC) – ENRESA team is to validate (to the extent that is possible) current Thermo-Hydro-Geochemical (THG) codes for coupled water flow, heat transfer and multicomponent reactive transport. In other words, the objective is to test the ability of these codes to cope with the complex hydrogeological and hydrochemical settings which are expected to be found in a real HLW repository.

As it was said before, setting up a fully coupled groundwater flow and reactive transport model requires solid hydrogeological and hydrochemical models and, in addition, implies to make a big effort of integration. For this reason, the Task #5 provides to the ULC-ENRESA team a unique opportunity to finally reach the proposed main goal.

1.3 Site description

The Äspö Hard Rock Laboratory is located around 500 m below the Äspö island. This island is situated in the southeast part of Sweden, 400 km south of Stockholm, and geographically is a granitic coastal island in the Baltic Sea, separated to the mainland and several other islands by shallow sea branches (see Figure 1.1).

The rocks of the area are predominantly granitoids, belonging to the TransScandinavian Igneous Belt. This rocks together with some volcanics others were emplaced and extruded during several pulses of Precambrian magmatism (Larson & Berglund, 1992). This granitoids have a range of mineralogical composition between true granites, which occur on Ävrö island and the Southern part of Äspö, to granodioritic to dioritic composition, which is most common on the northern part of Äspö (Kornfalt & Wikman, 1988).

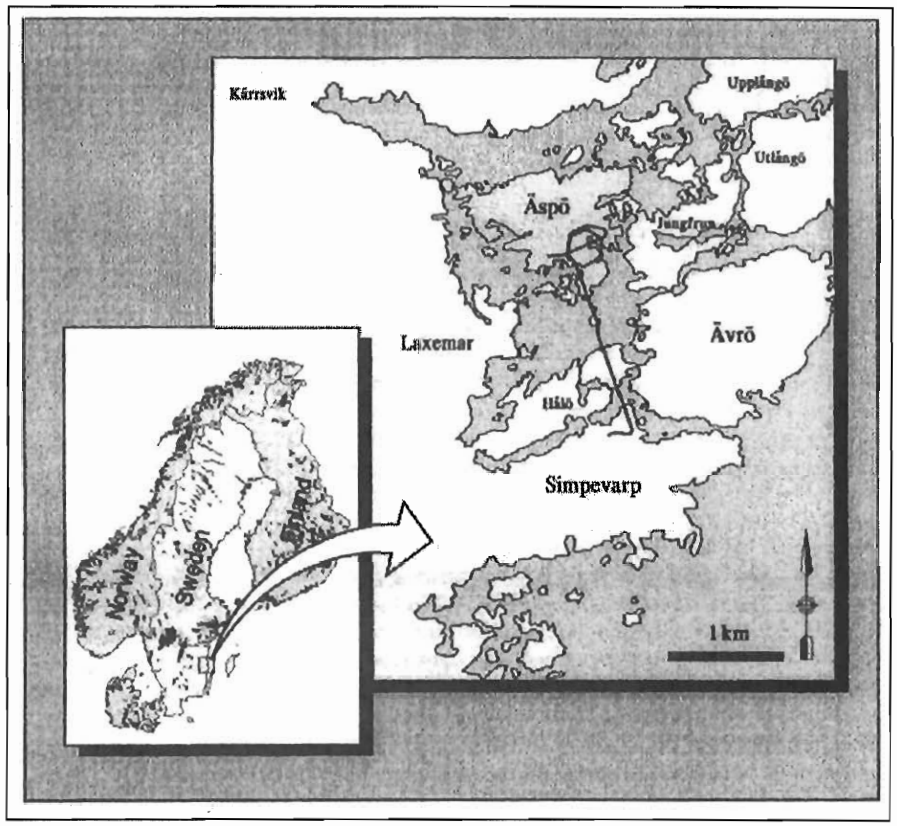

Figure 1.1 Geographical location of the Äspö HRL, after Rhén et al., 1997.

2 CONCEPTUAL MODEL

The huge amount of research efforts done during the pre-investigation and construction phases (years 1986-1995) at Äspö site has provided strong conceptual models about the geology (litology and structure), hydrogeology and hydrochemistry. An excellent compilation of these topics can be found in Rhén et al. (1997a) and Rhén et al. (1997b). In order to introduce some concepts and ideas used in the numerical model, a brief summary of the conceptual models is presented in this chapter. Most data and concepts have been found in Rhén et al. (1997 a,b).

2.1 Surface hydrology

The land surface of Äspö is slightly undulating, with a maximum height of 14 m. There are no perennial streams on the island, and the surface water is drained to the sea by the peatlands, sediments or directly to the sea.

The mean precipitation in the area is about 675 mm/year and about 18% falls as snow. The calculated actual evapo-transpiration (ET) is 490

mm/year and the potential ET is 616 mm/year. Run off for the area around Äspö is estimated to be between 150 and 200 mm/year. The annual mean temperature (presently) is around 6.5 °C.

Svensson (1997) studied the ground water recharge by means of numerical modelling. He concluded that the value of the infiltration depends on the local level of the water table ranging between 0.4 mm/year in natural conditions and 134 mm/year with the tunnel construction completed.

2.2 Ground water level

The ground water level under natural conditions ranges between 0-4 m above mean sea level and approximately follows the. Due to the drawdown caused by the inflow to the tunnel, the elevation of the water table decreased during its construction. The minimum water table elevation in 1995 was about 100 m below sea level and the piezometric levels measured are more or less stable since the excavation was ended in February 1995 (Stanfors et al., 1999).

2.3 Temperature and salinity

The salinity of the Baltic Sea around Äspö is approximately 6 g/l, but varies with location and time of sampling. There is a clear depth dependence of the salinity in the groundwater of Äspö site. The fresh water lens below Äspö has a thickness of 100-200 m under natural conditions and below this level the salinity increases to reach a value about 20 g/l at a depth of 800 m. The temperature gradient is more or less 15 °C/km (Ahlbom et al, 1995).

2.4 Materials and geometry

The Äspö site scale model covers an area of 2x2 km with a depth of 1 km, with the Äspö island located approximately in the middle of the top surface. Geometrically the model comprises two fundamental concepts:

a) Hydraulic conductors domains, which are large two-dimensional features with hydraulic properties different from the surrounding rock. They are generally defined geologically as major discontinuities but in some cases they may mainly be defined by interpretation of results from hydraulic interference testing.
b) Hydraulic rock mass domains are geometrically defined volumes in space with properties different from surrounding domains (rock mass or conductors). They may either be defined by lithological domains or purely by interpretation of results from hydraulic test.

Figure 2.1 shows the schematic description of these two main geohydrological concepts.

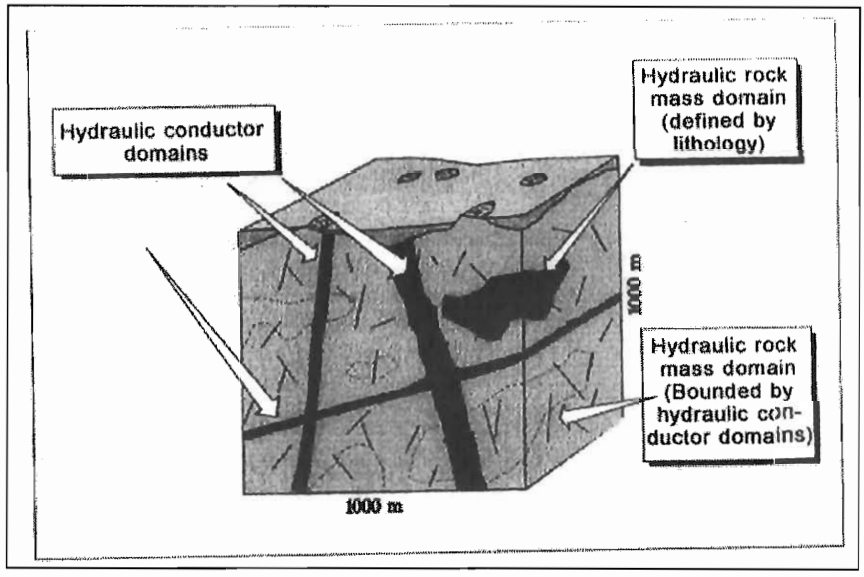

Figure 2.1 Schematic description of two main hydrogeological concepts: hydraulic conductors domains and hydraulic rock mass domains. Rhén et al. (1997 a).

Figure 2.2 shows a map of the hydraulic conductor and rock mass domains of the Äspö site scale conceptual model

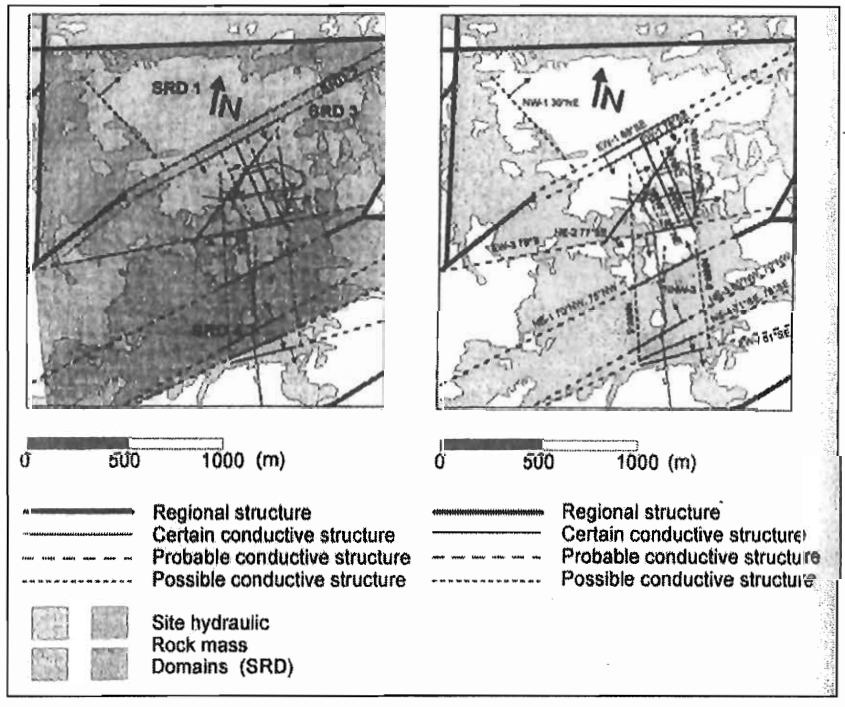

Figure 2.2 Hydraulic rock mass and conductor domains of the conceptual model. Rhén et al (1997b).

The exact location and the hydrogeological parameters of each domain can be found in Rhén et al (1997 b). For hydraulic conductor domains the transmisivity and the storage coefficient is provided deterministically, meanwhile for rock mass domains the properties are assigned stochastically.

The evaluated transmissivities for the hydraulic conductors domains are generally within the range $10^{-6} - 10^{-4}$ m^2/s with a median about 10^{-5} m^2/s. The maximum transmissivity is $3x10^{-4}$ m^2/s for hydraulic conductor domain NE-1. For the rock mass domains the hydraulic conductivity takes values around 3×10^{-10} m/s.

There are a few interference tests at Äspö HRL that are judged to be useful for evaluation of the storage coefficient. This is mainly because it is difficult to assume the radial flow condition in a fractured media. However it was possible to assume the radial flow condition in some test, mainly within a subplanar feature highly conductive, and using these data, Rhén et al (1997 b) obtain the following relationship:

$$S = a \cdot T^b \qquad (2.1)$$

where T is the transmissivity (m^2/s), S is the storage coefficient, a = 0.00922, b=0.785. The relationship was adjusted using 5 values obtained with a test scale of 100 m. The correlation coefficient was ρ = 0.71.

2.5 Transport of solutes

In order to estimate the transport properties of the rocks in the Äspö area, a few tests have been performed. Most of the data concerning transport of contaminants were evaluated from the LPT2 test, the NE-1 test and the TRUE project.

Rhén et al. (1997b) obtained a relationship between the kinematic porosity (n_e) and the hydraulic conductivity (K in m/s). The equation 2.2 shows this relationship:

$$n_e = 34.87K^{0.753} \qquad (2.2)$$

Values for matrix porosity have been measured in samples of different rocks. This values ranges from the minimum of the fine-grained granites (0.23%-0.27%) to the maximum of the Äspö diorite (0.40%-0.45%).

An important parameter concerning the transport of solutes is the dispersivity. This parameter takes into account the heterogeneity of the velocity field. Actual flow paths in porous and fractured media are highly irregular and some water particles move faster than the average velocity while others displace more slowly. Rhén et al (1997b) plotted the available values of the dispersivity coefficients (α) as a function of the spatial scale (s in m) fitting a linear approximation between Log_{10} (s) and Log_{10} (α). The obtained relationship was:

$$\alpha = 0.053\ s^{1.21} \qquad (2.3)$$

3 MATHEMATICAL MODEL

3.1 Groundwater Flow

Water flow through porous media is governed by Darcy's Law which in its most general form relates water flux $\mathbf{q}$ to the gradient of water pressure p and elevation z through

$$\mathbf{q} = -\frac{k}{\mu}(\nabla p + \rho \mathbf{g}) \tag{3.1}$$

where ρ and μ are water density (mass per unit volume) and dynamic viscosity, k is intrinsic permeability and $\mathbf{g}$ is a vertical vector pointing downwards of modulus equal to gravity acceleration. When density changes are negligible, Darcy's Law can be written in terms of hydraulic head h as

$$\mathbf{q} = -\mathbf{K}\nabla h \tag{3.2}$$

where

$$\mathbf{K} = \frac{\rho \mathbf{g}}{\mu}\mathbf{k} \tag{3.3}$$

and

$$h = \frac{p}{\rho \mathbf{g}} + z \tag{3.4}$$

Here $\mathbf{K}$ is the hydraulic conductivity tensor. By combining Darcy's Law and the mass balance equation one has

$$\nabla \cdot (K \nabla h) + w = S_s \frac{\partial h}{\partial t} \tag{3.5}$$

where w represents fluid sink/sources per unit volume of medium and S_s is the specific storage coefficient defined as the volume of water

delivered per unit time and unit volume of medium in response to a unit change of hydraulic head.

At the boundary Γ of the domain R either the head or its gradient (water flux) are known. Possible conditions include:

(1) Dirichlet condition

$$h(x,y,z,t)\big|_{\Gamma 1} = H \tag{3.6}$$

(2) Neumann condition

$$T\nabla h \cdot n\big|_{\Gamma 2} = Q \tag{3.7}$$

(3) Mixed condition

$$T\nabla h \cdot n\big|_{\Gamma 3} = \alpha(H - h) \tag{3.8}$$

where H and Q are specified heads and fluxes and α is a leakage coefficient (LT^{-1}).

3.2 Transport of conservative solutes

Dissolved species in saturated media are subject to various physical and chemical processes. The main transport processes are: (1) advection, (2) molecular diffusion and (3) hydrodynamic dispersion. Each of these processes produces a solute mass flux **F** (mass of solutes crossing a unit surface area of medium per unit time).

3.2.1 Advection

Advection refers to solute migration associated to water flow. Solutes move with water. If water flows at a specific discharge $\mathbf{q}$ (volumetric water flux), the advective mass flux $\mathbf{F}_A$ is given by

$$\mathbf{F}_A = \mathbf{q}\, c \tag{3.6}$$

where c is solute concentration, usually expressed as solute mass grams (or moles in reactive solute transport) per unit fluid volume. Solutes migrate at an average velocity $\mathbf{v}$ given by

$$\mathbf{v} = \frac{\mathbf{q}}{\theta} \tag{3.7}$$

where θ is the volumetric water content which is equal to the porosity ϕ for saturated media. The advective mass flux can also be obtained as

$$\mathbf{F}_A = \theta \mathbf{v} c \tag{3.8}$$

3.2.2 Molecular diffusion

Molecular diffusion is a transport mechanism related to the continuous Brownian motion of solute and fluid molecules. For pure water, molecular diffusion produces a mixing effect which obeys Fick's Law. This law states that the diffusive solute flux $\mathbf{F}_D$ is proportional to the concentration gradient ∇c :

$$\mathbf{F}_D = -D_0 \nabla c \tag{3.9}$$

where D_0 is the molecular diffusion coefficient in water. The diffusion coefficient of very small, near-spherical, particles in water is given by the Stokes-Eistein relationship

$$D_0 = \frac{kT}{6\pi\mu_w r} \tag{3.10}$$

where k is Boltzmann's constant, μ_w is the absolute viscosity of water and r is hydrodynamic radius of the particle. Although this relationship does not take into account chemical interactions between the solute and the solvent, it does provide a correct order of magnitude estimate of D_0 for many dissolved species in water. For hydrated ions, r is the radius of the hydration shell. Chemical species diffusing through the solution-filled pore spaces of a porous medium encounter along their path an irregular network of pore channels and frequently collide with the walls of these channels. Diffusion through this porous space is slower than it would be in the absence of the mineral framework. Based on these simple concepts of the diffusional process, the physical characteristics of the rock responsible for slowing down molecular diffusion are generally considered to be the water content θ itself, the pore size distribution (represented by a constrictivity term) and the tortuosity, τ, of the diffusional paths.

In a porous medium solutes can only diffuse along fluid pores following tortuous paths. This means that the effective molecular diffusion coefficient for a porous medium, D_e, is smaller than that for pure water. Usually D_e is related to D_0 through

$$D_e = \theta D_0 \tau \tag{3.11}$$

where τ is the medium tortuosity. For partially saturated porous media, tortuosity is related to water content through relationships such as that used by Simunek and Suares (1993)

$$\tau = \frac{\theta^{7/3}}{\theta_s^2} \tag{3.12}$$

where θ_s is saturated volumetric water content which can be taken equal to the total porosity. Therefore, the diffusive flux in porous media is given by:

$$\mathbf{F}_D = -D_e \nabla c \tag{3.13}$$

3.2.3 Hydrodynamic Dispersion

In addition to molecular diffusion there is a mixing phenomenon known as hydrodynamic dispersion which also produces both longitudinal and transverse solute spreading. This mixing effect is caused by medium heterogeneities. Actual flow paths are highly irregular. Some water particles move faster than the average velocity while others displace more slowly. The overall effect of all heterogeneities is a solute spreading in all directions. Laboratory and field evidence indicates that this phenomenon can also be described by Fick's Law, so that the hydrodispersive flux $\mathbf{F}_H$ can be described as

$$\mathbf{F}_H = -\theta \, \mathbf{D}_h \nabla c \tag{3.14}$$

where $\mathbf{D}_h$ is the hydrodynamic or mechanical dispersion tensor. Its principal directions coincide with the flow direction and its normals. The component along the flow direction D_L is the largest and is given by

$$D_L = \alpha_L |v| \tag{3.15}$$

while the smallest components D_T occur along the transverse directions and are given by

$$D_T = \alpha_T |v| \tag{3.16}$$

where $|v|$ is the modulus of the velocity vector **v**, α_L and α_T are the longitudinal and transverse dispersivities which are characteristic parameters of the medium having dimensions of length which measure the scale of the spatial heterogeneities.

In general, $\mathbf{D}_h$ is a symmetric tensor whose components in two dimensions are:

$$D_{xx} = \frac{\alpha_L v_x^2 + \alpha_T v_y^2}{|v|} \tag{3.17a}$$

$$D_{yy} = \frac{\alpha_L v_y^2 + \alpha_T v_x^2}{|v|} \tag{3.17b}$$

$$D_{xy} = D_{yx} = (\alpha_L - \alpha_T)\frac{v_x v_y}{|v|} \tag{3.17c}$$

For practical purposes, the effects of molecular diffusion and hydrodynamic dispersion are usually lumped together in a single dispersion tensor **D** which takes the form:

$$\theta \mathbf{D} = I D_e + \theta \mathbf{D}_h \tag{3.18}$$

where **I** is the identity tensor.

3.2.4 Solute transport equations

The equation governing solute transport through porous media is derived from the principle of mass conservation. This principle states that for any reference elementary volume of medium, the net flux plus sink/source terms must be equal to the time rate of change of the solute mass contained in the reference volume. Solute mass per unit volume of medium is equal to θc. The net mass flux is given by minus the divergence of the total flux vector. Therefore, mass conservation leads to the following equation:

$$-\nabla\cdot\left(\mathbf{F}_A+\mathbf{F}_D+\mathbf{F}_H\right)=\frac{\partial(\theta c)}{\partial t} \tag{3.19}$$

where $\nabla\cdot(\ )$ is the divergence operator which when applied to a vector $\mathbf{F}$ of components $\left(F_x,F_y,F_z\right)$ is equal to

$$\nabla\cdot(\mathbf{F})=\frac{\partial F_x}{\partial x}+\frac{\partial F_y}{\partial y}+\frac{\partial F_z}{\partial z} \tag{3.20}$$

Substitution of mass fluxes $\mathbf{F}_A$, $\mathbf{F}_D$ and $\mathbf{F}_H$ into the continuity Equation 3.19 leads to

$$\nabla\cdot(\theta\mathbf{D}\nabla c)-c\nabla\cdot\mathbf{q}-\nabla c\cdot\mathbf{q}=\frac{\partial(\theta c)}{\partial t} \tag{3.21}$$

Possible solute sinks and sources are added to the left-hand-side of this equation. For a fluid source of water flux w (per unit volume of medium) having a concentration c^*, and a solute sink/source term R (solute mass added per unit time and unit fluid volume) the transport equation becomes

$$\nabla\cdot(\theta\mathbf{D}\nabla c)-\mathbf{q}\cdot\nabla c+w(c^*-c)+\theta R=\theta\frac{\partial c}{\partial t} \tag{3.22}$$

where the following identity, which derives from the flow equation, has been taken into account

$$\left(-\nabla\cdot\mathbf{q}+w-\frac{\partial\theta}{\partial t}\right)c=0 \tag{3.23}$$

The solution of the transient solute transport equation requires knowing:

(1) transport parameters which include: water content θ, molecular diffusion coefficient $D_0\tau$, and dispersivities (α_L,α_T).

(2) sink/sources: w, c^* and R.

(3) initial conditions: $c_0(x,y)$ at $t=t_0$

(4) boundary conditions

The initial condition c_0 is either known or may correspond to the solution of a steady-state transport problem such as

$$\nabla\cdot(\theta\mathbf{D}\nabla c_0)-\mathbf{q}\nabla c_0+w_0(c_0^*-c_0)+\theta R_0=0 \tag{3.24}$$

At the boundary of the domain, either concentration or a function of its gradient must be known. Possible types of boundary conditions include:

(1) Dirichlet condition. The points lying at this part of the boundary Γ_1 satisfy the following condition

$$c\big|_{\Gamma_1}=\tilde{c} \tag{3.25}$$

where $\tilde{c}$ is a specified concentration, which may vary in space and time.

(2) Neumann condition. Let $\mathbf{n}$ be the unit vector normal to Γ_2, the part of Γ at which the dispersive flux F_D' is known. This type of condition is

$$-\theta \mathbf{D} \nabla c \cdot \mathbf{n}\Big|_{\Gamma_2} = F_D' \tag{3.26}$$

This equation states that the component of the dispersive flux normal to the boundary is known. This condition is usually imposed at impervious boundaries where F_D' is equal to zero.

(3) Cauchy mixed condition. Some parts of the boundary Γ_3 may have a condition in terms of the total mass flux:

$$\left(-\theta \mathbf{D} \nabla c + \mathbf{q} c\right) \cdot \mathbf{n}\Big|_{\Gamma_3} = F_0 \tag{3.27}$$

The imposed flux is given by F_0. Usually F_0 is taken equal to the advective flux $cq \cdot n$. At outflow boundaries it is usually assumed that the solute mass flux is given by the product of the water flux $q \cdot n$ times the concentration c of the flowing water. In this case, $F_0 = cq \cdot n$ and therefore the boundary condition reduces to

$$-\theta \mathbf{D} \nabla c \cdot \mathbf{n}\Big|_{\Gamma_3} = 0 \tag{3.28}$$

which is a particular case of the type (2) condition.

When the transport equation is integrated over aquifer thickness b, the result is

$$\nabla\cdot(\theta b\mathbf{D}\nabla c) - b\mathbf{q}\nabla c + r(c^* - c) + b\theta R = b\theta\frac{\partial c}{\partial t} \qquad (3.29)$$

where r is the fluid source term per unit surface area.

4 NUMERICAL TOOL

The code used to solve the equations of the numerical model was TRANMEF-3 (Juanes, 1997) developed in the Hydrogeology Group of the University of La Coruña.

TRANMEF-3 is a general numerical code for solving groundwater flow, multicomponent weakly-reactive solute transport and heat transport in heterogeneous (fractured) formations.

All the capabilities of the program are explained in the User's Manual (Juanes, 1997). TRANMEF-3 solves water flow, solute transport and heat transport simultaneously, or any of then separately. The Finite Element Method is used for discretization of space while a general Finite Difference scheme is used for time discretization.

The program performs an "exact" treatment of the Boundary Conditions, by fully integrating along boundaries. TRANMEF-3 handles six (6) different type of elements, that can be used arbitrarily together in any simulation problem. Moreover, and here stays the most interesting point, these elements do not need to have the same dimensions (they can be either 1-D, 2-D or 3-D). This capability allows to simulate, for example, 1-D and 2-D fracture networks in a general 3-D porous medium. Numerical Integration through the elements and element faces is taken into account, using Gauss quadrature in any dimension varying from 1 to 3, and order of integration between 1 and 4 for any kind of element.

5 NUMERICAL MODELLING

5.1 Modelling Approach

5.1.1 Introduction

In order to deal with the wide variety of flow and transport problems in fractured media, a number of modelling approaches have been developed. Following the classification of modelling approaches proposed by Berkowitz (1994) there are tree main types categories for fractured hydrogeological models: (1) Discrete fracture models, (2) Continuum models and, (3) Hybrid models. Other approaches are possible, such as stochastic and hierarchical models.

Discrete fracture models consider flow and transport processes within isolated (and normally connected) fractures. Analysis of problems with this approach has provided fundamental understanding of behaviour of relevant processes (Berkowitz, 1994). The main problem of this approach is the geometrical definition of the system. A number of conceptualizations have been developed proposed, which range from the simplest parallel plate model to 3-D fracture networks with variable aperture. Channelling models (Moreno et al., 1988) are also a particular type of this approach.

Continuum models consider the whole fractured medium as an equivalent porous medium. This approach is valid as long as it is possible to define a REV (Representative Elemental Volume) for the problem of interest. These models are applicable when the system allows sufficient interaction between fractures and porous blocks to allow establishment of local equilibrium. This approach solves the geometrical problem, but usually it is very difficult to find an adequate REV in fractured media.

Hybrid models are in the middle of the two approaches described above. This approach combines continuum representation of the domain with a discrete representation of the primary fractures in the formation.

5.1.2 Modelling approach and methodology for the Äspö Site Scale Model

As was mentioned in Chapter 4, the numerical tool used (TRANMEF-3) has the capability to handle multidimensional finite elements. This fact allows to simulate three-dimensional blocks of rock together with the main fractures defined as two-dimensional planes. The multidimensional capability is useful to reduce the number of elements and thus save CPU time and computer memory requirements.

The original plans of the ULC group for coping with the Äspö model were based on the use of a hybrid approach, including 3-D rock domains and 2-D conductor domains.

Methodologically, the numerical model was started as a continuum model (with 3-D elements) as a starting point before including the 2-D conductor domains. However, preliminary results obtained with the continuum model indicated the need to account for discrete fractures. Therefore, the discrete fracture approach was adopted. This decision was taken because:

1) The computed flow rate into the tunnel was less than a 7 % of the measured value even with an equivalent permeability larger than the median of the measured permeability.
2) The analysis of the measured flow rates indicates that the sections containing no hydraulic conductor domains contribute very little to the total flow rate.
3) Using a discrete fracture network approach allows us to save a lot of CPU time and memory. This is an important point due to the large number of calibration runs that are foreseen.

Table 5.1 shows the adopted methodology for the numerical modelling of the Äspö site.

Table 5.1 Methodology for the numerical modelling of the Äspö site

Set of Runs	*Characteristics*
Run_0	Steady-state flow Equivalent Porous media Simplified Boundary Conditions
Run_1	Steady-state flow Realistic Boundary Conditions
Run_2	Steady-state flow Discrete Fracture Networks
Run_3	Transient flow Discrete Fracture Networks
Run_4	Transport of conservative solutes Discrete Fracture Networks Hybrid approach to be considered
Run_5	2D-Reactive transport Redox Zone
Run_6	3D-Reactive transport Äspö site scale model

5.2 Spatial discretization

5.2.1 Geometry

The model domain consists in a three dimensional block of 2 x 2 km on the upper surface and 1 km depth (Figure 5.1). Inside this volume 19 of the 20 hydraulic conductor (HCD) domains have been considered (Figure 5.1). SFZ-14 is not considered because it is not crossed by the tunnel and neither connected with any other HCD. Then, in a Discrete Fracture Networks model this HCD is not playing any role. On the other hand, 11 out of the 19 HCD cross the Äspö HRL tunnel and elevator (Figure 5.1).

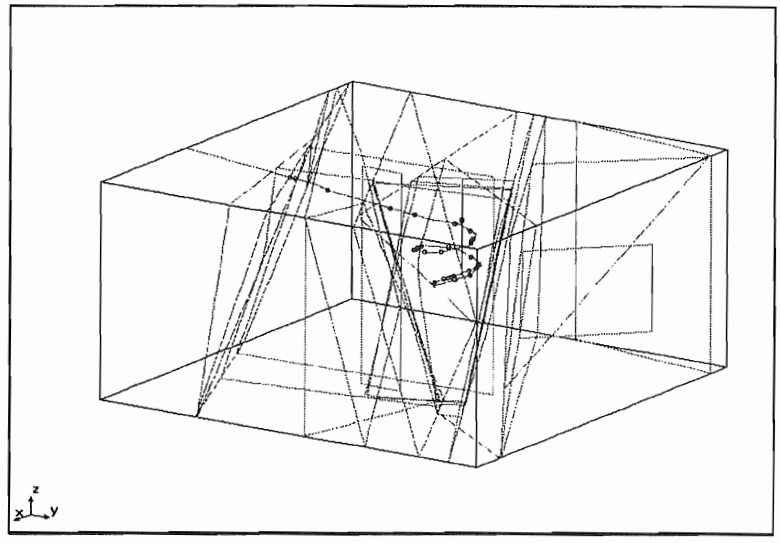

Figure 5.1 Model domain considered in the numerical model with the 20 hydraulic conductor domains, the Äspö HRL tunnel and the elevator. The points represent the intersection between the tunnel-elevator and the hydraulic conductor domains.

5.2.2 Spatial discretization for the Equivalent Porous Media Model

A finite elements mesh was generated for the continuum approach (Run_0 and Run_1). The mesh consists on 93,000 nodes and 87,500 3-D (prismatic) elements. In addition, 124 1-D elements were generated to represent the tunnel geometry. Figure 5.2 shows the 3-D mesh used in the continuum approach models. The mesh was progressively refined towards the central-upper part (near the tunnel position).

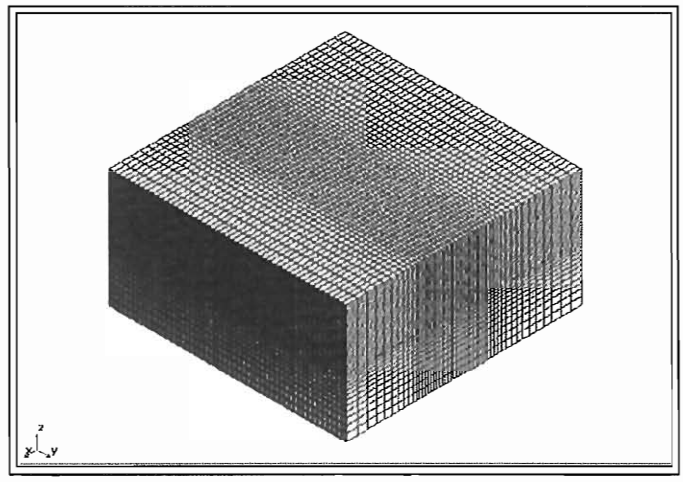

Figure 5.2 3D finite element mesh generated for Continuum Approach models

5.2.3 Spatial discretization for the Discrete Fracture Networks

The finite elements mesh generated for the Discrete Fracture Networks Models consists on 12,847 nodes and 14,273 elements. Most of them are 2-D quadrilateral elements for the hydraulic conductor domains discretization but, there are also 1-D linear elements to represent intersections between HCD and between de conductors and the external boundaries. HRL tunnel and elevator have been also discretized by means of 1-D linear elements.

Figures 5.3, 5.4, 5.5 and 5.6 show the details of the spatial discretization for the Discrete Fracture Networks Models.

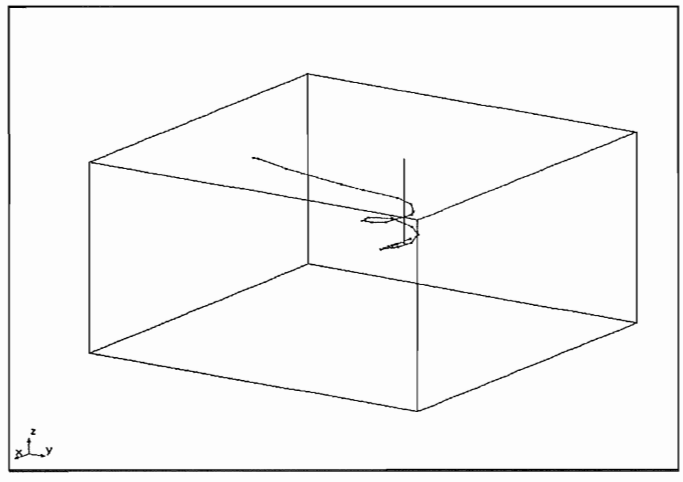

Figure 5.3 1D finite elements representing the HRL tunnel and elevator

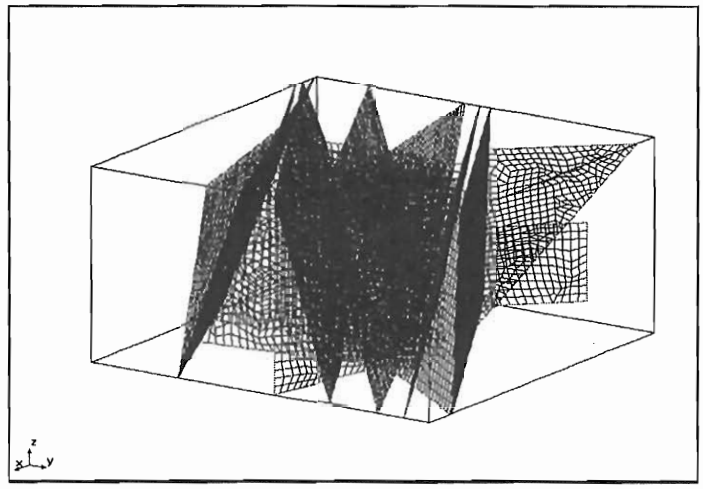

Figure 5.4 Spatial discretization used for the Hydraulic Conductor Domains using 2-D finite elements.

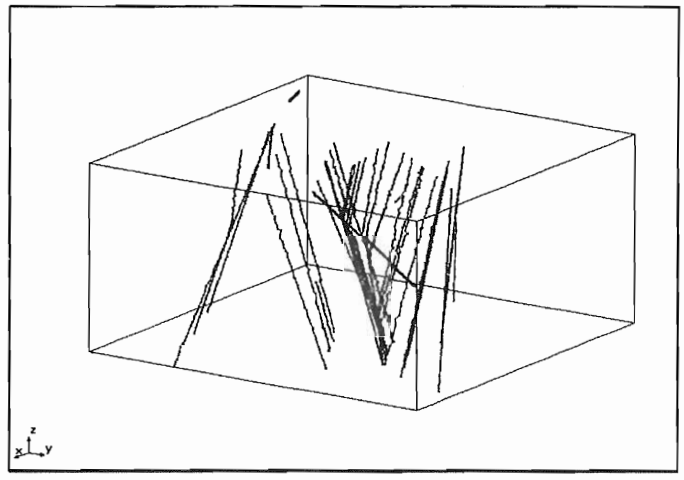

Figure 5.5 1-D elements used to represent Hydraulic Conductor Domains intersections.

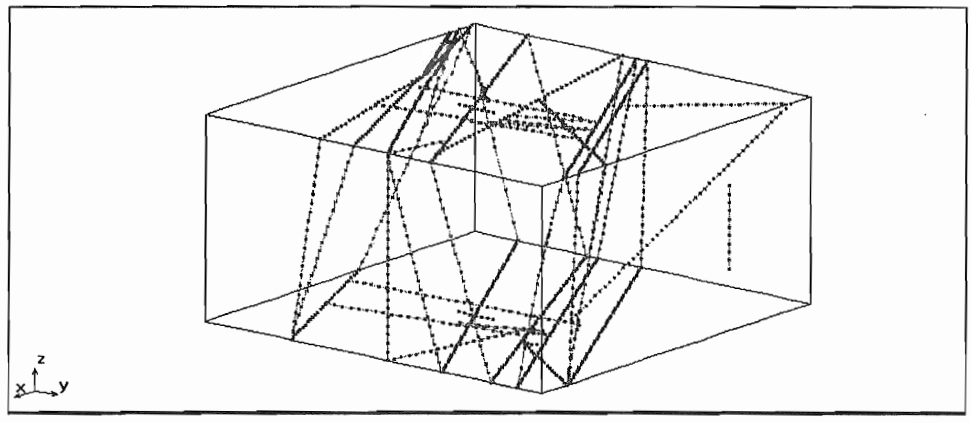

Figure 5.6 1-D elements used to represent the intersections between the Hydraulic Conductors Domains and the external boundaries.

5.3 Time discretization

For the Task #5 exercise the proposed model was specified to start on 1990-10-01. Instead of this date, the Discrete Fracture Networks model starts on 1991-06-27, because this is the date in which the tunnel crossed the first Hydraulic Conductor Domain (EW-7). The final time for the model is the 1997-01-01. Therefore, the numerical model covers a period of 2013 days.

Time discretization (Δt) are equal to 1 day, except for the dates when the tunnel crosses a HCD when Δt is ten times smaller. This discretization criterion for the time leads to a total of 2275 time steps.

A key point of the model is de simulation of the tunnel construction process. There are two decisions to be taken concerning with this issue:

1) How many stages must be considered to simulate de tunnel front movement.
2) The way to introduce the tunnel advance into the numerical model.

To simulate the tunnel advance there are two possibilities: (1) to simulate each stage with a single computer run, using as initial conditions the results computed by the previous run and, (2) to simulate the whole tunnel construction (all the stages) with a single run. A single run for the whole tunnel construction is a time-saving option which avoids reading and writing intermediate computed results. In addition, this is a better option in order to prevent possible mistakes. However, to model the entire construction in a single run the code must be able to handle with time varying.

In the numerical model presented in this report a mixed condition was adopted for the tunnel internal boundary. Using the mixed boundary condition, a minor change in the numerical code must be done in order to be able to model the whole process of the tunnel advance using only a single run. The change consists on introduce the capability of handle with leakage coefficients values variable in time. In this way, the leakage coefficient of a node will have a zero value (no boundary condition) for the time before the tunnel arrive to the node location, and will have a non-zero value after this time.

The tunnel front movement has been simulated by using 29 stages, one stage for each time that the tunnel crossed a Hydraulic Conductor Domain. Table 5.2 shows a summary of the characteristics of the simulation of the tunnel advance adopted in the numerical model.

Table 5.2 Stages for the simulation of tunnel and elevator construction

Model day	*Date*	*H.C.D. crossed*
0	91/06/27	EW-7
34	91/07/31	NE-4N
133	91/11/07	NE-3
313	92/05/06	NE-1
412	92/08/13	EW-3
432	92/09/02	NE-2
486	92/10/26	NNW-7
509	92/11/18	NNW-1
524	92/12/03	NNW-2
525	92/12/04	NE-2
572	93/01/20	NNW-4
600	93/02/17	NNW-4
614	93/03/09	Elevator
634	93/03/23	NNW-2
642	93/03/31	NNW-1
656	93/04/14	NNW-7
683	93/05/11	NE-2
697	93/05/25	NNW-7
914	93/12/28	NNW-1
928	94/01/11	NNW-2
944	94/01/27	NE-2
958	94/02/10	NNW-4
986	94/03/10	NNW-4
1103	94/07/05	NNW-2
1112	94/07/14	NNW-1
1123	94/07/25	NE-2
1125	94/07/27	NNW-7
1137	94/08/08	NNW-5
2013	01/01/97	Stop model

5.4 Boundary and initial conditions

5.4.1 Groundwater flow

- Side boundaries: Dirichlet condition with h* = 1000 m.
- Bottom boundary: Neumann condition (impervious, Q* = 0).
- Upper boundary I (Baltic sea):Dirichlet condition with h* = 1000m.
- Upper boundary II (Lands): Specified groundwater recharge R = 5 mm/year.
- Inner Boundaries (tunnel & elevator): Dirichlet condition with a prescribed pressure head equal to atmospheric pressure.

Figure 5.7 shows the 1-D elements used to represent the intersections between HCD and the upper external boundary. In this figure it is possible to distinguish the elements corresponding to emerged lands (with surface recharge) and the elements under the Baltic sea (prescribed head pressure).

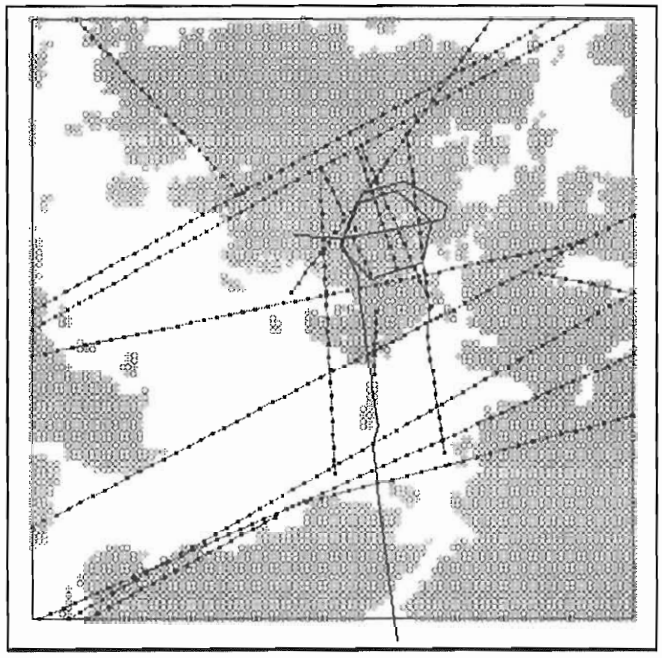

Figure 5.7 1D elements used to represent the intersection between H.C.D. and the upper boundary. In the figure it is represented the emerged land (grey) and the Baltic sea (white). Elements on the land have recharge boundary condition while elements on the sea have Dirichlet condition.

An initial hydraulic head of 1000 m was assigned to the whole domain.

5.4.2 Transport of solutes

- Side boundaries: Solute Flux associated to water flux (no dispersion).
- Bottom boundary: No flux.
- Upper boundary I (Baltic sea): Dirichlet condition with Baltic sea water concentration.
- Upper boundary II (Lands): Dirichlet condition with meteoric concentration.
- Inner Boundaries (tunnel & elevator): Solute flux associated to water flux.

To define the initial conditions of solute transport it is needed to interpolate from the 3-D data grid provided by Task #5 data deliveries to the nodes of our finite element mesh. For finding out the values to apply in the finite element mesh, the first adopted solution (the easiest) was to find the closest point of the data grid to each one of the nodes and use that concentration value. This is a very poor approach, because it is possible to find in the data grid two neighbour points having very different solute concentrations (even 15000 times different for the case of chlorides).

A better solution consists on using an interpolation method based on the concentration values (c_1) of the 3-D data grid. One can calculate the solute concentration (c_2) at any point of co-ordinates (x,y,z) as:

$$c_2(x,y,z) = \sum_{i=1}^{8} c_1^i \cdot N_i(x,y,z) \tag{5.1}$$

where $N_i(x,y,z)$ are the interpolation functions of concentration.

The same shape functions used by the code TRANMEF-3 (Juanes, 1997) have been used as interpolation functions. The shape functions use local co-ordinates (Figure 5.8) so, it is needed to make a transformation:

$$\begin{aligned} \xi &= \frac{(x_2 - x_c)}{\Delta x_1} \\ \eta &= \frac{(y_2 - y_c)}{\Delta y_1} \\ \zeta &= \frac{(z_2 - z_c)}{\Delta z_1} \end{aligned} \tag{5.2}$$

where:

(ξ,η,ζ) are local co-ordinates of the cube
(x_2,y_2,z_2) are global co-ordinates of the point in which we want to calculate the solute concentration
(x_c,y_c,z_c) are global co-ordinates of the centre of the cube
$(\Delta x_1, \Delta y_1, \Delta z_1)$ represent the length of the three sides of the cube (distance between the data grid points).

Knowing the local co-ordinates of the interpolation point, the values of the interpolation functions at that point can be computed according to:

$$\begin{aligned} N_1(\xi,\eta,\zeta) &= \frac{1}{8}\cdot(1-\xi)\cdot(1-\eta)\cdot(1-\zeta) \\ N_2(\xi,\eta,\zeta) &= \frac{1}{8}\cdot(1+\xi)\cdot(1-\eta)\cdot(1-\zeta) \\ N_3(\xi,\eta,\zeta) &= \frac{1}{8}\cdot(1+\xi)\cdot(1+\eta)\cdot(1-\zeta) \\ N_4(\xi,\eta,\zeta) &= \frac{1}{8}\cdot(1-\xi)\cdot(1+\eta)\cdot(1-\zeta) \\ N_5(\xi,\eta,\zeta) &= \frac{1}{8}\cdot(1-\xi)\cdot(1-\eta)\cdot(1+\zeta) \\ N_6(\xi,\eta,\zeta) &= \frac{1}{8}\cdot(1+\xi)\cdot(1-\eta)\cdot(1+\zeta) \\ N_7(\xi,\eta,\zeta) &= \frac{1}{8}\cdot(1+\xi)\cdot(1+\eta)\cdot(1+\zeta) \end{aligned} \tag{5.3}$$

$$N_8(\xi,\eta,\zeta)=\frac{1}{8}\cdot(1-\xi)\cdot(1+\eta)\cdot(1+\zeta)$$

Using interpolation functions (5.3) and with the equation (5.1) the solute concentration in each node of the finite elements mesh can be obtained.

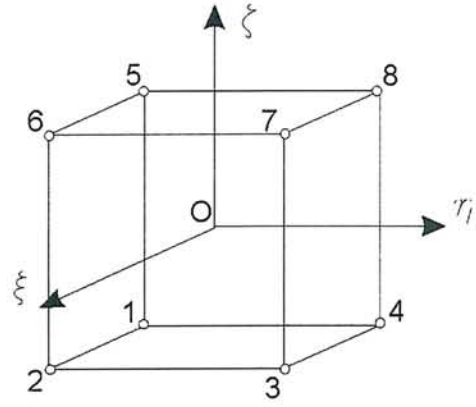

Figure 5.8 Local co-ordinate system of the shape functions used as interpolation functions to generate initial conditions of solute transport

Figure 5.9 shows the initial conditions for chloride concentration interpolated by using the shape functions described above.

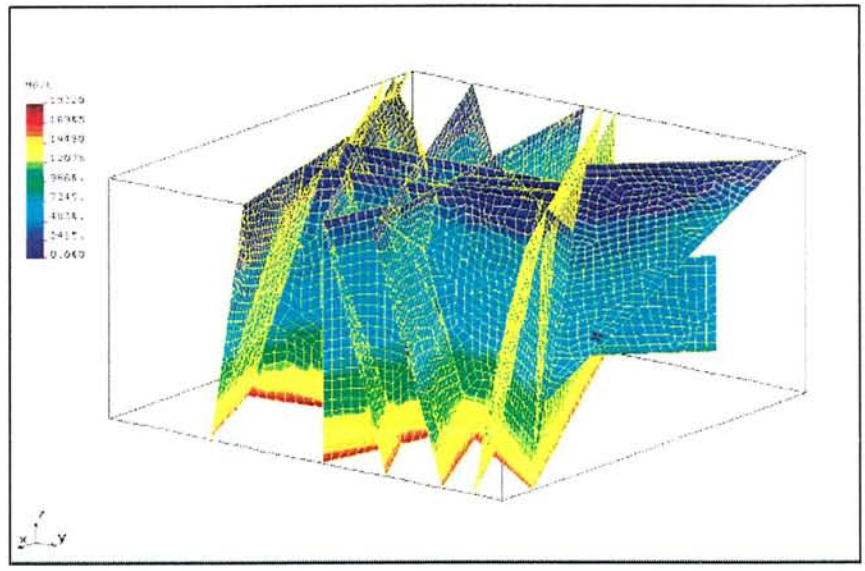

Figure 5.9 Initial chloride concentrations interpolated by using interpolation functions described above.

5.5 Parameters

The main material parameters for the numerical model are hydraulic conductivity (K) and specific storage coefficient (Ss) concerning to the groundwater flow, and kinematic porosity (n_e) and dispersivity (α) concerning to the transport of solutes.

Table 5.3 shows the values of transmisivity and width for each HCD. These values were taken from Rhén et al. (1997 b) and correspond to the median of the measured values. There are also 3 measured values of the storage coefficient. The rest of values of the storage coefficient and those adopted for the transport have been deduced with the equations 2.1, 2.2 and 2.3, introduced in Chapter 2.

Table 5.3 Flow parameters used in the numerical model (Rhén et al., 1997 b)

H.C.D.	Width (m)	T (m2/s)	S (-) meas
EW-1N	30	1,50E-06	
EW-1S	30	2,20E-05	
EW-3	15	2,40E-05	
EW-7	10	6,80E-05	
NE-1	30	3,00E-04	2,60E-05
NE-2	5	4,10E-07	
NE-3	50	2,90E-04	
NE-4N	40	3,00E-05	
NE-4S	40	3,00E-05	
NNW-1	20	1,10E-05	5,00E-06
NNW-2	20	5,60E-05	2,00E-06
NNW-4	10	1,50E-04	
SFZ-11	20	3,60E-06	
NW-1	10	1,70E-07	
NNW-5	20	2,00E-06	
NNW-6	20	1,40E-05	
NNW-7	20	4,80E-06	
NNW-8	20	1,00E-05	
NNW-3	20	2,00E-05	

6 RESULTS

6.1 Introduction

The main results concerning steady-state and transient modelling are presented in this chapter. Due to the delay of ULC in joining the Task Force #5 (in September of 1998), it has been not possible to present results of the transport modelling in this report. Therefore, no predictions of the concentrations and mixing proportions at the selected control points are available for April.

The results of the transient flow are good, however, results the numerical model of groundwater flow need to be improved with further calibrations.

The Äspö HRL site scale model constitutes a good opportunity to apply last generation numerical codes because the amount of data and conceptual knowledge generated by SKB is extremely large. It is important to recall that the complexity of the geometry and the space scale of the problem require a big deal of computational effort (in terms of memory and mainly of CPU time). This fact together with the amount of observation data to be checked after every run makes the calibration process a tedious, painfully long and difficult work. For all these reasons, the ENRESA+University of La Coruña team is in total agreement with the proposal of M. Uchida (99-03-09) to extend the modelling until August of 1999, and encourage the Task's members to join it. In our point of view the improvements of the results with this new schedule will be not only because our need of time but because the methodology. The comparison of the results presented in April and August and the analyses of possible discrepancies could be a very instructive exercise.

6.2 Steady-state groundwater flow

As was introduced in Chapter 5, the steady-state groundwater flow numerical model corresponds to a set of computation runs called Run_2.

These runs were the first attempt to calibrate the hydraulic conductivity field of the HCD. The starting values of the hydraulic conductivity field were those shown in table 5.3 and correspond to the median of the measured values (Rhén et al., 1997 b).

One of the important points extracted from the study of the Run_2 results is the role of transmissivities of the Hydraulic Conductors Domains in the numerical model. A sensitivity analysis of this parameter was done, and the results can be seen in the Figure 6.1. This figure shows a comparison of measured and computed flow rates into the tunnel for Run_2a and Run_2b. Transmissivities used in both runs

coincide with those values provided by (Rhén et al., 1997 b), but the difference is in the values used for the intersections.

Run_2a transmissivities of the intersections were equal to the arithmetic mean values of the intersected domains, while in Run_2b they were equal to 1000 m^2/day for each intersection.

Figure 6.1 illustrates that the model is not sensitive to the value of the transmissivities of these intersections, at least in terms of flow rates into the tunnel. Of course, the computed pressure head distribution around the intersection is different for both runs.

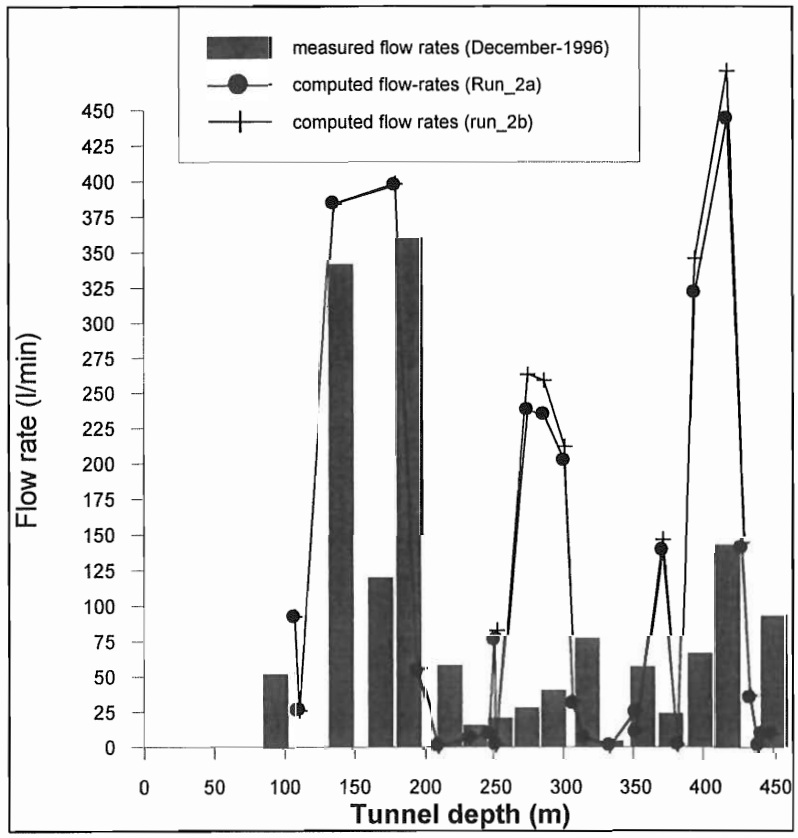

Figure 6.1 Results of Run_2a and Run_2b. Sensitivity analyses with respect to the intersections of transmissivity

Figure 6.2 shows the results of Run_2a and Run_2g. The last run was the best hydraulic conductivity calibration reached before starting with the transient flow modelling.

Due to the relatively small computational requirements needed to solve for steady-state flow (in comparison with transient flow), the set of computations run_2 was used to debug and check the model, for anomalies, mistakes in input data files, and specially for checking the behaviour of the intersections among HCD

Figure 6.3 shows the computed drawdowns in HCD NE1, NNW3 and NNW-7. It must be noticed that the tunnel cross all these three domains.

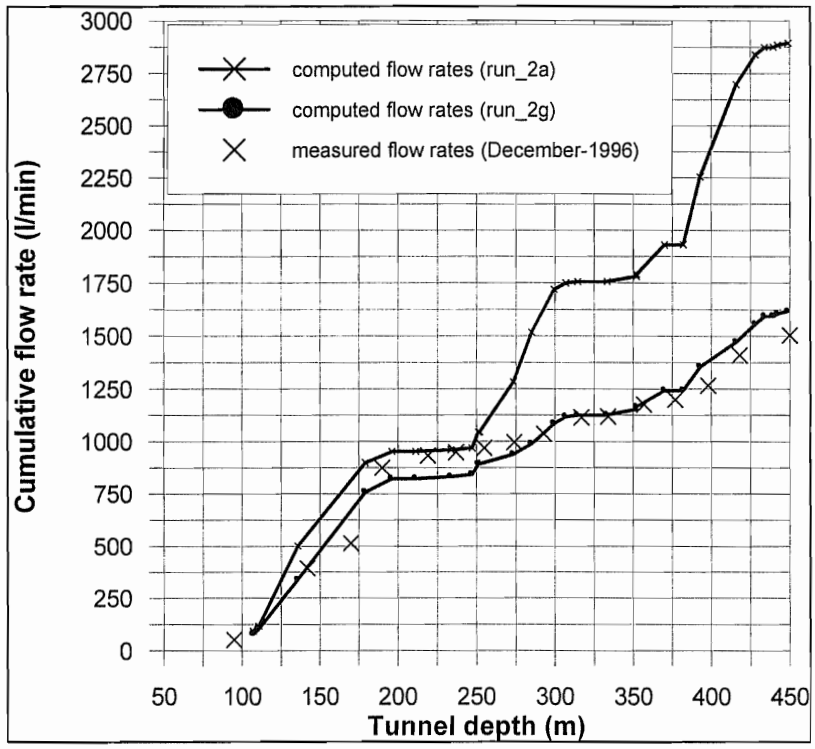

Figure 6.2 Measured and computed steady-state flow rates into the tunnel. Run_2g was the best calibration obtained for steady-state computations.

Figure 6.4 shows the computed drawdowns in the HCD NNW-4 and EW-1S. The difference of this figure is that only the NNW-4 HCD is crossed by the tunnel and then, the computed drawdowns in EW-1S are due to the connection with other domains. In Figure 6.4 it is possible to see the expected pattern of pressure head around the intersection.

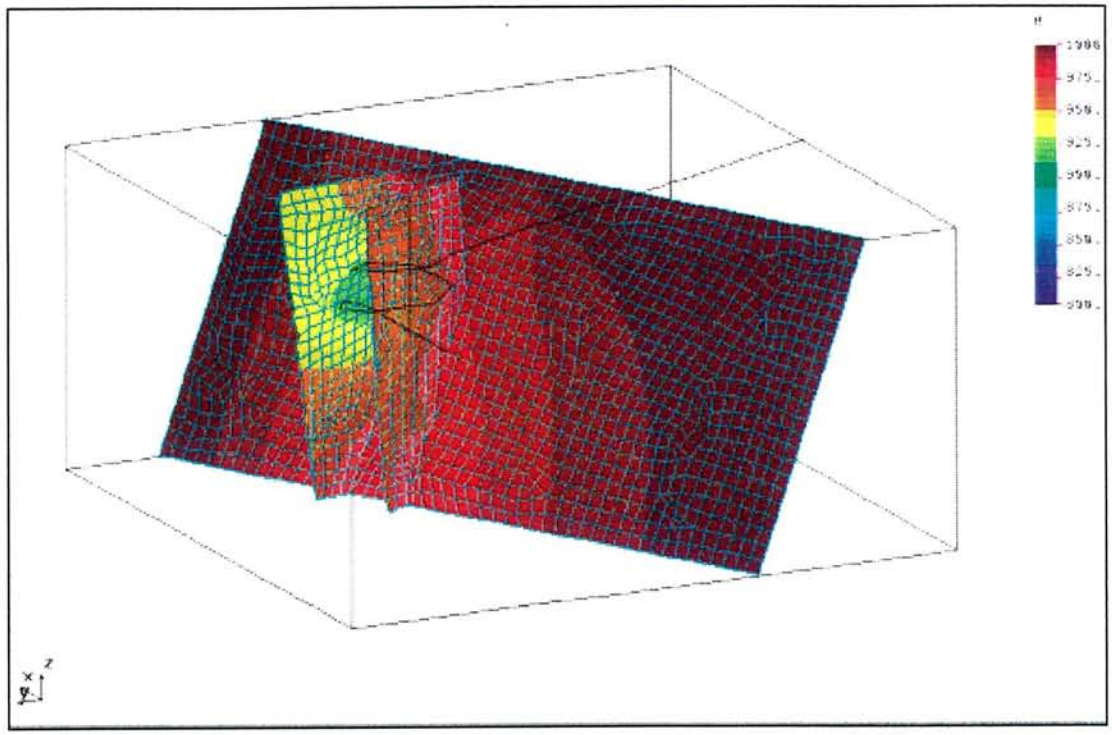

Figure 6.3 Computed steady-state pressure heads in HCD NE-1,NNW-3 and NNW-7.

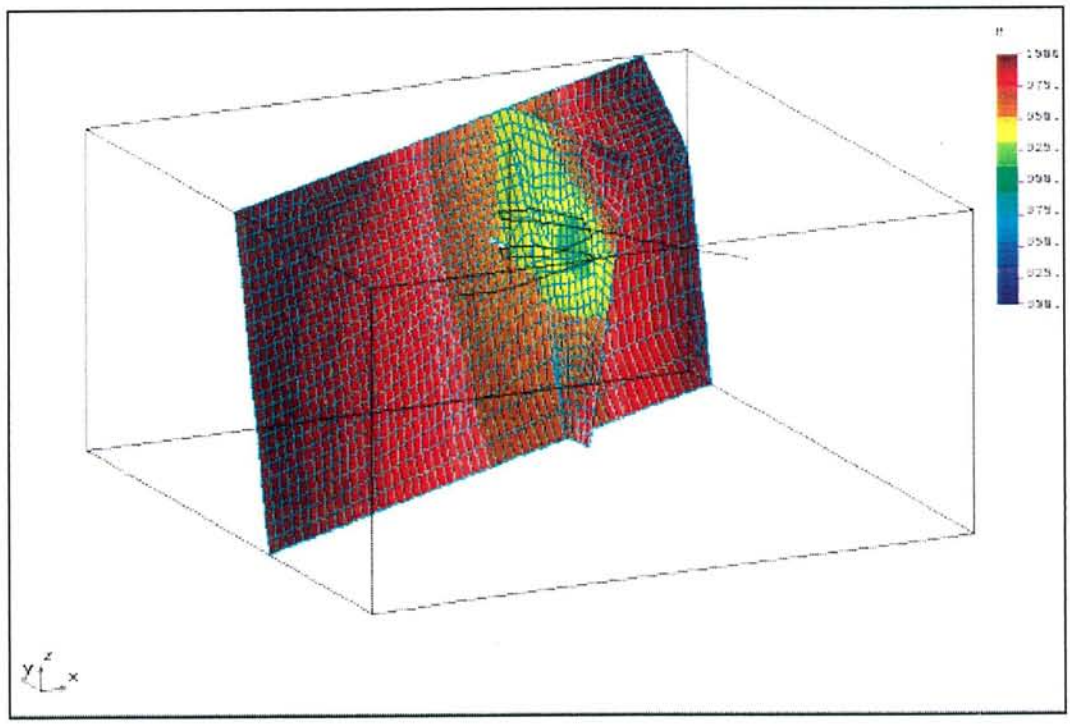

Figure 6.4 Computed steady-state pressure heads in HCD NNW-4 and EW-1S. Notice that EW-1S domain is not crossed by the tunnel.

6.3 Transient groundwater flow

The transient groundwater flow numerical model corresponds to a set of computation runs called Run_3. In this report the results of the Run_3l are presented. Run_3l is the best calibration run reach for the moment but as mentioned later further calibration must be done in the future.

It must be recalled that a mixed flow condition has been used for the inner boundary of the tunnel and elevator. This means that the flow rates into the tunnel are computed by the model and not prescribed as a boundary condition. Thus, measured flow rates into the tunnel can be compared to computed values. Finally, if the model is able to reproduce the system, it can be concluded that a model being able to reproduce flow rates and heads has more confidence than a model fitting only one of them, separately.

The observation points used to compare measured values with model results are listed in Table 6.1. In terms of head pressure the observation points are the sections of the boreholes KAS02 to KAS09, KAS12 and KAS14 crossing al least one HCD. In terms of flow rates the observation points are all the tunnel sections crossing at least one HCD. Despite the numerical model takes into account also the elevator, computed flow rates in the shafts have not yet been compared.

Table 6.1 List of observation points

Flow rate observation point	*Pressure heads Observation point*
MA1030G	KAS02(346-799)
MA1372G	KAS03(107-252)
MA1584G	KAS03(253-376)
MA1745G	KAS04(0-185)
MA1883G	KAS04(288-331)
MA2028G	KAS05(440-550)
MA2178G	KAS06(0-190)
MA2357G	KAS06(191-249)
MA2496G	KAS06(331-390)
MA2699G	KAS07(191-290)
MA2840G	KAS07(411-500)
MA2994G	KAS07(501-604)
MA3179G	KAS08(503-601)
MA3411G MA3426G MF0061G	KAS09(0-115)
	KAS14(0-130)

Figures 6.5 through 6.18 show the comparison between measured and computed flow rates into the tunnel at observation points. The analysis of these results indicates that there is an excellent agreement between computed and measured values. The main discrepancy can be found in section MA3179G (Figure 6.17) where the model is not able to reproduce the pattern of the evolution of the measured flow rate. Sections MA1745G and MA2496G show differences but must be noticed that these sections contribute only a little amount of water (around 20 and 4 l/min respectively) to the total flow rate of about 1600 l/min, and the model is able to reproduce the pattern evolution.

Figure 6.19 shows the evolution of total amount of water flowing into the tunnel. The model is able to reproduce patterns of measured data. The largest error is on the order of 20%. The model is not accounting for the contribution of the rock domains so it is reasonable to expect a computed flow rate smaller than the measured value. Once steady-state is reached, the model reproduce perfectly the measured data.

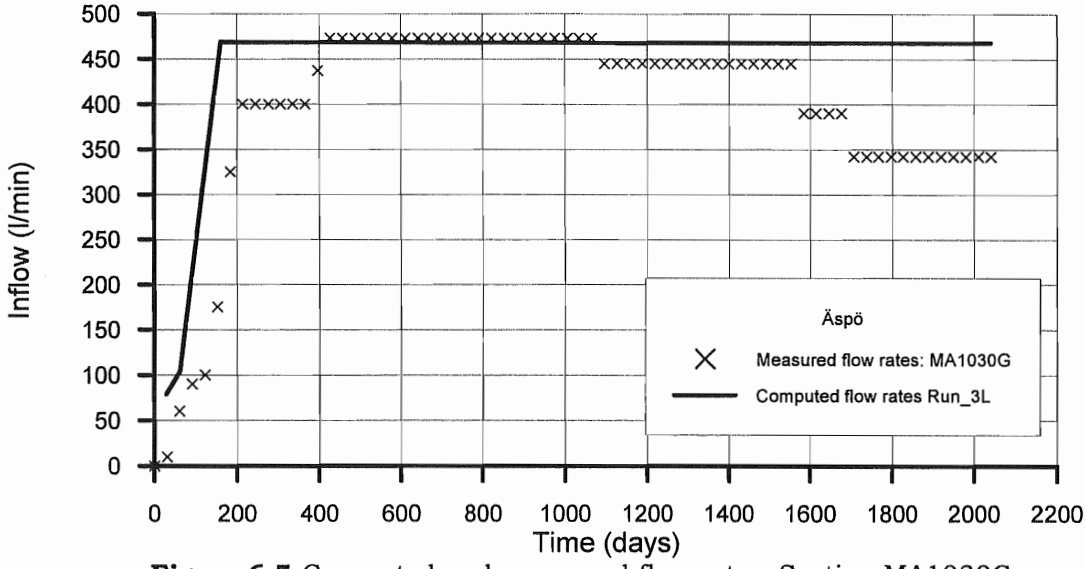

Figure 6.5 Computed and measured flow rates. Section MA1030G

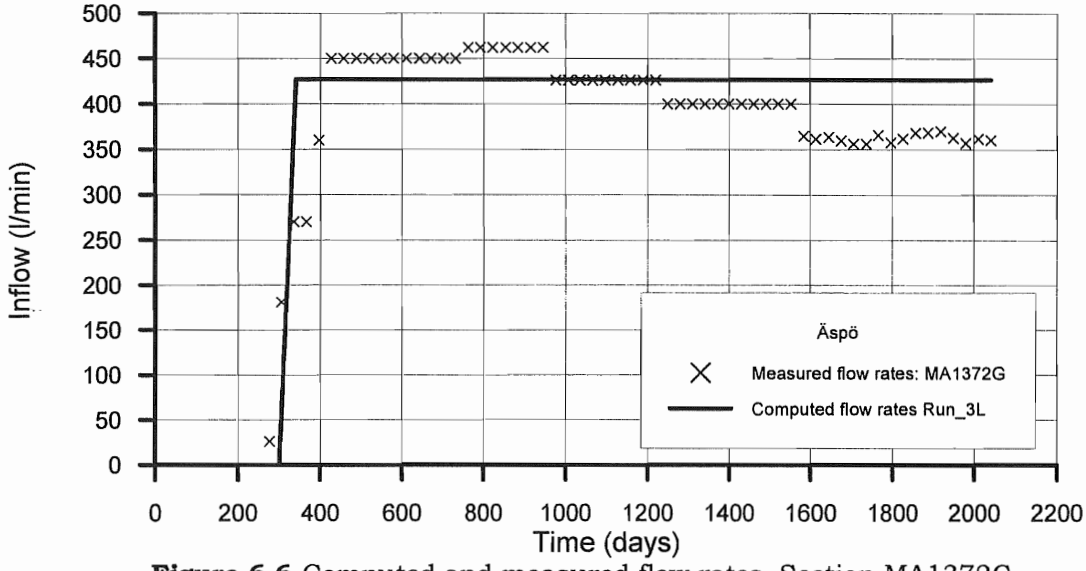

Figure 6.6 Computed and measured flow rates. Section MA1372G

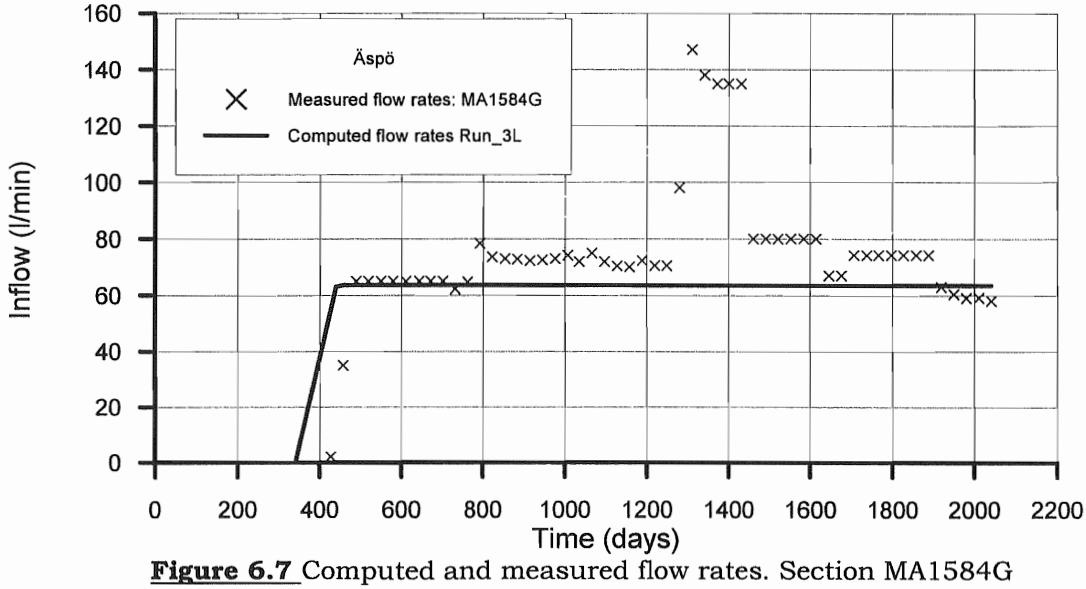

Figure 6.7 Computed and measured flow rates. Section MA1584G

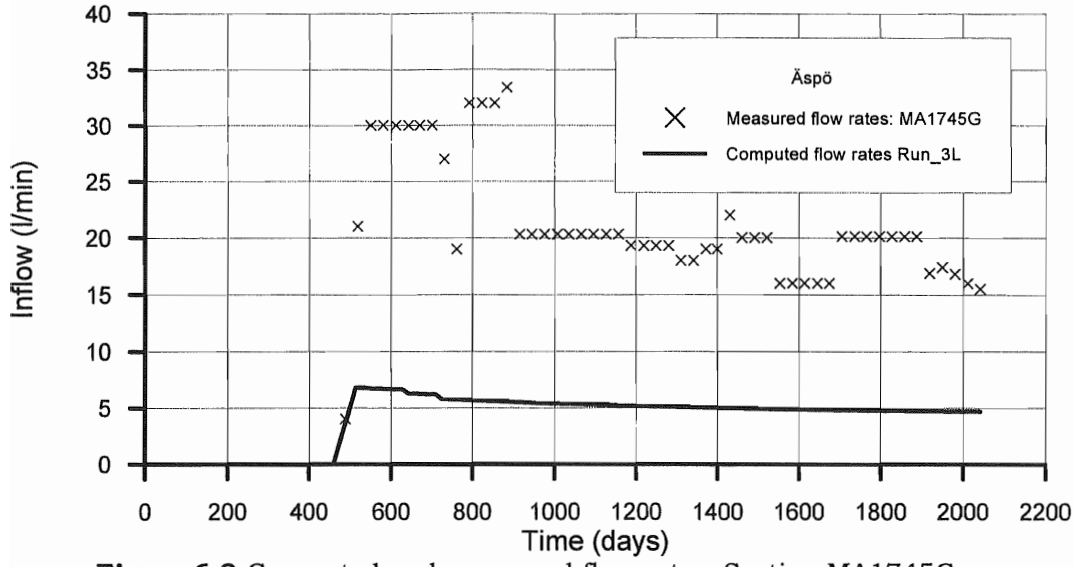

Figure 6.8 Computed and measured flow rates. Section MA1745G

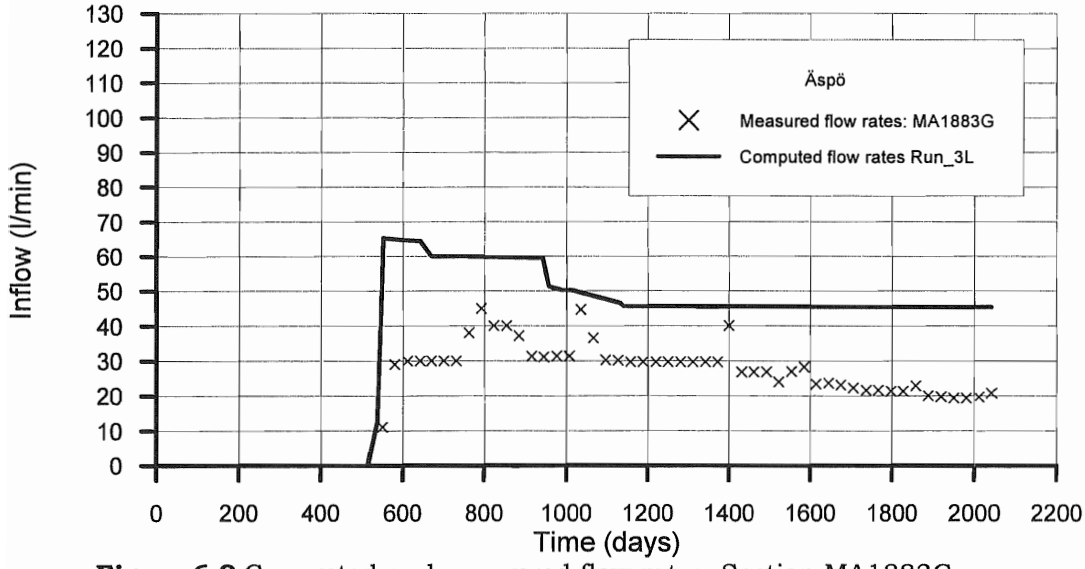

Figure 6.9 Computed and measured flow rates. Section MA1883G

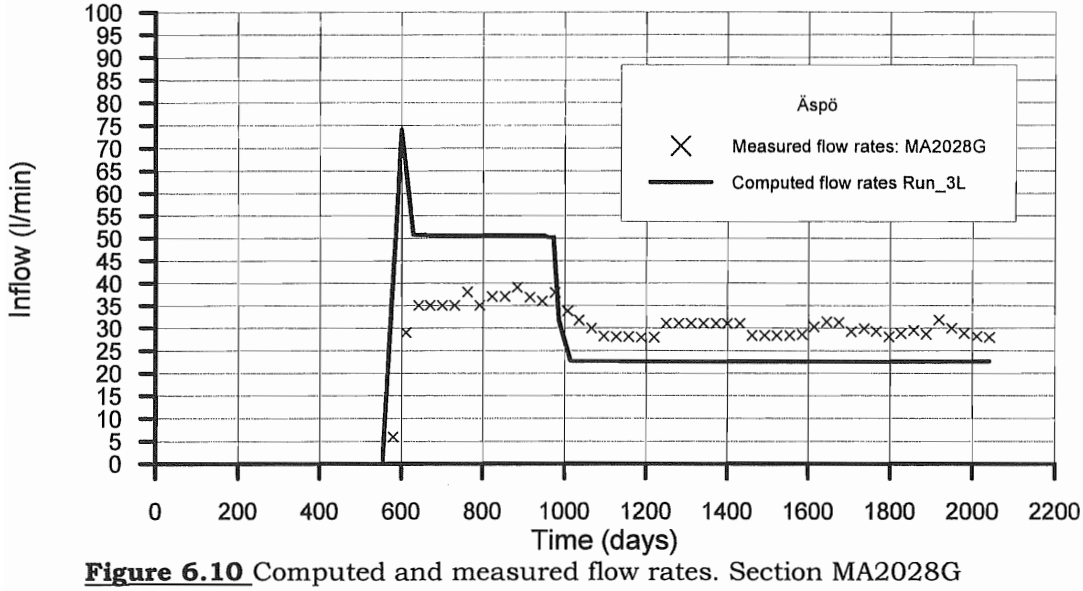

Figure 6.10 Computed and measured flow rates. Section MA2028G

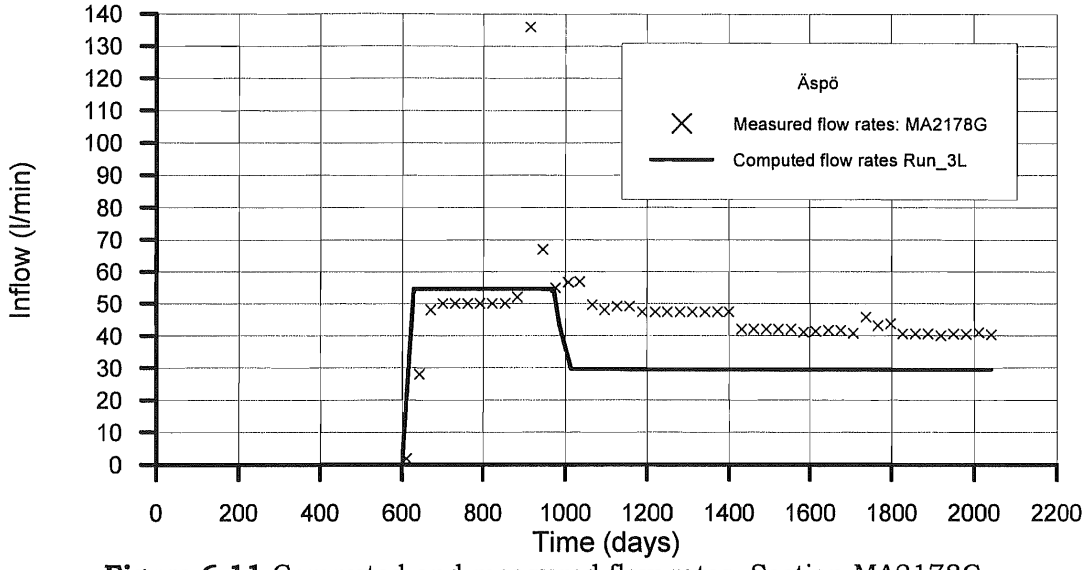

Figure 6.11 Computed and measured flow rates. Section MA2178G

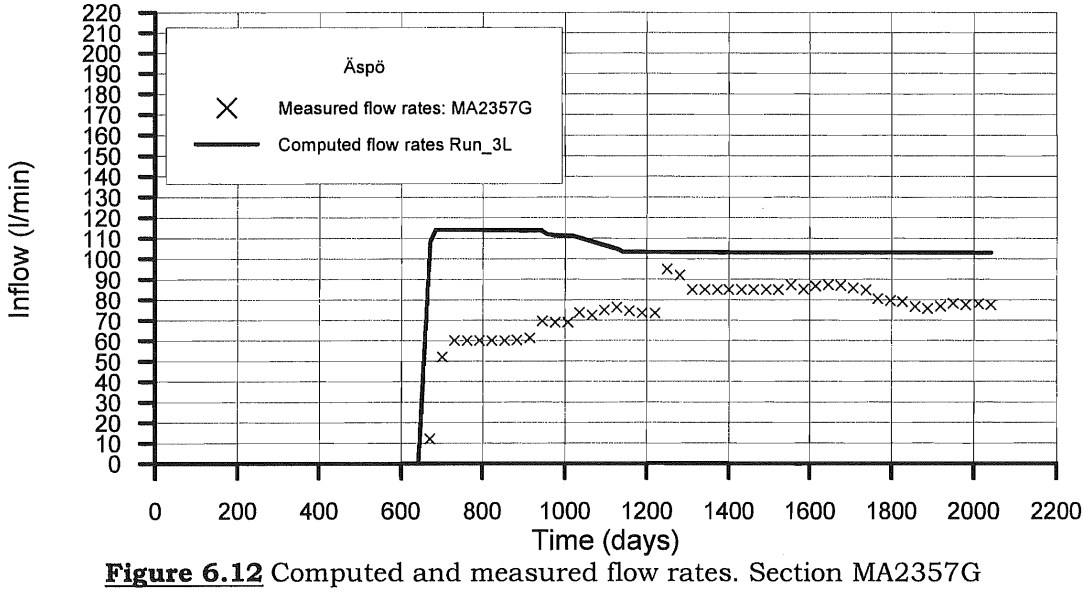

Figure 6.12 Computed and measured flow rates. Section MA2357G

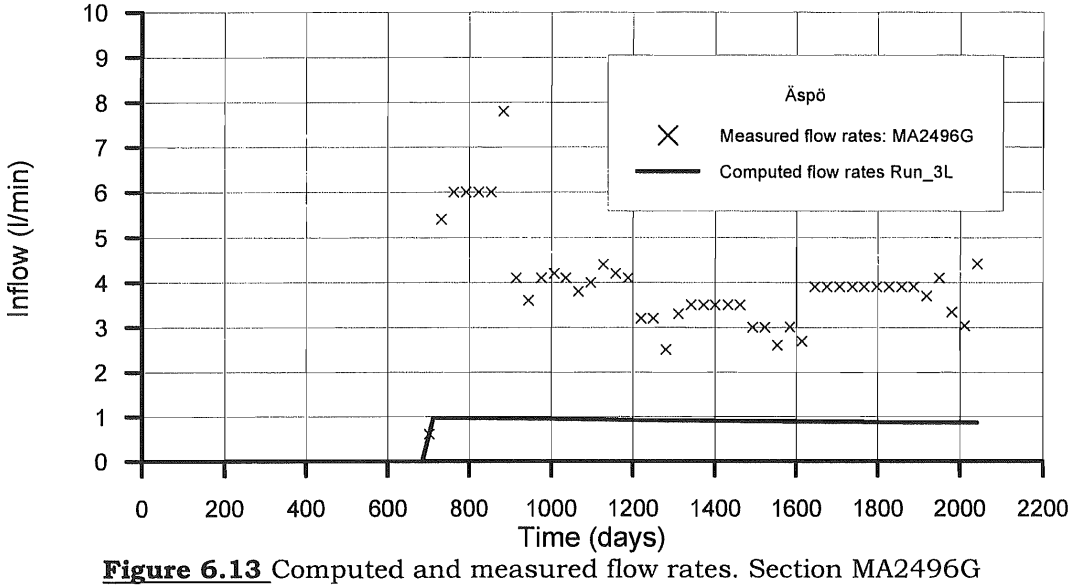

Figure 6.13 Computed and measured flow rates. Section MA2496G

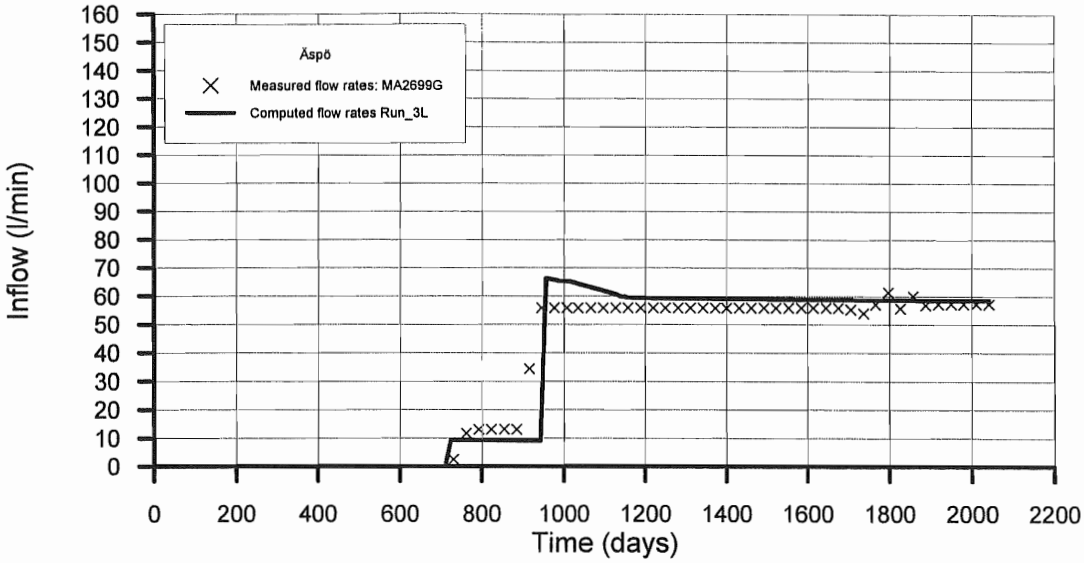

Figure 6.14 Computed and measured flow rates. Section MA2699G

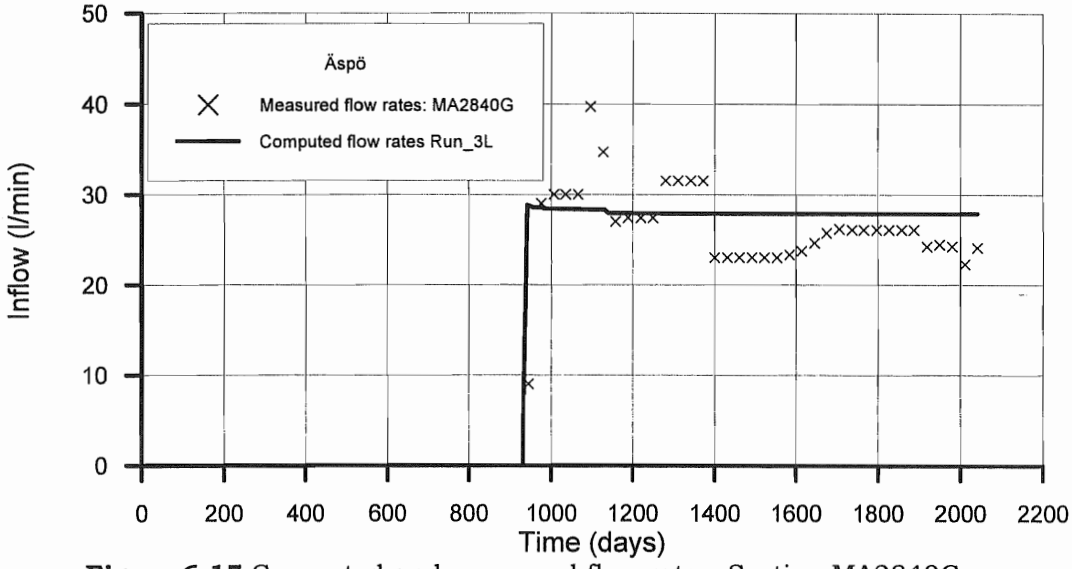

Figure 6.15 Computed and measured flow rates. Section MA2840G

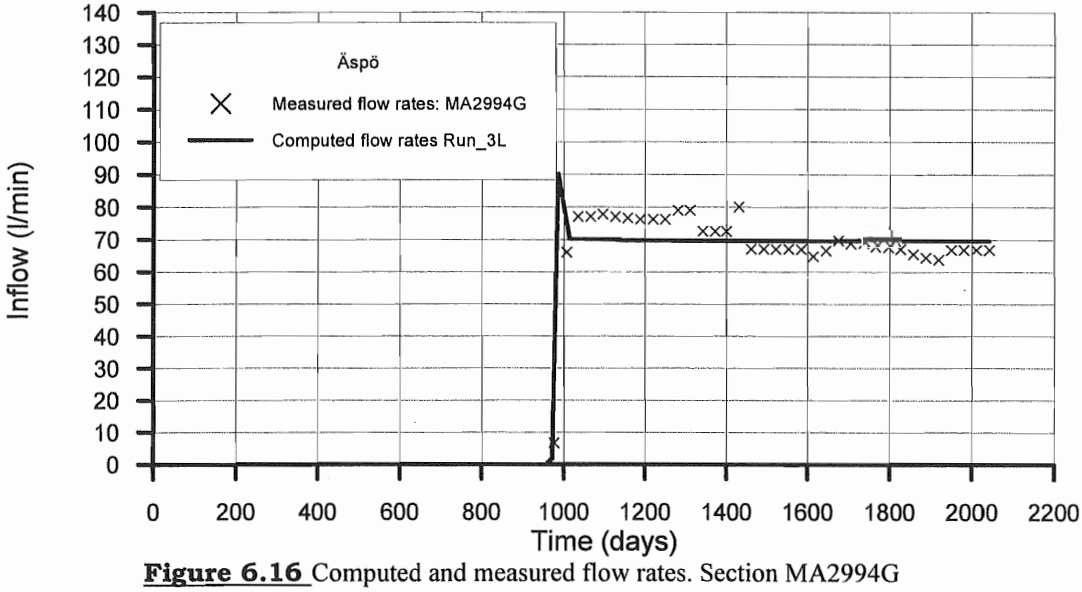

Figure 6.16 Computed and measured flow rates. Section MA2994G

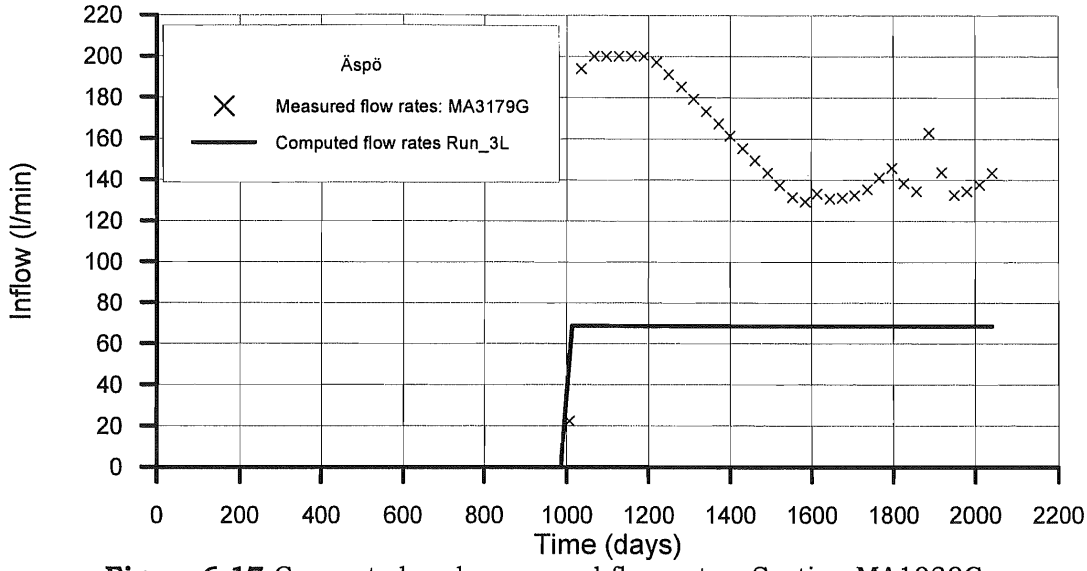

Figure 6.17 Computed and measured flow rates. Section MA1030G

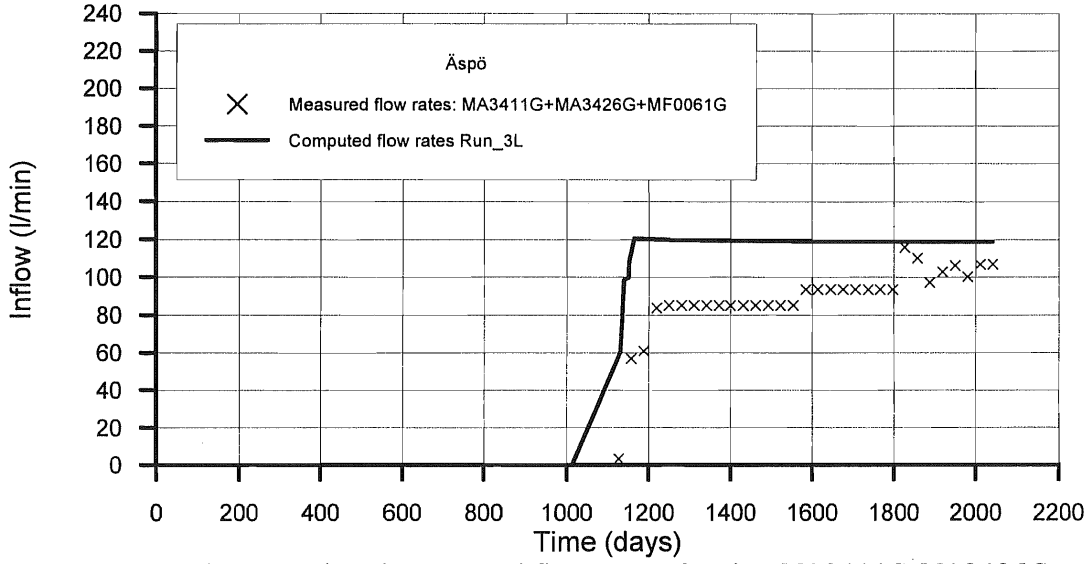

Figure 6.18 Computed and measured flow rates. Section MA3411G-MA3426G-MF0061G

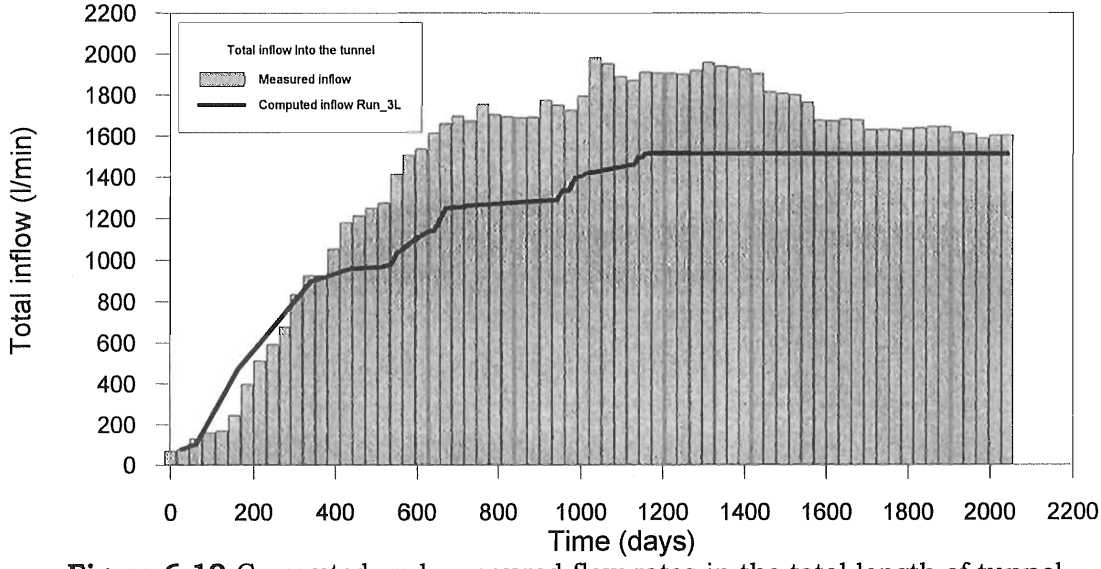

Figure 6.19 Computed and measured flow rates in the total length of tunnel

Figures 6.20 though 6.34 show the comparison between measured and computed pressure heads (freshwater head) in meters above sea level.

The analysis of head residuals indicates three major patterns. There are some observations points showing a good agreement between the measured and computed values. The best example is illustrated in Figure 6.24, which shows the comparison at borehole KAS04 (section 288-331). This section of the borehole cross the HCD EW-1S which is not crossed by the tunnel, and the agreement between model results and measured values is almost perfect.

Other points show some discrepancies between measured and computed values, but still the model is able to reproduce the behaviour (evolution) of measured heads. Figure 6.29 is a good example of this kind of results. Further efforts must be done in the calibration of the model, especially concerning the calibration of storage coefficients of the fractures crossing these borehole sections. In general, the model computes drawdowns which are smaller than measured values. Probably the model is using too large storage coefficient values.

Finally there are some observation points showing abnormal computed results. The model is not computing any drawdown in borehole KAS06 (0-190), while there is a clear influence of the tunnel construction in the measured data. These kind of major discrepancies could be caused by an improper connection between some domains that must be checked in the numerical model.

It can be concluded that, in general, the numerical model is in good agreement with measured data. The results will be improved in further calibration, which will require:

(1) Reviewing the connections between currently considered HCD.
(2) Checking the role of other HCD not included in the model.
(3) Reviewing the boundary conditions.
(4) Continuing with calibration of the values of T and S.
(5) Calibrating the values of leakage coefficient which control the inner boundary conditions in the tunnel

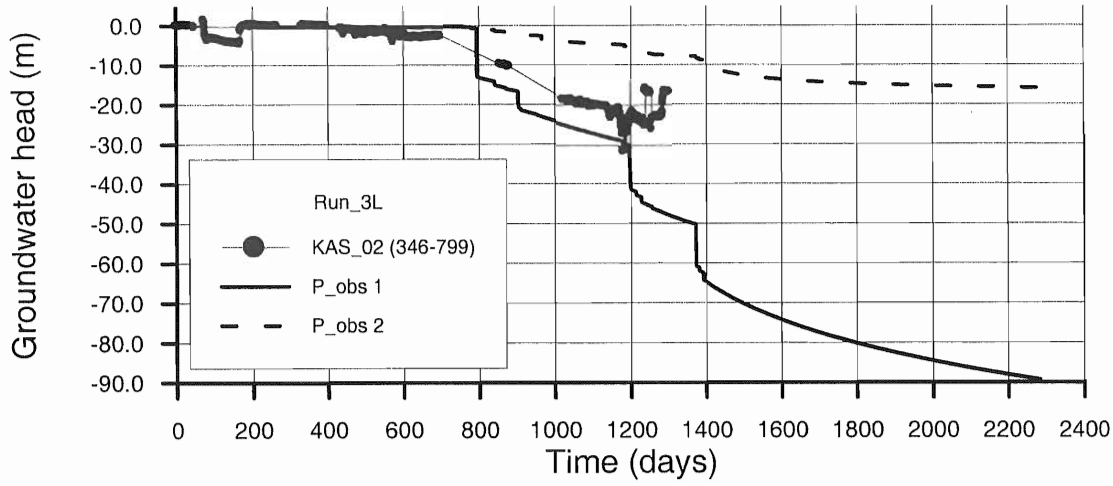

Figure 6.20 Computed and measured values KAS02 (346-799).

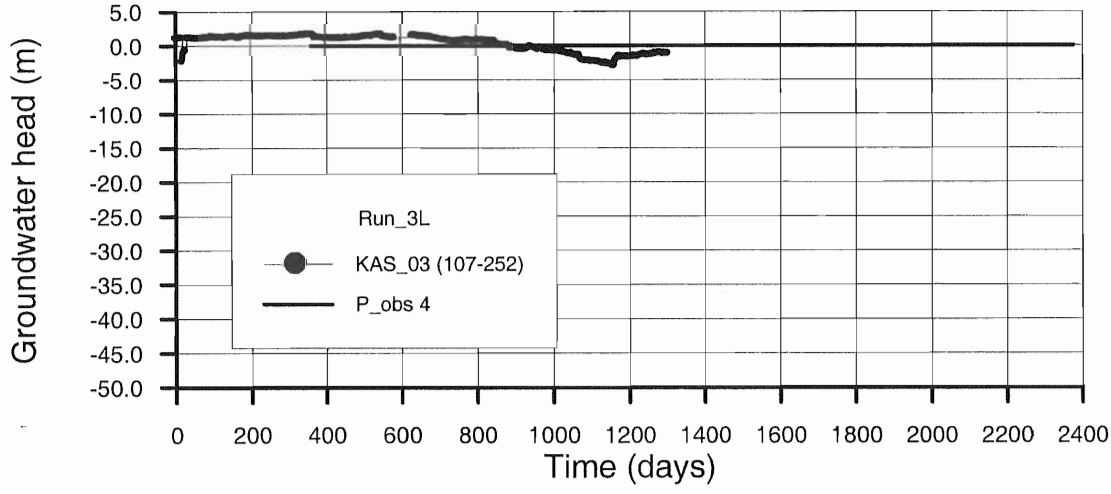

Figure 6.21 Computed and measured values KAS03 (107-252).

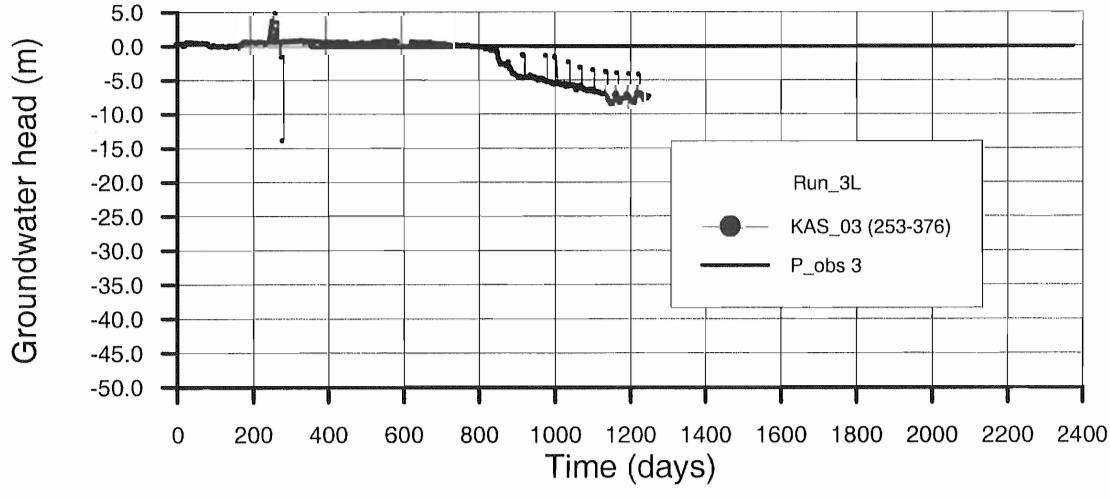

Figure 6.22 Computed and measured values KAS03 (253-376).

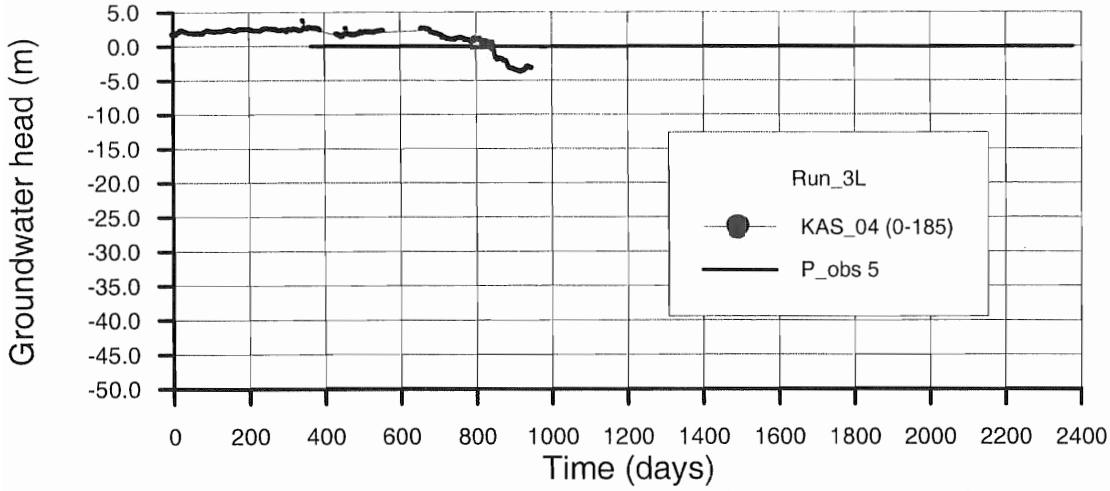

Figure 6.23 Computed and measured values KAS04 (0-185).

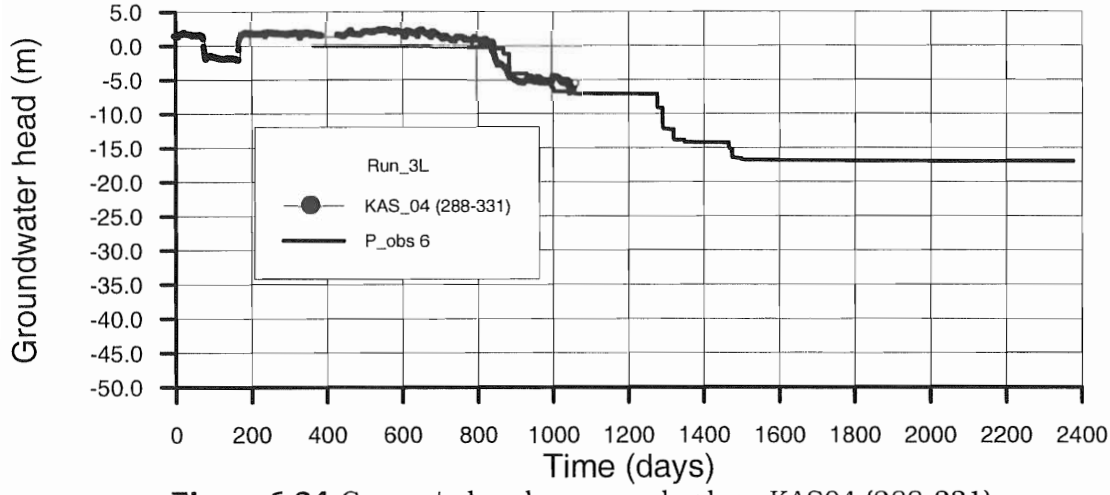

Figure 6.24 Computed and measured values KAS04 (288-331).

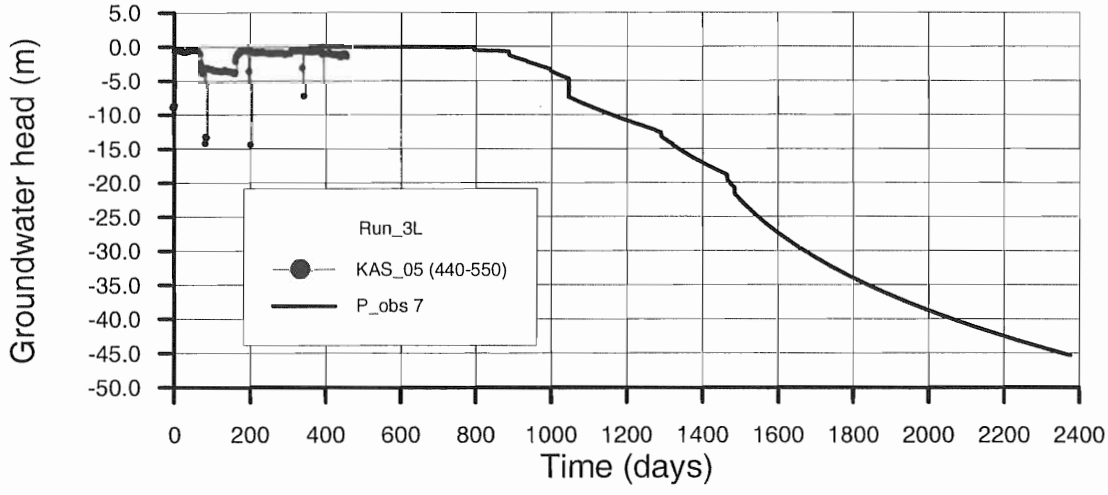

Figure 6.25 Computed and measured values KAS05 (440-550).

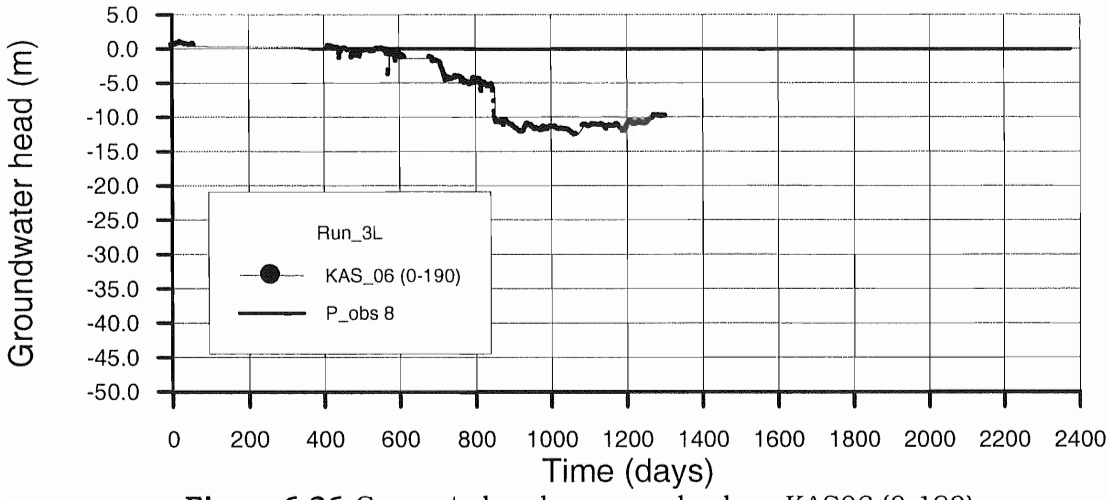

Figure 6.26 Computed and measured values KAS06 (0-190).

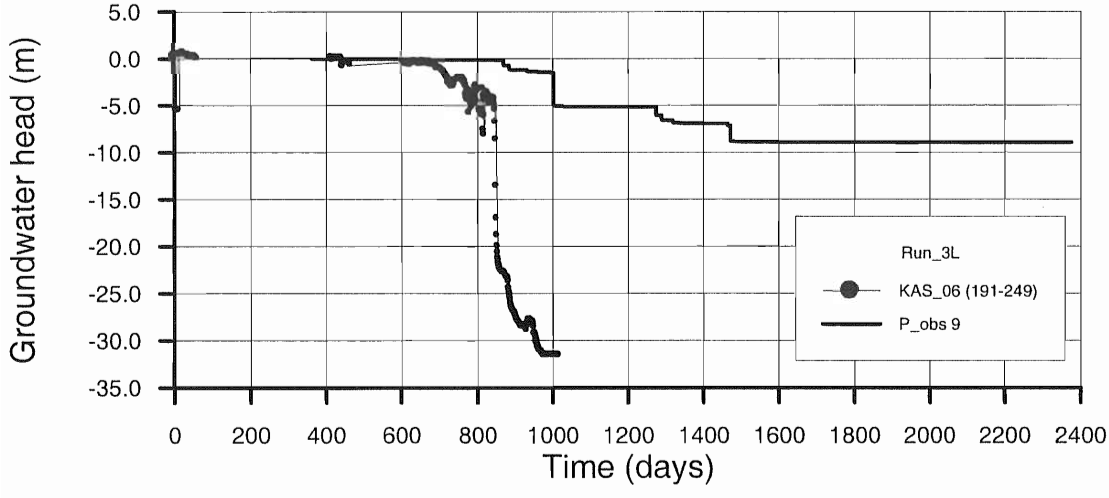

Figure 6.27 Computed and measured values KAS06 (191-249).

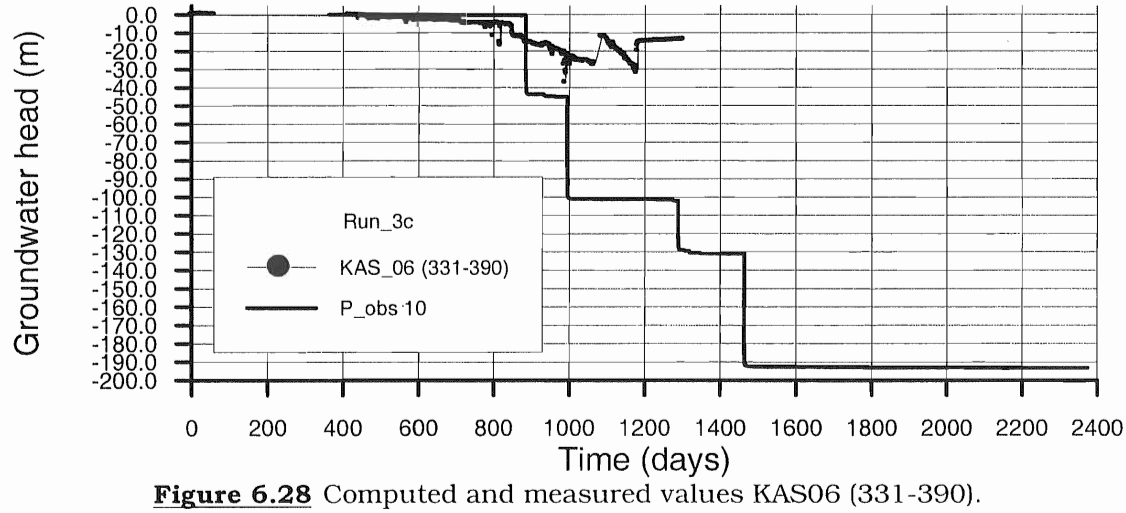

Figure 6.28 Computed and measured values KAS06 (331-390).

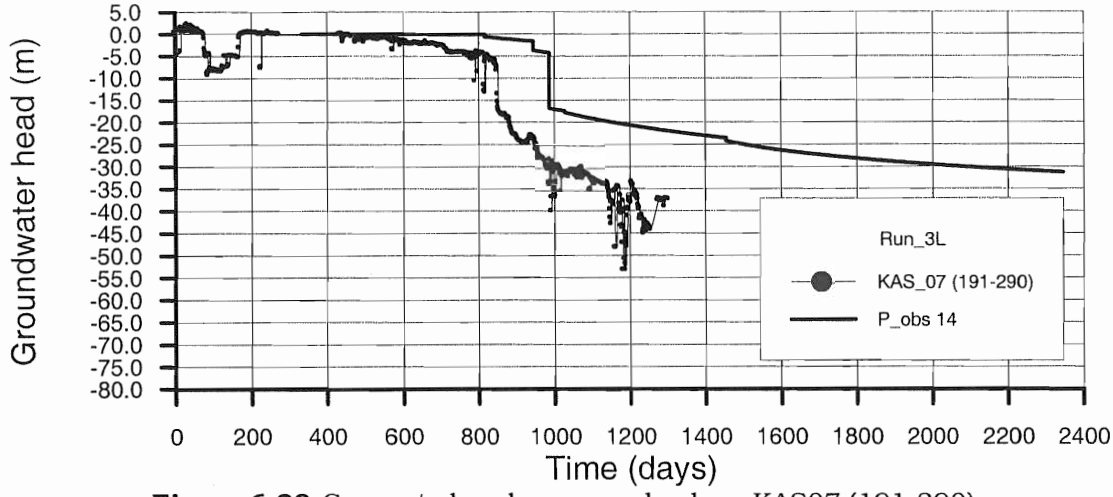

Figure 6.29 Computed and measured values KAS07 (191-290).

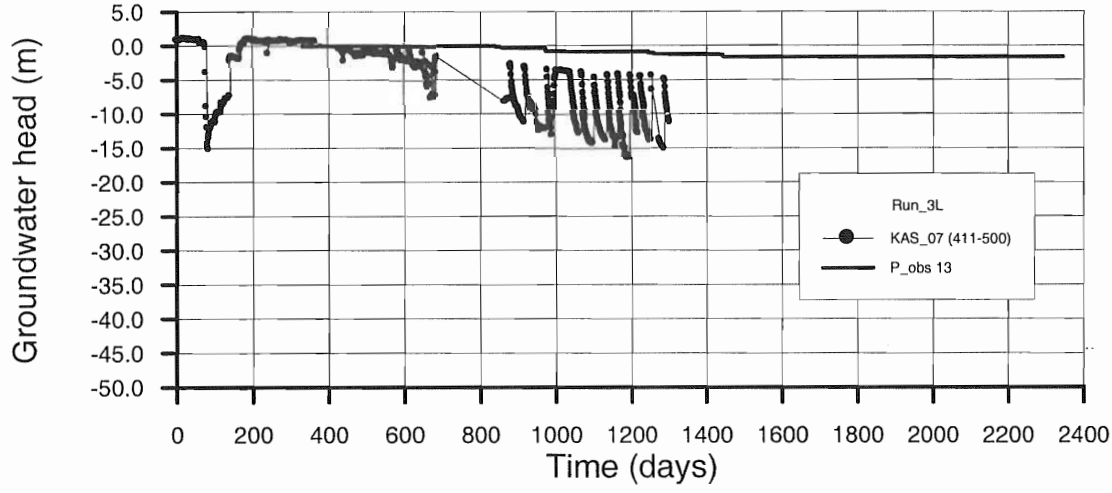

Figure 6.30 Computed and measured values KAS07 (411-500).

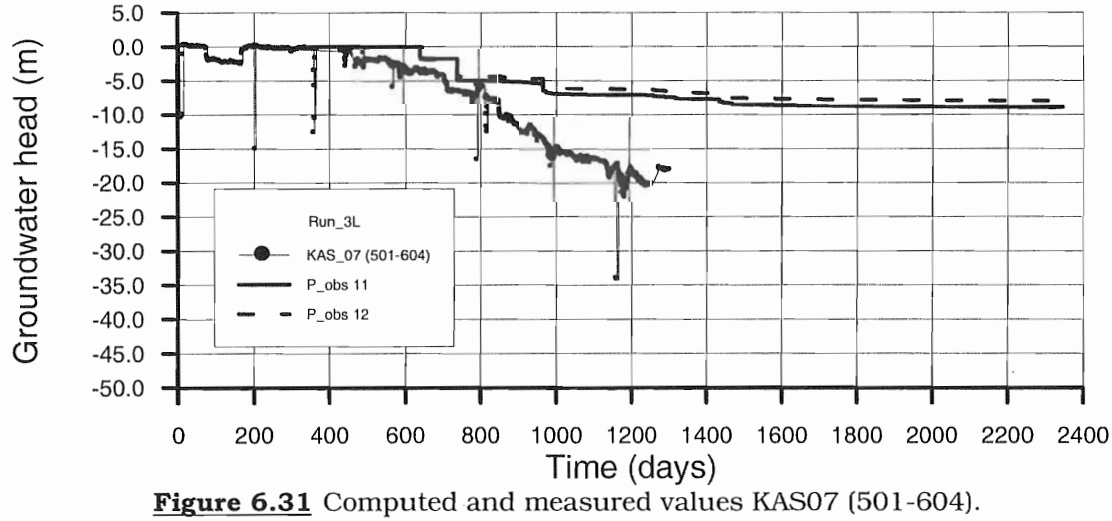

Figure 6.31 Computed and measured values KAS07 (501-604).

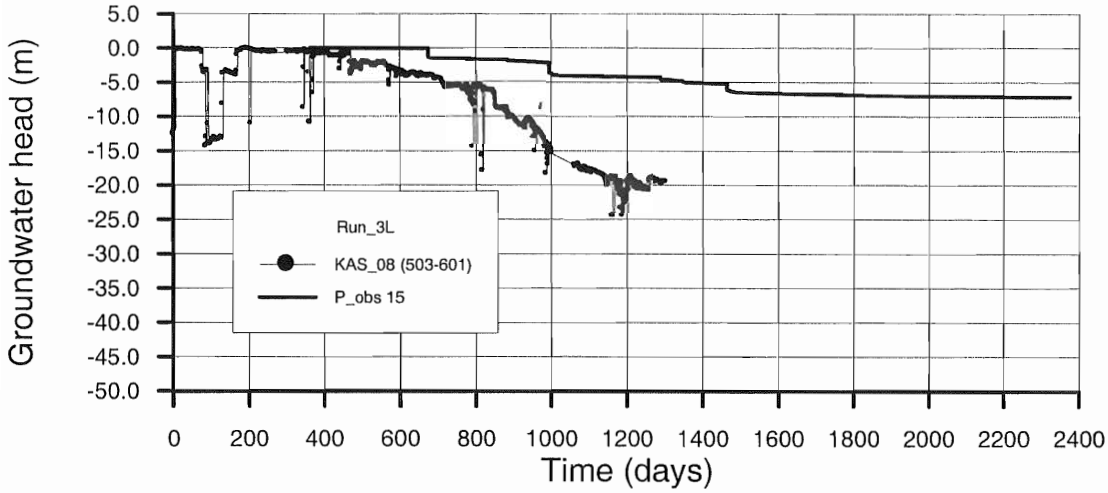

Figure 6.32 Computed and measured values KAS08 (503-601).

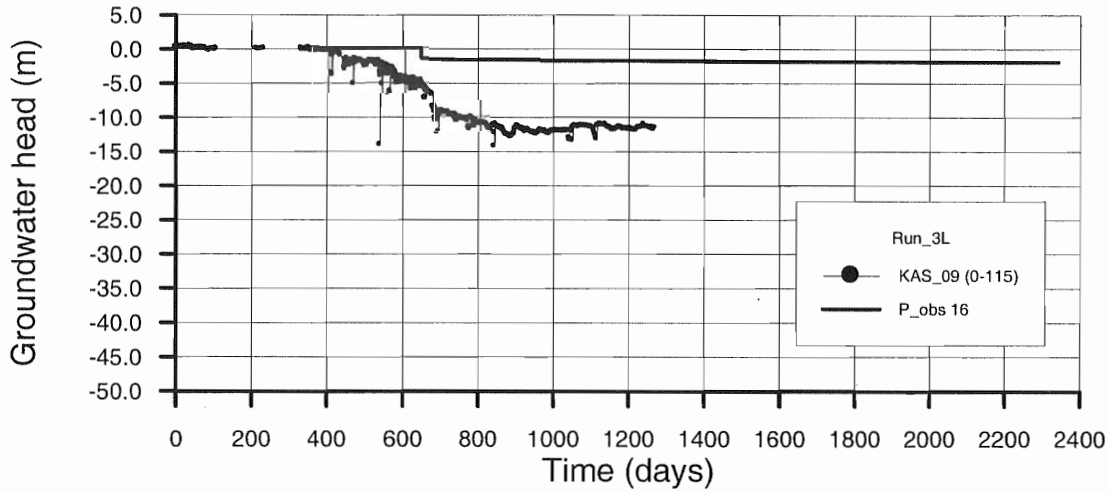

Figure 6.33 Computed and measured values KAS09 (0-115).

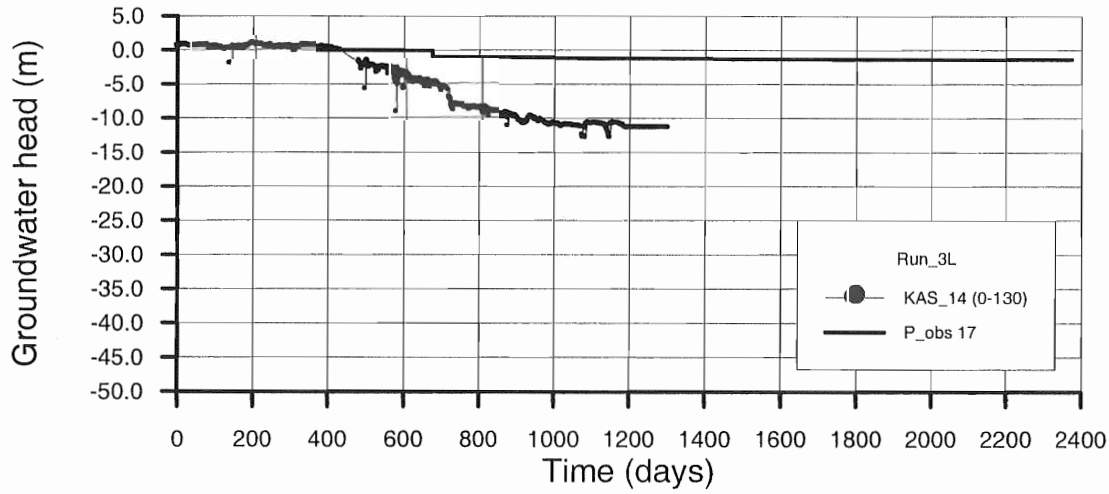

Figure 6.34 Computed and measured values KAS14 (0-130).

7 CONCLUSIONS

The numerical modelling of the groundwater flow of the Äspö site has been presented.

The numerical model was started with an Equivalent Porous Media Approach. However, the total computed flow rate into the tunnel was less than a 7 % of the measured value, even using an equivalent permeability larger than the median of the measured permeability.

A sensitivity analysis of the transmissivities of the intersections among Hydraulic Conductors Domains was done. The model was not sensitive to the value of the transmissivities of these intersections, at least in terms of steady-state flow rates into the tunnel.

The tunnel construction process has been simulated by means of 29 stages for the transient groundwater flow model. The flow rates into the tunnel are computed by the model and not prescribed as a boundary condition.

In terms of flow rates the computed results show an excellent agreement with the measured data in most of the tunnel sections. The comparison of the computed pressure heads and the measured values indicates that in general the numerical model is able to reproduce the measured drawdowns.

The results will be improved in further calibration making special attention to the connections between currently considered conductor domains, transsmisivity and storage coefficients values.

8 REFERENCES

Ahlbom, K.; Olsson, O. & Sehlstedt, S. (1995): Temperature conditions in the SKB study sites. SKB TR 95-16.

Berkowitz, B. (1994): Modelling flow and contaminant transport in fractured media. Advances in Porous Media. Chapter 6. M.Y. Corapcioglu (Ed). Elsevier

Juanes, R. (1997): Un código para la modelización tridimensional de flujo y transporte. Proyecto Técnico. ETS Ingenieros de Caminos, Canales y Puertos. Universidad de La Coruña. Unpublished.

Kornfalt, K.A. & Wikman, H. (1988): The rocks of the Äspö island. Description of the detailed maps of solid rocks including maps of 3 uncovered tranches. SKB PR 25-88-12.

Larson, S.A. & Berglund, J. (1992) : A Geochronological subdivision of the Transscandinavian Igneous Belt – three magmatic episodes. Geologiska Foreningens i Stockholm Forhandlingar, 114, 459-461.

Moreno, L.; Tsang, Y.W.; Tsang, C.F.; Hale, F.V. & Neretnieks, I. (1988): Flow and tracer transport in a single fracture: A stochastic model and its relation to some field observations. Water Resources Research, 24 (12): 2033-2048.

Rhén, I.; Bäckblom, G.; Gustafson, G.; Stanfors, R. & Wikberg, P. (1997b): Results from pre-investigations and detailed site characterization. Summary report. SKB TR 97-03.

Rhén, I.; Gustafson, G.; Stanfors, R. & Wikberg, P. (1997 b): Models based on site characterization 1986-1995. SKB TR 97-06.

Stanfors, R.; Rhén, I.; Tullborg, E-L & Wikberg, P. (1999): Overview of geological and hydrogeological conditions of the Äspö Hard Rock Laboratory site. Reference Unknown. Task #5 4th Workgroup Meeting Attachments.

Svensson, U. (1997): A regional analysis of groundwater flow and salinity distribution in the Äspö area. SKB TR 97-09.

APPENDIX 1.

Table A.1: Calibrated values of T and S used in RUN_31

H.C.D.	*T (m^2/s)*	*S (-)*
EW-1N	1,50E-06	1,75E-07
EW-1S	2,20E-05	1,44E-06
EW-3	1,74E-02	1,55E-06
EW-7	2,27E-05	3,50E-06
NE-1	1,74E-03	1,12E-05
NE-2	4,10E-07	6,34E-08
NE-3	1,57E-04	1,09E-05
NE-4N	3,00E-05	1,84E-06
NE-4S	3,00E-05	1,84E-06
NNW-1	2,31E-05	8,38E-07
NNW-2	3,54E-06	3,01E-06
NNW-4	2,60E-06	6,52E-06
SFZ-11	3,61E-06	3,49E-07
NW-1	1,70E-07	3,18E-08
NNW-5	4,63E-05	2,20E-07
NNW-6	1,40E-05	1,01E-06
NNW-7	4,79E-06	4,37E-07
NNW-8	1,00E-05	7,78E-07
NNW-3	2,00E-05	1,34E-06

APPENDIX 2. Mean error and accuracy of the model

Definitions:

ERROR:

Average residuals:

$$dh = \frac{\sum_{i=1}^{n}\left(h_i^m - h_i^c\right)}{n}$$

Average of absolute value of residuals:

$$dh(abs) = \frac{\sum_{i=1}^{n}\left|h_i^m - h_i^c\right|}{n}$$

ACCURACY:

Mean square error:

$$Dh = \sqrt{\frac{\sum_{i=1}^{n}\left(h_i^m - h_i^c - dh\right)^2}{n-1}}$$

Where:

n: Number of points with measured data used to compare with calculated points.

h: Piezometric level (freshwater head masl)

index m: Measured value

index c: Calculated value

* Time zero correspond to the 1990/07/01

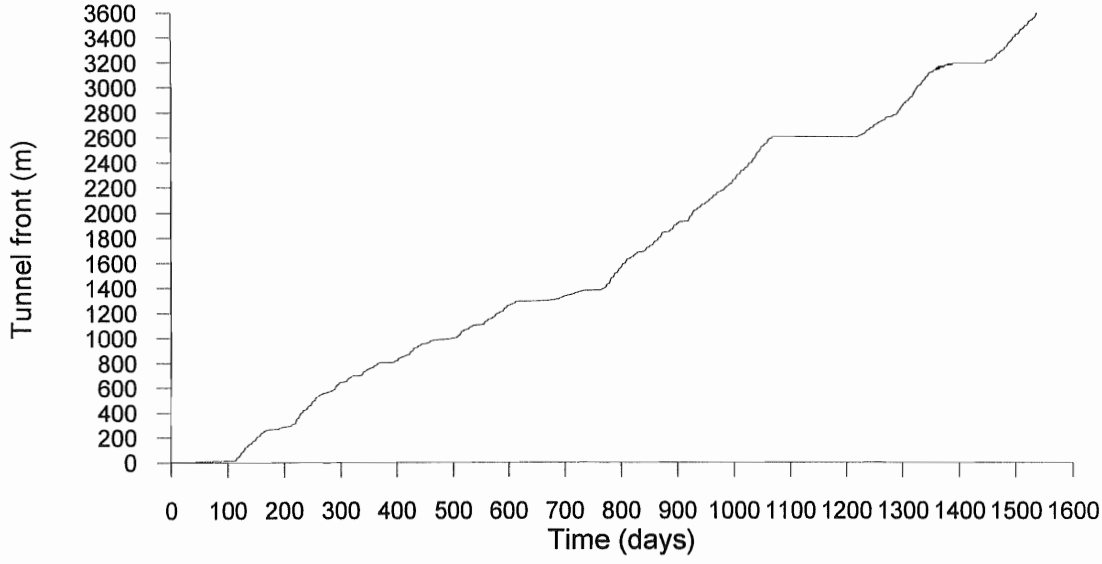

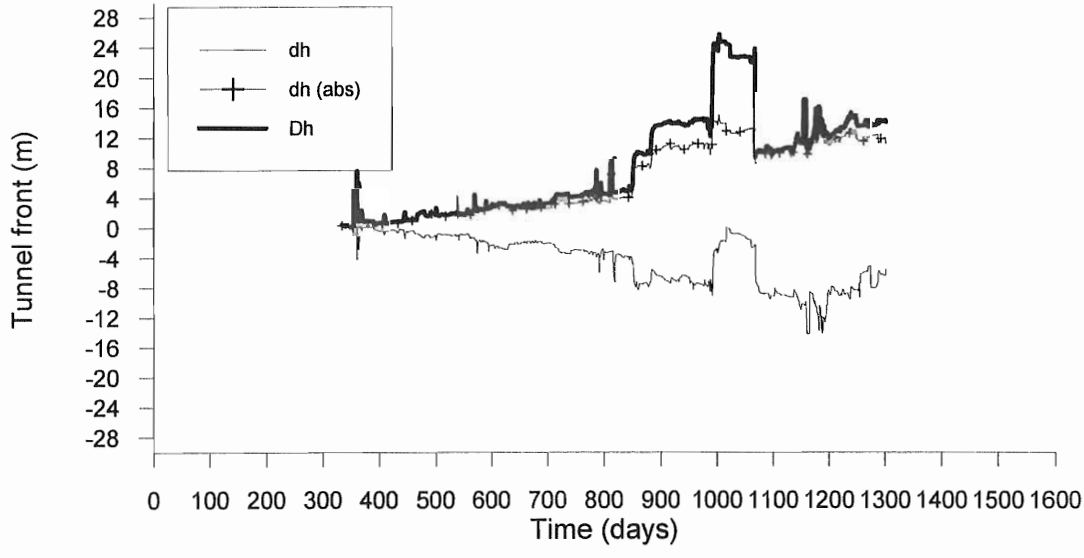

Prediction of water composition using M3.

M. Laaksoharju (SKB/Intera)

DRAFT

TASK#5: PREDICTIONS OF THE GROUNDWATER CHANGES ASSOCIATED WITH THE CONSTRUCTION OF ÄSPÖ HRL

M. Laaksoharju, C. Andersson, I. Gurban,

INTERA KB, Stockholm

April 1999

ABSTRACT

This report predicts influence of the tunnel construction on the groundwaters' at the Äspö Hard Rock Laboratory and is part of the Task 5 exercise. This information is used to support the integration between groundwater chemistry and hydrogeological modelling within Task 5.

The method used was to trace changes in samples taken in the time series from boreholes during the tunnel construction. The prevailing conditions such as: a transient lowering of hydraulic head by 80m and samples taken from sections with a similar hydraulic conductivity of around 10^{-7} m^2/s were assumed to determine the changes in the groundwater chemistry. This change was transformed into mixing proportions using M3. The general changes in mixing portions can be used as a "recipe" for predictions. M3 was used to add or remove mixing portions from the measured sample to predict new values for the major components and isotopes.

A test was made where the first sample in the time series was modified according to the general recipe that simulates the time span used in the sampling. The predicted compositions were compared with the measured ones and seemed to fit reasonably well. In order to avoid the risk of the model being site-specific further tests are suggested.

TABLE OF CONTENTS

1 INTRODUCTION TO THE TASK

Swedish Nuclear Fuel and Waste Management Company (SKB) is responsible for the safe handling and disposal of nuclear wastes in Sweden. This responsibility includes conducting studies into the siting of a deep repository for high-level nuclear waste. This report predicts the changes in groundwater composition associated with the tunnel construction at the Äspö Hard Rock Laboratory. The work presented in this study concerns groundwater predictions based on data distributed within the TASK#5 exercise.

2 SHORT SITE AND GROUNDWATER DESCRIPTION

The underground experimental Äspö Hard Rock Laboratory (HRL) (Figure 1), in south-east Sweden was initiated by the Swedish Nuclear Fuel and Waste Management company (SKB). This site is an important test and research facility which is used as part of the Swedish programme to dispose of spent nuclear fuel in crystalline bedrock.

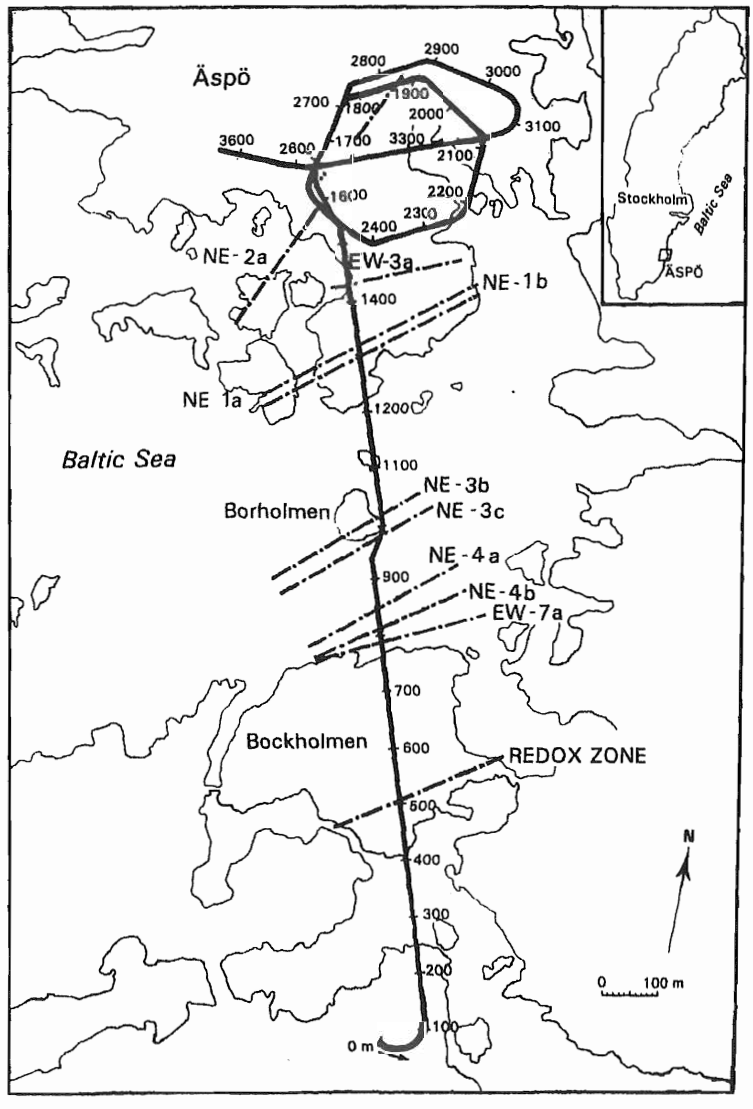

Figure 1 *Location and outline of the Äspö Hard Rock Laboratory in relation to the major fracture zones.*

The boreholes drilled from the surface at the Äspö site consist of percussion drilled boreholes to a depth of around 100m and deep core drilled boreholes with an approximate depth of 1000m; one core borehole reaches a depth of around 1700m. The probe boreholes drilled along and into the bedrock from the HRL tunnel wall generally have a length of 20m. The total length of the tunnel is approximately 3600m and the tunnel spiral reaches a maximum depth of 450m.

The boreholes at the Äspö site have been used for almost 10 years for various measurements, investigations and descriptions such as: hydrogeochemical (Smellie and Laaksoharju, 1992; Banwart et al. 1993; Banwart ed., 1995; Nilsson, 1995; Laaksoharju et al. 1995; Laaksoharju and Skårman, 1995; Laaksoharju and Wallin (eds.), 1997), hydrogeological (Rhén et al., 1993; 1994; Rhén and Stanfors, 1993) and geological (Stanfors et al., 1992; 1993 a,b; 1994).

The present day conditions at Äspö are: A thin lens of meteoric fresh water to a depth of 250m. A saline water consisting of a proportion of present and ancient Baltic Sea water and glacial melt water to a depth of 400-600 metres. Below this level the saline water still contains a proportion of glacial water and brine water of which a large portion has not been in contact with the atmosphere for a very long time, millions of year. During the HRL tunnel construction changes occurred in the composition of the water flowing into the tunnel at different locations. The variation in e.g. salinity was however relatively small, while the variation in the mixing proportions of the different reference waters varied considerably. The effects from different pre- and postglacial events have affected the groundwater composition at Äspö. (Laaksoharju and Wallin (ed)., 1997).

3 DATA, STRATEGY AND TOOLS USED FOR PREDICTIONS

3.1 DATA USED

The data set used in this work is the geochemical data distributed within TASK#5 including control points (CP) with time series and reported by Gurban et al. 1998.

3.2 STRATEGY

The strategy for the work was to:

- Evaluate the changes in the groundwater chemistry caused by the tunnel construction
- Use a new modelling technique (M3, see below) to decode this information.
- Based on the above, formulate a "recipe" for the hydrochemical changes
- Apply the recipe on initial conditions to predict changes due to the tunnel construction.

3.3 M3 DESCRIPTION

The origin and evolution of the groundwater can be described if the effect from mixing and reactions can be examined separately. In order to do this separation a new method named Multivariate Mixing and Mass balance calculations (abbreviated to M3) was constructed (Laaksoharju *et. al.*, 1997 and 1998). The model consists of 3 steps where the first step is a standard principal component analysis, followed by mixing, and finally by mass balance calculations as described below (see, Figure 2):

1. A standard multivariate technique called Principal Component Analysis (PCA) is used for the clustering of the data using the major components Cl, Ca, Na, Mg, K, SO_4 and HCO_3 in combination with the isotopes δ^2H, $\delta^{18}O$ and ^3H. PCA aims to describe as much of the information from the ten variables in the first equation (called the first principal component) as possible. As much as possible of the remaining information is described by the second principal component. The principal components are equations of linear combinations that describe most of the information in the data. The weights for the different variables in the equations are calculated automatically by the PCA. For the Äspö data set the first two principal components can be used to describe 70% of the information in the data set. The third or fourth principal components generally do not contain useful

information but this depends on the complexity of the examined data and the chosen variables. If the first two principal components contain most of the information, an x, y scatter plot can be drawn. The x is the equation for the first principal component and y the equation for the second principal component. The plot is named the M3 plot and is used to visualise the clustering of the data as well as to identify reference waters. A reference water is a selected water composition used to compare the other samples with. A reference groundwater can be any water composition but generally extreme waters such as rain water or deep water is used. Lines are drawn between the reference waters so a polygon is formed. The polygon defines the observations, which can be described by the selected reference waters. By definition the selected reference waters can describe the observations inside the polygon. The groundwater composition of an observation inside the polygon is compared to the chosen reference water compositions.

2. Mixing calculations are used to calculate the mixing portions. The mixing portions describe the contribution of the reference water composition to the observed water. The calculated mixing portion can be used to describe the origin of the groundwater. The mixing portions are equal to the distance of a sample to the selected reference waters in the M3 plot. From a two-dimensional surface, mixing portions containing a maximum of three reference waters can be calculated so that a mathematically unique solution is obtained. To avoid this shortcoming and to be able to use more than three reference waters in the model a control point with a known mixing portion was added to the calculations. A polygon containing say five reference waters contains a portion of 25% of each reference water in the centre point. By using this addition a mathematically unique solution can be achieved from a two dimensional plane with more than three reference waters (Laaksoharju et al., 1998). A mixing portion calculation of less than 10% is regarded as under the detection limit for the M3 method and is therefore uncertain. The overall accuracy of the model applied to Äspö data has been determined at ±10%.

3. Mass balance calculations are used to define the sources and sinks for different elements which deviate from the ideal mixing model used in the mixing calculations. The mixing portions are used to predict new values for the elements. No deviation from the measured value indicates that mixing can explain the element behaviour. A source or sink is due to mass balance reactions. The evolution of the groundwater can thus be described.

a)

Sample no	Variable 1	Variable 2	Variable 3	Variable 4	Variable 5
1	8500	45.5	19300	2.12	14.1
2	613	2.4	162	21	61
3	1960	95	93.7	234	90
4	11.5	2.3	15.4	1.9	63
5	2140	35.1	504	195	760
6	3020	7.3	4380	49.5	11
7	0	0	0	0	3
8	3179.8	154.1	152.0	379.6	146.0
9	0	0	0	2	7
10	2144	91.8	103	258	793
11	2320	26	818	217	227
12	2250	28	741	244	219
13	335	14	80	36	235
14	338	12	87	39	235
15	228	4	27	4	373

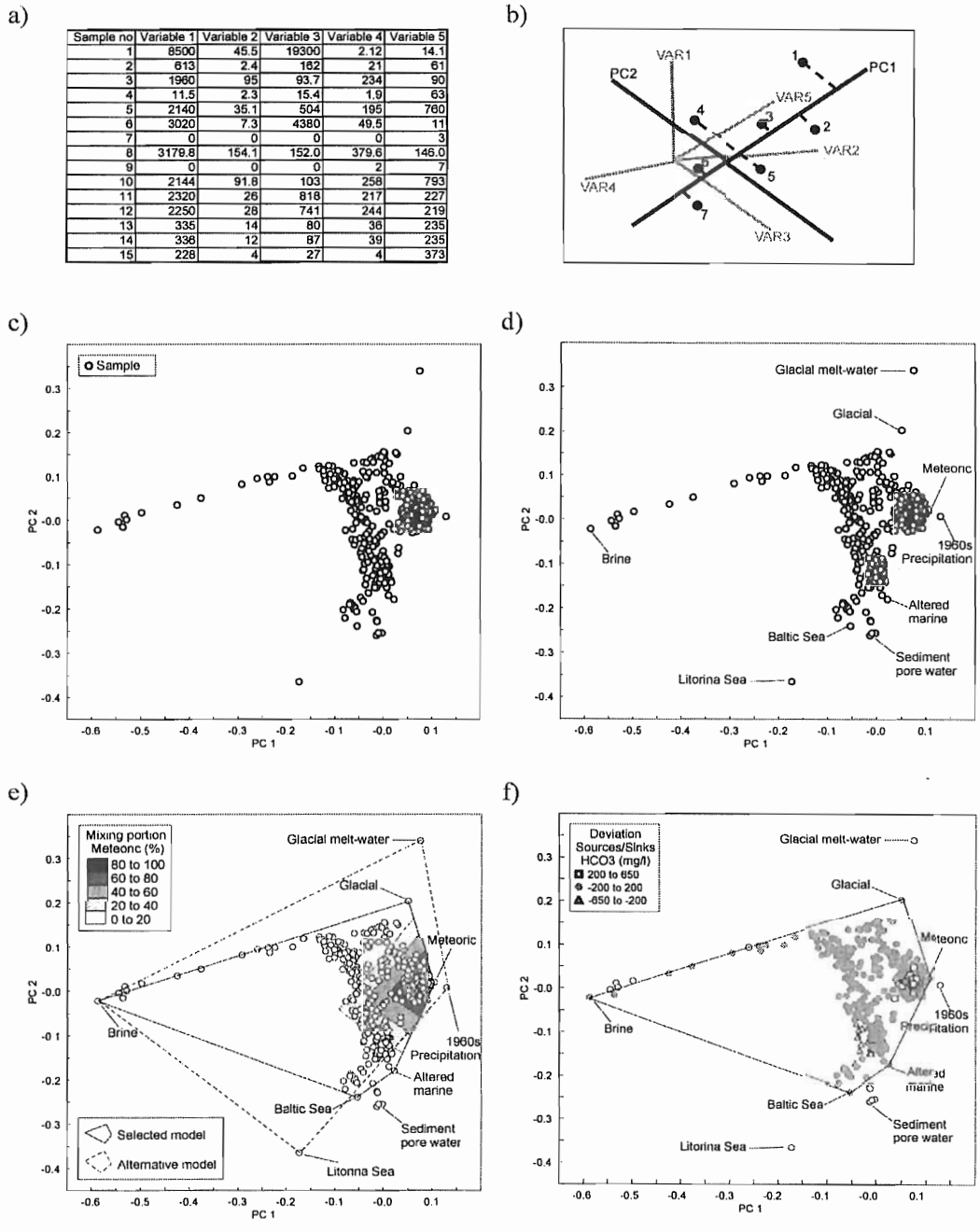

Figure 2*. Different steps in the M3 modelling; a) Data table containing groundwater compositions., b) The principle for principal component analysis; seven groundwater samples and their location in the multivariate space (VAR1-VAR5) and their projection on the principal component 1 (PC1) are shown. Principal component analysis is used to obtain the maximum resolution of the data set. c) The result of the principal component analysis showing principal components 1 and 2. d) Selection of possible reference waters- the other groundwaters are compared to these, e) Mixing calculations – the linear distance of a sample to the reference waters e.g. the portions of meteoric water (%) are calculated in the figure for the selected ideal mixing model, the alternative model uses a new set of reference waters. f) Mass balance calculations – the sources and sinks (mg/l) of carbonate (HCO_3) are shown which cannot be accounted for by using the ideal mixing model. The M3 model is applied to data from the Äspö Hard Rock Laboratory.*

It is important to note that the modelling is always relative to the selected reference waters. The modelling constraints can be changed depending on the selection of reference waters. It is important to note that the M3 model deals only with chemical information; no space or time constraints are included in the model. The calculation steps are described in more detail by Laaksoharju and Wallin (eds., 1997).

3.4 VOXEL ANALYST

In order to interpolate and visualise the measured and predicted values, the Voxel Analyst computer code was used. Voxel Analyst is a general-purpose data visualisation and analysis tool that helps to understand the relationship between different attributes within a 3-dimensional volume data set.

4 RESULTS OF THE MODELLING

4.1 SELECTION OF REFERENCE WATERS FOR M3 MODELLING

The PCA plot is a useful tool when choosing suitable reference waters in relation to the hydrodynamic conceptual model (Laaksoharju and Wallin, (eds) 1997). The variables Na, K, Ca, Mg, Cl, HCO_3, SO_4, ^2H, ^3H and ^{18}O are included in the PCA analysis. The reference waters identified are Brine, Glacial, Meteoric and Marine. The selected reference waters for the current modelling are shown in Figure 3 in relation to the sampled groundwaters at Äspö. The uncertainty range of ±10% for one sample in the model is shown in Figure 3.

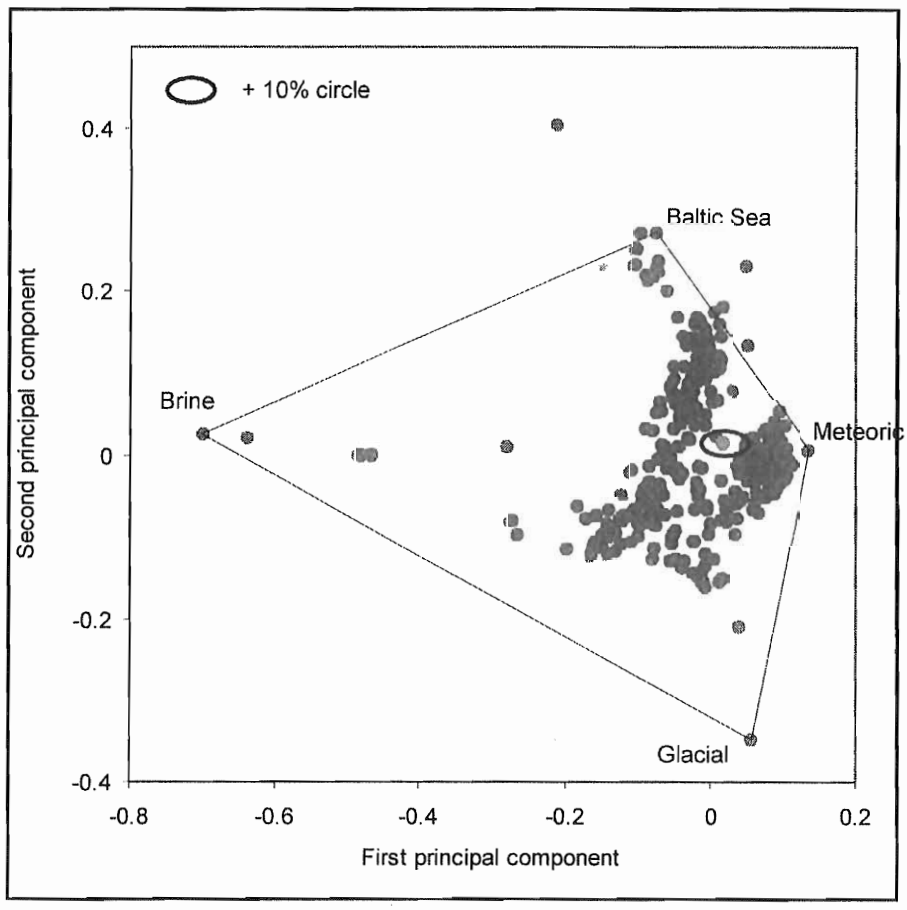

Figure 3. *PCA plot used as a basis for the M3 calculations. The reference waters for the groundwater modelling are shown. The polygon defines the samples that can be modelled by the selected reference waters. The uncertainty range of ±10% for the model is shown for one sample.*

The reference waters were selected so that most of the samples are inside the polygon and can be described. By definition the criteria are that a sample inside the polygon can be described by the selected reference waters. The closer to the reference water a groundwater observation plots in PCA the more of that type of water the sample contains. The reason for modelling all the observations simultaneously by using the same reference waters is that we can obtain information about the whole system and compare the changes of the groundwater associated with the tunnel construction.

The selected reference waters for the current M3 modelling are (the analytical composition is listed in Gurban et al., 1998):

- **Meteoric: represents precipitation in 1960 and infiltration water**
- **Baltic Sea water: represents modern Sea water from Baltic Sea**
- **Brine water: represents deep (1700m) groundwater from KLX02 at Laxemar**
- **Glacial water: represents meltwater from the last glaciation**

4.2 CHANGES IN THE GROUNDWATER COMPOSITION DUE TO THE TUNNEL CONSTRUCTION

The changes of the groundwater composition due to the tunnel construction are shown in different ways by using PCA in M3 (Figure s 4, 5 and 6). The *first sample* refers to the first sample in the time series sampled from a borehole at the Äspö site. The *last sample* refers to the last sample in the time series sampled from a borehole at the Äspö site. The length of the time series can vary from some months to years (see, Gurban et al., 1998).

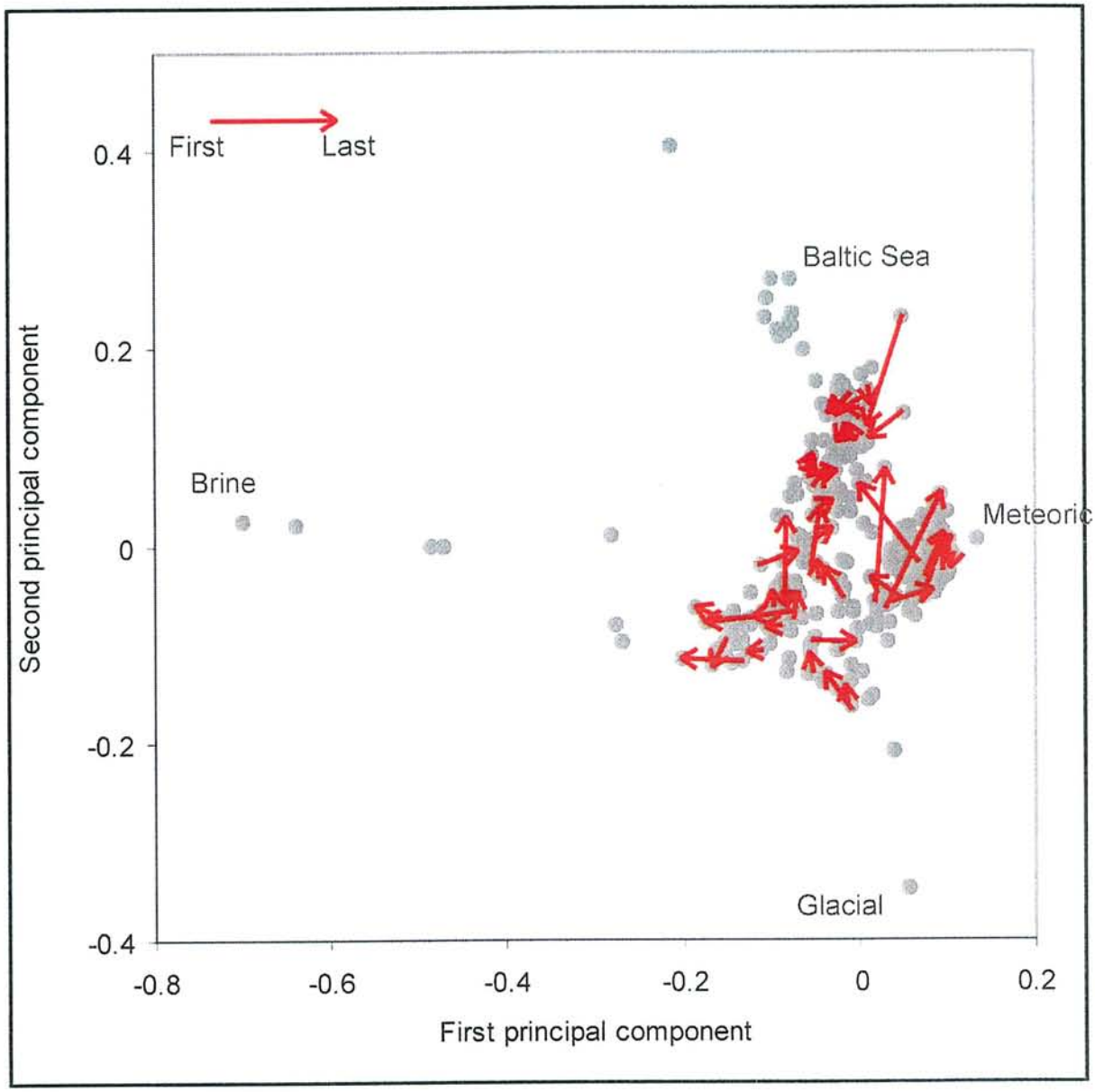

Figure 4. *PCA plot used to show the changes in the groundwater composition due to the tunnel construction. First refers to the first sample taking from the time series Last refers to the last sample of that time series.*

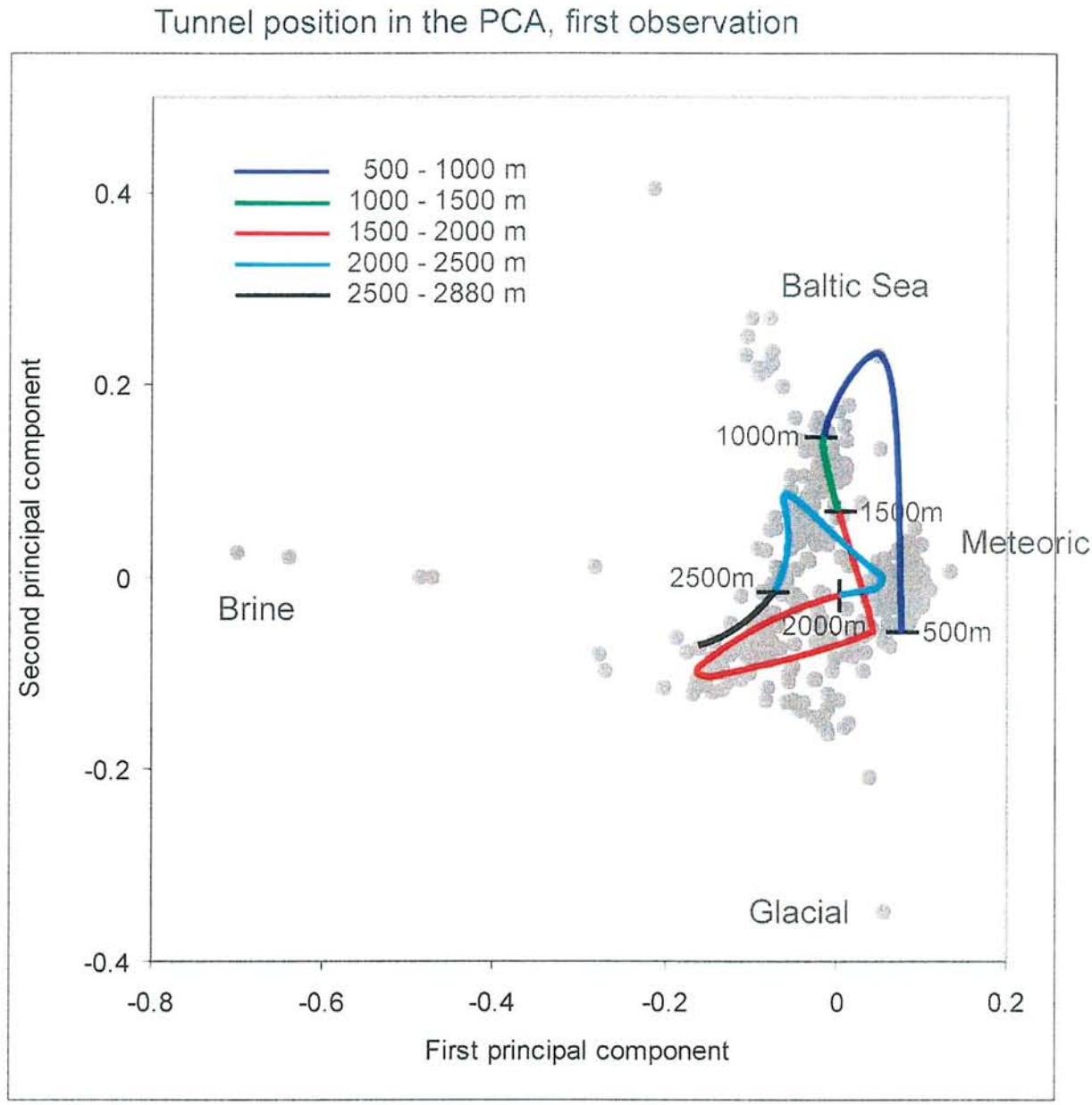

Figure 5. *PCA plot used to show the general (simplified) changes in groundwater composition in the samples along the tunnel for the first sample in the time series. The tunnel length is indicated for orientation, see Figure 1.*

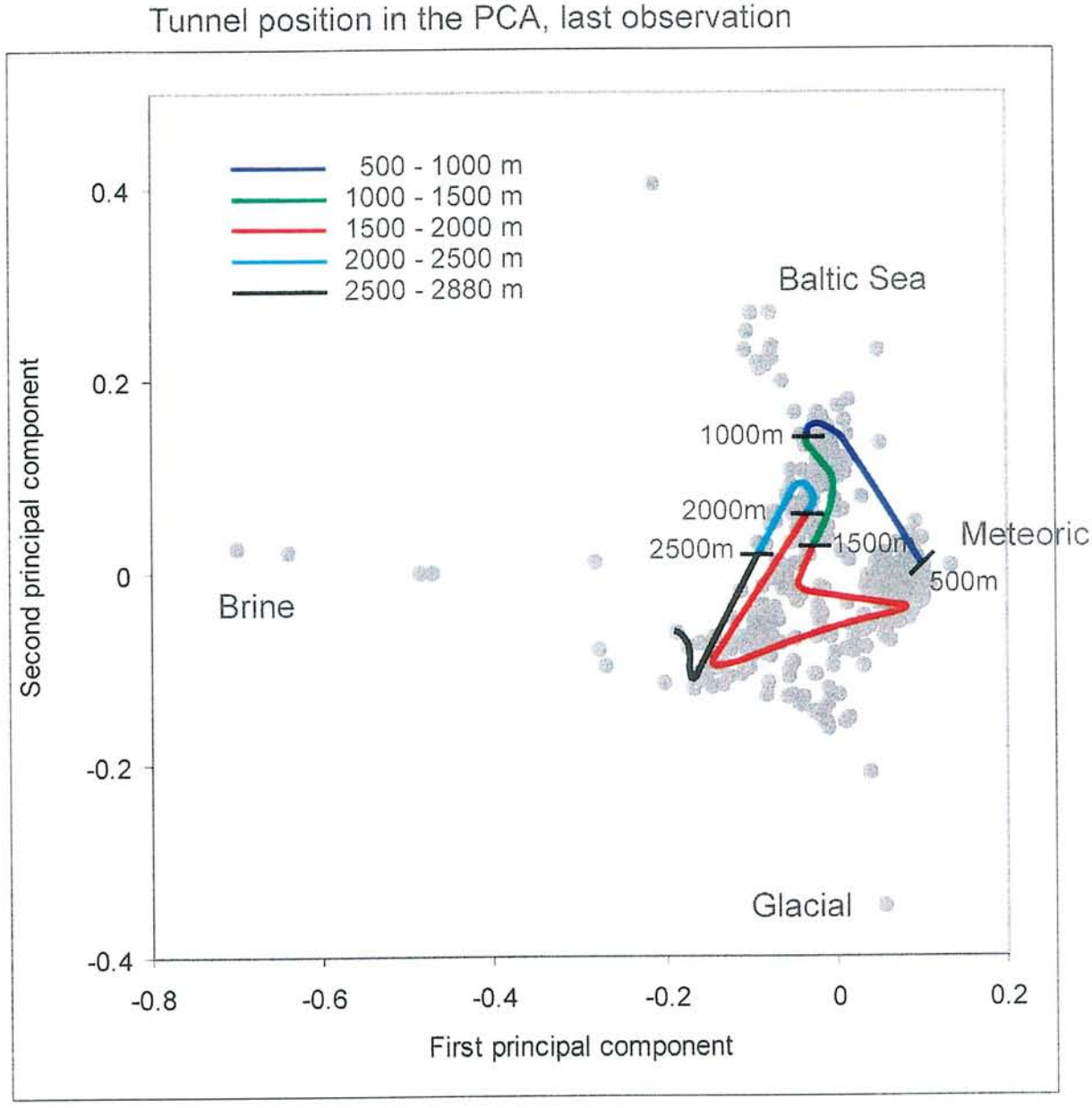

Figure 6. *PCA plot used to show the general (simplified) changes in groundwater composition in the samples along the tunnel for the last sample in the time series. The tunnel length is indicated for orientation see Figure 1.*

From Figure 4 the following conclusions are drawn: Where the first sample is dominated by meteoric water the last sample is as well. Although same samples migrate towards a more marine signature, samples with a marine origin seem to move to a less marine signature. Glacial water samples seem to change to a water composition with less glacial water. Saline groundwater seems to have more brine component in the last sample. The general trend is that the waters tend to be more mixed with time and move therefore towards the centre of the plot. Figures 5 and 6 show a similar trend where the tunnel construction seems to induce more mixed water. The water that is pumped out from the tunnel has a Cl concentration of around 6000mg/l which coincides with the Cl concentration obtained for samples close to the centre of the plot.

In order to be able to relate the groundwater changes to the geometry of the Äspö site, depth (Figure 7) and x, y co-ordinates (Figures 8 and 9) where plotted versus calculated changes in mixing portions. A systematic change could indicate a correlation which could be used when constructing the *groundwater prediction model* for the site.

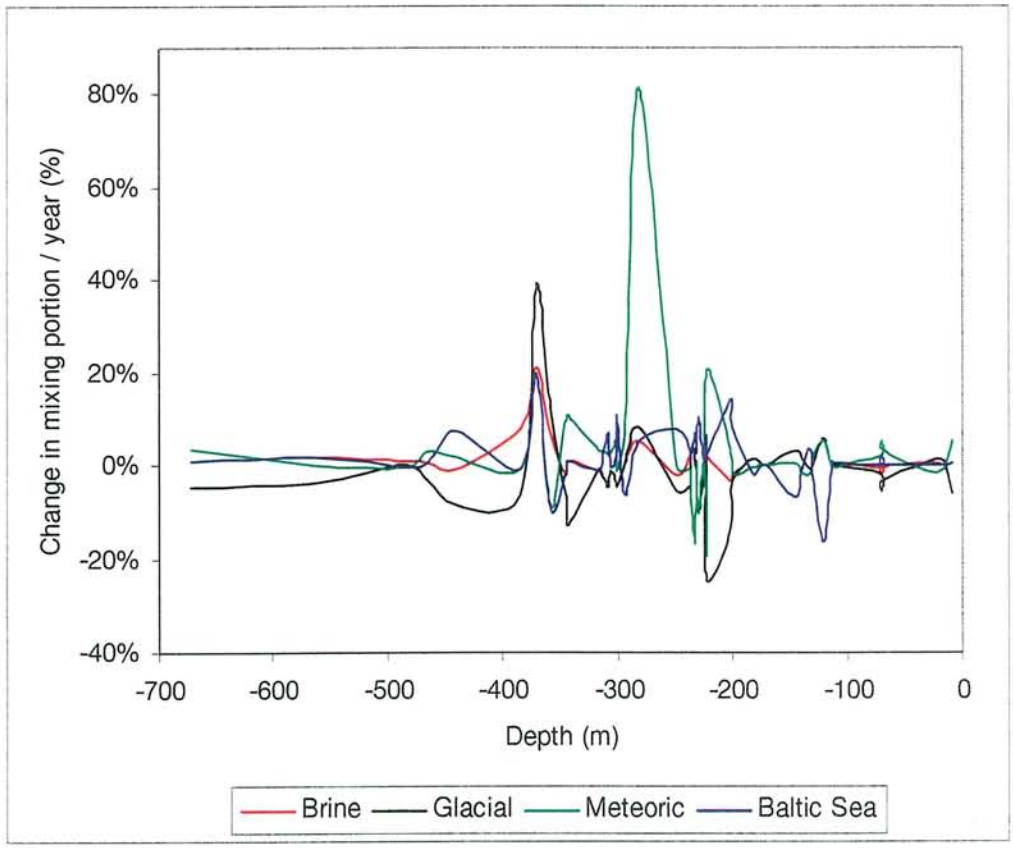

Figure 7. *Depth plotted versus calculated changes in mixing portions between the first and last sample in the time series from Äspö. The calculations were made for changes in Brine, Baltic Sea, Glacial and Meteoric water portions.*

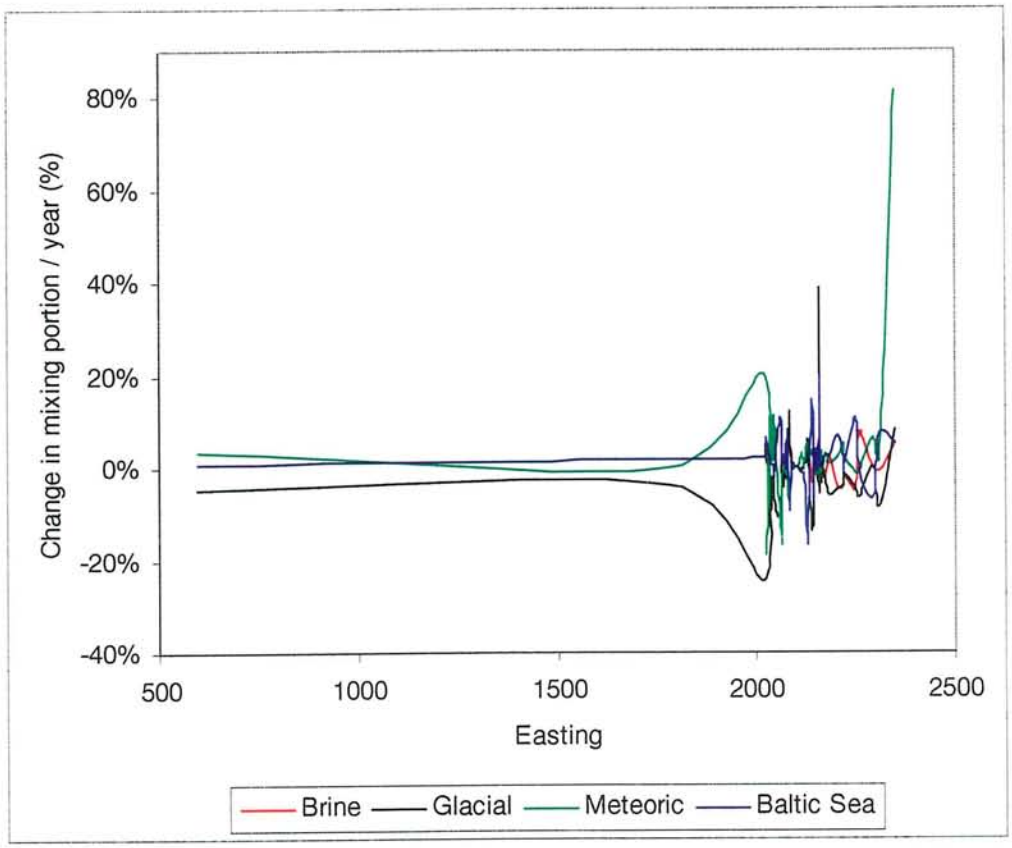

Figure 8. *x co-ordinates (easting) plotted versus the calculated changes in mixing portions between the first and last sample in the time series from Äspö. The calculations were made for changes in Brine, Baltic Sea, Glacial and Meteoric water portions.*

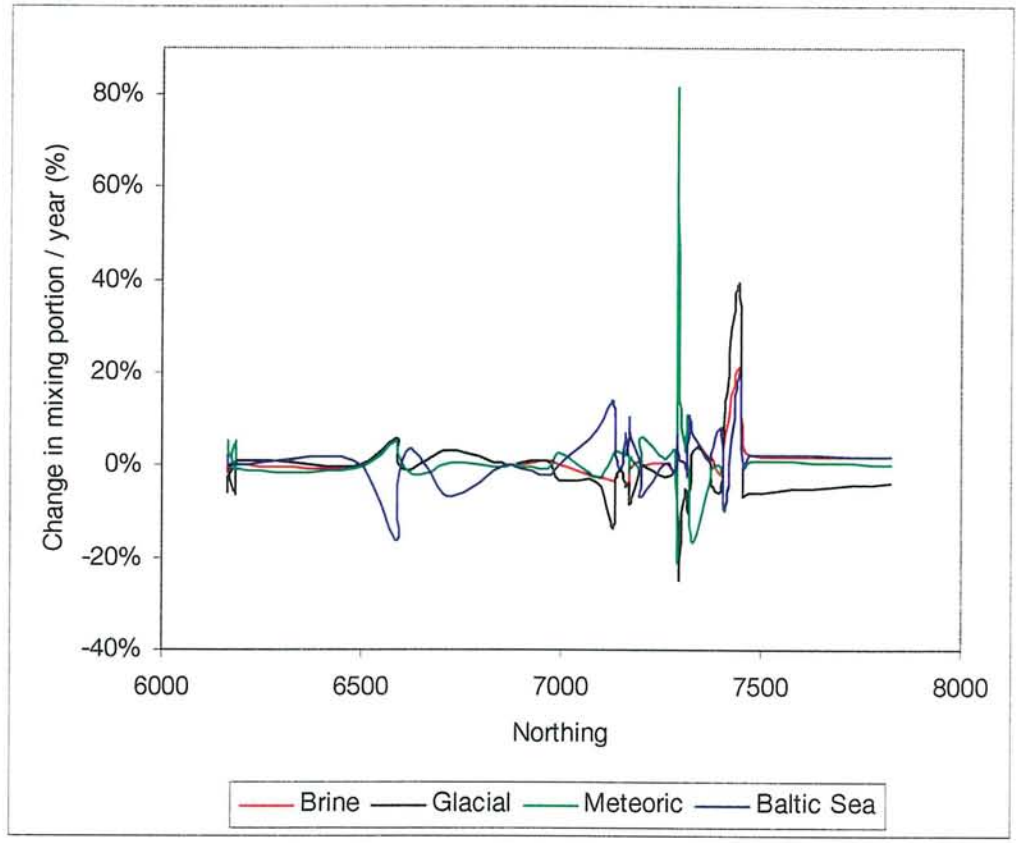

Figure 9. *y co-ordinates (northing) plotted versus the calculated changes in mixing portions between the first and last sample in the time series from Äspö. The calculations were made for changes in Brine, Baltic Sea, Glacial and Meteoric water portions.*

Figures 7, 8 and 9 show a complex relation between the changes in mixing portions and location. The only clear trend is an increasing Brine portion with depth in Figure 7. This shows the complexity of the changes due to the tunnel construction.

4.3 PREDICTIONS OF THE GROUNDWATER CHANGES

Several test were made to create a *Groundwater Prediction Model* or a "recipe" for the changes in the groundwater composition due to the tunnel construction. The following strategy and model were selected:

- Divide the groundwaters into classes using PCA where the dominating mixing portion in the first sample in the time series determines its class (Meteoric, Baltic, Glacial or Brine).
- Use the fact that the changes in groundwater chemistry are due to a complex relation between location and prevailing hydraulic properties and conditions.
- Calculate the changes in mixing portions between the first and last sample in the time series.
- Normalise the mixing portion changes with time (changes/year) to make the comparison easier.
- Calculate a mean mixing change per year.
- Use the mean mixing change to add or remove mixing portions from the first sample in the time series.
- Use the new mixing portions based on the reference water composition to predict a new water composition.
- Compare the predicted water composition with the measured one (last sample).
- The model should reflect the mean changes due to prevailing hydrogeological conditions (where most of the samples are collected from fracture zones with a hydraulic conductivity around 10^{-7} m^2/s and which have undergone a transient change where the groundwater level has been lowered by 80m due to the tunnel construction).

To collect information for the groundwater prediction model the changes in the mixing portions for the whole Äspö site (Table#1) and for a limited data set containing data from the Äspö island (Table#2) were examined. To make the comparison easier the mixing portions were normalised to changes in mixing portions (%) per year.

Table 1: Observations from the *Äspö site* (regional model) divided into three classes (Glacial, Meteoric and Baltic Sea) depending on the dominating mixing portion in the first sample taken from the time series. Mean depth for the classes, the mean changes in mixing portions per year and the mean values for Cl and $\delta^{18}O$ were calculated. The information was summarised as a total mean for the depth and changes in mixing portions and for the water conservative elements Cl and $\delta^{18}O$.

Äspö data (regional), difference per year								
	Mean depth		Brine	Glacial	Meteoric	Baltic Sea	Cl (mg/l)	δO18 (‰ SMOW)
Mean Glacial	-373.466	diff/y	2.2%	-3.3%	1.0%	0.0%	876	0.3
Mean Meteoric	-186.214	diff/y	0.0%	-3.8%	-0.6%	4.4%	350	0.5
Mean Baltic Sea	-190.175	diff/y	0.6%	0.6%	1.4%	-2.7%	-548	-0.2
Total mean	-246.694	diff/y	0.9%	-2.6%	0.4%	1.4%	326	0.3

Table 2: Observations from the *Äspö island* (local model) divided into three classes (Glacial, Meteoric and Baltic Sea) depending on the dominating mixing portion in the first sample from the time series. Mean depth for the classes, the mean changes in mixing portions per year and the mean values for Cl and $\delta^{18}O$ were calculated. The information was summarised as a total mean for the depth and changes in mixing portions and for the water conservative elements Cl and $\delta^{18}O$.

Äspö data and tunnel data >1200m distance from tunnel entrance (local)								
	Mean depth		Brine	Glacial	Meteoric	Baltic Sea	Cl (mg/l)	δO18 (‰ SMOW)
Mean Glacial	-350.432	diff/y	2.3%	-3.2%	0.8%	0.0%	952	0.2
Mean Meteoric	-267.940	diff/y	0.1%	-4.8%	-2.0%	6.7%	649	0.7
Mean Baltic Sea	-227.694	diff/y	-0.7%	-0.7%	1.2%	0.3%	-404	0.0
Total mean	-294.744	diff/y	0.9%	-3.3%	-0.2%	2.6%	584	0.3

The general mean changes in Tables 1 and 2 indicate that for the regional and the local models there is 0.9% more Brine, -2.6% to –3.3% less Glacial, 0.4% to –0.2% changes in Meteoric and 1.4% to 2.6% more of Baltic Sea water per year due to the tunnel construction. Knowing these general changes in mixing portions during prevailing hydrogeological conditions, the accuracy of these models can be tested. The regional and local models were used to modify the calculated mixing portions for the first sample according to the mean changes above. The mean changes in mixing portion per year were calculated to reflect the actual time for the last sample in the time series. Tests showed that the difference in the predicted values generally did not differ considerably if the regional or local model was used. In order to be able to predict more observations we therefore used the regional model in the predictions. Some test results using the regional model are shown in Figure 10. When judging the outcome of the predictions it is important to note that the groundwater chemistry varies naturally during sampling and due to model errors.

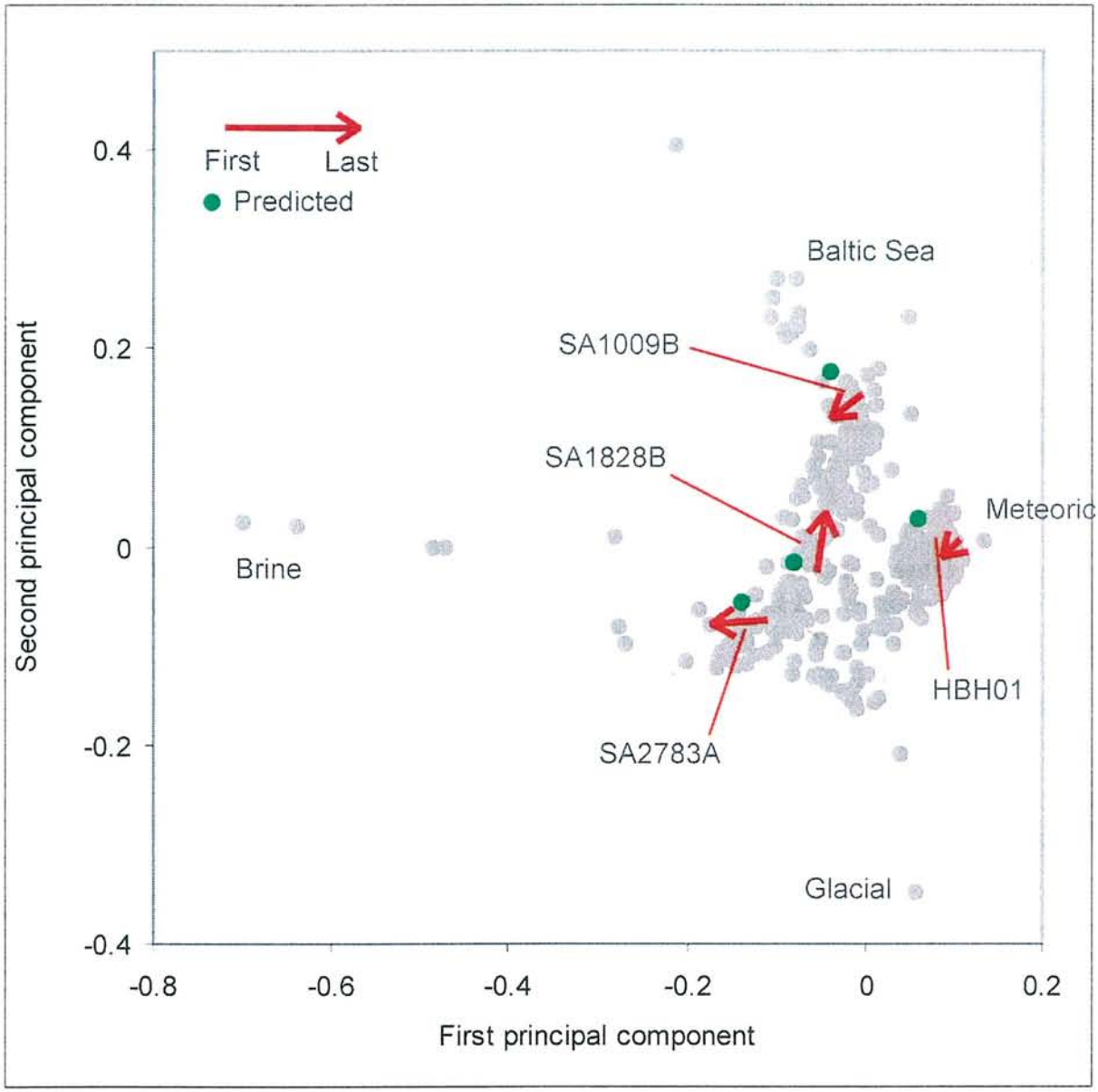

Figure 10. *Regional model used to predict the groundwater changes (green dot) for some observations. The arrow represents the development in the measured groundwater composition between the first and last sample in the time series.*

Figure 10 shows that some compositions are rather well predicted whereas other observations deviate. The predictions are relative close to the measured values considering the effect from natural or unnatural variations and uncertainties in the groundwaters. A more detailed comparison between the predicted and measured values based on all groundwater observations are listed in Table 3 for the mixing portions and in Table 4 for the major elements and isotopes.

Table 3: Comparison between average difference for mixing portion calculations between predicted and measured values. The comparison is based on all TASK#5 data with the time series.

	Brine	Glacial	Meteoric	Baltic Sea	Total difference	
Average difference	**1.2%**	**-0.9%**	**-0.1%**	**-0.3%**	**8.9%**	

Table 4: Comparison between average difference for major elements, stable isotopes and tritium between predicted and measured values. The comparison is based on all TASK#5 data with the time series.

	Na (mg/l)	K (mg/l)	Ca (mg/l)	Mg (mg/l)	CO3 (mg/l)	Cl (mg/l)	SO4 (mg/l)
Average difference	**-91**	**18**	**1356**	**-31**	**-128**	**2199**	**-99**

	D (o/oo)	Tr (TU)	O18 (o/oo)
Average difference	**-8**	**39**	**-1**

Table 3 shows that the difference in mixing portions between the predicted and the measured values is less than 10%. Table 4 shows that the major components vary in the way that some are over predicted (positive values) and others are under predicted (negative values). It is important to note that during sampling a variation of 2199 mg/l Cl or more is normally obtained. The average difference for $\delta^{18}O$ is less 1 unit which is regarded as high accuracy. For more details concerning the deviation between the predicted and measured values for the different groundwater samples please see Appendix 1. The conclusion is that the deviation in most of the cases seems to be within acceptable ranges.

4.4 VISUALISATION AND COMPARISON OF MEASURED AND PREDICTED VALUES

In order to visualise and compare the predictions with the measured values the following properties were selected: Cl, $\delta^{18}O$ (water conservative), the mixing portion calculations for Meteoric water and HCO_3 which were affected by reactions (Figures 11, 12, 13 and 14). The interpolations and the visualisation were performed using the computer code Voxel Analyst.

Figures 11, 12, 13 and 14 show a reasonable agreement between the measured and predicted groundwater properties. The deviations are generally smaller than the known uncertainties from natural variation, sampling uncertainties and modelling variations.

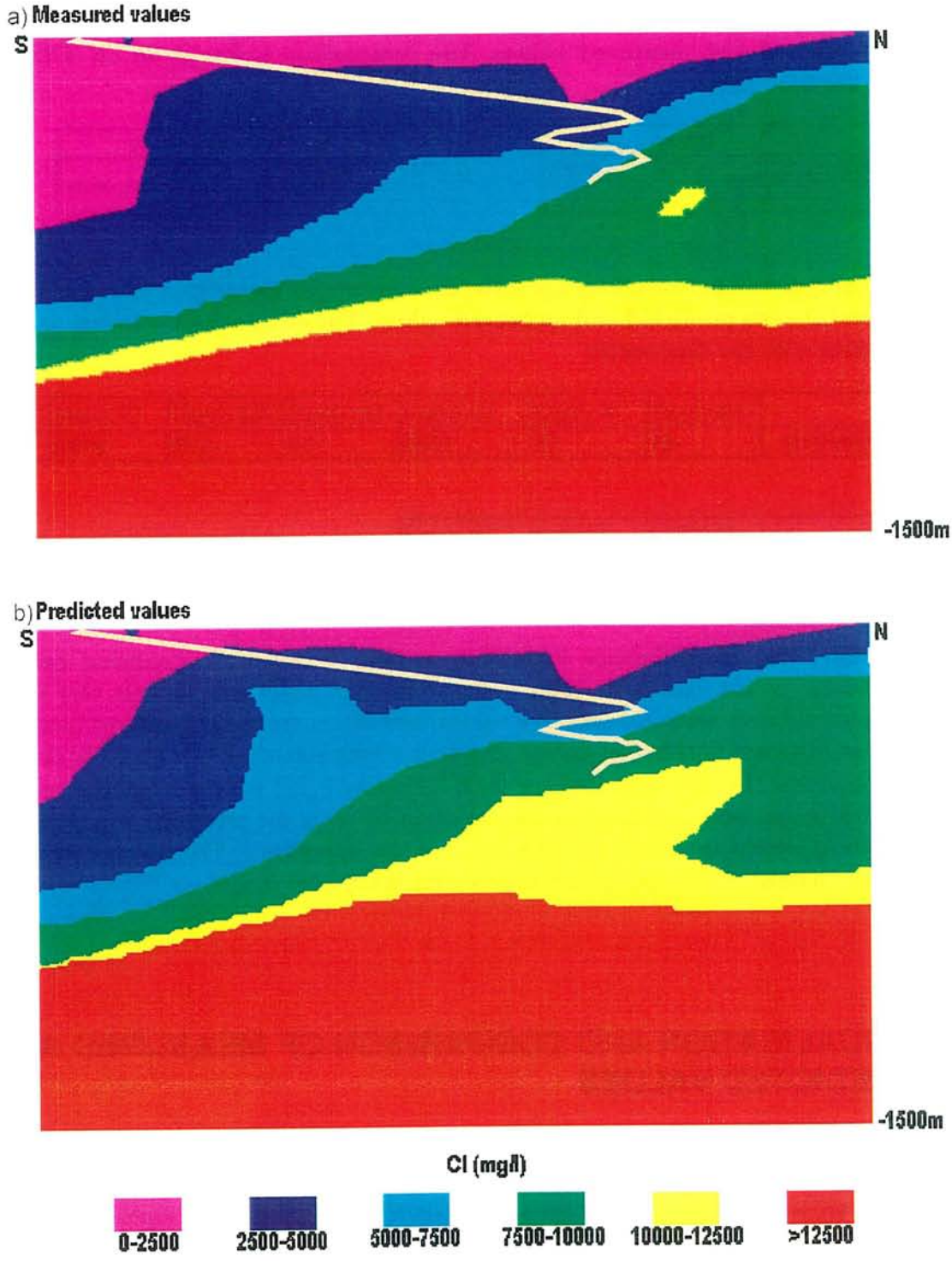

Figure 11. *Visualisation of the Cl concentration for the measured and predicted values. The cutting plane is N-S along the Äspö HRL tunnel.*

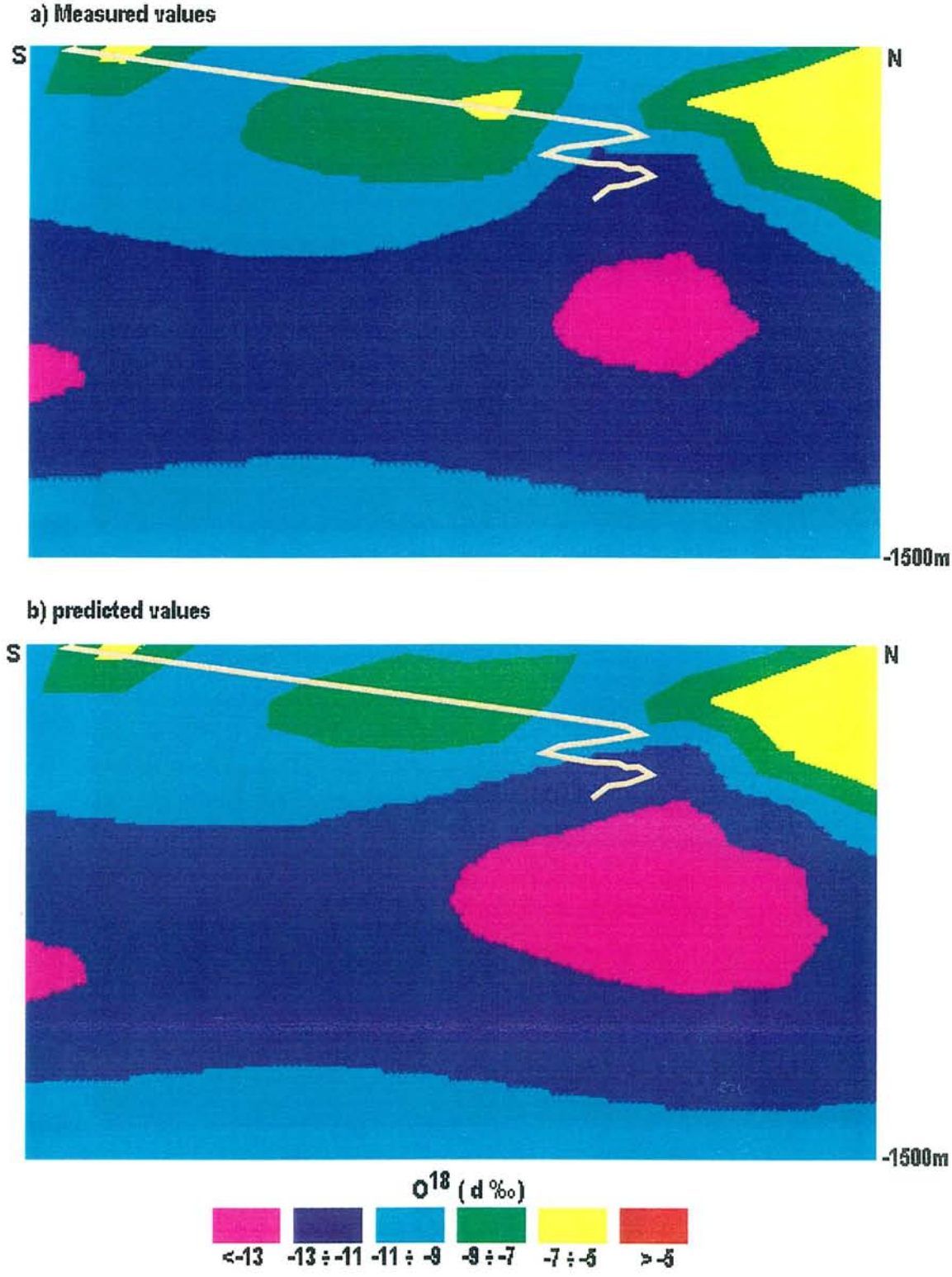

Figure 12. *Visualisation of $\delta^{18}O$ content for the measured and predicted values. The cutting plane is N-S along the Äspö HRL tunnel.*

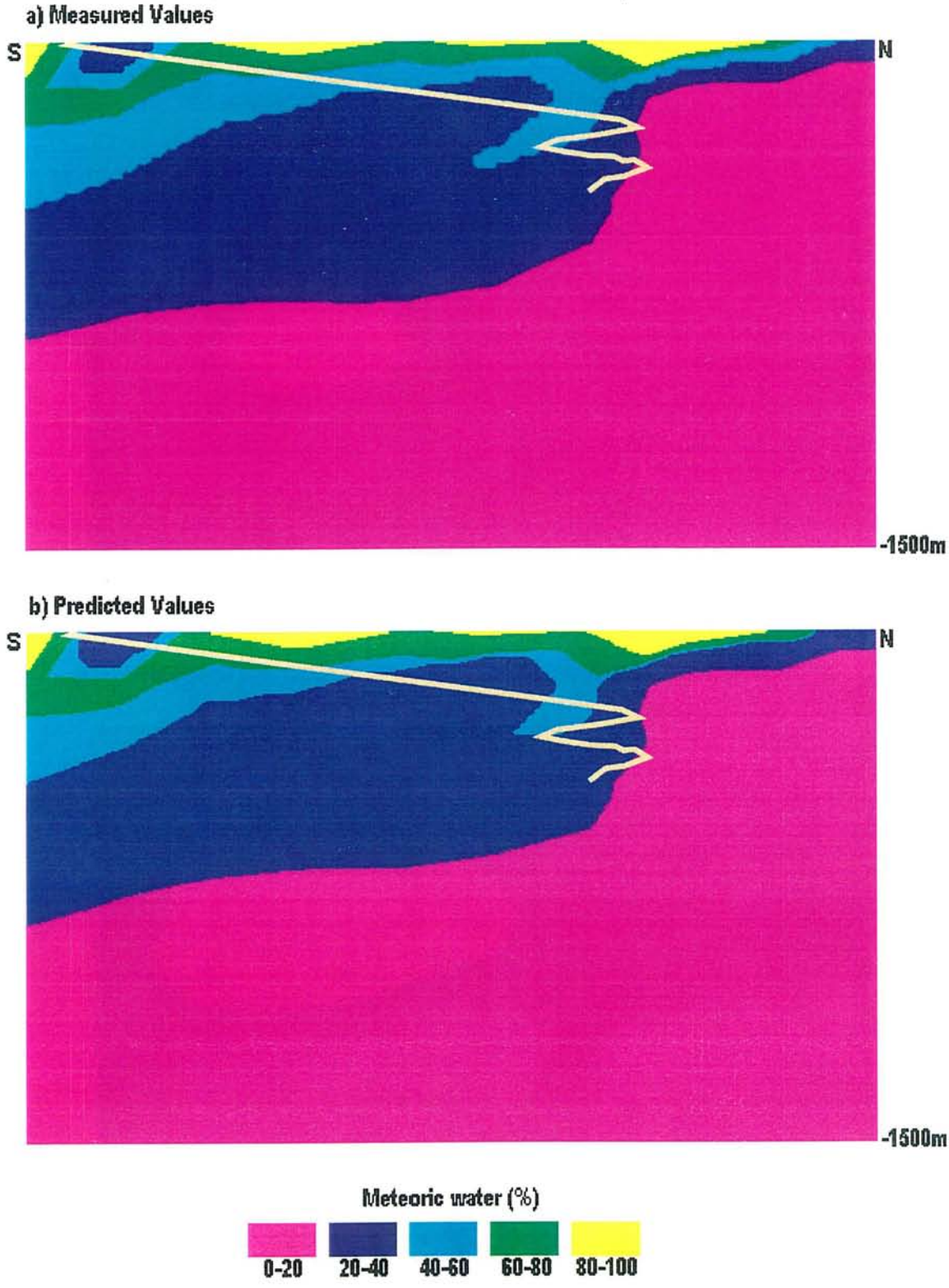

Figure 13. *Visualisation of the mixing portion calculations for Meteoric water showing the mixing calculations based on measured and predicted groundwater compositions. The cutting plane is N-S along the Äspö HRL tunnel.*

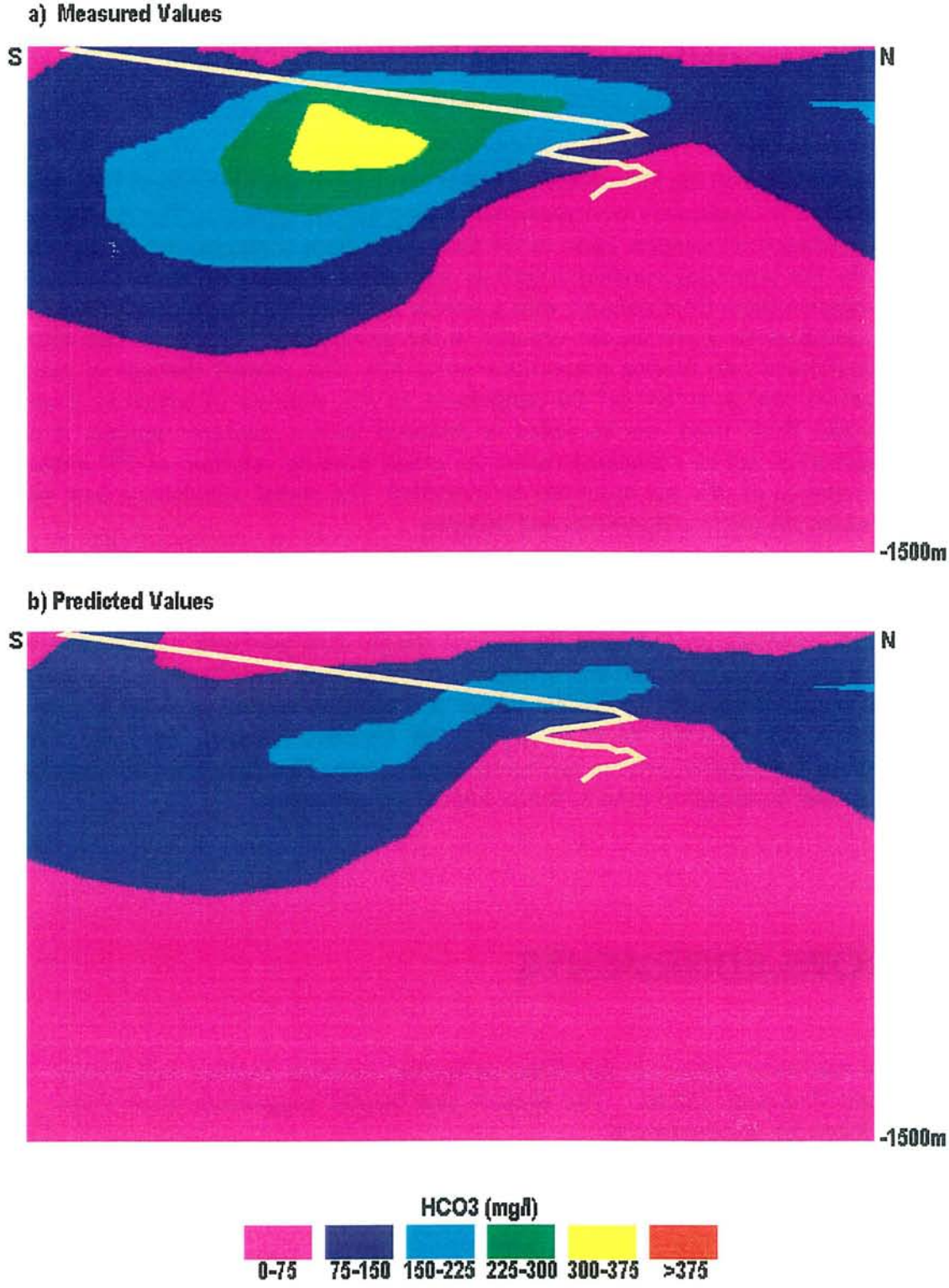

Figure 14. Visualisation of HCO_3 concentration for the measured and predicted values. The cutting plane is N-S along the Äspö HRL tunnel.

5 CONCLUSIONS OF THE MODELLING

The conclusion based on the M3 modelling is that the changes due to the Äspö HRL tunnel construction can be reasonably well predicted using a simple approach. The method used was to trace changes in samples taken in the time series from boreholes during the tunnel construction. The prevailing conditions such as: a transient lowering of hydraulic head by 80m and samples taken from sections with a similar hydraulic conductivity of around 10^{-7} m^2/s were assumed to determine the changes in the groundwater chemistry. This change can be transformed into mixing proportions using M3. The general changes in mixing portions can be used as a "recipe" for predictions. In M3, portions of Meteoric, Glacial, Baltic Sea and Brine water can be added or removed from a measured sample. A new water composition can be calculated where the effect from eg. addition of 5% meteoric water and removal of 8% sea water can be modelled. The model calculates a new water composition for the major components and isotopes.

A test was made where the first sample in the time series was modified according to the general recipe compensating for the time. A new water composition was calculated by adding mixing portions according to the general recipe. This predicted composition was compared with the measured one and seemed to fit reasonably well. In order to avoid the risk of the model being only applicable to the prevailing conditions at Äspö the model should be run in a reverse mode to predict the transient situation from the tunnel construction to the situation prior to the tunnel construction. The changes in the individual boreholes should be related to local hydrogeological measurements.

ACKNOWLEDGEMENTS

This study has been supported and financed by the Swedish Nuclear and Waste Management Company (SKB). The support and helpful suggestions from Peter Wikberg (SKB) are acknowledged.

REFERENCES

Banwart S (ed), Laaksoharju M, Skårman C, Gustafsson E, Pitkänen P, Snellman M, Landström O, Aggeryd I, Mathiasson L, Sundblad B, Tullborg E-L, Wallin B, Pettersson C, Pedersen K, Arlinger J, Jahromi N, Ekendahl S, Hallbeck L, Degueldre C, Malmström M, 1995. Äspö Hard Rock Laboratory. The Redox Experiment in Block Scale. Final reporting of results from the three year project. SKB Progress Report PR 25-95-06, Stockholm, Sweden.

Banwart S, Gustafsson E, Laaksoharju M, Nilsson A-C, Tullborg E-L, Wallin B, 1993. The large scale Redox experiment: Redox processes in a Granitic coastal aquifer. SKB Progress Report PR 25-93-03, Stockholm, Sweden.

Gurban I, Laaksoharju M, Andersson C (1998). Influences of the tunnel construction on the groundwater chemistry at Äspö. SKB Technical note: TN-98-16g.

Laaksoharju M, Skårman C, Skårman E, 1998. Multivariate Mixing and Mass balance (M3) calculations, a new tool for decoding hydrogeochemical information. Submitted to Applied Geochemistry.

Laaksoharju M, Wallin B (eds), 1997. Evolution of the groundwater chemistry at the Swedish Äspö Hardrock Laboratory site. Proceedings of the second Äspö international geochemistry workshop. SKB International Cooperation Report 97-04, Stockholm, Sweden.

Laaksoharju M, Skårman C, 1995. Groundwater sampling and chemical characterisation of the HRL tunnel at Äspö, Sweden. SKB-Progress report PR 25-95-29, Stockholm, Sweden.

Laaksoharju M, Smellie J, Nilsson A-C, Skårman C, 1995. Groundwater sampling and chemical characterisation of the Laxemar deep borehole KLX02. SKB Technical Report TR 95-05, Stockholm, Sweden.

Nilsson A-C, 1995. Compilation of groundwater chemistry data from Äspö 1990-1994. SKB Progress Report PR 25-95-02, Stockholm, Sweden.

Rhén I, Danielsson P, Forsmark T, Gustafson G, Liedholm M, 1993. Äspö Hard Rock Laboratory. Geohydrological evaluation of the data from section 700-1475m. SKB Progress Report PR 25-93-06, Stockholm, Sweden.

Rhén I, Danielsson P, Forsmark T, Gustafson G, Liedholm M, 1994. Äspö Hard Rock Laboratory. Geohydrological evaluation of the data from section 2265-2874m. SKB Progress Report PR 95-94-20, Stockholm, Sweden.

Rhén I, Stanfors R, 1993. Passage through water-bearing fracture zones. Evaluation of investigations in fracture zones NE-1, EW-7 and NE-3, SKB Progress Report PR 25-92-18, Stockholm, Sweden.

Smellie J, Laaksoharju M, 1992. The Äspö Hard Rock Laboratory: Final evaluation of the hydrogeochemical pre-investigations in relation to existing geological and hydraulic conditions. SKB Technical Report TR 92-31, Stockholm, Sweden.

Smellie J, Laaksoharju M, Wikberg P, 1995. Äspö, SE Sweden: A natural groundwater flow model derived from hydrogeochemical observations. Journal of Hydrogeology 172 (1995) 147-169.

Stanfors R, Gustafson G, Munier R, Olsson P, Stille H, Wikberg P, 1992. Evaluation of geological predictions in the access ramp 0-700m. SKB Progress Report PR 25-92-02, Stockholm, Sweden.

Stanfors R, Liedholm M, Munier R, Olsson P, Stille H, 1993a. Geological-structural evaluation of data from section 700-1475m. SKB Progress Report PR 25-93-05, Stockholm, Sweden.

Stanfors R, Liedholm M, Munier R, Olsson P, Stille H, 1993b. Äspö Hard Rock Laboratory. Geological-structural evaluation of data from tunnel section 1475-2265m. SKB Progress Report PR 25-93-10, Stockholm, Sweden.

Stanfors R, Liedholm M, Munier R, Olsson P, Stille H, 1994. Äspö Hard Rock Laboratory. Geological-structural evaluation of data from tunnel section 2265-2874m. SKB Progress report PR 25-94-19, Stockholm, Sweden.

APPENDIX 1: Data used

The difference between the predicted and measured values for the data set containing the time series. The difference for the mixing portions, major components and isotopes are listed.

ID code	Secup	Seclow	Centr.	Date	Days from 1990-10-14 =0	Days from 1st obs.	Years from 1st obs.	Northing	Easting	Elevation	SNO
KAS02	309	345	327	920819	675	1422	3,9	7287,165	2114,836	-318,178	1990
KAS03	533	626	579,5	940412	1276	601	1,6	7825,385	1781,814	-566,304	2234
KAS05	440	549,6	494,8	940412	1276	588	1,6	7197,769	2074,653	-483,321	2235
KAS07	191	290	240,5	940406	1270	583	1,6	7131,309	2139,342	-201,271	2228
KAS07	501	604	552,5	940906	1423	736	2,0	6995,844	2042,233	-464,993	2273
KAS08	503	601	552	940406	1270	583	1,6	7172,453	2307,591	-441,306	2229
KAS09	116	150	133	951012	1824	1136	3,1	6857,829	2089,529	-110,585	2333
KAS12	234	277	255,5	930907	1059	371	1,0	7475,856	2182,879	-231,657	2161
KLX01	680	702,11	691,06	891101	-347	363	1,0	7307,837	595,69	-672,907	1633
HBH01	31	50,6	40,8	950324	1622	1182	3,2	6183,527	2166,468	-30,879	2307
HBH02	21	32,4	26,7	950324	1622	1181	3,2	6190,937	2161,031	-15,296	2308
HBH05	11	22	16,5	931112	1125	380	1,0	6185,414	2144,279	-8,697	2198
KR0012B	5	10,57	7,785	960521	2046	1798	4,9	6167,254	2165,756	-69,196	2361
KR0013B	7,05	16,94	11,995	951010	1822	1592	4,4	6166,277	2159,071	-69,269	2324
KR0015B	19,82	30,31	25,065	960521	2046	1504	4,1	6168,049	2144,354	-69,537	2363
HA1327B	3,5	29,5	16,5	931214	1157	377	1,0	6963,062	2118,058	-182,949	2208
KA1639A	13,4	14,4	13,9	930929	1081	90	0,2	7289,736	2021,422	-223,187	2177
KA1639A	15,4	25,9	20,65	930927	1079	48	0,1	7296,386	2020,416	-222,622	2171
KA1750A	4,4	5,4	4,9	930929	1081	90	0,2	7373,065	2068,565	-237,243	2179
KA1755A	88	160		960521	2046	222	0,6				2359
KBH02	240,25	372,85	306,55	931214	1157	111	0,3	6583,47	2128,279	-120,472	2210
SA0813B	5,6	19,5	12,55	960521	2046	1628	3,3	6479,609	2152,822	-112,929	2353
SA0923A	6	20	13	930207	847	434	1,2	6588,708	2125,893	-128,407	2075
SA0958B	5	19,7	12,35	940607	1332	349	1,0	6618,921	2151,272	-133,195	2254
SA1009B	6	19,5	12,75	960521	2046	1058	2,9	6672,091	2152,899	-139,744	2356
SA1062B	6	20	13	921202	780	223	0,6	6724,883	2145,887	-146,969	2050
SA1229A	6	20,5	13,25	960521	2046	1001	2,7	6885,159	2105,455	-171,291	2357
SA1420A	6	50	28	960521	2046	1376	3,6	7092,329	2080,819	-200,592	2358
SA1614B	5,8	19,3	12,55	940606	1331	564	1,5	7257,869	2039,086	-224,037	2249
SA1680B	6	20	13	930203	843	106	0,3	7317,959	2060,113	-230,324	2066
SA1696B	5,9	19,2	12,55	940606	1331	594	1,6	7332,421	2065,722	-232,645	2250
SA1730A	5,6	20	12,8	951011	1823	980	2,7	7369,317	2065,943	-237,012	2331
SA1828B	5,8	20	12,9	940606	1331	564	1,5	7401,58	2157,075	-249,511	2252
SA2074A	6	38,7	22,35	950518	1677	832	2,3	7290,03	2348,258	-281,676	2317
SA2175B	5,8	20	12,9	940530	1324	168	0,5	7200,014	2294,498	-293,825	2244
SA2240B	5,7	19,8	12,75	931207	1150	70	0,2	7172,049	2249,831	-301,544	2204
SA2273A	5,8	20	12,9	960521	2046	903	2,5	7149,762	2221,715	-305,968	2355

ID code	Secup	Seclow	Centr.	Measured Na (mg/l)	Measured K (mg/l)	Measured Ca (mg/l)	Measured Mg (mg/l)	Measured HCO3 (mg/l)	Measured Cl (mg/l)	Measured SO4 (mg/l)	Measured D (o/oo)	Measured Tr (TU)	Measured O18 (o/oo)
KAS02	309	345	327	1150	7,5	671	48,5	138	3250	249	-94,9	8	-13,3
KAS03	533	626	579,5	1564	6,7	1162	48,4	38	4637	270	-106,3	6,8	-13,6
KAS05	440	549,6	494,8	2450	10	2560	42,1	5	8402	534	-96,8	8,4	-13
KAS07	191	290	240,5	1479	10,2	559	125	335	3743,8	74,4	-65,4	22	-8
KAS07	501	604	552,5	1890	9,5	1610	59,6	13	5960	446	-80,4	12,7	-11,2
KAS08	503	601	552	2180	13,3	1522	144,8	63	6452	391	-73,8	13	-9,2
KAS09	116	150	133	1465,1	33,89	198,9	139,7	175	2804,3	298,34	-56,7	33,8	-7
KAS12	234	277	255,5	1650	12,5	1070	107	61	4860	233	-82	4,2	-10,5
KLX01	680	702,11	691,06	1610	7,3	1330	24	24	4680	390	-98,8	0,6	-11,8
HBH01	31	50,6	40,8	286	3,8	94,4	16,2	290	550	103	-72,7	31	-9,8
HBH02	21	32,4	26,7	45,9	1,4	38	3,8	170	100	13,8	-73,9	35	-9,9
HBH05	11	22	16,5	25,4	2,6	42,6	8,8	172	27,6	36,6	-64,7	24	-9,4
KR0012B	5	10,57	7,785	326,9	3,73	83,6	14,4	302	495,6	102	-70,4	38	-9,9
KR0013B	7,05	16,94	11,995	620	4	270	47,1	267	1458,9	125,53	-70,6	71	-9,5
KR0015B	19,82	30,31	25,065	442	3,45	143	23	340	726	110	-72,9	34	-9,7
HA1327B	3,5	29,5	16,5	1760	13,7	684	157	259	4310	255	-54,5	13	-7,4
KA1639A	13,4	14,4	13,9	2218	8,2	1967	68,3	23	6960	480	-90,2	4,2	-12,4
KA1639A	15,4	25,9	20,65	1620	6	774	45,9	19	4230	130	-107,6	12	-14,6
KA1750A	4,4	5,4	4,9	2062	7,8	1684	71,2	33	6230	462	-80	8,4	-11,6
KA1755A	88	160		2836	9,47	3540,5	37,6	8	10565	611	-96,1	10	-12,8
KBH02	240,25	372,85	306,55	1800	21	638	160	340	4210	228	-59,2	6,8	-7,7
SA0813B	5,6	19,5	12,55	1522,7	19,39	275,5	111,6	319	2963,9	251,98	-53,2	19,4	-6,8
SA0923A	6	20	13	1800	30	678	162	655	4310	128	-59,7	8,4	-7,7
SA0958B	5	19,7	12,35	1634,1	21,4	477,8	125,1	274	3641	303	-55,6	22,8	-7,2
SA1009B	6	19,5	12,75	1598,1	35,94	239,4	150	110	3169,5	371,03	-57,4	24,5	-7
SA1062B	6	20	13	1930	34	545	177	403	4350	187	-58	8	-7,7
SA1229A	6	20,5	13,25	1639,8	28,04	413,1	137,2	303	3392,9	248	-46,3	15,2	-6,5
SA1420A	6	50	28	1315,8	21,1	245,4	119,1	214	2676,7	280,88	-60,3	23,7	-7,1
SA1614B	5,8	19,3	12,55	1831,3	7,37	1207	98,3	109	5176,1	333	-77,6	8,4	-10,4
SA1680B	6	20	13	1100	10	583	63,3	137	2790	194	-85,5	17	-10,7
SA1696B	5,9	19,2	12,55	1932,5	9,14	1740,4	71,4	89	6275,2	459	-81	7	-11,1
SA1730A	5,6	20	12,8	2384,2	8,23	2616,5	56,4	36	8650,5	530,46	-87,1	8,45	-11,9
SA1828B	5,8	20	12,9	1861,5	11,67	1063,9	138,8	111	5123	251	-67,8	8,4	-8,9
SA2074A	6	38,7	22,35	1454	9,3	560,4	119,3	128	3414,1	262	-65,1	33	-8,4
SA2175B	5,8	20	12,9	1959,5	15,29	1037,1	161,6	127	5442	267	-62	8,4	-8,2
SA2240B	5,7	19,8	12,75	2110	17,5	1010	180	171	5460	254	-57,3	5,9	-8,1
SA2273A	5,8	20	12,9	1804,9	14	823,8	134,6	175	4530,9	273,72	-62,8	20,3	-8,1

ID code	Secup	Seclow	Centr.	Mixing Brine	Mixing Glacial	Mixing Meteoric	Mixing Baltic Sea	Predicted Brine	Predicted Glacial	Predicted Meteoric	Predicted Baltic Sea
KAS02	309	345	327	10%	38%	41%	10%	18%	31%	30%	20%
KAS03	533	626	579,5	13%	49%	25%	13%	11%	51%	26%	12%
KAS05	440	549,6	494,8	23%	46%	16%	16%	22%	41%	17%	19%
KAS07	191	290	240,5	4%	4%	60%	32%	11%	22%	56%	12%
KAS07	501	604	552,5	18%	29%	35%	18%	19%	31%	30%	20%
KAS08	503	601	552	17%	17%	37%	30%	19%	26%	34%	20%
KAS09	116	150	133	3%	3%	39%	54%	6%	-5%	42%	58%
KAS12	234	277	255,5	15%	21%	49%	15%	14%	24%	48%	14%
KLX01	680	702,11	691,06	15%	45%	26%	15%	15%	47%	23%	15%
HBH01	31	50,6	40,8	4%	5%	87%	4%	6%	-6%	92%	8%
HBH02	21	32,4	26,7	2%	8%	87%	2%	5%	-3%	91%	7%
HBH05	11	22	16,5	3%	5%	88%	3%	4%	8%	83%	4%
KR0012B	5	10,57	7,785	3%	3%	89%	5%	8%	7%	73%	11%
KR0013B	7,05	16,94	11,995	1%	1%	81%	18%	11%	14%	60%	14%
KR0015B	19,82	30,31	25,065	4%	4%	87%	6%	8%	2%	79%	11%
HA1327B	3,5	29,5	16,5	6%	6%	42%	45%	6%	2%	43%	49%
KA1639A	13,4	14,4	13,9	19%	41%	20%	19%	18%	39%	24%	18%
KA1639A	15,4	25,9	20,65	10%	51%	28%	10%	10%	54%	26%	10%
KA1750A	4,4	5,4	4,9	19%	31%	31%	19%	18%	32%	32%	18%
KA1755A	88	160		28%	44%	14%	14%	28%	42%	14%	15%
KBH02	240,25	372,85	306,55	6%	6%	42%	45%	5%	4%	41%	51%
SA0813B	5,6	19,5	12,55	3%	3%	48%	46%	7%	-5%	51%	48%
SA0923A	6	20	13	1%	1%	45%	53%	1%	-3%	42%	59%
SA0958B	5	19,7	12,35	5%	5%	43%	47%	7%	3%	45%	45%
SA1009B	6	19,5	12,75	6%	6%	33%	55%	5%	-5%	39%	62%
SA1062B	6	20	13	4%	4%	37%	54%	3%	1%	37%	59%
SA1229A	6	20,5	13,25	2%	2%	38%	57%	5%	-5%	39%	61%
SA1420A	6	50	28	5%	5%	49%	42%	16%	8%	58%	18%
SA1614B	5,8	19,3	12,55	16%	20%	48%	16%	17%	19%	47%	18%
SA1680B	6	20	13	10%	19%	60%	10%	7%	22%	63%	8%
SA1696B	5,9	19,2	12,55	18%	29%	35%	18%	9%	19%	63%	9%
SA1730A	5,6	20	12,8	22%	39%	20%	20%	20%	28%	32%	21%
SA1828B	5,8	20	12,9	13%	13%	46%	28%	17%	17%	47%	18%
SA2074A	6	38,7	22,35	8%	8%	54%	31%	7%	2%	82%	8%
SA2175B	5,8	20	12,9	11%	11%	38%	39%	12%	10%	36%	42%
SA2240B	5,7	19,8	12,75	10%	10%	35%	45%	11%	11%	35%	43%
SA2273A	5,8	20	12,9	9%	9%	45%	37%	14%	5%	39%	42%

				Predicted	Predicted	Predicted	Predicted	Predicted	Predicted	Predicted	Predicted	Predicted	Predicted
ID code	Secup	Seclow	Centr.	Na	K	Ca	Mg	HCO3	Cl	SO4	D	Tr	O18
				(mg/l)	(mg/l)	(mg/l)	(mg/l)	(mg/l)	(mg/l)	(mg/l)	(o/oo)	(TU)	(o/oo)
KAS02	309	345	327	1949	28	3542	48	25	9378	232	-92	40	-13
KAS03	533	626	579,5	1169	17	2138	28	15	5647	139	-113	31	-15
KAS05	440	549,6	494,8	2282	28	4357	45	22	11324	266	-99	26	-14
KAS07	191	290	240,5	1139	16	2082	27	19	5499	136	-90	62	-12
KAS07	501	604	552,5	2009	28	3687	47	24	9725	238	-92	39	-13
KAS08	503	601	552	2037	28	3747	48	25	9874	241	-88	43	-12
KAS09	116	150	133	1600	57	1118	135	58	4773	238	-59	67	-7
KAS12	234	277	255,5	1429	20	2630	33	21	6930	169	-90	55	-12
KLX01	680	702,11	691,06	1566	22	2886	36	19	7601	185	-107	30	-14
HBH01	31	50,6	40,8	627	10	1076	19	19	2912	77	-71	96	-9
HBH02	21	32,4	26,7	563	9	983	16	18	2643	69	-74	94	-10
HBH05	11	22	16,5	412	6	744	10	15	1974	50	-84	85	-11
KR0012B	5	10,57	7,785	932	15	1635	26	20	4388	113	-80	78	-11
KR0013B	7,05	16,94	11,995	1247	19	2231	33	21	5943	150	-83	67	-11
KR0015B	19,82	30,31	25,065	925	14	1638	25	20	4379	112	-76	84	-10
HA1327B	3,5	29,5	16,5	1464	49	1204	114	50	4662	213	-67	64	-8
KA1639A	13,4	14,4	13,9	1897	26	3512	43	22	9234	224	-99	33	-13
KA1639A	15,4	25,9	20,65	1079	15	1997	25	14	5250	128	-116	30	-16
KA1750A	4,4	5,4	4,9	1905	26	3526	43	23	9271	225	-94	40	-13
KA1755A	88	160		2697	27	5472	36	19	13912	305	-99	22	-14
KBH02	240,25	372,85	306,55	1403	50	981	119	51	4185	209	-68	62	-8
SA0813B	5,6	19,5	12,55	1490	48	1308	112	50	4880	215	-61	71	-8
SA0923A	6	20	13	1269	57	300	139	59	2826	205	-62	67	-7
SA0958B	5	19,7	12,35	1447	46	1311	106	47	4806	207	-68	64	-9
SA1009B	6	19,5	12,75	1619	61	985	145	61	4590	245	-58	65	-7
SA1062B	6	20	13	1413	58	617	139	58	3609	220	-64	62	-8
SA1229A	6	20,5	13,25	1595	60	968	143	60	4519	241	-58	65	-7
SA1420A	6	50	28	1710	24	3103	42	25	8220	204	-76	66	-10
SA1614B	5,8	19,3	12,55	1771	25	3255	42	24	8581	210	-84	55	-11
SA1680B	6	20	13	787	11	1454	18	16	3826	94	-92	67	-12
SA1696B	5,9	19,2	12,55	919	13	1674	22	17	4428	110	-90	67	-12
SA1730A	5,6	20	12,8	2083	29	3811	50	26	10064	247	-89	41	-12
SA1828B	5,8	20	12,9	1845	26	3392	43	25	8942	219	-82	55	-11
SA2074A	6	38,7	22,35	764	11	1374	20	18	3652	92	-77	86	-10
SA2175B	5,8	20	12,9	1828	46	2300	100	44	7125	245	-72	54	-9
SA2240B	5,7	19,8	12,75	1805	46	2219	101	45	6950	243	-73	54	-9
SA2273A	5,8	20	12,9	2006	46	2727	98	44	8150	263	-68	57	-9

ID code	Secup	Seclow	Centr.	Difference Brine	Difference Glacial	Difference Meteoric	Difference Baltic Sea	Total diff. +	Total diff. -
KAS02	309	345	327	8%	-7%	-11%	10%	18%	-18%
KAS03	533	626	579,5	-2%	2%	1%	-1%	3%	-3%
KAS05	440	549,6	494,8	0%	-4%	1%	3%	5%	-5%
KAS07	191	290	240,5	7%	17%	-4%	-20%	24%	-24%
KAS07	501	604	552,5	1%	2%	-5%	2%	5%	-5%
KAS08	503	601	552	2%	10%	-3%	-9%	12%	-12%
KAS09	116	150	133	2%	-8%	3%	3%	8%	-8%
KAS12	234	277	255,5	-2%	3%	-1%	-1%	3%	-3%
KLX01	680	702,11	691,06	0%	2%	-3%	1%	3%	-3%
HBH01	31	50,6	40,8	2%	-11%	5%	4%	11%	-11%
HBH02	21	32,4	26,7	3%	-11%	4%	5%	11%	-11%
HBH05	11	22	16,5	0%	4%	-5%	1%	5%	-5%
KR0012B	5	10,57	7,785	5%	4%	-16%	6%	16%	-16%
KR0013B	7,05	16,94	11,995	11%	14%	-21%	-4%	25%	-25%
KR0015B	19,82	30,31	25,065	5%	-2%	-8%	5%	10%	-10%
HA1327B	3,5	29,5	16,5	0%	-4%	1%	3%	4%	-4%
KA1639A	13,4	14,4	13,9	-1%	-2%	5%	-1%	5%	-5%
KA1639A	15,4	25,9	20,65	0%	3%	-3%	0%	3%	-3%
KA1750A	4,4	5,4	4,9	0%	0%	0%	0%	1%	-1%
KA1755A	88	160		0%	-2%	0%	1%	2%	-2%
KBH02	240,25	372,85	306,55	-1%	-3%	-1%	5%	5%	-5%
SA0813B	5,6	19,5	12,55	4%	-8%	3%	1%	8%	-8%
SA0923A	6	20	13	0%	-4%	-3%	7%	7%	-7%
SA0958B	5	19,7	12,35	2%	-2%	2%	-2%	4%	-4%
SA1009B	6	19,5	12,75	-1%	-11%	6%	7%	12%	-12%
SA1062B	6	20	13	-1%	-4%	0%	5%	5%	-5%
SA1229A	6	20,5	13,25	2%	-7%	1%	4%	7%	-7%
SA1420A	6	50	28	11%	3%	9%	-24%	24%	-24%
SA1614B	5,8	19,3	12,55	1%	-1%	-2%	2%	2%	-2%
SA1680B	6	20	13	-3%	2%	3%	-3%	5%	-5%
SA1696B	5,9	19,2	12,55	-10%	-9%	28%	-9%	28%	-28%
SA1730A	5,6	20	12,8	-2%	-11%	12%	1%	13%	-13%
SA1828B	5,8	20	12,9	5%	4%	1%	-10%	10%	-10%
SA2074A	6	38,7	22,35	0%	-5%	28%	-23%	28%	-28%
SA2175B	5,8	20	12,9	0%	-1%	-3%	4%	4%	-4%
SA2240B	5,7	19,8	12,75	1%	0%	0%	-2%	2%	-2%
SA2273A	5,8	20	12,9	5%	-4%	-6%	5%	10%	-10%

				Difference	Difference	Difference	Difference	Difference	Difference	Difference	Difference	Difference	Difference
ID code	Secup	Seclow	Centr.	Na	K	Ca	Mg	HCO3	Cl	SO4	D	Tr	O18
				(mg/l)	(mg/l)	(mg/l)	(mg/l)	(mg/l)	(mg/l)	(mg/l)	(o/oo)	(TU)	(o/oo)
KAS02	309	345	327	799	20	2871	-1	-113	6128	-17	2	32	1
KAS03	533	626	579,5	-395	10	976	-20	-23	1010	-131	-7	24	-2
KAS05	440	549,6	494,8	-168	18	1797	3	17	2922	-268	-2	18	-1
KAS07	191	290	240,5	-340	6	1523	-98	-316	1756	61	-25	40	-4
KAS07	501	604	552,5	119	18	2077	-12	11	3765	-208	-12	26	-1
KAS08	503	601	552	-143	15	2225	-97	-38	3422	-150	-15	30	-3
KAS09	116	150	133	135	24	920	-5	-117	1968	-60	-2	33	0
KAS12	234	277	255,5	-221	7	1560	-74	-40	2070	-64	-8	51	-2
KLX01	680	702,11	691,06	-44	14	1556	12	-5	2921	-205	-8	29	-3
HBH01	31	50,6	40,8	341	7	982	3	-271	2362	-26	1	65	0
HBH02	21	32,4	26,7	517	8	945	12	-152	2543	55	0	59	0
HBH05	11	22	16,5	387	4	701	2	-157	1947	14	-19	61	-2
KR0012B	5	10,57	7,785	605	11	1552	12	-282	3892	11	-9	40	-1
KR0013B	7,05	16,94	11,995	627	15	1961	-15	-246	4484	24	-13	-4	-2
KR0015B	19,82	30,31	25,065	483	11	1495	2	-320	3653	2	-3	50	0
HA1327B	3,5	29,5	16,5	-296	35	520	-43	-209	352	-42	-12	51	-1
KA1639A	13,4	14,4	13,9	-321	18	1545	-25	-1	2274	-256	-9	29	-1
KA1639A	15,4	25,9	20,65	-541	9	1223	-21	-5	1020	-2	-8	18	-1
KA1750A	4,4	5,4	4,9	-157	18	1842	-28	-10	3041	-237	-14	32	-1
KA1755A	88	160		-139	18	1932	-2	11	3347	-306	-3	12	-1
KBH02	240,25	372,85	306,55	-397	29	343	-41	-289	-25	-19	-9	55	-1
SA0813B	5,6	19,5	12,55	-33	29	1032	0	-269	1916	-37	-8	52	-1
SA0923A	6	20	13	-531	27	-378	-23	-596	-1484	77	-2	59	0
SA0958B	5	19,7	12,35	-187	25	833	-19	-227	1165	-96	-13	41	-1
SA1009B	6	19,5	12,75	21	25	746	-5	-49	1421	-126	0	40	0
SA1062B	6	20	13	-517	24	72	-38	-345	-741	33	-6	54	0
SA1229A	6	20,5	13,25	-44	32	555	5	-243	1126	-7	-12	50	-1
SA1420A	6	50	28	394	3	2858	-77	-189	5543	-77	-15	43	-3
SA1614B	5,8	19,3	12,55	-60	17	2048	-57	-85	3405	-123	-7	46	-1
SA1680B	6	20	13	-313	1	871	-45	-121	1036	-100	-7	50	-2
SA1696B	5,9	19,2	12,55	-1013	4	-67	-49	-72	-1847	-349	-9	60	-1
SA1730A	5,6	20	12,8	-302	21	1195	-7	-10	1413	-283	-2	33	0
SA1828B	5,8	20	12,9	-16	14	2328	-96	-86	3819	-32	-15	47	-2
SA2074A	6	38,7	22,35	-690	2	814	-100	-110	238	-170	-12	53	-2
SA2175B	5,8	20	12,9	-131	31	1263	-62	-83	1683	-22	-10	46	-1
SA2240B	5,7	19,8	12,75	-305	29	1209	-79	-126	1490	-11	-16	48	-1
SA2273A	5,8	20	12,9	201	32	1903	-36	-131	3619	-11	-5	37	-1

					Days from	Days from	Years from				
ID code	Secup	Seclow	Centr.	Date	1990-10-14 =0	1st obs.	1st obs.	Northing	Easting	Elevation	SNO
SA2273B	5,8	20	12,9	940530	1324	181	0,5	7162,946	2217,931	301,932	2245
SA2289B	6	19,4	12,7	940530	1324	181	0,5	7158,515	2202,689	-307,718	2246
SA2322A	6	20,1	13,05	940527	1321	241	0,7	7136,119	2174,475	-312,606	2243
SA2583A	5,7	20	12,85	940518	1312	72	0,2	7301,166	2035,311	-343,513	2240
SA2600A	5,8	19,4	12,6	960521	2046	806	2,2	7315,455	2044,414	-345,048	2351
SA2703A	5,7	19,6	12,65	940517	1311	83	0,2	7411,496	2082,084	-358,592	2237
SA2783A	5,8	19,9	12,85	960520	2045	826	2,3	7442,809	2160,694	-371,361	2352
SA2880A	11,92	13,92	12,92	960412	2007	170	0,5	7455,116	2259,267	-384,736	2349
Average difference											

				Measured	Measured	Measured	Measured	Measured	Measured	Measured	Measured	Measured	Measured
ID code	Secup	Seclow	Centr.	Na	K	Ca	Mg	HCO3	Cl	SO4	D	Tr	O18
SA2273B	5,8	20	12,9	1761,7	7,82	1135,1	127,5	117	5105,2	196	-71,3	10,1	-9,5
SA2289B	6	19,4	12,7	1952,7	12,16	968,6	162,1	178	5167,3	219	-60,8	8,4	-8
SA2322A	6	20,1	13,05	1908,3	9,44	977,4	142,5	184	5034,3	213	-68	8,4	-8,6
SA2583A	5,7	20	12,85	2170	8,51	1859,6	73,9	44	6895,6	492	-85,9	5,9	-10,7
SA2600A	5,8	19,4	12,6	2125,4	9,1	1485,7	85	114	5920,7	403,81	-75,5	11	-9,8
SA2703A	5,7	19,6	12,65	2824	7,79	3581,3	40,3	12	10591,6	600	-93,7	4,2	-13,1
SA2783A	5,8	19,9	12,85	3053,2	10,89	4061,5	48,6	15	12054	616	-90	22	-12,5
SA2880A	11,92	13,92	12,92	3156,4	13,64	4378,1	41,1	22	12956,3	626	-84,5	21	-12,1
Average difference													

				Mixing	Mixing	Mixing	Mixing	Predicted	Predicted	Predicted	Predicted
ID code	Secup	Seclow	Centr.	Brine	Glacial	Meteoric	Baltic Sea	Brine	Glacial	Meteoric	Baltic Sea
SA2273B	5,8	20	12,9	13%	13%	53%	21%	16%	14%	50%	20%
SA2289B	6	19,4	12,7	10%	10%	42%	39%	12%	11%	41%	36%
SA2322A	6	20,1	13,05	11%	11%	48%	29%	14%	11%	46%	29%
SA2583A	5,7	20	12,85	20%	32%	29%	20%	20%	34%	27%	20%
SA2600A	5,8	19,4	12,6	18%	18%	46%	18%	24%	28%	23%	25%
SA2703A	5,7	19,6	12,65	28%	45%	13%	13%	27%	42%	16%	16%
SA2783A	5,8	19,9	12,85	29%	38%	16%	16%	23%	33%	21%	23%
SA2880A	11,92	13,92	12,92	31%	34%	17%	17%	28%	36%	18%	18%
Average difference											

				Predicted	Predicted	Predicted	Predicted	Predicted	Predicted	Predicted	Predicted	Predicted	Predicted
ID code	Secup	Seclow	Centr.	Na	K	Ca	Mg	HCO3	Cl	SO4	D	Tr	O18
SA2273B	5,8	20	12,9	1721	27	3016	48	27	8099	208	-80	59	-11
SA2289B	6	19,4	12,7	1765	40	2442	84	39	7241	230	-74	56	-10
SA2322A	6	20,1	13,05	1727	34	2671	68	33	7545	218	-76	59	-10
SA2583A	5,7	20	12,85	2061	28	3818	47	24	10037	243	-94	36	-13
SA2600A	5,8	19,4	12,6	2536	35	4661	60	29	12289	300	-86	35	-12
SA2703A	5,7	19,6	12,65	2590	27	5195	37	20	13260	295	-99	23	-14
SA2783A	5,8	19,9	12,85	2419	33	4488	55	27	11790	285	-91	31	-13
SA2880A	11,92	13,92	12,92	2714	30	5364	44	23	13766	311	-94	27	-13
Average difference													

				Difference	Difference	Difference	Difference	Total diff.	Total diff.
ID code	Secup	Seclow	Centr.	Brine	Glacial	Meteoric	Baltic Sea	+	-
SA2273B	5,8	20	12,9	2%	1%	-2%	0%	3%	-3%
SA2289B	6	19,4	12,7	3%	1%	-1%	-3%	4%	-4%
SA2322A	6	20,1	13,05	2%	0%	-2%	-1%	2%	-2%
SA2583A	5,7	20	12,85	0%	2%	-2%	0%	2%	-2%
SA2600A	5,8	19,4	12,6	6%	10%	-23%	7%	23%	-23%
SA2703A	5,7	19,6	12,65	-1%	-3%	2%	2%	5%	-5%
SA2783A	5,8	19,9	12,85	-6%	-5%	4%	7%	11%	-11%
SA2880A	11,92	13,92	12,92	-3%	2%	0%	1%	3%	-3%
Average difference				**1%**	**-1%**	**0%**	**0%**	**9%**	**-9%**

				Difference	Difference	Difference	Difference	Difference	Difference	Difference	Difference	Difference	Difference
ID code	Secup	Seclow	Centr.	Na	K	Ca	Mg	HCO3	Cl	SO4	D	Tr	O18
SA2273B	5,8	20	12,9	-40	19	1881	-79	-90	2994	12	-9	49	-1
SA2289B	6	19,4	12,7	-187	28	1473	-78	-139	2074	11	-14	48	-2
SA2322A	6	20,1	13,05	-181	24	1693	-75	-151	2510	5	-8	50	-2
SA2583A	5,7	20	12,85	-109	19	1959	-27	-20	3141	-249	-8	30	-2
SA2600A	5,8	19,4	12,6	411	26	3176	-25	-85	6369	-104	-11	24	-2
SA2703A	5,7	19,6	12,65	-234	20	1613	-3	8	2669	-305	-5	19	-1
SA2783A	5,8	19,9	12,85	-634	22	426	6	12	-264	-331	-1	9	0
SA2880A	11,92	13,92	12,92	-442	17	986	2	1	810	-315	-9	6	-1
Average difference				**-91**	**18**	**1356**	**-31**	**-128**	**2199**	**-99**	**-8**	**39**	**-1**